Numerical methods for high frequency scattering by multiple obstacles

Andrew Gibbs

University of Reading

A thesis submitted for the degree of

Doctor of Philosophy

March 2017

Declaration

I confirm that this is my own work and that the use of all material from other sources has been properly and fully acknowledged.

In addition to my three supervisors, Chapter 5 is the result of collaboration with Dr. Euan Spence.

Acknowledgements

Firstly, I owe a great deal of thanks to my supervisors Andrea Moiola, Stephen Langdon and Simon Chandler-Wilde for all of your help and enthusiasm over the past three years. I've really enjoyed working with all of you, and I'm very grateful that you have been able to dedicate so much time to my project, and for opportunities you have given me. Thank you to EPSRC for funding the project.

Alongside my supervisors, I've crossed paths with many interesting academics during the project. I would like to thank Dave Hewett, Sam Groth, Justin Prince, Alexey Chernov, Tristan Pryer and Timo Betcke for many helpful conversations throughout my PhD. I am incredibly grateful to Daan Huybrechs for our conversations about quadrature, Euan Spence for our conversations about mild trapping and DtN maps, and finally Nick Biggs for introducing me to Embedding Formulae. More generally, I would like to thank everyone in the Maths and Stats Department at Reading who have made the last four years so much fun.

A particularly enjoyable six months of my PhD was spent at Maquarie University, Sydney. I would like to thank the Australian Bicentennial scholarship for funding this opportunity, and Stuart Hawkins for the very warm welcome and supervision that I received, alongside all of the staff and students who made the experience so special.

Finally, I owe a great deal of thanks to my friends and family. In particular Hasen, my parents, Nikki and the McCarthy family for supporting me and giving me somewhere to stay during the final months of my PhD.

Abstract

For problems of time harmonic wave scattering, standard numerical methods (using piecewise polynomial approximation spaces) require the computational cost to grow with the frequency of the problem, in order to maintain a fixed accuracy. This can make many problems of practical interest difficult or impossible to solve at high frequencies. The *Hybrid Numerical Asymptotic Boundary Element Method* (HNA BEM) overcomes this by enriching the approximation space with oscillatory basis functions, in such a way that accuracy may be maintained with a computational cost that grows only modestly with frequency. HNA methods have previously been developed for a range of problems, including screens in two and three dimensions, also convex, non-convex and penetrable polygons in two dimensions. To date, all HNA methods have been developed for problems of plane wave scattering by a single obstacle. **The key aim of this thesis is to extend the HNA method to multiple obstacles**.

A range of extensions to the HNA method are made in this thesis. Previous HNA methods for convex polygons use an approximation space on two overlapping meshes, here we use HNA on a single mesh. This single-mesh approach is easier to implement, and we prove that the frequency-dependence of the size of the approximation space is the same as for the overlapping mesh. We generalise HNA theory to provide a priori error estimates for a broader range of incident fields than just the plane wave, including point sources, beam sources, and Herglotz-type incidence. We also extend the HNA ansatz to include multiple obstacles.

In addition to the development of HNA methods, we also consider other ideas and developments related to multiple scattering problems. This includes the first (to the best knowledge of the author) mesh and frequency explicit condition for well-posedness of Galerkin BEM for multiple scattering.

We investigate numerical implementation of *Embedding Formulae*, which provide the far-field pattern for any incident plane wave, given the far-field patterns induced by a small (frequency independent) number of plane waves. We establish points at which a naive implementation of the theory can cause numerical instabilities and present alternative, numerically stable Embedding Formulae. We also extend the Embedding Formulae to produce the far-field pattern of any Herglotz-type wave. The recently developed *Tmatrom* method, a numerically stable T-matrix method, is explored as an alternative means of extending the HNA method from single to multiple obstacles. Tmatrom typically requires a number of single scattering problems to be

solved, and this number grows (more than) linearly with the frequency of the problem. Using the numerically stable Embedding Formulae, we show that Tmatrom can be applied by solving a number of problems that depends only on the geometry of the obstacle, and not the frequency of the incident wave.

Contents

Notational rules of thumb

Each chapter of this thesis will consider a different problem on different geometric configurations. Whilst definitions will be stated as and when they are used, a general rule of thumb is that Γ_j denotes the jth side of the polygon with boundary Γ, whilst γ_i denotes the boundary of the ith obstacle (not to be confused with the imaginary unit $\mathrm{i} := \sqrt{-1}$). Moreover, n_Γ denotes the number of sides of Γ, whilst n_γ denotes the number of disconnected obstacles that comprise γ. We typically write N (with a subscript depending on the problem) to denote *number of degrees of freedom*.

Chapter 1

Introduction

1.1 General problem statement and formulation

Problems of high-frequency time harmonic scattering arise in a range of real world problems, including seismic imaging, noise reduction, and atmospheric modelling. In this thesis, the focus is on two-dimensional acoustic waves, although many of the ideas may be extended to electromagnetic or elastic waves. Naturally, three-dimensional problems are more common in practical applications. We expect that with further work, much of the theory in this thesis may be extended to three dimensions, possible extensions are discussed at the end of each chapter. Indeed, three-dimensional HNA methods have already been developed in [33], extending the two dimensional screen problem of [34]. However, the two-dimensional setting is a more sensible starting point for new methodology and theory.

The Helmholtz equation is named after Hermann Ludwig Ferdinand von Helmholtz, and is often referred to as the *reduced* or *time-harmonic* wave equation. This is because solutions of the Helmholtz equation correspond to *time-harmonic* (periodic in time) solutions of the wave equation. We introduce the problem from this starting point of the two-dimensional wave equation (see, e.g., [17, (§2.1)] for a derivation),

$$\left(\frac{1}{c^2}\frac{\partial^2}{\partial t^2} - \Delta\right) U = 0, \quad \text{in } \Omega \times [0,\infty), \tag{1.1}$$

modelling waves $U(\mathbf{x},t)$ propagating at speed $c > 0$ with $\mathbf{x} := (x_1, x_2) \in \Omega \subset \mathbb{R}^2$, with the two-dimensional Laplacian operator

$$\Delta := \frac{\partial^2}{\partial x_1^2} + \frac{\partial^2}{\partial x_2^2}.$$

A time-harmonic wave may be represented as

$$U(\mathbf{x},t) = \mathrm{Re}\left\{ u(\mathbf{x})\mathrm{e}^{-\mathrm{i}\omega t}\right\}, \quad \text{for } \omega > 0, \tag{1.2}$$

hence inserting (1.2) into (1.1) yields the Helmholtz equation

$$(\Delta + k^2)u = 0, \quad \text{in } \Omega, \tag{1.3}$$

where $k := \omega/c$ denotes the *wavenumber*. We assume throughout this thesis that the wavenumber k does not vary in space. As an example, the sound of a piano will satisfy the wave equation (1.1), however it will peak at the moment when the key is pressed and the hammer hits the string, the amplitude $|U(\mathbf{x}, t)|$ will decay in time t. Hence it cannot be considered *time-harmonic*; there will exist no U of the form (1.2) with component $u(\mathbf{x})$ satisfying (1.3). In contrast, an organ sound is produced by a constant stream of air forcing a pipe to vibrate, and may be considered *time-harmonic*; hence there exists a u corresponding to the sound of an organ which satisfies (1.3).

1.1.1 Boundary Value Problem

Let $\Omega_- \subset \mathbb{R}^2$ be a bounded, Lipschitz open set (see for example [13, Definition A.2] for a definition of this) with boundary $\partial\Omega$, and define the exterior scattering domain as the complement of the closure of this set, that is $\Omega_+ := \mathbb{R}^2 \setminus \overline{\Omega_-}$. The unit normal vector $\mathbf{n}$ is perpendicular to $\partial\Omega$, defined almost everywhere on $\partial\Omega$. For example, the normal vector $\mathbf{n}$ is not defined at corner points. We assume that the wavenumber $k > 0$ does not vary in $\mathbb{R}^2$; an essential requirement for the boundary integral equation formulation that follows in §1.1.2. The incident field u^{inc} is the (known) wave which will be excited by the obstacle Ω_-. Constraints on u^{inc} will change throughout the thesis, however they all fit inside the following general definition:

DEFINITION 1.1 (Incident field/wave)**.** *We say $u^{inc} \in L^2_{\text{loc}}(\mathbb{R}^2)$ is an* incident field *or an* incident wave *if there exists some open neighbourhood $\mathcal{N} \subset \mathbb{R}^2$ such that Ω_- is compactly embedded inside of $\mathcal{N}$ and u^{inc}*

(i) is in $C^\infty(\mathcal{N})$,

(ii) satisfies the Helmholtz equation (1.3) *in $\mathcal{N}$.*

We are interested in the interaction between an incident wave u^{inc} and an obstacle (or collection of obstacles) Ω_-. We aim to solve the following Boundary Value Problem (BVP): given the incident field u^{inc}, determine the total field $u \in C^2(\Omega_+) \cap C(\bar{\Omega}_+)$ (see Definition A.1, and more generally §A.1 for a summary of function spaces) such that

$$(\Delta + k^2)u = 0 \qquad \text{in } \Omega_+, \tag{1.4}$$

$$u = 0 \qquad \text{on } \partial\Omega_+ \tag{1.5}$$

and the scattered field $u^s := u - u^{\text{inc}}$ satisfies the Sommerfeld radiation condition, that is

$$\left(\frac{\partial}{\partial r} - \mathrm{i}k\right) u^s = o(r^{-1/2}), \quad \text{where } r = |\mathbf{x}|, \quad \text{as } |\mathbf{x}| \to \infty. \tag{1.6}$$

The condition (1.5) is typically referred to as the Dirichlet sound-soft boundary condition. Such boundary conditions occur in electromagnetic problems [17, §6.4]; if Ω_- can be modelled as a perfectly conductive infinitely long cylinder. Such cylindrical problems are referred to as *axis invariant* (see e.g. [45, pp5-6]) and may be modelled in two-dimensions, in which the total electric field is *transverse electric*, whilst perfect conductivity implies that the total electric field (analogous to u) vanishes inside of Ω_-, and satisfies a Dirichlet boundary condition equivalent to (1.5). It follows that the problem (1.4)-(1.6) is uniquely solvable (see for example [42, Theorem 9.10]).

The problem we currently describe is a *general problem statement*, whereas each chapter that follows will contain a *specific problem statement*, which fits inside of this general framework, but will contain specific constraints on the geometry of the scatterer Ω_-, and the incident field u^{inc}.

Explicit solutions to (1.4)-(1.6) only exist for special geometries, for example when Ω_- is a circle. This has motivated a significant amount of research into numerical methods for scattering problems in recent years. If a standard finite difference/element scheme is used, one typically approximates the solution u by a series of piecewise polynomials. As k grows, the number of degrees of freedom must typically grow by more than $O(k^2)$ to maintain accuracy, in order to resolve the oscillations and account for pollution effects. Moreover, it is necessary to truncate the domain Ω_+ and construct an artificial boundary, as it is impossible to consider a problem on an infinite domain with finite computational cost. These drawbacks of domain-based methods motivate *Boundary Element Methods*, which will be introduced shortly in §1.1.4.

1.1.2 Boundary integral equation formulation

Provided that k does not vary in space, the BVP (1.4)-(1.6) can be reformulated as a *Boundary Integral Equation* (BIE). Our BIE will make use of the fundamental solution to (1.3),

$$\Phi(\mathbf{x}, \mathbf{y}) := \frac{\mathrm{i}}{4} H_0^{(1)}(k|\mathbf{x} - \mathbf{y}|), \quad \mathbf{x} \neq \mathbf{y}, \tag{1.7}$$

for $\mathbf{x}$ and $\mathbf{y}$ in $\mathbb{R}^2$, where $H_n^{(1)}$ denotes the Hankel function of the first kind, order n. If u satisfies the BVP (1.4)–(1.6), we may construct an open ball B_R centred at the origin, with radius $R > 0$ chosen sufficiently large such that $\Omega_- \subset B_R$, and a second open ball $B_\epsilon(\mathbf{x})$ centred at $\mathbf{x}$ of radius $\epsilon > 0$, and apply Green's second identity ([13, Theorem 2.19]) to u^s and $\Phi(\mathbf{x}, \cdot)$ in $\Omega_+ \cap B_R \setminus B_\epsilon(\mathbf{x})$. Considering the limit as $\epsilon \to 0$ and $R \to \infty$, it follows from the radiation condition (1.6) and the asymptotics of (1.7) that

$$u^s(\mathbf{x}) = \int_{\partial\Omega} \left[-\Phi(\mathbf{x}, \mathbf{y}) \frac{\partial u^s}{\partial \mathbf{n}}(\mathbf{y}) + u^s(\mathbf{y}) \frac{\partial \Phi(\mathbf{x}, \mathbf{y})}{\partial \mathbf{n}(\mathbf{y})} \right] \mathrm{d}s(\mathbf{y}), \quad \mathbf{x} \in \Omega_+, \tag{1.8}$$

where

$$\frac{\partial}{\partial \mathbf{n}} := \mathbf{n} \cdot \nabla$$

denotes the *normal derivative*, which is often referred to as the *Neumann trace*, and shall also be denoted by the shorthand $\partial_{\mathbf{n}}^+$ in this thesis. A more formal definition can be found in Appendix A.2. For further details of (1.8) see [13, Theorem 2.21] or [17, Theorem 2.5]. Applying Green's second identity to u^{inc} and $\Phi(\mathbf{x}, \cdot)$ in Ω_-, we obtain

$$u^{\mathrm{inc}}(\mathbf{x}) = \int_{\partial\Omega} \left[-\Phi(\mathbf{x}, \mathbf{y}) \frac{\partial u^{\mathrm{inc}}}{\partial \mathbf{n}}(\mathbf{y}) + u^{\mathrm{inc}}(\mathbf{y}) \frac{\partial \Phi(\mathbf{x}, \mathbf{y})}{\partial \mathbf{n}(\mathbf{y})} \right] \mathrm{d}s(\mathbf{y}), \quad \mathbf{x} \in \Omega_+. \tag{1.9}$$

For further details see [13, Theorem 2.20] or [17, Theorem 2.1]. Summing (1.8) and (1.9) and noting the boundary condition (1.5) we obtain

$$u = u^{\mathrm{inc}} - S_k \partial_{\mathbf{n}}^+ u \quad \text{in } \Omega_+, \tag{1.10}$$

where $S_k : H^{s-1/2}(\partial\Omega) \to H^{s+1}_{\mathrm{loc}}(\mathbb{R}^2)$ for $s \in [-1/2, 1/2]$,

$$S_k \varphi(\mathbf{x}) := \int_{\partial\Omega} \Phi(\mathbf{x}, \mathbf{y}) \varphi(\mathbf{y}) \, \mathrm{d}s(\mathbf{y}), \quad \mathbf{x} \in \Omega_+, \tag{1.11}$$

denotes the acoustic single layer operator (see [13, Theorem 2.15] for detailed discussion of its mapping properties). Typically, one may obtain a BIE by taking a combination of traces (relevant operators introduced in §A.2) of the representation (1.10).

For $s \in [-1/2, 1/2]$, the single layer operator $\mathcal{S}_k : H^{s-1/2}(\partial\Omega) \to H^{s+1/2}(\partial\Omega)$ is defined by

$$\mathcal{S}_k \varphi(\mathbf{x}) := 2 \int_{\partial\Omega} \Phi(\mathbf{x}, \mathbf{y}) \varphi(\mathbf{y}) \, \mathrm{d}s(\mathbf{y}), \quad \mathbf{x} \in \partial\Omega,$$

the double layer operator $\mathcal{D}_k : H^{s+1/2}(\partial\Omega) \to H^{s+1/2}(\partial\Omega)$ is defined by

$$\mathcal{D}_k \varphi(\mathbf{x}) := 2 \int_{\partial\Omega} \frac{\partial \Phi(\mathbf{x}, \mathbf{y})}{\partial \mathbf{n}(\mathbf{y})} \varphi(\mathbf{y}) \, \mathrm{d}s(\mathbf{y}), \quad \mathbf{x} \in \partial\Omega,$$

whilst its adjoint $\mathcal{D}_k' : H^{s-1/2}(\partial\Omega) \to H^{s-1/2}(\partial\Omega)$ is defined by

$$\mathcal{D}_k'\varphi(\mathbf{x}) := 2\int_{\partial\Omega} \frac{\partial\Phi(\mathbf{x},\mathbf{y})}{\partial\mathbf{n}(\mathbf{x})}\varphi(\mathbf{y})\,\mathrm{d}s(\mathbf{y}), \quad \mathbf{x}\in\partial\Omega.$$

We have the following relationship between these operators and S_k of (1.11), from [13, (2.41)]:

$$2\tau_\pm S_k = \mathcal{S}_k, \quad 2\partial_n^\pm S_k = \mp\mathcal{I} + \mathcal{D}_k', \tag{1.12}$$

where $\tau_\pm$ and $\partial_{\mathbf{n}}^\pm$ denote the Dirichlet and Neumann interior and exterior traces (see §A.2), and $\mathcal{I}$ denotes the identity operator. We will also make use of the vector valued integral operator: the surface gradient of the single layer,

$$\nabla_{\partial\Omega}\mathcal{S}_k\varphi(\mathbf{x}) := 2\int_{\partial\Omega} \nabla_{\partial\Omega,\mathbf{x}}\Phi(\mathbf{x},\mathbf{y})\varphi(\mathbf{y})\,\mathrm{d}s(\mathbf{y}), \quad \mathbf{x}\in\partial\Omega, \tag{1.13}$$

where the kernel is defined by

$$\nabla_{\partial\Omega,\mathbf{x}}\Phi(\mathbf{x},\mathbf{y}) := \nabla_{\mathbf{x}}\Phi(\mathbf{x},\mathbf{y}) - \mathbf{n}(\mathbf{x})\frac{\partial\Phi(\mathbf{x},\mathbf{y})}{\partial\mathbf{n}(\mathbf{x})}$$

and the integral (1.13) is to be understood in the Cauchy principle value sense.

We seek a BIE of the form

$$\mathcal{A}\partial_{\mathbf{n}}^+ u = f, \quad \text{on } \partial\Omega, \tag{1.14}$$

where $\mathcal{A} : L^2(\partial\Omega) \to L^2(\partial\Omega)$ is a boundary integral operator, and $f \in L^2(\partial\Omega)$, where $\partial_{\mathbf{n}}^+$ denotes the Neumann trace (see (A.6) for a formal Definition). By taking the Dirichlet trace (as in (A.5)) of (1.10), we obtain the formulation with $\mathcal{A} = \mathcal{S}_k$ and $f = \tau_+ u^{\mathrm{inc}}$. However $\mathcal{S}_k$ is non-invertible for certain values of k, so in practice this is not a suitable formulation. In what follows, we will describe two suitable choices for $\mathcal{A}$, which are invertible. Throughout the thesis, $\mathcal{A}$ may refer to either of these two operators. By combining the Dirichlet and Neumann trace, we obtain the following formulation.

DEFINITION 1.2 (Combined potential formulation)**.** *The standard combined potential operator $\mathcal{A}_{k,\eta} : H^{s-1/2}(\partial\Omega) \to H^{s-1/2}(\partial\Omega)$, for $s \in [-1/2, 1/2]$ (see e.g. [13, 17]) and the corresponding BIE formulation is defined as*

$$\mathcal{A} = \mathcal{A}_{k,\eta}' := \mathcal{I} + \mathcal{D}_k' - \mathrm{i}\eta\mathcal{S}_k,$$

where $\eta \in \mathbb{R}\setminus\{0\}$ is the coupling parameter, with

$$f = f_{k,\eta} := 2\left(\frac{\partial}{\partial\mathbf{n}} - \mathrm{i}\eta\right)u^{inc}.$$

It follows from [13, Theorem 2.27] that $\mathcal{A}'_{k,\eta}$ is invertible for $k > 0$ and $\eta \neq 0$. In §5.4 we will make use of $\mathcal{A}_{k,\eta}$ (defined in (5.42)), the adjoint of $\mathcal{A}'_{k,\eta}$.

The second formulation (which we state shortly in Definition 1.4) is new for multiple scattering problems and may be considered a generalisation of the star-combined operator of [52] to multiple star-shaped obstacles. This will be discussed in greater detail in Chapter 5. Indeed, for a single star shaped Ω_-, the definition is equivalent to that of [52]. First, some additional terminology is required.

DEFINITION 1.3 (Star- and constellation-shaped)**.** *A bounded open set Ω_i with boundary γ_i is 'star-shaped' if there exists $\mathbf{x}_i^c \in \Omega_i$ and a Lipschitz continuous $g_i : S^1 \to \mathbb{R}$, where $S^1 := \{\hat{\mathbf{x}} \in \mathbb{R}^2 : |\hat{\mathbf{x}}| = 1\}$, such that $g_i(\hat{\mathbf{x}}) > 0$ for all $\hat{\mathbf{x}} \in S^1$ with*

$$\gamma_i = \{g_i(\hat{\mathbf{x}})(\hat{\mathbf{x}} - \mathbf{x}_i^c) : \hat{\mathbf{x}} \in S^1\}.$$

Intuitively, this may be interpreted as the following: Given any $\mathbf{x} \in \Omega_i$, one can draw a straight line from $\mathbf{x}_i^c$ to $\mathbf{x}$, without leaving Ω_i.

We say a domain Ω_- is 'constellation-shaped' if it can be represented as the union of $n_\gamma \in \mathbb{N}$ star-shaped, pairwise disjoint obstacles. Hence we can write $\Omega_- = \cup_{i=1}^{n_\gamma} \Omega_i$, where each component Ω_i is star-shaped.

DEFINITION 1.4 (Star/Constellation combined formulation)**.** *For a star/constellation shaped domain Ω_- with boundary γ, with γ_i the boundary of each star-shaped component (as in Definition 1.3), we define the star/constellation-combined operator $\mathcal{A}_k : L^2(\gamma) \to L^2(\gamma)$ as*

$$\mathcal{A} = \mathcal{A}_k := (\mathbf{Z} \cdot \mathbf{n})\,(\mathcal{I} + \mathcal{D}'_k) + \mathbf{Z} \cdot \nabla_\gamma \mathcal{S}_k - \mathrm{i}\hat{\eta}\mathcal{S}_k$$

where $\mathbf{Z}(\mathbf{x}) = \mathbf{x} - \mathbf{x}_i^c$ (with $\mathbf{x}_i^c$ chosen as in Definition 1.3 above) on γ_i, for $i = 1, \ldots, n_\gamma$. with $\hat{\eta}(\mathbf{x}) := k|\mathbf{Z}(\mathbf{x})| + \mathrm{i}/2$. Choosing $\mathcal{A} = \mathcal{A}_k$, the right-hand side data for the corresponding BIE formulation (1.14) *is*

$$f = f_k := 2\,(\mathbf{Z} \cdot \nabla - \mathrm{i}\hat{\eta})\,u^{inc}, \quad \text{on } \gamma.$$

In Theorem 5.6 we show that the constellation combined operator is invertible on constellation-shaped domains.

There are two key advantages of a BIE formulation such as (1.14) over the BVP (1.4)-(1.6), in particular in solving for $\partial^+_{\mathbf{n}} u$ on $\partial\Omega$ instead of u in Ω_+. Firstly, we have reduced the dimension of our problem by one, which makes for easier implementation of any numerical approximation. Secondly, we are solving for a function defined on the compact $\partial\Omega$, as opposed to the unbounded Ω_+. This removes the requirement of an artificial boundary that arises in domain based methods.

REMARK 1.5 (Formulational conventions)**.** *It is worth noting the equivalent formulations in other BIE literature. Many formulations contain a* $1/2$ *in front of the identity component* $\mathcal{I}$ *of* $\mathcal{A}$*, and do not contain the factor* 2 *in the boundary operator definition, or the function* f*. Here (as in [16]) we include this factor of* 2*, which corresponds to an alternative scaling. Note also that this effect follows through to quantities such as the coercivity constant of the star-combined operator of Definition 1.4. Moreover, the extensive review article [13] uses calligraphic notation for the operators which map from the domain* Ω_+*, with non-calligraphic for the operators mapping from and to the boundary, which is the opposite of the convention adopted in this thesis (also in [35] and [15]).*

On multiple occasions, we will make use of the following definition, which is useful when considering single obstacles in a multiple obstacle configuration.

DEFINITION 1.6 (Operator restriction)**.** *Denote by* $H^{s_1}(\partial\Omega)$ *and* $H^{s_2}(\partial\Omega)$ *two Sobolev spaces on* $\partial\Omega$*. For* $\mathcal{T} : H^{s_1}(\partial\Omega) \to H^{s_2}(\partial\Omega)$ *with* X *and* $Y \subset \partial\Omega$*,* s_1 *and* s_2 *in* $\mathbb{R}$*, we define the operator* $\mathcal{T}_{Y\to X} : H^{s_1}(\partial\Omega) \to H^{s_2}(X)$ *by*

$$\mathcal{T}_{Y\to X}\varphi := (\mathcal{T} \circ \mathcal{Q}_Y\varphi)\,|_X,$$

where the operator $\mathcal{Q}_Y : H^{s_1}(\partial\Omega) \to \{\varphi \in H^{s_3}(\partial\Omega) : \operatorname{supp}\varphi \subset Y\}$*, with* $s_3 \in (-\infty, s_1] \cap (-\infty, 1/2)$*, is defined as*

$$\mathcal{Q}_Y\varphi = \begin{cases} \varphi, & \text{on } Y, \\ 0, & \text{on } \partial\Omega \setminus Y. \end{cases} \tag{1.15}$$

We will also use the same notation for $\mathcal{T} : H^{s_1}(Y) \to H^{s_2}(X)$ *for* $Y \subset \partial\Omega$ *where no confusion can arise, replacing* $\partial\Omega$ *in the definition* (1.15) *with* Y*. Note also that for an operator* $\mathcal{T} : \mathcal{H}^{s_1}(Y) \mapsto \mathcal{H}^{s_2}(X)$*, we write* $\|\mathcal{T}\|_{\mathcal{H}^{s_1}(Y)\to\mathcal{H}^{s_2}(X)}$ *as a convenient shorthand for* $\|\mathcal{T}_{Y\to X}\|_{\mathcal{H}^{s_1}(Y)\to\mathcal{H}^{s_2}(X)}$*, (also) where no confusion can arise.*

The operator $\mathcal{T}_{Y\to X}$ in the above Definition 1.6 may be interpreted as the contribution to the scatterer X from the scatterer Y, in the operator $\mathcal{T}$.

A concept that is useful when relating solutions of the BVP to solutions of the BIE is the following:

DEFINITION 1.7 (Dirichlet-to-Neumann map)**.** *We denote the Dirichlet-to-Neumann map by* $P^+_{DtN} : H^{1/2}(\partial\Omega) \to H^{-1/2}(\partial\Omega)$*. This maps Dirichlet boundary data* $\tau_+ u^s = -u^{inc}|_{\partial\Omega}$ *to the Neumann trace of the scattered field* $\partial^+_{\mathbf{n}} u^s$*. A detailed discussion can be found in [13, §2.7].*

We note that the DtN map is defined for traces of functions which satisfy (1.4) and (1.6), hence is typically applied to $\tau_+ u^s$ and not $\tau_+ u$.

We will consider waves of the following type in several places in this thesis.

DEFINITION 1.8 (Herglotz-type functions)**.** *Suppose that φ is an entire solution of* (1.4) *and satisfies*

$$\lim_{R\to\infty} \int_{B_R} |\varphi|^2 \,\mathrm{d}V < \infty,$$

where B_R is a ball of radius R centred at the origin, then there exists a 'Herglotz kernel' $g_{Herg} \in L^2(0, 2\pi)$ such that, (see for example [17, Theorem 3.30])

$$\varphi(\mathbf{x}) = \int_0^{2\pi} g_{Herg}(\theta) \mathrm{e}^{\mathrm{i}k\mathbf{x}\cdot\mathbf{d}_\theta} \,\mathrm{d}\theta, \quad \textit{for } \mathbf{x} \in \mathbb{R}^2,$$

where $\mathbf{d}_\theta := (\cos\theta, -\sin\theta)$. We say that φ is a 'Herglotz-type' function.

We solve problems of Herglotz-type incidence in §3.1.

1.1.3 The far-field pattern

A quantity of practical interest is the *far-field pattern* of the scattered field u^s (also referred to as the *far-field coefficient*), which describes the distribution of energy of the scattered field u^s (of a solution to (1.4)-(1.6)) far away from Ω_-. We can represent the asymptotic behaviour of the scattered field (as in [35, §6]) by

$$u^s(\mathbf{x}) \sim u^\infty(\theta) \frac{\mathrm{e}^{\mathrm{i}(kr+\pi/4)}}{2\sqrt{2\pi kr}}, \quad \text{as } r = |\mathbf{x}| \to \infty,$$

where the term $u^\infty(\theta)$ denotes the *far-field coefficient* at observation angle $\theta \in [0, 2\pi)$, which we can represent via the Neumann trace of the total field:

$$u^\infty(\theta) := -\int_{\partial\Omega} \mathrm{e}^{-\mathrm{i}k[y_1\cos\theta + y_2\sin\theta]} \frac{\partial u}{\partial \mathbf{n}}(\mathbf{y}) \,\mathrm{d}s(\mathbf{y}), \quad \theta \in [0, 2\pi), \quad \mathbf{y} = (y_1, y_2). \tag{1.16}$$

The following concept for the *far-field map* will also be useful

$$\mathcal{F}_\infty \varphi(\theta) := -\int_{\partial\Omega} \mathrm{e}^{-\mathrm{i}k[y_1\cos\theta + {}_2\sin\theta]} \left[-P_{\mathrm{DtN}}\tau_+ + \partial^+_{\mathbf{n}}\right] \varphi(\mathbf{y}) \,\mathrm{d}s(\mathbf{y}), \tag{1.17}$$

for φ satisfying the conditions of Definition 1.1, chosen such that $\mathcal{F}_\infty(u^{\mathrm{inc}}) = u^\infty$, where u^{inc} is the incident field of problem (1.4)-(1.6).

1.1.4 Boundary Element Methods

We now introduce the standard version of the Boundary Element Method (BEM), which underpins many of the numerical experiments in this thesis. BEM is the approach of approximating the boundary solution $\partial^+_{\mathbf{n}} u$ on $\partial\Omega$.

Given a suitable choice for $\mathcal{A}$ of (1.14), we seek an approximation $v_N \approx \partial^+_{\mathbf{n}} u \in H^s(\partial\Omega)$ for some $s \in \mathbb{R}$, inside a finite dimensional subspace $V_N \subset H^s(\partial\Omega)$. We choose a basis $\Lambda_N = \{\phi_i\}_{i=1}^N$ of V_N. The Galerkin method seeks a solution such that

$$(\mathcal{A}v_N, \varphi)_{H^s(\partial\Omega)} = (f, \varphi)_{H^s(\partial\Omega)}, \quad \text{for all } \varphi \in V_N, \tag{1.18}$$

holds, where $(\cdot, \cdot\cdot)_{H^s(\partial\Omega)}$ denotes the $H^s(\partial\Omega)$ inner product (see Appendix A.2 for a definition). It is therefore an equivalent condition to (1.18) that

$$(\mathcal{A}v_N, \phi_i)_{H^s(\partial\Omega)} = (f, \phi_i)_{H^s(\partial\Omega)}, \quad \text{for all } \phi_i \in \Lambda_N.$$

Alternatively, we may use the collocation method, such that for a chosen set of points $X = \{x_1, \ldots, x_N\} \subset \partial\Omega$, the following holds:

$$\mathcal{A}v_N(x_i) = f(x_i), \quad \text{for all } x_i \in X. \tag{1.19}$$

A comparison of collocation and Galerkin within the context of the high frequency methods of this thesis will be seen in Remark 2.12. There are extensions to both methods, for example Petrov Galerkin methods permit the space of the test functions φ to be different to the solution space V_N, whilst a least squares collocation approach allows for a number of collocation points greater than N. The Nyström method, offers another alternative, although it will not be discussed in this thesis (see for example [3, Chapter 4] for a summary).

Given a BEM approximation to the solution of the problem (1.14) $v_N \approx \partial^+_{\mathbf{n}} u$, we can approximate the solution to the problem (1.4)-(1.6), by inserting the approximation into (1.10) to obtain

$$u \approx u^i - S_k v_N, \quad \text{in } \Omega_+.$$

For BEM, when an approximation space V_N of piecewise polynomials is used, the number of degrees of freedom N must increase at least linearly with k to maintain accuracy. Hybrid Numerical Asymptotic methods overcome this by enriching the approximation space with oscillatory basis functions, as we shall see in §2.2.

1.2 Motivation and aims of this thesis

Before outlining *what* this thesis contains, we aim to explain *why* all of the work was necessary, approximately in chronological order (which is not the order that the chapters are presented).

If the dimension of the approximation space of a numerical method does not need to grow with the wavenumber k to maintain a fixed accuracy, we describe the method as k- or frequency- independent. This term will be used throughout the thesis. Hybrid Numerical Asymptotic (HNA) methods have shown to produce frequency independent results, and are provably no more than $\log^2 k$ dependent. Methods have been developed for a range of Ω_-: convex polygons in [35], non-convex polygons in [15], penetrable obstacles in [31] and the two- and three- dimensional screen in [34] and [33] respectively. All of these methods are for single obstacles, with plane wave incidence.

A key motivation for this thesis is to extend previous methods to multiple obstacles. We now briefly summarise two well-researched multiple scattering approaches here, the *Iterative* and *T-matrix* methods. Iterative multiple scattering methods may be interpreted as solving many successive single scattering problems, in which the scattered field at the previous step becomes the incident field at the current step. Mathematically this requires the problem to be reformulated as a Neumann series, which will diverge if the obstacles are sufficiently close together. A detailed analysis of such methods can be found in [1]. The T-matrix method originally presented in [55] has recently been adapted to a more stable approach in [23], which has been implemented into the software package *Tmatrom*. This extends naturally to multiple obstacles and although certain restrictions are imposed on the separation of the obstacles, these are more concrete than with a standard iterative approach.

The starting point for the thesis was an extension of the HNA ansatz to multiple obstacles, which is outlined in Chapter 4. This method is well suited to certain configurations, and places almost no restriction on the separation of the obstacles. A disadvantage when compared with single scattering HNA methods for polygons was that no coercive formulation was available, and we were forced to seek alternative means when obtaining conditions for well-posedness. This was the entire motivation for Chapter 5, in which stability of the Galerkin method for multiple scattering h-BEM is explored, and a coercive formulation is presented.

A second consequence of the work of Chapter 4 was the motivation to explore alternative approaches to extend HNA to multiple obstacles, in particular using the

well-studied iterative and T-matrix methods of [1] and [23]. Both methods require the solutions of many single scattering problems, with a special type of incident field. This motivated the work of Chapter 3, in which the single scattering HNA method is generalised to solve for a far broader range of incident fields. The beam source incidence may be used in conjunction with iterative methods (although we do not explore this here) whilst the Herglotz-type incidence enables the HNA method to solve for radiating wavefunction incidence, allowing the HNA method to be used in conjunction with the Tmatrom T-matrix method, for multiple scattering problems. The Tmatrom method (discussed in Chapter 7) requires the far-field of $O(k)$ single scattering problems of radiating wavefunction incidence. As the HNA method is designed for high frequency problems, this motivated an attempt to reduce the number of far-field patterns required using the Embedding Formulae of [9], which provide the far-field pattern induced by any Herglotz-type incident field, given the far-field induced by a k-independent number of plane waves. However a naive implementation of these Embedding Formulae can lead to numerical instabilities at certain points. Understanding and overcoming these instabilities was the motivation for Chapter 6.

1.3 Outline of thesis

Chapter 2 introduces the HNA method, inside of a framework more general than has been seen in previous works, with the intention of extending the method to a broader class of problems. HNA methods for polygons have previously utilised an approximation space defined on two overlapping meshes, for which numerical implementation can be quite complicated. Here we present an alternative approximation space on a single mesh, and prove a new best approximation result analogous to the overlapping mesh case. This mesh will also be used in the multiple scattering configuration that follows in Chapter 4. Finally, the Galerkin method for a single convex polygon HNA BEM is explained, and a range of known results are discussed.

In Chapter 3 we use the framework of Chapter 2 to generalise the HNA method from plane waves to new types of incidence, including point source, beam source and Herglotz-type functions (see Figure 1.1). A general formulation for source-type incidence is presented, and the theory for the HNA method is extended further to source-type incidence, permitting less regular incident fields. Numerical results for the point source are presented, demonstrating exponential convergence of the method. Chapter 4 aims to generalise the HNA method to multiple obstacles. Here we extend the HNA ansatz to obtain a representation for the solution on a single side of a convex polygon, when there is one (or many) other obstacle(s) present (see Figure 1.2). The

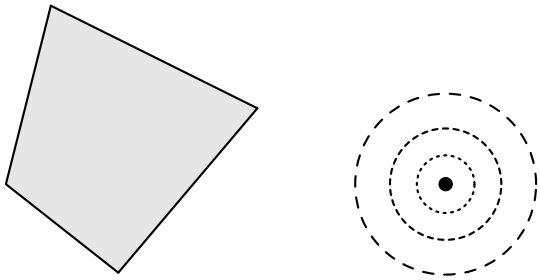

Figure 1.1: Diagram of the type of source-type incidence scattered by a convex polygon, which is considered in Chapter 3. Analysis holds for cases where the source point is at least $1/k$ from the corners of the obstacle.

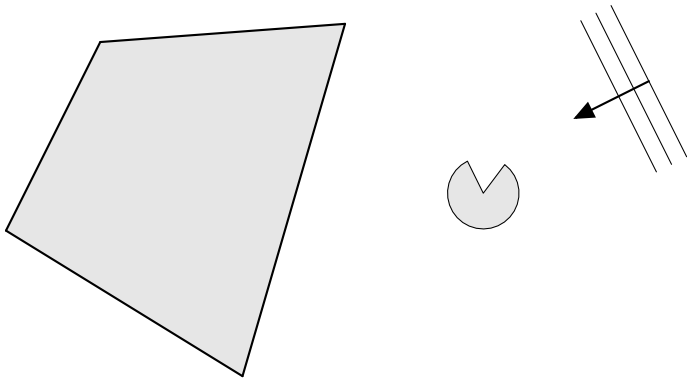

Figure 1.2: Diagram of plane wave scattering by multiple obstacles, which is considered in Chapter 4. Analysis holds for cases where the convex polygon is at least $1/k$ from the other obstacle(s).

other obstacle(s) need not be polygonal for the representation to hold. The method we propose then constructs an oscillatory basis (either on an overlapping or single mesh as described in Chapter 2) on the convex polygon, with a standard *hp*-BEM basis of piecewise polynomials on the other obstacle(s). Under certain assumptions, exponential convergence is predicted, which is subsequently demonstrated by numerical results. This Chapter also introduces a new bound on the solution in the domain for non-trapping polygonal scatterers, which may also be applied to non-convex polygons. An alternative wavenumber-independent method for multiple convex polygons is also presented.

Chapter 5 begins to answer more general questions about well-posedness for multiple scattering BEM. The new theory in this Chapter leads to two key results, both

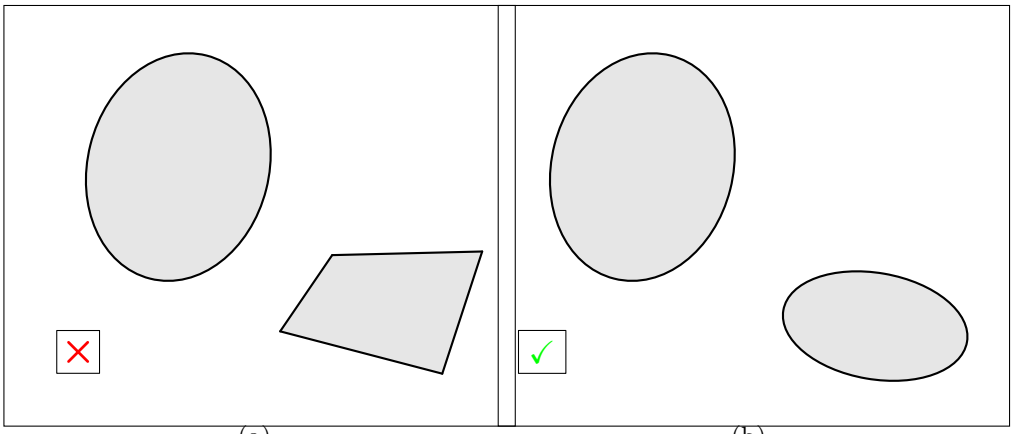

Figure 1.3: Diagram (b) shows a mild-trapping configuration, for which h-BEM Galerkin stability estimates are derived in Chapter 5. Such analysis does not hold for stability estimates of configuration (a), which contains a non-smooth obstacle.

of which provide information about the stability constant and conditions for existence and uniqueness of a solution to the Galerkin equations. Firstly, we show that if the obstacles are star-shaped and sufficiently far apart, then the *constellation combined* operator of Definition 1.4 is coercive. Secondly, we obtain wavenumber-explicit conditions for uniqueness of the Galerkin equations with the standard combined operator (of Definition 1.2), for configurations of multiple smooth obstacles with strictly positive curvature (with no restriction on the separation of the obstacles, see Figure 1.3). Additionally, Chapter 5 contains standard h-BEM approximation on multiple convex polygons, and k-explicit bounds on the inverse of the constellation combined operator.

Chapter 6 explains how instabilities can arise when numerically implementing Embedding Formulae (of [9]) and proposes a novel reformulation which is numerically stable. The formulae considered hold only for rational polygons, for which each external angle is a rational multiple of π (see Figure 1.4). We also provide numerical analysis of this new method, which provides an upper bound on the global error in terms of the key parameters of the problem, and this stability is backed up by numerical results. Additional notes on implementation of such a method, including a new algorithm for fast computation of far-field derivatives, can be found in Appendix C.

Chapter 7 summarises the Tmatrom method of [23], and explains different ways that this may be combined with the HNA method. The type of multiple obstacle configurations which may be solved using Tmatrom are summarised in Figure 1.5.

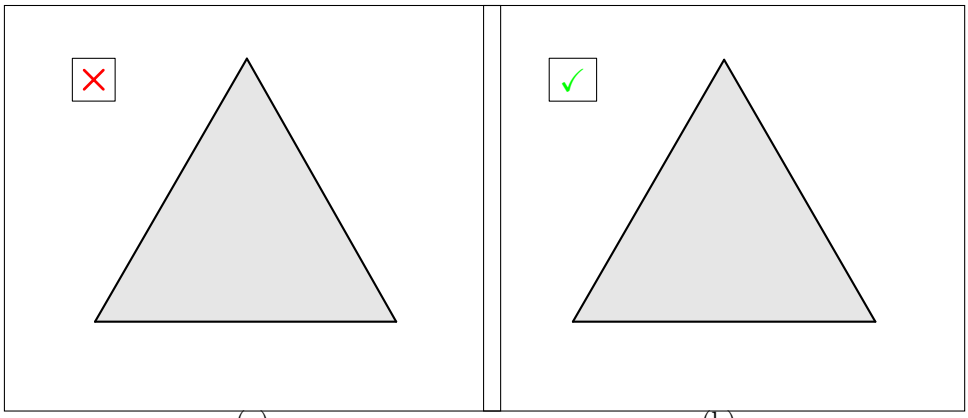

Figure 1.4: Embedding formulae of Chapter 6 hold for rational polygons of type (a), which has external angles $5\pi/3$. Our method cannot be applied to irrational polygons such as (b), which has external angles $\{(5+\epsilon)\pi/3, (5-\epsilon)\pi/3, 5\pi/3\}$, where $\epsilon = 2^{-1/2}/10 \notin \mathbb{Q}$.

The first approach utilises the Herglotz representation of Chapter 3, whilst the second combines this with the Embedding Formulae of Chapter 6. A numerical example combining Tmatrom with the Embedding Formulae of Chapter 6 with MPSpack of [4] is presented.

In Chapter 8, we summarise the work presented in the thesis alongside ideas for future work. The majority of the results of the thesis is partitioned into two distinct methods, which are compared. We also compare the single- and overlapping-mesh approximation spaces.

Appendix A provides a formal definition of the majority of terms used throughout the thesis. This includes a definition of trace spaces, Bessel potential spaces, and k-weighted norms. Fundamental bounds and regularity results for the fundamental solution (1.7) are also presented.

Appendix B summarises quadrature rules used to generate numerical examples throughout the thesis. Much of the information of this section can be obtained elsewhere, although having it all contained in one place may be useful. Issues arising with *near singularities* are discussed, alongside related issues arising when computing singular integrals on long and thin domains. An explanation for the latter of these issues is provided, which to the best knowledge of the author, is new.

Appendix C provides further details for implementation of the Embedding Formulae of Chapter 6. This includes an algorithm for fast computation of derivatives of the far-field pattern, assuming that an approximation to the Neumann trace is available. An alternative algorithm for computing the far-field pattern at unstable

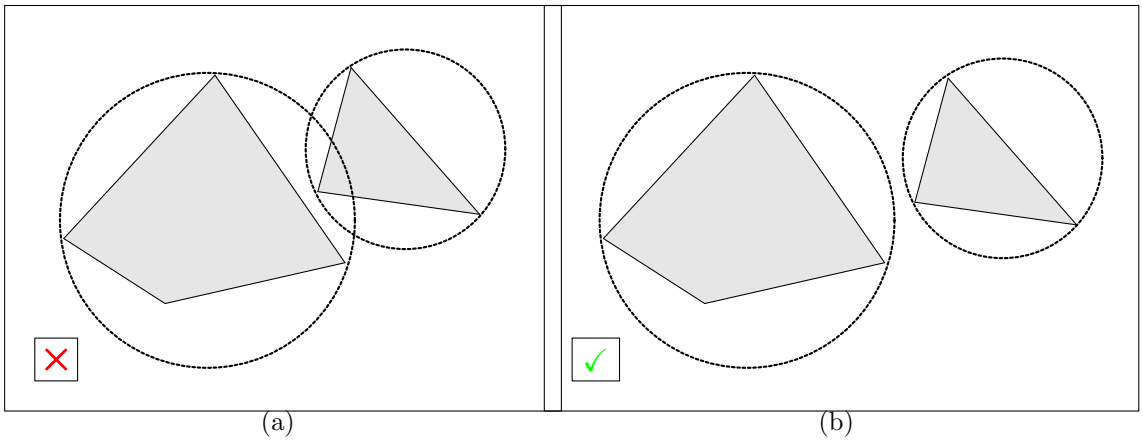

Figure 1.5: T-matrix method of Chapter 7 requires that each obstacle can sit inside of a ball, such that the intersection of any two of these balls is empty. Hence, our method is applicable to Configuration (a), but not configuration (b).

points, which is outside of the scope of Chapter 6, is outlined. These enable the Embedding Formulae to become controllably accurate at any observation point, at any observation angle.

Chapter 2

General HNA framework

In this chapter we summarise much of the single scattering HNA work prior to this thesis, inside a general framework which will also encompass a broader class of problems in Chapters 3 and 4. We also introduce and analyse a new approximation space, as an alternative to what has been used previously.

2.1 Representation on a single side

In related literature, there appears to be no single consistent definition of the term *polygon*, so we shall clarify a definition that is appropriate for what follows.

DEFINITION 2.1 (Polygon)**.** *We say Ω_- is a polygon if it is a bounded Lipschitz open set with a boundary $\partial\Omega$ consisting only of straight line segments, such that the endpoint of every segment is connected to one other endpoint of another segment.*

We note that Definition 2.1 permits multiple disconnected shapes, whereas other conventions in the literature do not. Many results that follow hold for a subclass of polygons, which we define now (as in e.g., [50, Definition 1.1])

DEFINITION 2.2 (Non-trapping polygon)**.** *We say that a polygon Ω_- (in the sense of Definition 2.1) is non-trapping if:*

(i) No three vertices of $\partial\Omega$ are co-linear, i.e. they lie in a straight line.

(ii) For a ball B_R with radius $R > 0$ sufficiently large that $\Omega_- \subset B_R$, there exists a $T(R) < \infty$ such that all billiard trajectories that start inside of $B_R \setminus \Omega_-$ that start at time zero $T = 0$ and miss the vertices of $\partial\Omega$ will leave B_R by time $T(R)$.

In this chapter we assume that scattering obstacle Ω_- of the general problem statement of §1.1 is a convex polygon, which we denote Ω_Γ with boundary $\partial\Omega = \Gamma$. We

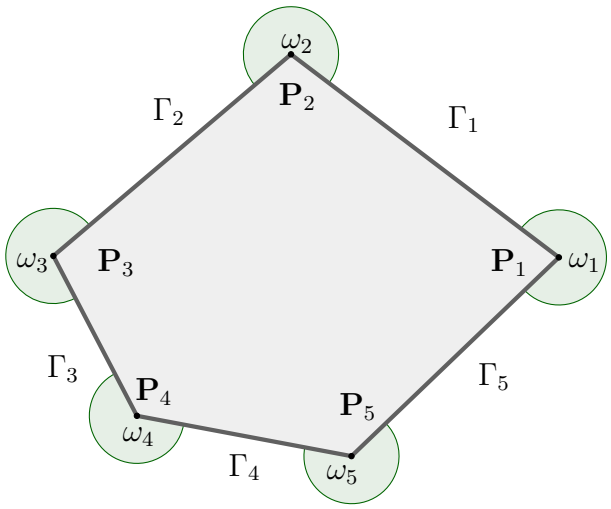

Figure 2.1: Example of a five-sided polygon ($n_\Gamma = 5$) with boundary Γ.

now define a range of parameters related to the geometry of Ω_Γ, on which subsequent bounds will depend. The parameters in these definitions will hold for any convex polygon in this thesis.

DEFINITION 2.3 (Parameters of a convex polygon)**.** *For an n_Γ-sided polygon (in the sense of Definition 2.1) with boundary Γ, we denote by $\mathbf{P}_j$ and $\mathbf{P}_{j+1}$ the nodes at the endpoints of each side Γ_j, for $j = 1, \ldots, n_\Gamma$ setting $\mathbf{P}_{n_\Gamma+1} := \mathbf{P}_1$. Conventionally, the vertices are indexed anti-clockwise. We denote by $L_j := |\mathbf{P}_{j+1} - \mathbf{P}_j|$ the length of Γ_j, $\tilde{L}_j := \sum_{\ell=1}^{j} L_\ell$, and $L_\Gamma := \tilde{L}_{n_\Gamma}$. The jth exterior angle is denoted ω_j, hence for a convex polygon we have $\omega_j \in (\pi, 2\pi)$. Finally we choose the constant $c_* > 0$ such that $kL_j \geq c_*$ for $j = 1, \ldots, n_\Gamma$ (e.g. $c_* = \min_j\{kL_j\}$), and $L_* := \max_j\{L_j\}$*

Figure 2.1 depicts a five-sided polygon with certain parameters of Definition 2.3. We parametrise Γ by

$$\mathbf{x}_\Gamma(s) = \mathbf{P}_j + \frac{s - \widetilde{L}_{j-1}}{L_j}(\mathbf{P}_{j+1} - \mathbf{P}_j), \quad s \in [\widetilde{L}_{j-1}, \widetilde{L}_j), \quad j = 1, \ldots, n_\Gamma \tag{2.1}$$

and $\Gamma_j^- \cup \Gamma_j \cup \Gamma_j^+$, which is the straight line containing Γ_j, extended infinitely in both directions (defined in more detail in Chapter 3), by

$$\mathbf{y}_j(s) = \mathbf{P}_j + \frac{s - \widetilde{L}_{j-1}}{L_j}(\mathbf{P}_{j+1} - \mathbf{P}_j), \quad s \in \mathbb{R}, \quad j = 1, \ldots, n_\Gamma.$$

Now we consider the scattering problem (1.4)-(1.6), with solution u, for the case where the scattering object Ω_- is a convex polygon. In such a case, there are two

key physical components of the scattered field u^s. Firstly, the waves *reflected* by the edges Γ_j, for $j = 1, \ldots, n_\Gamma$. As we will see, these can be written explicitly without the need for numerical approximation. The second type of wave which contributes to the scattered field are the *diffracted* waves emanating from the corners $\mathbf{P}_j$, for $j = 1, \ldots, n_\Gamma$. Recall that with a BIE formulation (1.14), we are instead solving for $\partial^+_{\mathbf{n}} u$. In such a case, the diffracted waves move in just two directions along each side Γ_j, for $j = 1, \ldots, n_\Gamma$, making this formulation an ideal approach for approximating the diffracted waves. Moreover, it is possible to separate explicitly the oscillatory behaviour of these two diffracted terms; the remaining (unknown) term which must be approximated numerically is non-oscillatory [16, Corollary 3.4]. The full mathematical derivation depends on the incident wave u^i (see [16, §3] for plane waves, see Chapter 3 of this thesis for more general incidence), however the HNA ansatz for a single impenetrable convex polygon may be written as:

$$\frac{\partial u}{\partial \mathbf{n}}(\mathbf{x}_\Gamma(s)) = \overbrace{\Psi(\mathbf{x}_\Gamma(s))}^{\text{Reflected terms}} + \overbrace{\underbrace{v_j^+(\mathbf{x}_\Gamma(s-\tilde{L}_{j-1}))}_{\text{First unknown envelope}}\, \mathrm{e}^{\mathrm{i}ks} + \underbrace{v_j^-(\mathbf{x}_\Gamma(\tilde{L}_j - s))}_{\text{Second unknown envelope}}\, \mathrm{e}^{-\mathrm{i}ks}}^{\text{Diffracted terms}}, \quad (2.2)$$

where $s \in [\tilde{L}_{j-1}, \tilde{L}_j]$, for $j = 1, \ldots, n_\Gamma$, with $\mu(z) := \mathrm{e}^{-\mathrm{i}z} H_1^{(1)}(z)/z$, the (unknown) amplitudes of the diffracted waves are represented by

$$\begin{aligned} v_j^+(s) &:= \frac{\mathrm{i}k^2}{2} \int_0^\infty \mu\big(k(s+t)\big) \mathrm{e}^{\mathrm{i}k(t-\widetilde{L}_{j-1})} u\big(\mathbf{y}_j(\widetilde{L}_{j-1} - t)\big)\, \mathrm{d}t, \qquad s \in [0, L_j], \\ v_j^-(s) &:= \frac{\mathrm{i}k^2}{2} \int_0^\infty \mu\big(k(s+t)\big) \mathrm{e}^{\mathrm{i}k(\widetilde{L}_j+t)} u\big(\mathbf{y}_j(\widetilde{L}_j + t)\big)\, \mathrm{d}t, \qquad s \in [0, L_j], \end{aligned} \quad (2.3)$$

whilst Ψ represents the leading order asymptotics corresponding physically to the reflected terms, hence we shall see later that Ψ is zero on the sides which are not illuminated by the incident wave. The term Ψ is often referred to as the *Physical Optics Approximation* for single scatterers, an approximation which ignores diffracted waves. Intuitively, this approximation may be interpreted as twice the normal derivative on the sides that can *see* the incident waves. At sufficiently high frequencies, this may be a suitable approximation, however it is not controllably accurate. The Hybrid Numerical Asymptotic method improves on the Physical Optics Approximation by approximating the diffracted waves numerically. In previous methods such as [35], Ψ can be written explicitly in terms of u^{inc}, although an approximate representation may be sufficient. This is the case for the penetrable obstacles of [31], in which a beam tracing algorithm is used to approximate reflections inside Ω_Γ. This takes the form of an infinite series, which must be truncated, and is thus only approximate (although in

theory, controllably accurate). However, the representation for the diffracted waves for penetrable Ω_Γ is more complex, and does not fit within the framework (2.2). Similarly, the ansatz for non-convex obstacles of [15] contains an additional term, and does not fit within (2.2).

It is the envelopes $v_j^\pm$ that are approximated numerically, indeed our *hp* approximation will converge exponentially (from [35, Theorem 5.2]) if the following assumption holds.

ASSUMPTION 2.4. *There exists a term $M(u)$ such that:*

(i) The functions $v_j^\pm$, for $j = 1, \ldots, n_\Gamma$, are analytic in the right half-plane $\mathrm{Re}[s] > 0$, where they satisfy the bounds

$$|v_j^\pm(s)| \leq \begin{cases} C_j^\pm M(u) k |ks|^{-\delta_j^\pm}, & 0 < |s| \leq 1/k, \\ C_j^\pm M(u) k |ks|^{-1/2}, & |s| > 1/k, \end{cases}$$

where $\delta_j^+, \delta_j^- \in (0, 1/2)$ are given by $\delta_j^+ := 1 - \pi/\omega_j$ and $\delta_j^- := 1 - \pi/\omega_{j+1}$, C_j^+ depends only on c_* and ω_j, C_j^- depends only on c_* and ω_{j+1}

(ii) $M(u)$ depends on the size of the solution u to (1.4) − (1.6) grows at most algebraically with k, i.e. there exists a $\beta \geq 0$ such that

$$M(u) \lesssim k^\beta, \quad \text{for all } k \geq 0, \tag{2.4}$$

where $a \lesssim b$ means that $a \leq cb$, where the constant c depends only on the geometry of Ω_-.

To summarise, in order to design HNA methods we must be able to do the following:

(i) Represent leading order behaviour accurately via Ψ.

(ii) Show that Assumption 2.4 holds.

Prior to this thesis, HNA methods have only been designed for problems of plane wave incidence, which are defined as:

$$u^{\mathrm{inc}}(\mathbf{x}) = u^{\mathrm{inc}}_{PW}(\mathbf{x}; \alpha) := \mathrm{e}^{\mathrm{i}k\mathbf{d}_\alpha \cdot \mathbf{x}}, \quad \text{where } \mathbf{d}_\alpha := (\cos\alpha, -\sin\alpha). \tag{2.5}$$

Unlike previous HNA papers (for e.g. [16, §2]), we choose α to be the angle that the plane wave is emanating from, measured against the x_1-axis. This is to be consistent with previous literature on Embedding Formulae, which we explore in Chapter 6.

REMARK 2.5 (The constant $M(u)$ for plane waves)**.** *For problems of plane wave incidence (as in* (2.5)*) scattering by a single convex polygon Ω_-, Assumption 2.4 has been shown to hold with*

$$M(u) = M_\infty(u) := \sup_{\mathbf{x}\in\Omega_+} |u(\mathbf{x})|,$$

[35, Theorem 3.2]. Numerical experiments of [16] and [15] suggest that for problems of plane wave incidence with convex Ω_-, we have $M_\infty(u) \sim 1$, although the strongest theoretical bound is currently $M_\infty(u) \lesssim k^{1/2}\log^{1/2} k$, for $k \geq k_0$ where k_0 is a constant independent of k, (see [35, Theorem 4.3] for star shaped polygons, this is generalised to non-trapping polygons in Corollary 4.7 of this thesis). In §3.2.1 we will consider cases for which Assumption 2.4(i) holds, but with $M_\infty(u)$ unbounded, hence requiring a different choice of $M(u)$.

The framework we present does not include the non-convex work of [15]; this requires an extra term in the ansatz which captures the oscillatory nature of the waves diffracted by the corners, as they are reflected by the non-convex sides.

2.2 Approximation space

We now design an approximation space to represent efficiently the diffracted waves emanating from the corners of the convex polygon Γ,

$$v_\Gamma(s) := \frac{1}{k}\left(v_j^+(s-\widetilde{L}_{j-1})\mathrm{e}^{\mathrm{i}ks} + v_j^-(\widetilde{L}_j - s)\mathrm{e}^{-\mathrm{i}ks}\right), \quad s \in \left[\widetilde{L}_{j-1}, \widetilde{L}_j\right],\ j = 1,\ldots,N_\Gamma, \tag{2.6}$$

a term containing all of the unknown components of (2.2) (recall that the reflected waves can be represented explicitly). The scaling by $1/k$ ensures that v_Γ is dimensionless. Instead of approximating v_Γ by piecewise polynomials, we use our knowledge of the oscillations $\mathrm{e}^{\pm\mathrm{i}ks}$ and approximate both $v_j^+(s-\widetilde{L}_{j-1})$ and $v_j^-(\widetilde{L}_{j-1}-s)$ by piecewise polynomials. Both of these are singular as s tends to zero, thus the polynomial space requires a graded mesh to ensure a strong approximation. In this section we present two such approximation spaces, both graded and enriched with oscillatory basis elements. First we present the *overlapping-mesh* space, which has been used in all previous HNA methods, included here for completeness and for an easy comparison against the new mesh. This space consists of two overlapping meshes, graded towards opposite corners. Secondly we propose a new alternative approach, the *single-mesh* space; motivated by potentially easier implementation.

We shall see in Chapter 4 that the approximation spaces we present here are not only appropriate for a new class of incident fields, but may also be used on a convex polygon inside a multiple scattering configuration.

The overlapping-mesh hybrid space

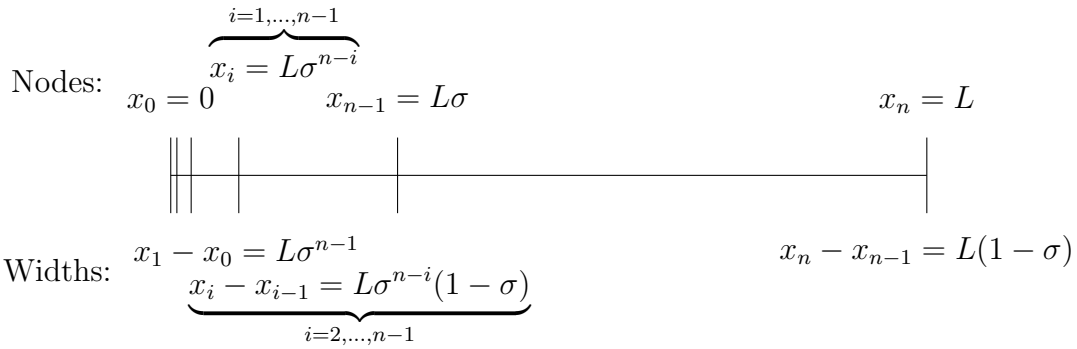

Figure 2.2: The nodes and widths of the mesh as described in Definition 2.6

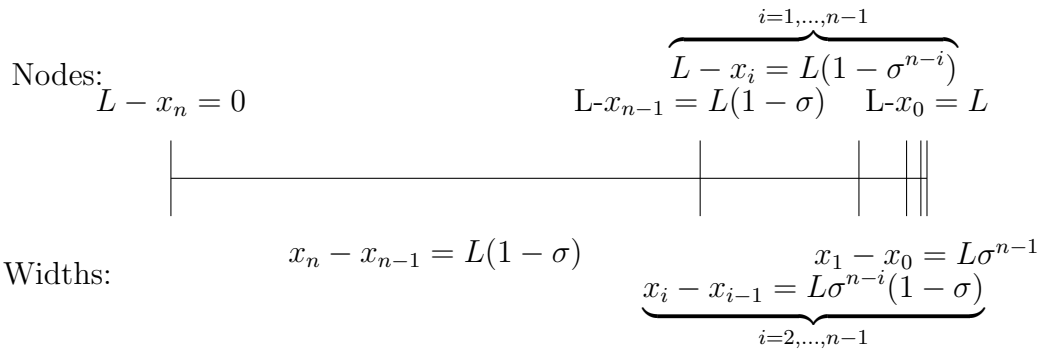

Figure 2.3: The nodes and widths of the mesh as described in Definition 2.6 subtracted from L, to construct a mesh graded in the opposite direction.

DEFINITION 2.6. *Given $L > 0$, $n \in \mathbb{N}$ and a grading parameter $\sigma \in (0,1)$, we denote by $\mathcal{M}_n^<(0,L) = \{x_0, \ldots, x_n\}$ the geometrically graded mesh on $[0,L]$ with n layers graded towards 0, whose $n+1$ meshpoints x_i are defined by*

$$x_0 := 0, \quad x_i := L\sigma^{n-i}, \quad \text{for } i = 1, \ldots, n.$$

For a vector $\mathbf{p} = (p_1, \ldots, p_n) \in (\mathbb{N}_0)^n$ we denote by $\mathcal{P}_{\mathbf{p},n}^<$ the space of piecewise polynomials on $\mathcal{M}_n^<(0,L)$ with degree vector $\mathbf{p}$, i.e.

$$\mathcal{P}_{\mathbf{p},n}^<(0,L) := \Big\{ \rho \in L^2(0,L) : \rho|_{(x_{i-1},x_i)}$$

is a polynomial of degree at most p_i for $i = 1, \ldots, n$ $\Big\}$.

Where $p_i = p$ for $i = 1, \ldots, n$, we write $\mathcal{P}^<_{p,n}$ for $\mathcal{P}^<_{\mathbf{p},n}$.

The space $\mathcal{P}^<_{\mathbf{p},n}(0, L_j)$ is designed to approximate v_j^+, enrichment with oscillatory functions provides a space suitable to approximate $v_j^+ \mathrm{e}^{\pm \mathrm{i}ks}$. We first define two spaces for each side Γ_j, $j = 1, \ldots, n_\Gamma$, using $n_j \in \mathbb{N}$ to determine the degree of mesh grading and the vectors $\mathbf{p}_j$ to determine the polynomial degree on each mesh element:

$$\overline{\overline{V}}_j^+ := \Big\{ v \in L^2(0, L_\Gamma) : v|_{(\widetilde{L}_{j-1}, \widetilde{L}_j)}(s) = \widetilde{\rho}(s - \widetilde{L}_{j-1}) \mathrm{e}^{\mathrm{i}ks}, \quad \widetilde{\rho} \in \mathcal{P}^<_{\mathbf{p}_j, n_j}(0, L_j), \\ \rho|_{(0,L_\Gamma)\setminus(\widetilde{L}_{j-1}, \widetilde{L}_j)} = 0 \Big\},$$

$$\overline{\overline{V}}_j^- := \Big\{ v \in L^2(0, L_\Gamma) : v|_{(\widetilde{L}_{j-1}, \widetilde{L}_j)}(s) = \widetilde{\rho}(\widetilde{L}_j - s) \mathrm{e}^{-\mathrm{i}ks}, \quad \widetilde{\rho} \in \mathcal{P}^<_{\mathbf{p}_j, n_j}(0, L_j), \\ \rho|_{(0,L_\Gamma)\setminus(\widetilde{L}_{j-1}, \widetilde{L}_j)} = 0 \Big\}.$$

In the space $\overline{\overline{V}}_j^-$, the argument of $\tilde{\rho}$ decreases as s increases. This is related to the mesh depicted in Figure 2.3. The overlapping-mesh approximation space can now be defined as

$$\overline{\overline{V}}_N^{\mathrm{HNA}}(\Gamma) := \mathrm{span} \left\{ \bigcup_{j=1}^{n_\Gamma} (\overline{\overline{V}}_j^+ \cup \overline{\overline{V}}_j^-) \right\},$$

where N refers to the number of degrees of freedom in the space $\overline{\overline{V}}_N^{\mathrm{HNA}}(\Gamma)$, and depends on parameters $\mathbf{p}_j$ and n_j for $j = 1, \ldots, n_\Gamma$.

The single-mesh hybrid space

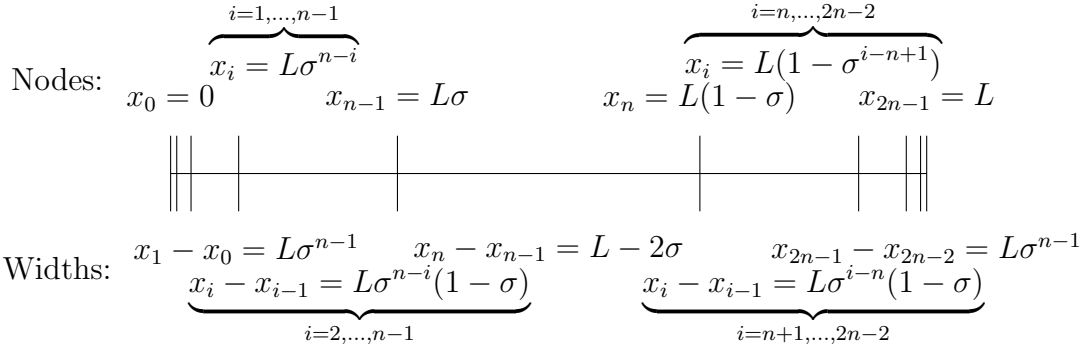

DEFINITION 2.7. *Given $L > 0$, $n \in \mathbb{N}$ and a grading parameter $\sigma \in (0, 1/2)$, we denote by $\mathcal{M}_n(0, L) = \{x_0, \ldots, x_{2n-1}\}$ the symmetric geometrically graded mesh on*

$[0, L]$ *with* n *layers in each direction, whose* $2n$ *meshpoints* x_i *are defined by*

$$\begin{array}{lll} x_0 := 0, & x_i := L\sigma^{n-i}, & \text{for } i = 1, \ldots, n-1, \\ x_i := L(1-\sigma^i), & \text{for } i = n, \ldots, 2n-2, & x_{2n-1} := L. \end{array}$$

For a vector $\mathbf{p} = (p_1, \ldots, p_n) \in (\mathbb{N}_0)^n$ *we denote by* $\mathcal{P}_{\mathbf{p},n}$ *the space of piecewise polynomials on* $\mathcal{M}_n(0, L)$ *with degree vector* $\mathbf{p}$*, i.e.*

$$\mathcal{P}_{\mathbf{p},n}(0, L) := \left\{ \begin{array}{c} \rho \in L^2(0, L) : \rho|_{(x_{i-1}, x_i)} \text{ and } \rho|_{(x_{2n-1-i}, x_{2n-i})} \\ \text{are polynomials of degree at most } p_i \text{ for } i = 1, \ldots, n \end{array} \right\}.$$

In the case where $p_i = p$ *for* $i = 1, \ldots, n$*, we write* $\mathcal{P}_{p,n}$ *for* $\mathcal{P}_{\mathbf{p},n}$*.*

We first define two spaces for each side Γ_j, $j = 1, \ldots, n_\Gamma$, using $n_j \in \mathbb{N}$ to determine the degree of mesh grading and the vectors $\mathbf{p}_j$ to determine the polynomial degree on each mesh element:

$$\begin{aligned} \overline{V}_j^+ := \Big\{ & v \in L^2(0, L_\Gamma) : v|_{(\widetilde{L}_{j-1}, \widetilde{L}_j)}(s) = \widetilde{\rho}(s - \widetilde{L}_{j-1}) \mathrm{e}^{\mathrm{i}ks}, \widetilde{\rho} \in \mathcal{P}_{\mathbf{p}_j, n_j}(0, L_j), \\ & \rho|_{(0,L_\Gamma)\setminus(\widetilde{L}_{j-1}, \widetilde{L}_j)} = 0 \Big\}, \end{aligned}$$

$$\begin{aligned} \overline{V}_j^- := \Big\{ & v \in L^2(0, L_\Gamma) : v|_{(\widetilde{L}_{j-1}, \widetilde{L}_j)}(s) = \widetilde{\rho}(\widetilde{L}_j - s) \mathrm{e}^{-\mathrm{i}ks}, \widetilde{\rho} \in \mathcal{P}_{\mathbf{p}_j, n_j}(0, L_j), \\ & \rho|_{(0,L_\Gamma)\setminus(\widetilde{L}_{j-1}, \widetilde{L}_j)} = 0 \Big\}. \end{aligned}$$

As is explained in Remark 2.8, to avoid ill conditioning of the discrete system we must remove certain basis functions.

$$\widetilde{V}_j := \operatorname{span}\left(\left\{ v \in V_j^- : v|_{[\widetilde{L}_{j-1}, \widetilde{L}_{j-1} + x_{\tilde{n}_j}]} = 0 \right\} \cup \left\{ v \in V_j^+ : v|_{[\widetilde{L}_j - x_{\tilde{n}_j}, \widetilde{L}_j]} = 0 \right\} \right)$$

where

$$x_{\tilde{n}_j} := \max \left\{ x_i \in \mathcal{M}_{n_j}(0, L_j) \text{ such that } x_i \leq \alpha_j \frac{2\pi}{k} \right\} \tag{2.7}$$

and α_j is a parameter chosen such that $0 < \alpha_j < L_j k/(4\pi)$, bounded independently of k and and $\mathbf{p}_j$, used to fine tune the space. Put simply, there are two basis functions on elements sufficiently far from the corners, and one basis element on elements close to the corners. The parameter α_j determines the threshold referring to precisely what is meant by *sufficiently close*. Hence the single-mesh approximation space is defined as

$$\overline{V}_N^{\mathrm{HNA}}(\Gamma) := \operatorname{span} \bigcup_{j=1}^{n_\Gamma} \tilde{V}_j.$$

REMARK 2.8 (Why elements of $\overline{V}_j^{\pm}$ are removed)**.** *Since the mesh is strongly graded to approximate the singularities of $v_j^{\pm}$, some of its elements are much smaller than the wavelength of the problem, thus $\mathrm{e}^{\pm \mathrm{i}ks}$ are roughly constant on them and the functions of $\overline{V}_j^{+}$ supported on these elements are numerically indistinguishable from those on $\overline{V}_j^{-}$, leading to an ill-conditioned discrete system of Galerkin methods set in $\overline{V}_j^{+} \cup \overline{V}_j^{-}$. To avoid this, in these elements we maintain only one of these two contributions. Intuitively, α_j can be thought of as the value such that in all elements with distance from one of the segment endpoints smaller than α_j, the space $\widetilde{V}_j$ supports polynomials multiplied with only one of the waves $\mathrm{e}^{\pm \mathrm{i}ks}$. As the parameter α_j increases, fewer degrees of freedom are used and the conditioning of the discrete system is improved, but the accuracy of the method is reduced, hence care must be taken when selecting α_j.*

As has become standard for HNA BEM (see e.g. [35]), in the numerical experiments of §3.2.3 and §4.5 we choose a grading parameter of $\sigma = 0.15$, which is a prudent over-refinement of the value suggested by [32, Theorem 3.2]. We note that our definition of each approximation space results in symmetric grading and distribution of polynomial degrees. For the more complex asymmetric definition on the overlapping mesh, see for example [35, §5].

We shall shortly present a new result, a best approximation result analogous to the overlapping mesh case of [35, Theorem 5.4], adapted for the single mesh. First, we motivate why a modification to the overlapping mesh theorem is required, outlining the differences between the two spaces. The basis functions on the graded regions of the mesh, which are designed to handle the singularities of $v_j^{\pm}$, will also be used to approximate a smooth wave propagating in the opposite direction, for which the grading is not necessary. The elements of the space $\widetilde{V}_j$ supported on the larger central $2(n_j - \widetilde{n}_j) - 1$ elements $[\widetilde{L}_{j-1} + x_{\widetilde{n}_j}, \widetilde{L}_{j-1} + x_{\widetilde{n}_j+1}], \ldots, [\widetilde{L}_j - x_{\widetilde{n}_j+1}, \widetilde{L}_{j-1} + x_{\widetilde{n}_j}]$ coincide with those of $\mathrm{span}(\overline{V}_j^{+} \cup \overline{V}_j^{-})$, thus the HNA approximation results of [35, §5] apply. However, on the first and final $\widetilde{n}_j$ mesh elements of $\mathcal{M}_n(0, L_j)$, the elements of the discrete space contain only one of the two oscillating factors $\mathrm{e}^{\pm \mathrm{i}ks}$. For example, in the first $\widetilde{n}_j$ smaller elements $[\widetilde{L}_{j-1}, \widetilde{L}_{j-1} + x_1], \ldots, [\widetilde{L}_{j-1} + x_{\widetilde{n}_j-1}, \widetilde{L}_{j-1} + x_{\widetilde{n}_j}]$, the basis functions of the form $\mathrm{e}^{\mathrm{i}ks}\rho(s - \widetilde{L}_{j-1})$ for a polynomial ρ, need to approximate both the singular function $v_j^{+}(s - \widetilde{L}_{j-1})\mathrm{e}^{\mathrm{i}ks}$. Here the approximation theory of [35] applies again, and the smooth function $v_j^{-}(\widetilde{L}_j - s)\mathrm{e}^{-\mathrm{i}ks}$, for which we prove approximation bounds in the next theorem. These correspond to the approximation of $v_j^{-}(\widetilde{L}_j - s)\mathrm{e}^{-2\mathrm{i}ks}$ away from its singularity with piecewise polynomials. In particular we want to control the

dependence of the error on the wavenumber k. In the remaining $\widetilde{n}_j$ elements closest to $\widetilde{L}_j$ the same reasoning applies with basis functions of the form $\mathrm{e}^{-\mathrm{i}ks}\rho(\widetilde{L}_j - s)$.

For the overlapping-mesh space, best approximation estimates were derived in [35, Theorem 5.4] (summarised shortly in Corollary 2.11). The single-mesh space is a relatively new approach to HNA methods, and prior to this thesis no analogous result had been derived. The following theorem provides such estimates, and illustrates the dependence of the best approximation on the parameter α_j.

THEOREM 2.9. *Suppose that the polynomial degree p_j is constant across the elements of the side Γ_j, that Assumption 2.4 holds, $n_j \geq c_j p_j$ for $c_j > 0$ of Definition 2.3, and $x_{\tilde{n}_j} \leq L_j k/(2+\epsilon_j)\pi$ for some $0 < \epsilon_j \leq 1$. Then we have the following bound, concerning the best approximation of the single-mesh space, on a single side Γ_j of a convex polygon:*

$$\inf_{w_N \in \widetilde{V}_j} \left\| v_j^{\pm} \mathrm{e}^{\pm \mathrm{i}k\cdot} - w_N \right\|_{L^2(0,L_j)} \tag{2.8}$$

$$\leq C_j M(u) \sqrt{k} \Big((kL_j)^{1/2-\delta_j^{\pm}} + \log^{1/2}(2+kL_j) + \sqrt{k}(kI_j)^{-\delta_j^{\pm}} \Big) \mathrm{e}^{-p_j \tau_j^{\pm}} \tag{2.9}$$

where

$$\tau_j^{\pm} := \min \left\{ c_j^{\pm} |\log\sigma| (1/2 - \delta_j^{\pm}),\ \log \frac{1+\sigma^{1/2}(2-\sigma)^{1/2}}{1-\sigma},\ \log\left(1+\epsilon_j+\epsilon_j^{1/2}(2+\epsilon_j)^{1/2}\right) \right\},$$

$I_j := L_j - x_{\tilde{n}_j}(1+\epsilon_j/2) > 0$, *and*

$$C_j := \max \left\{ C_4, \max_{\pm}\{C_j^{\pm}\} \sqrt{x_{\tilde{n}_j}} \frac{2}{\epsilon_j + \epsilon_j^{1/2}(2+\epsilon_j)^{1/2}} \mathrm{e}^{2\alpha_j \pi \sqrt{\epsilon_j(\epsilon_j+2)}} \right\},$$

with C_4 as in [35, Theorem 5.5].

Proof. We give only the details for the case of v_j^+, that of v_j^- follows by similar arguments. From the definition of $\widetilde{V}_j$ and $\overline{V}_j^{\pm}$ we have

$$\inf_{w_N \in \widetilde{V}_j} \left\| v_j^+ \mathrm{e}^{\mathrm{i}k\cdot} - w_N \right\|^2_{L^2(0,L_j)} \leq$$
$$\inf_{w_N \in \overline{V}_j^+} \left\| v_j^+ \mathrm{e}^{\mathrm{i}k\cdot} - w_N \right\|^2_{L^2(0,L_j - x_{\tilde{n}_j})} + \inf_{w_N \in \overline{V}_j^-} \left\| v_j^+ \mathrm{e}^{\mathrm{i}k\cdot} - w_N \right\|^2_{L^2(L_j - x_{\tilde{n}_j}, L_j)}.$$

By Assumption 2.4, $g(z) = v_k^+(z/k)$ satisfies the estimates required in [35, Theorem 5.2], and using $|\mathrm{e}^{\mathrm{i}ks}| = 1$ the first term on the right-hand side is hence bounded as in [35, Theorem 5.4], leading to the first two terms in the brackets in (2.8). Focusing on the second term, we multiply by $\mathrm{e}^{\mathrm{i}k\cdot}$ and scale by a factor k:

$$\inf_{w_N \in \overline{V}_j^-} \left\| v_j^+ \mathrm{e}^{\mathrm{i}k\cdot} - w_N \right\|_{L^2(L_j - x_{\tilde{n}_j}, L_j)} = \inf_{P \in \mathcal{P}_{p_j,n}(0,L_j)} \left\| v_j^+ \mathrm{e}^{2\mathrm{i}k\cdot} - P \right\|_{L^2(L_j - x_{\tilde{n}_j}, L_j)}$$

$$= \frac{1}{\sqrt{k}} \inf_{P\in\mathcal{P}_{p_j,n}(0,kL_j)} \left\|v_j^+(\cdot/k)\mathrm{e}^{2\mathrm{i}\cdot} - P\right\|_{L^2(k(L_j-x_{\widetilde{n}_j}),kL_j)}$$
$$\leq \sqrt{x_{\widetilde{n}_j}} \inf_{P\in\mathcal{P}_{p_j,n}(0,kL_j)} \left\|v_j^+(\cdot/k)\mathrm{e}^{2\mathrm{i}\cdot} - P\right\|_{L^\infty(k(L_j-x_{\widetilde{n}_j}),kL_j)}.$$

To bound this term we define the open ellipse by $\mathcal{E} := \{w \in \mathbb{C} : |w - k(L_j - x_{\widetilde{n}_j})| + |w - kL_j| < R\}$ with $R := (1+\epsilon_j)kx_{\widetilde{n}_j}$ and appeal to [35, Lemma A.2] to obtain

$$\inf_{w_N\in\overline{V}_j^-} \left\|v_j^+\mathrm{e}^{\mathrm{i}k\cdot} - w_N\right\|_{L^2(L_j-x_{\widetilde{n}_j},L_j)} \leq \sqrt{x_{\widetilde{n}_j}}\frac{2}{\rho-1}\rho^{-p_j}\left\|v_j^+(\cdot/k)\mathrm{e}^{2\mathrm{i}\cdot}\right\|_{L^\infty(\mathcal{E})}$$
$$\leq \sqrt{x_{\widetilde{n}_j}}\frac{2}{\rho-1}\rho^{-p_j}\left\|\mathrm{e}^{2\mathrm{i}\cdot}\right\|_{L^\infty(\mathcal{E})}\left\|v_j^+(\cdot/k)\right\|_{L^\infty(\mathcal{E})},$$

where $\rho := (R + \sqrt{R^2 - (kx_{\widetilde{n}_j})^2})/kx_{\widetilde{n}_j} = 1 + \epsilon_j + \epsilon_j^{1/2}(2+\epsilon_j)^{1/2}$. Noting that $\sup\{|\operatorname{Im}(w)| : w \in \mathcal{E}\} = \frac{1}{2}\sqrt{R^2 - x_{\widetilde{n}_j}^2} = \frac{1}{2}kx_{\widetilde{n}_j}\sqrt{\epsilon_j(\epsilon_j+2)} \leq \alpha_j\pi\sqrt{\epsilon_j(\epsilon_j+2)}$ and $\inf\{\operatorname{Re}(w) : w \in \mathcal{E}\} = kL_j - kx_{\widetilde{n}_j}(1+\epsilon_j/2)$, it follows from Assumption 2.4 that

$$\inf_{w_N\in V_j^-} \left\|v_j^+\mathrm{e}^{\mathrm{i}k\cdot} - w_N\right\|_{L^2(L_j-x_{\widetilde{n}_j},L_j)}$$
$$\leq \sqrt{x_{\widetilde{n}_j}}\frac{2}{\rho-1}\rho^{-p_j}\mathrm{e}^{2\alpha_j\pi\sqrt{\epsilon_j(\epsilon_j+2)}}C_j^+M(u)k\left|k\big(L_j - x_{\widetilde{n}_j}(1+\epsilon_j/2)\big)\right|^{-\delta_j^+}$$

from which the result follows, recalling that $x_{\widetilde{n}} \leq \alpha_j 2\pi/k$. □

In this proof we have approximated $v_j^+(\cdot/k)\mathrm{e}^{2\mathrm{i}\cdot}$ over $\widetilde{n}_j$ small elements with a single polynomial of degree p_j; sharper estimates may be derived along the lines of the proof of [35, Theorem 5.2], which admits different polynomials in each element.

A slightly sharper bound may be achievable by choosing non-oscillating functions on the elements close to the corners, yielding the constant $\mathrm{e}^{\alpha_j\pi\sqrt{\epsilon_j(\epsilon_j+2)}}$ in place of $\mathrm{e}^{2\alpha_j\pi\sqrt{\epsilon_j(\epsilon_j+2)}}$. However this would also require separate bounds close to the singularity of $v_j^\pm$, we would be unable to use the bounds of [35, Theorem 5.2], making the proof more complex. If α_j is chosen independently of k and sufficiently small, then the first and the last $\widetilde{n}_j$ elements of $\mathcal{M}_n(0,L_j)$ are smaller than a given fraction of the wavelength of the problem.

Construction of the stiffness matrix will have approximately similar CPU time for the single- and overlapping-mesh approach (assuming that the same quadrature routine is used in each method) for similar degrees of freedom, because the inner products are very similar. Provided α_j is chosen correctly, we expect the implementation of the single-mesh to be advantageous because implementation is easier, as there are fewer types of inner products that need computing for the Galerkin method and it is easily adapted from a standard *hp* solver, which would not generally be defined

over an overlapping mesh. Secondly, controlling the number of degrees of freedom of the discrete space enables us to control the conditioning of the discrete system. Figure 2.4 suggests that the conditioning remains stable as the number of degrees of freedom increases, for $\alpha_j = \min\{(\mathbf{p})_i/2, 2\}$ on the ith mesh element, for $j = 1, 2, 3$, whilst the conditioning for the overlapping-mesh space appears to grow exponentially for a similar number of degrees of freedom. It should be noted that the value of α_j is larger here than that which is used to produce the numerical results in §3.2.3 and §4.5, and we would expect a larger value of α_j to produce less accurate results. Hence an advantage of the single-mesh approach is that the user has control over the conditioning of the discrete system (by tweaking the parameter α_j), but this may come at a cost (a loss of accuracy). Indeed, Figure 3.11 suggests that the condition number for $\alpha_j = \min\{(\mathbf{p})_i/8, 2\}$ grows exponentially, whilst Figure 4.4 suggests that the larger choice $\alpha_j = \min\{(\mathbf{p})_i/4, 2\}$ can lead to inaccurate results.

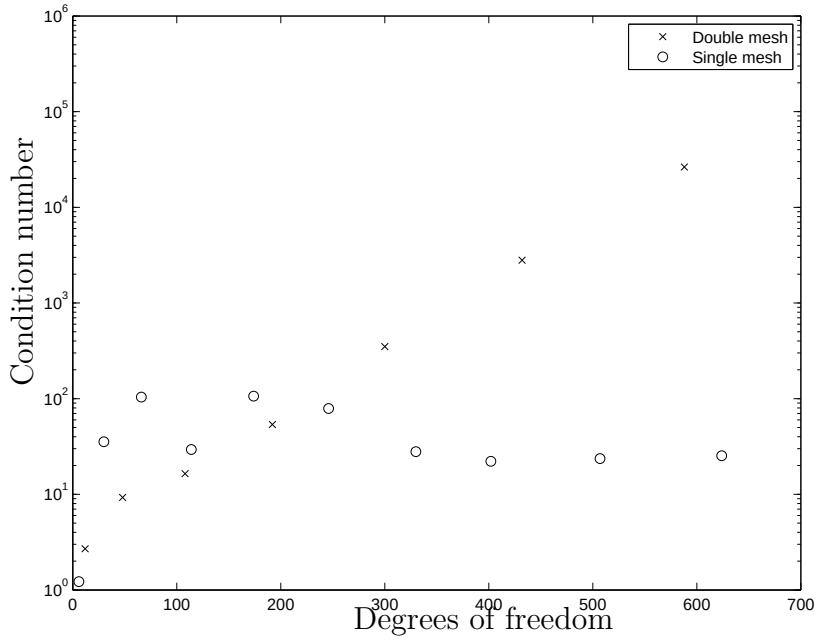

Figure 2.4: The condition number of the Galerkin stiffness matrix corresponding to scattering by a single regular triangle, with each side length 2π and wavenumber $k = 5$, for a single- and double-mesh discretisation as described in Remark 2.8. The maximal polynomial degrees used are $p = 0, \ldots, 9$ for the single-mesh space and $p = 1, \ldots, 7$ for the overlapping-mesh space; the polynomial degrees in the small elements are decreased as in Remark 2.10.

REMARK 2.10. *It is shown in [35, Theorem A.3] for* $\overline{\overline{V}}_N^{\mathrm{HNA}}(\Gamma)$ *that it is possible to reduce the number of degrees of freedom on* Γ*, whilst maintaining exponential convergence, by reducing the polynomial degree in the smaller mesh elements. For example,*

given $p > 1$, suppose that we define for each side Γ_j, $j = 1, \ldots, n_\Gamma$, a degree vector $\mathbf{p}$ by

$$(\mathbf{p})_i := \begin{cases} \left\lceil \frac{i-1}{n_*} p \right\rceil, & 1 \leq i \leq n_*, \\ p, & n_* + 1 \leq i \leq n, \end{cases}$$

where n_* is the largest $i \in \{1, \ldots, n-1\}$ such that $x_{i-1}/2 < 1$. Numerical experiments in §3.2.3 and §4.5 suggest that a similar result holds for $\overline{V}_N^{\mathrm{HNA}}(\Gamma)$, although we do not prove this here. To this purpose, one has to use the technique of [35, Theorem A.3], relying on different approximation bounds on each mesh element, while the technique used in the proof of Theorem 2.9 requires the presence of high-order polynomials on each element.

Now we present a result which compares the best approximation of the single-mesh and overlapping-mesh spaces, over the whole boundary Γ.

COROLLARY 2.11. *If Assumption 2.4 and the conditions for Theorem 2.9 hold for a convex polygon Γ, then we have the following best approximation bound for the diffracted wave v_Γ (see (2.6)):*

$$\inf_{w_N \in V_N^{\mathrm{HNA}}(\Gamma)} \|v_\Gamma - w_N\|_{L^2(\Gamma)} \leq C_\Gamma M(u) k^{-1/2} J(k) \mathrm{e}^{-p\tau_\Gamma}, \tag{2.10}$$

where C_Γ is a constant independent of k and

$$J(k) := \begin{cases} (1 + kL_*)^{1/2-\delta_*} + \log^{1/2}(2 + kL_*) + \sqrt{k}(kI_*)^{-\delta_*}, & V_N^{\mathrm{HNA}}(\Gamma) = \overline{V}_N^{\mathrm{HNA}}(\Gamma) \\ (1 + kL_*)^{1/2-\delta_*} + \log^{1/2}(2 + kL_*), & V_N^{\mathrm{HNA}}(\Gamma) = \overline{\overline{V}}_N^{\mathrm{HNA}}(\Gamma) \end{cases}$$

with $I_* := \min_j\{I_j\}$, $p := \min_j\{p_j\}$, $\tau_\Gamma := \min_{j,\pm}\{\tau_j^\pm p_j\}/p$, $\delta_* := \min_{j,\pm}\{\delta_j^\pm\}$. For the case $\overline{V}_N^{\mathrm{HNA}}(\Gamma)$, it follows that $C_\Gamma = \max_j\{C_j\}$. For the case $\overline{\overline{V}}_N^{\mathrm{HNA}}(\Gamma)$, C_Γ is equal to the constant C_4 of [35, Theorem 5.5].

Proof. For $\overline{V}_N^{\mathrm{HNA}}(\Gamma)$, the result follows by extending Theorem 2.9 to all sides, noting the scaling of (2.6). The case $\overline{\overline{V}}_N^{\mathrm{HNA}}(\Gamma)$ is proved in [35, Theorem 5.5]. □

In the above Corollary 2.11, we note that there is an additional term in the best approximation error of $\overline{V}_N^{\mathrm{HNA}}(\Gamma)$, namely $\sqrt{k}(kI_*)^{-\delta_*}$. By definition, for convex polygons we have that $\delta_* > 1/2$, hence it follows that $J(k) \sim \log^{1/2} k$ as $k \to \infty$.

REMARK 2.12 (Collocation vs Galerkin HNA BEM)**.** *The collocation (see (1.19)) HNA method for the problem of the two-dimensional screen was investigated in [47]. A key component of the investigation was a comparison between single- and overlapping-mesh collocation, although no conclusions were drawn regarding how the collocation*

points should be chosen when an overlapping mesh is used. In certain cases, choosing Chebyshev nodes resulted in a non-convergent numerical method. Given this result, the single-mesh space $\overline{V}_N^{\mathrm{HNA}}(\Gamma)$ *would be the recommended choice when coupled with a collocation HNA method. The key advantage of collocation is that the integrals in the discrete system are of one dimension less, making for easier implementation, and faster run time. The disadvantage of collocation is that there is (currently) no applicable theory on stability constants for collocation HNA BEM, however there are many problems (for example, looking ahead to multiple obstacle HNA BEM* (4.22)*) for which there are also no stability bounds available for the Galerkin method (see* (1.18)*) either, hence case there is no theoretical advantage to implementing the more complex Galerkin method. Stability analysis of collocation HNA BEM is a possible area for future work, as it has been proved (see for example [2]) for certain problems (not including HNA BEM), that collocation and Galerkin methods produce the same result, in which case the same error analysis can be applied. In summary, there are advantages and disadvantages to Collocation and Galerkin methods, depending on implementation time available and desirability of a priori error bounds.*

2.3 HNA Galerkin method for a single convex polygon

Here we summarise the HNA Galerkin method for a single convex polygon Γ. We write $V_N^{\mathrm{HNA}}(\Gamma)$ to denote either of the two approximation spaces of §2.2. The continuous BIE to solve may be written by combining (2.2), (2.6) and (1.14) with either choice of $\mathcal{A}$,

$$\mathcal{A}v_\Gamma = \frac{1}{k}\left(f - \mathcal{A}\Psi\right), \quad \text{on } \Gamma,$$

and the Galerkin problem (see (1.18)) to solve is: find $v_N \in V_N^{\mathrm{HNA}}(\Gamma)$ such that

$$(\mathcal{A}v_N, \varphi)_{L^2(\Gamma)} = \frac{1}{k}\left(f - \mathcal{A}\Psi, \varphi\right)_{L^2(\Gamma)}, \quad \text{for all } \varphi \in V_N^{\mathrm{HNA}}(\Gamma), \tag{2.11}$$

where $(\cdot,\cdot)_{L^2(\Gamma)}$ denotes the L^2 inner product on Γ (see §A.2). For $\mathcal{A} = \mathcal{A}_{k,\eta}$ it follows by [16, Theorem 5.2] that there exists an $N_0 > 0$ such that (2.11) has a unique solution for $N \geq N_0$. For $\mathcal{A} = \mathcal{A}_k$ we have $N_0 = 1$ (see Remark 2.13 for details). Provided the conditions of Assumption 2.4 and Corollary 2.11 are satisfied, we may bound the error in our approximation on a single convex scatterer,

$$\|v_\Gamma - v_N\|_{L^2(\Gamma)} \leq Ck^{-1/2}C_q(k)M(u)J(k)\mathrm{e}^{-p\tau_\Gamma}, \quad \text{for } N \geq N_0, \tag{2.12}$$

where C, p, J and τ_Γ are as in Corollary 2.11. The bound (2.12) follows by combining the best approximation error with [16, Theorem 5.2], and is a natural generalisation of [35, (5.11)] to multiple approximation spaces (recalling that J depends on the choice of approximation space). The constant $C_q(k) \geq 1$ denotes the *stability* or *quasi-optimality constant*, which determines the relationship between the best approximation available in the space $V_N^{\mathrm{HNA}}(\Gamma)$ and the solution to the Galerkin equations (2.11), as these need not be the same thing. The stability constant depends on the formulation used, and has been the subject of much investigation, which we will summarise now:

REMARK 2.13 (The stability constant C_q for HNA methods on convex polygons)**.** *Here C_q represents the quasi-optimality constant associated to the Galerkin method. If $\mathcal{A} = \mathcal{A}_k$ (of Definition 1.3) then $N_0 = 1$ and $C_q \lesssim k^{1/2}$ for $k \geq k_0$, where $k_0 > 0$ is fixed and independent of k. This follows from the coercivity of $\mathcal{A}_k$, by Céa's lemma (see [52] and [35, Theorem 6.1]). Numerical experiments of [8, Table 6.1] show that $\mathcal{A}_{k,k}$ is coercive for the square and equilateral triangle, with a coercivity constant uniform in k, hence $C_q \sim \|\mathcal{A}_{k,k}\|$; given the current best available bounds on $\mathcal{A}_{k,\eta}$ ([20, Theorem 1.4]), we have $C_q \lesssim k^{1/4} \log k$ in these particular cases. Such a result has not yet been proved for $\mathcal{A}_{k,\eta}$ with general convex polygonal scatterers. Instead we may use the more general theory (see for example [3, Theorem 3.1.1]), given that $\mathcal{A}_{k,\eta}$ is a compact perturbation of a coercive operator [16, p620] we have existence of N_0 and C_q, although this provides no mechanism to bound either in terms of known parameters.*

THEOREM 2.14. *Suppose that the stability constant $C_q(k)$ grows at most algebraically with k, that Assumption 2.4 holds, $\mathcal{A}$ is a compact perturbation of a coercive operator, and either approximation space is used with the following condition on the polynomial degree vector on the jth side:*

$$(\mathbf{p}_j)_i = p_j \leq n_j/c_j \quad \textit{for} \quad i = 1, \ldots, n_j \quad \textit{with} \quad c_j \geq 1 \quad \textit{for} \quad j = 1, \ldots n_\Gamma,$$

where c_j is the constant from Theorem 2.9. Then the solution of the Galerkin equations (2.11) *converges exponentially to the true solution of* (1.14) *as $p \to \infty$ on $L^2(\Gamma)$, where $p := \min_j\{p_j\}$.*

Proof. It follows by Assumption 2.4 and Corollary 2.11 that $C_q(k)M(u)J(k)$ grows only algebraically in k. Hence there exists an $N \geq N_0$, where N grows with p, such that $\mathrm{e}^{-p\tau_\Gamma}$ will dominate the algebraic terms, given the bound (2.12). □

The above theorem highlights the importance of obtaining algebraic bounds on $M(u)$ (thus showing that Assumption 2.4 holds), which is a key component of Chapter 3. Although much work has been done to understand the growth of the stability constant $C_q(k)$ for star-shaped Ω_- (as discussed in Remark (2.13)), Chapter 5 provides the first bound for multiple scattering problems. Given the solution of (2.11), we can approximate quantities of practical interest using the Definitions (2.2) and (2.6), noting that v_N is an approximation to v_Γ, to obtain

$$\partial^+_{\mathbf{n}} u \approx \nu_p := \Psi + k v_N, \quad \text{on } \Gamma,$$

where p is the polynomial degree used to obtain the approximation with N degrees of freedom (there are parameters other than p, in particular c_j, which determine N). From this, an approximation to the total field u of (1.10) follows immediately, by inserting into (1.10)

$$u \approx u_N := u^{\text{inc}} - S_k \nu_p, \quad \text{in } \Omega_+,$$

and we have (from [35, Theorem 6.3]) that

$$\|u - u_N\|_{L^\infty(\Omega_+)} \leq C M(u) k^{1/2} \log^{1/2}(2 + L_* k) J(k) \mathrm{e}^{-p\tau_\Gamma}.$$

Likewise, we have the following approximation to the far-field coefficient of (1.16)

$$u^\infty(\theta) \approx u^\infty_N(\theta) := \int_\Gamma \mathrm{e}^{-\mathrm{i}k[y_1 \cos\theta + y_2 \sin\theta]} \nu_p(\mathbf{y}) \, \mathrm{d}s(\mathbf{y}), \quad \theta \in [0, 2\pi), \tag{2.13}$$

with error estimate (from [35, Theorem 6.4])

$$\|u^\infty - u^\infty_N\|_{L^\infty(0,2\pi)} \leq C k^{3/2} M(u) \log^{1/2}(2 + k L_*) J(k) \mathrm{e}^{-p\tau_\Gamma}. \tag{2.14}$$

Chapter 3

Generalisation of incident fields solvable by HNA method

The results produced in this chapter will appear in [26].

To date, each version of the HNA method has been developed for solving problems of plane wave incidence (as in Figure 3.2(a), see Remark 2.5). However, point source incidence (see Definition 3.6(i) and Figure 3.2(c)) also occurs frequently in practical applications. For example, in acoustic modelling, most sounds originate from a source point; a plane wave model is only appropriate when the source is far away from the scattering obstacle (a plane wave may be interpreted as a point source at infinity). Moreover, a point source is more physically realistic (than a plane wave) as it satisfies the radiation condition (1.6). Perhaps less commonly studied is a generalisation of the point source; the beam source (see Definition 3.6(ii), and Figure 3.2(d)), for which the point source is smeared along a line. Our interest in the beam source is only partially motivated by direct application; we expect it will also be useful for iterative multiple scattering versions of HNA BEM, which are discussed briefly in Chapter 8.

We are also interested in scattering by a general Herglotz-type incident field (see Definition 1.8 and Figure 3.2(b) for an example with Herglotz kernel). As with the beam source incidence, solutions to such problems may not have as many immediate applications. Instead, our motivation is nested inside a larger idea for solving multiple scattering problems. The Tmatrom method of [23] requires an approximation of the far-field pattern of radiating wavefunctions, for which the Herglotz kernel can be written explicitly (see Chapter 7 for details). Hence it is necessary to understand such problems to develop HNA methods which are compatible with the Tmatrom method.

In this Chapter, we aim to generalise HNA methods to a broader class of obstacles, whilst restricting our attention to the case of the convex polygon Ω_-. For each new

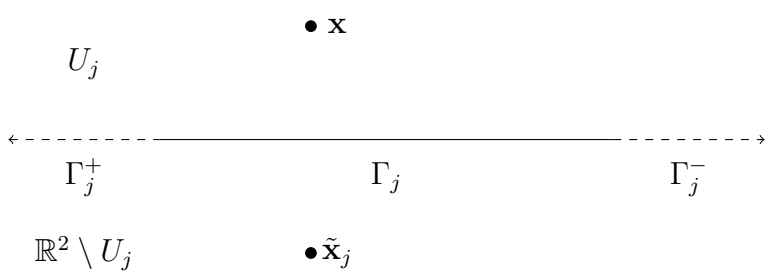

Figure 3.1: Example of a typical extension of a single side Γ_j, and the image of $\mathbf{x} \in U_j$ reflected in the infinite line $\Gamma_j^\infty = \Gamma_j^- \cup \Gamma_j \cup \Gamma_j^+$, to create the point $\tilde{\mathbf{x}}_j \in \mathbb{R}^2 \setminus U_j$.

problem considered, we will derive a boundary representation analogous to (2.2) using a half-plane formulation, extending a single side Γ_j (of the boundary Γ of the convex polygon Ω_-) infinitely in both directions to form the boundary of the half-plane (see Figure 3.6 for example of an extension of a typical side). Considering a single side Γ_j of a convex polygon Γ, $1 \leq j \leq n_\Gamma$, we define Γ_j^+ and Γ_j^- as the infinite extensions of Γ_j in the clockwise and anti-clockwise directions. Denote by U_j the (open) upper-half plane relative to $\Gamma_j^\infty := \Gamma_j^+ \cup \Gamma_j \cup \Gamma_j^-$, such that the unit normal $\mathbf{n}_j$ points into U_j. Finally, we define $\widetilde{\mathbf{x}}^j$ to be the reflection of $\mathbf{x}$ across Γ_j. Formally, $\mathbf{x} = \widetilde{\mathbf{x}}^j$ when $\mathbf{x} \in \Gamma_j$, otherwise $\widetilde{\mathbf{x}}^j \neq \mathbf{x}$ satisfies $\operatorname{dist}(\mathbf{x}, \Gamma_j^\infty) = \operatorname{dist}(\widetilde{\mathbf{x}}^j, \Gamma_j^\infty) = \frac{1}{2}|\mathbf{x} - \widetilde{\mathbf{x}}^j|$ (see Figure 3.1 for a visual example).

We will make multiple uses of the following representation from [10, (14)], which states that for $v \in C^2(U_j) \cap C(\overline{U_j})$ satisfying the Helmholtz equation (1.3) and the radiation condition (1.6), we have

$$v(\mathbf{x}) = 2 \int_{\Gamma_j^\infty} \frac{\partial \Phi(\mathbf{x}, \mathbf{y})}{\partial \mathbf{n}(\mathbf{y})} v(\mathbf{y}) \, \mathrm{d}s(\mathbf{y}), \quad \mathbf{x} \text{ in } U_j. \tag{3.1}$$

We note that this representation holds for $v = u^s$ (the scattered field component of the solution to (1.4)-(1.6)) and holds for plane waves propagating in direction $\mathbf{d}$, provided that $\mathbf{d} \cdot \mathbf{n}_j \geq 0$, i.e. propagating out of U_j (see [10], [16, §3]). Our representation for the Neumann trace of the solution to (1.4)–(1.6) will typically be of the form

$$\frac{\partial u}{\partial \mathbf{n}}(\mathbf{x}) = \Psi(\mathbf{x}) + 2 \int_{\Gamma_j^+ \cup \Gamma_j^-} \frac{\partial^2 \Phi(\mathbf{x}, \mathbf{y})}{\partial \mathbf{n}(\mathbf{x}) \partial \mathbf{n}(\mathbf{y})} u(\mathbf{y}) \, \mathrm{d}s(\mathbf{y}), \quad \mathbf{x} \text{ in } \Gamma_j. \tag{3.2}$$

This leads to the boundary representation (2.2), since

$$\frac{\partial^2 \Phi(\mathbf{x}, \mathbf{y})}{\partial \mathbf{n}(\mathbf{x}) \partial \mathbf{n}(\mathbf{y})} = \frac{\mathrm{i} H_1^{(1)}(k|\mathbf{x} - \mathbf{y}|)}{4|\mathbf{x} - \mathbf{y}|} = \frac{\mathrm{i}k^2}{4} \mathrm{e}^{\mathrm{i}k|\mathbf{x}-\mathbf{y}|} \mu(k|\mathbf{x}-\mathbf{y}|), \quad \text{where} \quad \mu(z) := \mathrm{e}^{-\mathrm{i}z} \frac{H_1^{(1)}(z)}{z},$$

see [16, eq. (3.6)].

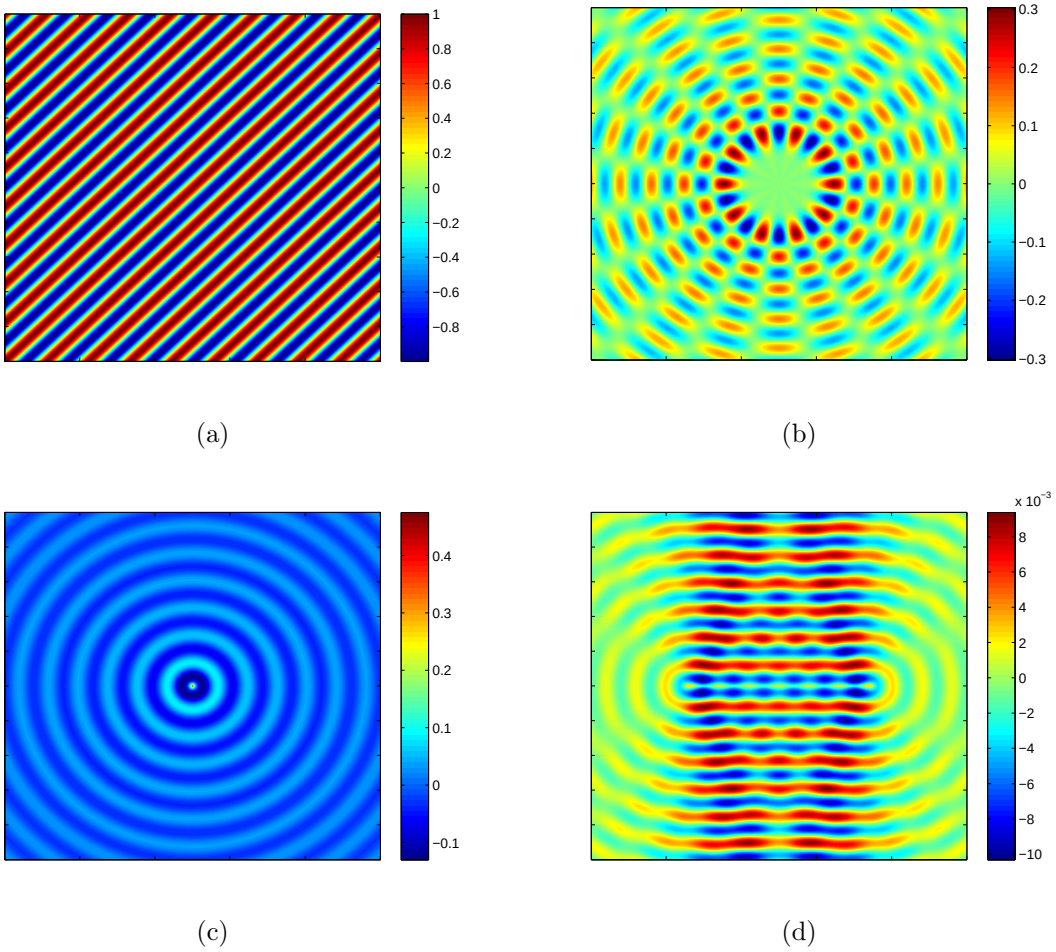

(a) (b)

(c) (d)

Figure 3.2: Examples of types of incident field solvable in this chapter, with wavenumber $k = 40$ (although the wavenumber is irrelevant for (a) and (c)). (a) Plane wave. (b) Herglotz-type wave with kernel $g_{\text{Herg}} = -\mathrm{e}^{-\mathrm{i}\ell\theta}/(2\pi)$. (c) Point source. (d) Beam source (see Definition 3.5) with $\gamma = \{(x_1, x_2) \in \mathbb{R}^2 : x_1 \in [-1/2, 1/2], x_2 = 0\}$ and $\varphi(\mathbf{x}) = 1/2 + x_1^2$.

As promised in Remark 2.5, we will generalise the definition of $M(u)$ (of Assumption 2.4) to problems where the incident field is unbounded at points inside the scattering domain Ω_+. This definition will continue to depend on the size of u in some sense. We will conclude this introduction with a theorem which will be used in each problem considered in this chapter, and the multiple scattering problems of Chapter 4. This theorem will enable us to bound the scattered field u^s in terms of the k-weighted norm (see (A.4)) of the incident field u^{inc} on the boundary $\partial\Omega$.

THEOREM 3.1. *For an obstacle Ω_- with boundary $\partial\Omega$ and incident field u^{inc} (in the sense of Definition 1.1), we have the following bounds on the corresponding scattered*

field $u^s = u - u^{inc}$, where u is the solution to (1.4)–(1.6):

(i) For star-shaped polygonal Ω_- with boundary $\Gamma = \partial\Omega$,

$$\|u^s\|_{L^\infty(\Omega_+)} \leq C_1 \left[2\,\mathrm{diam}(\Omega_-) + \frac{1}{2k}\right] k^{-1/2} \log^{1/2}(2 + kL_*)\|u^{inc}\|_{H^1_k(\Gamma)},$$

where

$$C_1 = \frac{\sqrt{5n_\Gamma/(8\log 2)}[1 + (2/\pi)(1 - \gamma_E + e^{1/4})]}{\operatorname*{ess\,inf}_{\mathbf{x}\in\Gamma}(\mathbf{x}\cdot\mathbf{n}(\mathbf{x}))},$$

where n_Γ is the number of sides of Γ, whilst L_* denotes the length of the longest side and $\gamma_E \approx 0.577$ denotes the Euler constant.

(ii) More generally, for a non-trapping polygon (in the sense of Definition 2.2) Ω_- with boundary $\partial\Omega$, given $k_0 > 0$,

$$\|u^s\|_{L^\infty(\Omega_+)} \lesssim k^{-1/2}\log^{1/2}(k)\|u^{inc}\|_{H^1_k(\partial\Omega)}, \quad \textit{for } k \geq k_0.$$

(Recall that $a \lesssim b$ is equivalent to $a \leq cb$, where c depends only on the geometry of Ω_-.)

Proof. (i) We have the representation $u^s = -S_k\mathcal{A}_k^{-1}f_k$ in Ω_+ (follows immediately from (1.10)), where $\mathcal{A}_k$ and f_k are as in Definition 1.4. As $u^{\mathrm{inc}} \in C^\infty(\mathcal{N})$ by Definition 1.1, it follows that $u^{\mathrm{inc}} \in H^1(\Gamma)$. Hence by the definition of f_k,

$$\begin{aligned}\|f_k\|_{L^2(\Gamma)} &\leq \mathrm{diam}(\Omega_-)\|\nabla u^{\mathrm{inc}}\|_{L^2(\Gamma)} + k(\mathrm{diam}(\Omega_-) + 1/2)\|u^{\mathrm{inc}}\|_{L^2(\Gamma)} \\ &\leq \left[2\,\mathrm{diam}(\Omega_-) + \frac{1}{2k}\right]\|u^{\mathrm{inc}}\|_{H^1_k(\Gamma)}. \end{aligned} \tag{3.3}$$

The result follows by combining (3.3) with the bound on S_k of [35, Lemma 4.1] and the bound on $\mathcal{A}_k^{-1}$ of [35, (4.5)] (noting that our definition of $\mathcal{A}_k$ is twice that of $\mathcal{A}_k$ in [52], as warned by Remark 1.5) with the bound

$$\|u^s\|_{L^\infty(\Omega_+)} \leq \|S_k\|_{L^2(\Gamma)\to L^\infty(\Omega_+)}\|\mathcal{A}_k^{-1}\|_{L^2(\Gamma)\to L^2(\Gamma)}\|f_k\|_{L^2(\Gamma)}. \tag{3.4}$$

(ii) In terms of the Dirichlet to Neumann map, we may consider the BVP with Dirichlet data $u^s = -u^{\mathrm{inc}}$ on the boundary $\partial\Omega$, hence $\partial^+_{\mathbf{n}}u^s = -P_{\mathrm{DtN}}\tau_+u^{\mathrm{inc}}$. We therefore have the representation

$$u^s = -S_k(\partial^+_{\mathbf{n}} - P_{\mathrm{DtN}}\tau_+)u^{\mathrm{inc}}, \quad \text{in } \Omega_+,$$

which we can bound

$$\|u^s\|_{L^\infty(\Omega_+)} \leq \|S_k\|_{L^2(\partial\Omega)\to L^\infty(\Omega_+)} \left(1 + \|P_{\mathrm{DtN}}\|_{H^1_k(\partial\Omega)\to L^2(\partial\Omega)}\right) \|u^{\mathrm{inc}}\|_{H^1_k(\partial\Omega)}.$$

We have that $\|S_k\|_{L^2(\partial\Omega)} \lesssim k^{-1/2}\log^{1/2} k$ from [35, Lemma 4.1] provided we choose $k_0 \geq \max\{2L_*, 2/L_*\}$, also k_0 must be chosen such that $\|P_{\mathrm{DtN}}\|_{H^1_k(\partial\Omega)\to L^2(\partial\Omega)} \lesssim 1$ ([6, Theorem 1.4]), this proves the assertion. □

In the above Theorem 3.1, the bound (i) is a special case of the more general bound (ii), choosing $k_0 = \max\{2L_*, 2/L_*\}$ and k-independent constant $c = C_1[2\,\mathrm{diam}(\Omega_-) + 1]\sqrt{2}$. In this chapter, we consider only convex polygons (a sub-class of star-shaped polygons, so all results concerning star-shaped obstacles hold), however Theorem 3.1(ii) is a general result which will also apply to multiple obstacles in Chapter 4, and to non-convex obstacles (this is discussed further immediately after Corollary 4.7).

3.1 Herglotz-type incidence

First, we extend the well-studied case of plane wave incidence to a weighted integral of plane waves. From the point of view of the numerical analysis, this is the simplest case we consider, as smoothness properties are inherited from the single plane wave case.

We aim to solve the problem (1.4)-(1.6) for a single convex polygon Ω_- with boundary $\Gamma = \partial\Omega$, where the incident field is a Herglotz-type function (in the sense of Definition 1.8), for which the Herglotz kernel $g_{\mathrm{Herg}} \in L^2(0, 2\pi)$ is known, hence

$$u^{\mathrm{inc}}(\mathbf{x}) = u^{\mathrm{inc}}_{\mathrm{Herg}}(\mathbf{x}; g_{\mathrm{Herg}}) := \int_0^{2\pi} g_{\mathrm{Herg}}(\theta)\mathrm{e}^{\mathrm{i}k\mathbf{x}\cdot\mathbf{d}_\theta}\,\mathrm{d}\theta, \quad \text{for } \mathbf{x} \in \mathbb{R}^2,$$

where $\mathbf{d}_\theta := (\cos\theta, -\sin\theta)$. We shall typically not specify the second argument (the Herglotz kernel) of $u^{\mathrm{inc}}_{\mathrm{Herg}}(\mathbf{x}; g_{\mathrm{Herg}})$, and instead write $u^{\mathrm{inc}}_{\mathrm{Herg}}(\mathbf{x})$. We now separate the leading order behaviour (reflected terms) of $\partial^+_{\mathbf{n}} u$, by splitting the incident wave $u^{\mathrm{inc}}_{\mathrm{Herg}}$ into incoming and outgoing waves relative to the half-plane U_j, to obtain a representation of the form (3.2). To do this, we require $Z_j^\downarrow := \{\theta \in [0, 2\pi) : \mathbf{d}_\theta \cdot \mathbf{n}_j < 0\}$ and $Z_j^\uparrow := \{\theta \in [0, 2\pi) : \mathbf{d}_\theta \cdot \mathbf{n}_j \geq 0\}$. We may now split the incident wave into plane waves partitioned over these sets, and use the representation (3.1) on $Z_j^\uparrow$ to obtain for $\mathbf{x}$ in U_j

$$u^{\mathrm{inc}}_{\mathrm{Herg}}(\mathbf{x}) \;=\; \int_{Z_j^\downarrow \cup Z_j^\uparrow} g_{\mathrm{Herg}}(\theta)\mathrm{e}^{\mathrm{i}k\mathbf{x}\cdot\mathbf{d}_\theta}\,\mathrm{d}\theta$$

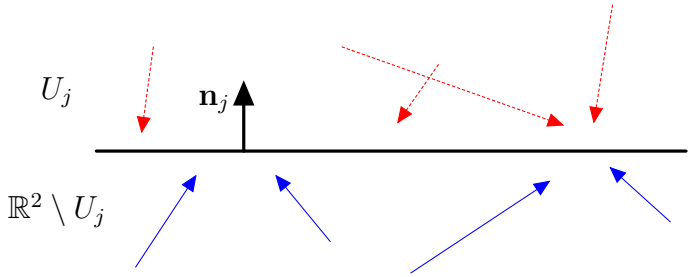

Figure 3.3: Example of the two types of waves split over the integral. Dashed arrows are those in $Z_j^{\downarrow}$, regular arrows are in $Z_j^{\uparrow}$.

$$= \int_{Z_j^{\downarrow}} g_{\text{Herg}}(\theta) \mathrm{e}^{\mathrm{i}k\mathbf{x}\cdot\mathbf{d}_\theta} \,\mathrm{d}\theta + 2\int_{\Gamma_j^{\infty}} \int_{Z_j^{\uparrow}} \frac{\partial \Phi(\mathbf{x},\mathbf{y})}{\partial \mathbf{n}(\mathbf{y})} g_{\text{Herg}}(\theta) \mathrm{e}^{\mathrm{i}k\mathbf{y}\cdot\mathbf{d}_\theta} \,\mathrm{d}\theta \,\mathrm{d}s(\mathbf{y}). \tag{3.5}$$

We cannot use the representation (3.1) over $Z_j^{\downarrow}$, instead we may consider

$$u^r(\mathbf{x}) = -\int_{Z_j^{\downarrow}} g_{\text{Herg}}(\theta) \mathrm{e}^{\mathrm{i}k\tilde{\mathbf{x}}_j\cdot\mathbf{d}_\theta} \,\mathrm{d}\theta, \quad \mathbf{x} \text{ in } U_j,$$

the integral of images of plane waves reflected in the line Γ_j^{∞} (see Figure 3.3). As this consists only of incident waves which are outgoing relative to $\tilde{\mathbf{x}}_j$, we can use the representation (3.1) with $v = u^s$ to obtain

$$0 = u^r(\mathbf{x}) + 2\int_{\Gamma_j^{\infty}} \int_{Z_j^{\downarrow}} \frac{\partial \Phi(\mathbf{x},\mathbf{y})}{\partial \mathbf{n}(\mathbf{x})} g_{\text{Herg}}(\theta) \mathrm{e}^{\mathrm{i}k\mathbf{y}\cdot\mathbf{d}_\theta} \,\mathrm{d}\theta \,\mathrm{d}s(\mathbf{y}), \quad \mathbf{x} \text{ in } U_j, \tag{3.6}$$

where $\tilde{\mathbf{y}}_j$ has been replaced by $\mathbf{y}_j$, as $\mathbf{y} = \tilde{\mathbf{y}}_j$ on Γ_j^{∞}. Summing (3.5), (3.6) and (3.1) with $v = u^s$ yields

$$u(\mathbf{x}) = \int_{Z_j^{\downarrow}} g_{\text{Herg}}(\theta) \left[\mathrm{e}^{\mathrm{i}k\mathbf{x}\cdot\mathbf{d}_\theta} - \mathrm{e}^{\mathrm{i}k\tilde{\mathbf{x}}\cdot\mathbf{d}_\theta}\right] \mathrm{d}\theta + 2\int_{\Gamma_j^{\infty}} \frac{\partial \Phi(\mathbf{x},\mathbf{y})}{\partial \mathbf{n}(\mathbf{y})} u(\mathbf{y}) \,\mathrm{d}s(\mathbf{y}), \quad \mathbf{x} \text{ in } U_j, \tag{3.7}$$

finally taking the Neumann trace gives the representation (3.2)

$$\frac{\partial u}{\partial \mathbf{n}}(\mathbf{x}) = \Psi_{\text{Herg}}(\mathbf{x}) + 2\int_{\Gamma_j^{+}\cup\Gamma_j^{-}} \frac{\partial^2 \Phi(\mathbf{x},\mathbf{y})}{\partial \mathbf{n}(\mathbf{x})\partial \mathbf{n}(\mathbf{y})} u(\mathbf{y}) \,\mathrm{d}s(\mathbf{y}), \quad \mathbf{x} \text{ in } \Gamma_j, \tag{3.8}$$

where

$$\Psi_{\text{Herg}}(\mathbf{x}) = 2\mathrm{i}k \int_{Z_j^{\downarrow}} [\mathbf{n}_j \cdot \mathbf{d}_\theta] g_{\text{Herg}}(\theta) \mathrm{e}^{\mathrm{i}k\mathbf{x}\cdot\mathbf{d}_\theta} \,\mathrm{d}\theta, \quad \mathbf{x} \text{ in } \Gamma_j.$$

We note that the representation (3.8) appears identical to (3.2), the key difference being the definition of $\Psi = \Psi_{\text{Herg}}$.

THEOREM 3.2. *Suppose that the incident field is a Herglotz-type function u^{inc}_{Herg} (in the sense of Definition 1.8), and Ω_- is a convex polygon. It follows that Assumption 2.4(i) holds, with*

$$M(u) = M_\infty(u) := \sup_{\mathbf{x}\in\Omega_+} |u(\mathbf{x})|,$$

hence the functions $v_j^\pm$, $j = 1, \ldots, n_\Gamma$, are analytic in the right half-plane $\mathrm{Re}[s] > 0$, where they satisfy the bounds

$$|v_j^\pm(s)| \leq \begin{cases} C_j^\pm M_\infty(u) k|ks|^{-\delta_j^\pm}, & 0 < |s| \leq 1/k, \\ C_j^\pm M_\infty(u) k|ks|^{-1/2}, & |s| > 1/k, \end{cases}$$

where $\delta_j^+, \delta_j^- \in (0, 1/2)$ are given by $\delta_j^+ := 1 - \pi/\omega_j$ and $\delta_j^- := 1 - \pi/\omega_{j+1}$. The constant C_j^+ depends only on c_*, and ω_j, whilst the constant C_j^- depends only on c_*, and ω_{j+1}. Here the constants c_* ω_j are as in Definition 2.3.

Proof. Given the boundary representation (3.8), [35, Theorem 3.1] describing the behaviour close to the corners holds for Herglotz-type functions, and the assertion follows by exactly the same arguments as [35, Theorem 3.2]. □

The estimates above can be rewritten in terms of known parameters using the following bound.

COROLLARY 3.3. *Suppose that u^{inc}_{Herg} and Ω_- are as in Theorem 3.2. Given the Herglotz kernel $g_{Herg} \in L^2(0, 2\pi)$ of u^{inc}_{Herg} we have the following bound*

$$M_\infty(u) \leq \|g_{Herg}\|_{L^2(0,2\pi)} \left(\sqrt{2\pi} + 2C_1\sqrt{\pi}|\Gamma|^{1/2} \left[2\,\mathrm{diam}(\Omega_-) + \frac{1}{2k} \right] k^{1/2} \log^{1/2}(2 + kL_*) \right),$$

where C_1 and L^* are as in Theorem 3.1. Hence, if there exists a $\beta' > 0$ such that $\|g_{Herg}\|_{L^2(0,2\pi)} \lesssim k^{\beta'}$, Assumption 2.4(ii) holds.

Proof. The bound on $M_\infty(u)$ follows by writing

$$M_\infty(u) \leq \|u^{\mathrm{inc}}_{\mathrm{Herg}}\|_{L^\infty(\Omega_+)} + \|u^s\|_{L^\infty(\Omega_+)} \tag{3.9}$$

and noting by Definition 1.8 it follows that $\|u^{\mathrm{inc}}_{\mathrm{Herg}}\|_{H^1_k(\Gamma)} \leq 2\sqrt{\pi}|\Gamma|^{1/2}k\|g_{\mathrm{Herg}}\|_{L^2(0,2\pi)}$, hence we may use Theorem 3.1 to bound $\|u^{\mathrm{inc}}_{\mathrm{Herg}}\|_{L^\infty(\Omega_+)}$ of (3.9), with $\|u^{\mathrm{inc}}_{\mathrm{Herg}}\|_{L^\infty(\Omega_+)} \leq \sqrt{2\pi}\|g_{\mathrm{Herg}}\|_{L^2(0,2\pi)}$, which again follows from Definition 1.8. □

Through Theorem 3.2 and Corollary (3.3), we have shown that both components of Assumption 2.4 hold, and thus by Theorem 2.14, exponential convergence of the

Galerkin method 4.4 for Herglotz-type incidence is guaranteed. We do not present numerical experiments for problems of Herglotz-type incidence here.

Although the theory was initially developed to integrate HNA methods with the T-matrix method of [23], we will develop a more efficient method in Chapter 6 which serves the same purpose, using the theory developed in Chapter 7. To implement the theory of this section, one may apply the method (2.11) to approximate $\partial_{\mathbf{n}}^{+}u$, noting that if we choose $\mathcal{A} = \mathcal{A}_k$ then fully explicit error estimates follow from (2.12) on any N-dimensional subspace $V_N^{\mathrm{HNA}}(\Gamma)$, by Corollary 3.3 and Remark 2.13.

3.2 Source-type incidence

In this section, we aim to generalise the HNA method to cases for which the incident field $u^{\mathrm{inc}} \notin C^{\infty}(\mathbb{R}^2)$. Naturally, some regularity is required for the HNA method to work. We aim to contain the *less regular* regions of the incident field, for example a point at which the incident field is unbounded, inside of a set that is sufficiently far from the scatterer Ω_- such that Assumption 2.4 holds, and therefore (by Theorem 2.14) the HNA method still converges at an exponential rate. We denote by Z a set inside of which this less regular behaviour is contained. Previous analyses of the HNA method utilised the boundedness of u when bounding the diffracted waves (see for example [35, Theorem 3.2 proof]); it follows from (3.2) that $v_{\pm}$ may be written as integrals along the extended line $\Gamma_j^{\pm}$. The idea is to take $M_{\infty}(u)$ outside of the integral using Hölder's inequality with $L^1(\Gamma_j^{\pm})$ and $L^{\infty}(\Gamma_j^{\pm})$ to obtain a bound on the diffracted waves. However, we will demonstrate here that if there exists a bounded open $Z \in \mathbb{R}^2$ outside of which u^{inc} is smooth, it is sufficient for u^{inc} to be L^2 integrable on $\Gamma_j^{\pm} \cap Z$, whilst Theorem 3.1 provides a bound on $\|u^s\|_{\Gamma_j^{\pm}}$. To ensure u^{inc} satisfies these conditions, we define the straight line

$$\ell_{c,\theta} := \left\{(x_1, x_2) \subset \mathbb{R}^2 : x_2 \cos\theta - x_1 \sin\theta = c\right\}, \quad \text{for } c \in \mathbb{R} \text{ and } \theta \in [0, \pi). \tag{3.10}$$

We will make use of the following norm, which considers the trace on the intersection of such lines with Z, for a function w

$$\|w\|_{\mathcal{L}(Z)} : H^{1/2+\epsilon}(Z) \to \mathbb{R}_+, \quad \|w\|_{\mathcal{L}(Z)} := \sup_{c\in\mathbb{R},\theta\in[0,\pi)} \|\tau_{\ell_{c,\theta}} w\|_{L^2(\ell_{c,\theta}\cap Z)}, \quad \text{for } \epsilon > 0, \tag{3.11}$$

where $\tau_{\ell_{c,\theta}}$ denotes the trace operator mapping to the line $\ell_{c,\theta}$. Given that $w \in H^{1/2+\epsilon}(Z)$ we know that w is continuous across $\ell_{c,\theta}$, hence the trace is the same regardless of the direction in which it is taken. Figure 3.4 depicts the type of lines considered, for a set Z.

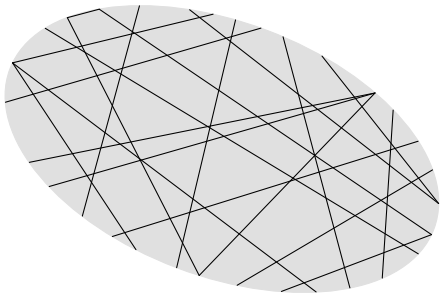

Figure 3.4: A finite set of lines intersecting some shaded region Z. The $\mathcal{L}(Z)$ norm considers the infinite set of all such lines, and bounds above the L^2 norm of a function restricted to any such straight line.

The following Theorem bounds the $L^2(\ell_{c,\theta} \cap Z)$ norm uniformly for any $c \in \mathbb{R}, \theta \in [0, \pi)$. This is useful given that our definition of $M(u)$ for source-type incidence will contain the $\mathcal{L}(Z)$ norm.

THEOREM 3.4. *If $u^{inc}|_Z \in H^s(Z)$ for $s \in (1/2, 3/2)$, where Z is a finite union of convex bounded sets open in $\mathbb{R}^2$, then*

$$\|u^{inc}\|_{\mathcal{L}(Z)} \leq C_\tau \|u^{inc}\|_{H^s(Z)},$$

where $C_\tau > 0$ depends only on Z.

Proof. Initially we consider the case for Z convex. We consider a line $\ell_{c,\theta}$ which intersects Z, and consider the two (also convex) sets formed via the bisection of the set Z by $\ell_{c,\theta}$. Denote by one of these two sets $\hat{Z}$, chosen to be the set inside of which the largest ball can be constructed, and assume for now that $\text{diam}(\hat{Z}) = 1$. Denote by $\partial\hat{Z}$ the boundary of $\hat{Z}$. It follows by [36, Lemma 4.4] that

$$\|w\|^2_{L^2(\partial\hat{Z})} \leq \hat{C}_\tau \left(\|w\|^2_{L^2(\hat{Z})} + |w|^2_{W^s(\hat{Z})} \right), \quad \text{for } w \in H^s(Z),$$

where $\hat{C}_\tau$ depends on $\hat{Z}$ and $|\cdot|_{W^s(\hat{Z})}$ denotes the Sobolev–Slobodeckij semi-norm, order s over $\hat{Z}$ (see e.g. [42, p74] for a definition). As $\ell_{c,\theta} \cap Z \subset \partial\hat{Z}$, and $\hat{Z} \subset Z$ we have

$$\|w\|^2_{L^2(\ell_{c,\theta} \cap Z)} \leq \hat{C}_\tau \left(\|w\|^2_{L^2(Z)} + |w|^2_{W^s(Z)} \right), \quad \text{for } w \in H^s(Z).$$

Given the conditions of [36, Lemma 4.4], we may choose $\hat{C}_\tau$ to be the constant corresponding to the $\ell_{c,\theta}$ which minimises the radius of the largest open ball that can be constructed inside of the set $\hat{Z}$. Given Z, this choice will produce the maximal

value of $\hat{C}_\tau$. Combining this maximal constant with the equivalence of the Sobolev–Slobodeckij and Bessel potential norms (see [42, Theorem 3.30(ii)]) we may write

$$\|w\|^2_{\mathcal{L}(Z)} \leq C_\tau \|w\|^2_{H^s(Z)}, \quad \text{for } w \in H^s(Z),$$

where C_τ depends only on Z. Repeated applications of the above steps extend this result to finite unions of convex sets. Likewise, scaling arguments can be used for the case $\operatorname{diam}(\hat{Z}) \neq 1$. □

Now we may define the space of source-type incident waves which we will solve via the HNA method.

DEFINITION 3.5 (Source-type incidence)**.** *Given a bounded open $Z \subset \mathbb{R}^2$ such that $\operatorname{dist}(Z, \Omega_+) \geq 1/k$, we define the set of source-type incidences as*

$$H_{\mathrm{src}}(\Omega_+; Z) := \{\varphi \in L^2_{\mathrm{loc}}(\mathbb{R}^2) : \varphi|_Z \in H^s(Z), \text{ for } \quad s > 1/2, \quad \varphi|_{\mathbb{R}^2 \setminus Z} \in C^\infty(\mathbb{R}^2 \setminus Z)\}.$$

The above definition takes into consideration the result of Theorem 3.4; by restricting to $\varphi|_Z \in H^s(Z)$ this ensures that $\|\varphi\|_{\mathcal{L}(Z)} < \infty$ for all functions in the space. We note also that classical $C^\infty(\mathbb{R}^2)$ incidences, for example plane or Herglotz-type waves, are accommodated by the above definition, in which case Z may be chosen to be empty.

Intuitively, the set Z can be thought of as the region in which the incident wave may be less regular, and all weakly singular behaviour should be strictly inside of Z. Given that we still have smoothness inside a neighbourhood of Γ, we can obtain the required bounds on $|v_\pm|$ of Assumption 2.4, for a carefully chosen $M(u)$.

3.2.1 Leading order behaviour for scattering by point and beam source incidence

We now restrict our attention to a particular class of source-type incident fields, so that the leading order behaviour can be separated, as is required to represent the solution in the form (3.2)

DEFINITION 3.6 (Localised source)**.** *The localised source $u^{inc} \in H_{\mathrm{src}}(\Omega_+, Z)$ is defined as*

$$u^{inc}(\mathbf{x}) = \langle \tilde{\varphi}, \Phi(\mathbf{x}, \cdot) \rangle, \quad \text{for } \mathbf{x} \in \mathbb{R}^2 \setminus Z,$$

where $\tilde{\varphi}$ is a distribution, and the values of Z for which $\mathbf{x}$ is defined depends on the particular choice of $\tilde{\varphi}$, as discussed in Remark 3.7 below. We are interested in two particular cases:

(i) The point source emanating from $\mathbf{s} \in Z$*, corresponding to* $\tilde{\varphi} = \delta_{\mathbf{s}}$*, where* $\delta_{\mathbf{s}}$ *is the Dirac Delta function translated to* $\mathbf{s}$*, for which*

$$u^{inc}(\mathbf{x}) = u^{inc}_{PS}(\mathbf{x}; \mathbf{s}) := \Phi(\mathbf{x}, \mathbf{s}), \quad \textit{for } \mathbf{x} \in \mathbb{R}^2 \setminus \{\mathbf{s}\}.$$

(ii) The beam source emanating from a Lipschitz curve γ *of Hausdorff dimension one, with density* $\varphi \in L^2(\gamma)$*,*

$$u^{inc}(\mathbf{x}) = u^{inc}_{BS}(\mathbf{x}; \varphi) := \int_\gamma \Phi(\mathbf{x}, \mathbf{y}) \varphi(\mathbf{y}) \, \mathrm{d}s(\mathbf{y}), \quad \textit{for } \mathbf{x} \in \mathbb{R}^2.$$

See Figure 3.6 for examples of typical Z for source type waves. Hereafter we shall often make the second arguments $\mathbf{s}$ and φ of u^{inc}_{PS} and u^{inc}_{BS} implicit, writing $u^{\mathrm{inc}}_{PS}(\mathbf{x})$ and $u^{\mathrm{inc}}_{BS}(\mathbf{x})$ instead.

REMARK 3.7 (Dependence on regularity of $\tilde{\varphi}$)**.** *We now explain in more detail the values of* $\mathbf{x} \in Z$ *for which* $u^{inc}(\mathbf{x})$ *is defined, given* $\tilde{\varphi}$*, noting the regularity of the fundamental solution,*

$$\Phi(\mathbf{x}, \cdot) \in H^{1-\epsilon}(\mathbb{R}^2), \quad \textit{for all } \epsilon > 0, \quad \textit{for all } \mathbf{x} \in \mathbb{R}^2. \tag{3.12}$$

(As we could not locate a derivation of the regularity (3.12) *in the literature, we present an argument in Appendix A.4.) Given that the inner product is well defined between any space and its dual, it follows from* (3.12) *that* $u^{inc}(\mathbf{x}) = \langle \tilde{\varphi}, \Phi(\mathbf{x}, \cdot) \rangle$ *is defined for all* $\mathbf{x} \in Z$ *(and therefore all* $\mathbf{x} \in \mathbb{R}^2$*) if* $\tilde{\varphi} \in H^{-1+\epsilon}(\mathbb{R}^2)$*, as is the case for the beam source of Definition 3.6(ii). However, this is not the case for the point source, as we have taken the less regular* $\tilde{\varphi} = \delta_{\mathbf{s}} \in H^{-1-\epsilon}(Z) \cap (C(Z))^*$*, for* $\mathbf{s} \in Z$ *and* $\epsilon > 0$*, yielding* $\Phi(\mathbf{x}, \mathbf{s})$*, for which* $\mathbf{x}$ *is undefined at* $\mathbf{s}$*. However, for the point source case, it follows from* (3.12) *that* $\Phi(\cdot, \mathbf{s}) \in H^s(\mathbb{R}^2)$ *for* $s \in (1/2, 1)$*, hence by Definition 3.5 we have that* $\Phi(\cdot, \mathbf{s}) \in H_{src}(\Omega_+; Z)$ *for* $\mathbf{s}$ *in a suitable* Z *containing* $\mathbf{s}$*. This is sufficient to prove the bounds on* $|v_\pm|$*, as required by Assumption 2.4(i).*

Now we derive a representation for $\partial^+_{\mathbf{n}} u$ which explicitly separates the leading order (reflected) terms in terms of known components of u^{inc}, for the case of the beam source and the point source. The general rule is that if the side Γ_j can *see* the source, then the leading order term Ψ is equal to $2\partial^+_{\mathbf{n}} u^{\mathrm{inc}}$, otherwise it is equal to zero.

THEOREM 3.8. *For a point source incidence $u^{inc} = u^{inc}_{PS}$ (as in Definition 3.6(i)), the leading order behaviour of* (3.2) *is*

$$\Psi = \Psi_{PS}(\mathbf{x}) := \begin{cases} 2\partial^+_{\mathbf{n}}\Phi(\mathbf{x},\mathbf{s}), & \mathbf{s} \in U_j, \\ 0, & \textit{otherwise}, \end{cases} \quad \textit{for } \mathbf{x} \in \Gamma_j, \tag{3.13}$$

where U_j denotes the upper half plane relative to Γ^∞_j (as defined at the start of this Chapter, depicted in Figure 3.1).

Proof. Define the half-plane Dirichlet Green's function

$$G_j(\mathbf{x},\mathbf{y}) := \Phi(\mathbf{x},\mathbf{y}) - \Phi(\widetilde{\mathbf{x}}^j,\mathbf{y}), \quad \mathbf{x} \neq \mathbf{y},$$

where $\widetilde{\mathbf{x}}^j$ is the reflection of $\mathbf{x}$ in the line Γ^∞_j, as defined at the beginning of this chapter. We split into three cases, depending on the position of the source point $\mathbf{s}$:

(i) For $\mathbf{s}$ in U_j, we apply Green's second identity to u^{inc}_{PS} and $G_j(\mathbf{x},\cdot)$ in $U_j \cap B_R(0) \cap B_\epsilon(\mathbf{s})$, where B_R is a ball chosen sufficiently large that Γ_j and $B_\epsilon(\mathbf{s})$ are inside it, for $\epsilon > 0$. Taking the limit as $\epsilon \to 0$ and $R \to \infty$ yields the result

$$u^{\text{inc}}_{PS}(\mathbf{x}) = G_j(\mathbf{x},\mathbf{s}) + 2\int_{\Gamma^\infty} \frac{\partial\Phi(\mathbf{x},\mathbf{y})}{\partial\mathbf{n}(\mathbf{y})} u^{\text{inc}}_{PS}(\mathbf{y})\,\mathrm{d}s(\mathbf{y}), \quad \mathbf{x} \in U_j. \tag{3.14}$$

Taking the Neumann trace gives the result

$$\frac{\partial u^{\text{inc}}_{PS}}{\partial\mathbf{n}}(\mathbf{x}) = 2\frac{\partial\Phi(\mathbf{x},\mathbf{s})}{\partial\mathbf{n}(\mathbf{x})} + 2\int_{\Gamma^\infty} \frac{\partial^2\Phi(\mathbf{x},\mathbf{y})}{\partial\mathbf{n}(\mathbf{x})\partial\mathbf{n}(\mathbf{y})} u^{\text{inc}}_{PS}(\mathbf{y})\,\mathrm{d}s(\mathbf{y}), \quad \mathbf{x} \in \Gamma_j, \tag{3.15}$$

as claimed.

(ii) For $\mathbf{s} \in \Gamma^\infty_j$, the same approach as (i) holds, although the factor of 2 in (3.14) is replaced by a 1, as only half of the ϵ-ball is in U_j. This makes no difference however, as $\partial_{\mathbf{n}} + \Phi(\mathbf{x},\mathbf{s}) = 0$ for $\mathbf{s} \in \Gamma^\infty_j$, so the leading order term Ψ is zero in this case.

(iii) For a source in the relative lower-half plane, $\mathbf{s} \in \mathbb{R}^2 \setminus U_j$, the representation (3.1) may be used, as u^{inc}_{PS} is smooth in the upper half plane U_j, hence

$$u^{\text{inc}}_{PS}(\mathbf{x}) = 2\int_{\Gamma^\infty_j} \frac{\partial\Phi(\mathbf{x},\mathbf{y})}{\partial\mathbf{n}(\mathbf{y})} u^{\text{inc}}_{PS}(\mathbf{y})\,\mathrm{d}s(\mathbf{y}), \quad \mathbf{x} \in U_j,$$

and taking the Neumann trace yields

$$\frac{\partial u^{\text{inc}}_{PS}}{\partial\mathbf{n}}(\mathbf{x}) = 2\int_{\Gamma^\infty_j} \frac{\partial^2\Phi(\mathbf{x},\mathbf{y})}{\partial\mathbf{n}(\mathbf{x})\partial\mathbf{n}(\mathbf{y})} u^{\text{inc}}_{PS}(\mathbf{y})\,\mathrm{d}s(\mathbf{y}), \quad \mathbf{x} \in \Gamma_j,$$

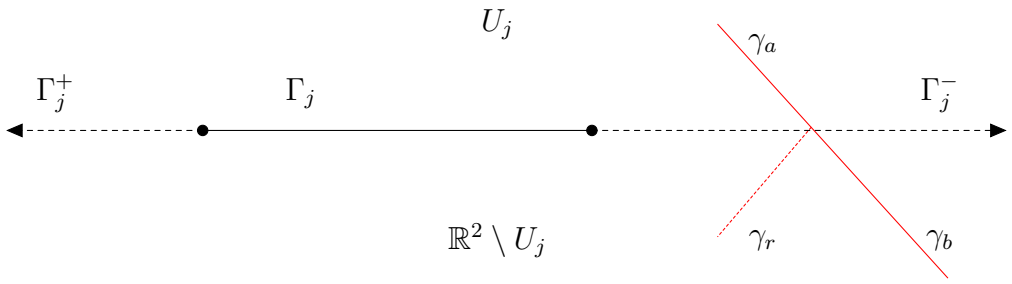

Figure 3.5: Depiction of the imaging argument used in the proof of Theorem 3.9. Here $\gamma_a := \gamma \cap U_j$, $\gamma_b := \gamma \setminus U_j$ and $\gamma_r := \{\tilde{\mathbf{x}}_j \in \mathbb{R}^2 : \mathbf{x} \in \gamma_a\}$. Physically, γ_r corresponds to the reflection of γ_a in the line $\gamma_j^\infty := \Gamma_j^- \cup \Gamma_j \cup \Gamma_j^+$. The wave u_a^{inc} emanates from γ_a, u_b^{inc} emanates from γ_b, and u_a^r may be interpreted as a wave emanating from γ_r (although it is formulated differently in (3.20)).

Combining each case, summing with the representation (3.19) of the Neumann trace of the scattered field u^s yields

$$\frac{\partial u}{\partial \mathbf{n}}(\mathbf{x}) = \Psi_{\text{PS}}(\mathbf{x}) + 2\int_{\Gamma_j^+ \cup \Gamma_j^-} \frac{\partial^2 \Phi(\mathbf{x},\mathbf{y})}{\partial \mathbf{n}(\mathbf{x}) \partial \mathbf{n}(\mathbf{y})} u(\mathbf{y})\, \mathrm{d}s(\mathbf{y}), \quad \mathbf{x} \in \Gamma_j,$$

as claimed □

THEOREM 3.9. *For a beam source incidence $u^{inc} = u_{BS}^{inc}$ with density $\varphi \in L^2(\gamma)$ (as in Definition 3.6(ii)), the leading order behaviour of* (3.2) *is*

$$\Psi_{BS}(\mathbf{x}) = 2\int_{U_j \cap \gamma} \frac{\partial \Phi(\mathbf{x},\mathbf{y})}{\partial \mathbf{n}(\mathbf{x})} \varphi(\mathbf{y})\, \mathrm{d}s(\mathbf{y}), \quad \textit{for } \mathbf{x} \in \Gamma_j. \tag{3.16}$$

Proof. We will use a *method of images* style argument (depicted in Figure 3.5). We split u_{BS}^{inc} into two components, corresponding to the contribution to the intensity at $\mathbf{x}$ from the components of the incident field above and below the extended line Γ_j^∞,

$$u_a^{\text{inc}}(\mathbf{x}) := \int_{\gamma \cap U_j} \Phi(\mathbf{x},\mathbf{y}) \varphi(\mathbf{y})\, \mathrm{d}s(\mathbf{y}), \quad \text{and} \quad u_b^{\text{inc}}(\mathbf{x}) := \int_{\gamma \setminus U_j} \Phi(\mathbf{x},\mathbf{y}) \varphi(\mathbf{y})\, \mathrm{d}s(\mathbf{y}), \tag{3.17}$$

noting that $u^{\text{inc}} = u_a^{\text{inc}} + u_b^{\text{inc}}$. Given that $u_b^{\text{inc}}|_{U_j} \in C^2(U_j) \cap C(\overline{U_j})$, we can apply (3.1) to obtain the representation

$$u_b^{\text{inc}}(\mathbf{x}) = \int_{\Gamma_j^\infty} \frac{\partial \Phi(\mathbf{x},\mathbf{y})}{\partial \mathbf{n}(\mathbf{y})} u_b^{\text{inc}}(\mathbf{y})\, \mathrm{d}s(\mathbf{y}), \quad \mathbf{x} \in U_j. \tag{3.18}$$

We note that the same representation holds for u^s, hence

$$u^s(\mathbf{x}) = \int_{\Gamma_j^\infty} \frac{\partial \Phi(\mathbf{x}, \mathbf{y})}{\partial \mathbf{n}(\mathbf{y})} u^s(\mathbf{y}) \, \mathrm{d}s(\mathbf{y}), \quad \mathbf{x} \in U_j. \tag{3.19}$$

For $\varphi \in L^2(\gamma)$, it follows from [13, Theorem 2.15] that $u_a^{\mathrm{inc}}|_{U_j} \in H^{3/2}_{\mathrm{loc}}(U_j) \not\subset C^2(U_j) \cap C(\overline{U_j})$, hence we cannot apply (3.1). Instead we make use of $u_a^r(\mathbf{x}) := -u_a^{\mathrm{inc}}(\tilde{\mathbf{x}}_j) \in C^2(U_j) \cap C(\overline{U_j})$, which physically corresponds to the reflection of u_a^{inc} in the extended line Γ_j^∞ (See Figure 3.5). Applying (3.1) yields

$$u_a^r(\mathbf{x}) = 2 \int_{\Gamma_j^\infty} \frac{\partial \Phi(\widetilde{\mathbf{x}}_j, \mathbf{y})}{\partial \mathbf{n}(\mathbf{y})} u_a^{\mathrm{inc}}(\mathbf{y}) \, \mathrm{d}s(\mathbf{y}) = -2 \int_{\Gamma_j^\infty} \frac{\partial \Phi(\mathbf{x}, \mathbf{y})}{\partial \mathbf{n}(\mathbf{y})} u_a^{\mathrm{inc}}(\mathbf{y}) \, \mathrm{d}s(\mathbf{y}), \tag{3.20}$$

for $\mathbf{x} \in U_j$. We may now add both sides of (3.20) to $u = u^{\mathrm{inc}} + u^s$, and split the incident field $u^{\mathrm{inc}} = u_a^{\mathrm{inc}} + u_b^{\mathrm{inc}}$ to obtain

$$u(\mathbf{x}) = \overbrace{u_a^{\mathrm{inc}}(\mathbf{x}) + u_b^{\mathrm{inc}}(\mathbf{x})}^{u^{\mathrm{inc}}} + u^s(\mathbf{x}) + u_a^r(\mathbf{x}) + \overbrace{2 \int_{\Gamma_j^\infty} \frac{\partial \Phi(\mathbf{x}, \mathbf{y})}{\partial \mathbf{n}(\mathbf{y})} u_a^{\mathrm{inc}}(\mathbf{y}) \, \mathrm{d}s(\mathbf{y})}^{-u^r(\mathbf{x})}, \quad \mathbf{x} \in U_j.$$

Substituting the representation for u_a^{inc} of (3.17) and (3.19), we obtain

$$u(\mathbf{x}) = u_a^{\mathrm{inc}}(\mathbf{x}) + u_a^r(\mathbf{x}) + 2 \int_{\Gamma_j^+ \cup \Gamma_j^-} \frac{\partial \Phi(\mathbf{x}, \mathbf{y})}{\partial \mathbf{n}(\mathbf{y})} u(\mathbf{y}) \, \mathrm{d}s(\mathbf{y}), \quad \mathbf{x} \in U_j.$$

Taking the Neumann trace to Γ_j yields

$$\frac{\partial u}{\partial \mathbf{n}}(\mathbf{x}) = 2 \int_{\gamma \cap U_j} \frac{\partial \Phi(\mathbf{x}, \mathbf{y})}{\partial \mathbf{n}(\mathbf{x})} \varphi(\mathbf{y}) \, \mathrm{d}s(\mathbf{y}) + 2 \int_{\Gamma_j^+ \cup \Gamma_j^-} \frac{\partial^2 \Phi(\mathbf{x}, \mathbf{y})}{\partial \mathbf{n}(\mathbf{x}) \partial \mathbf{n}(\mathbf{y})} u(\mathbf{y}) \, \mathrm{d}s(\mathbf{y}), \quad \mathbf{x} \in \Gamma_j,$$

as claimed. □

The definition of Ψ for a point source may be easily extended to multiple point sources by taking a linear combination of the leading order behaviour for each individual point source. Recalling that the beam source may become a useful concept in iterative multiple scattering methods, we remark that the case of a more general density $\varphi \in H^{-1/2}(\gamma)$ must be well understood for an iterative solution of a configuration of multiple screens, as this is the solution space of the screen problem. We hypothesise that a similar result holds in such a case, however one must be careful when *splitting* the beam source into $u^{\mathrm{inc}} = u_a^{\mathrm{inc}} + u_b^{\mathrm{inc}}$ (as in the proof of Theorem 3.9), as the integral now must be understood in the sense of distributions.

We will see in (4.1) that the leading order for beam source incidence (3.16) is closely related to our multiple scattering operator (4.12); the key difference is that φ becomes an unknown density in the multiple scattering case.

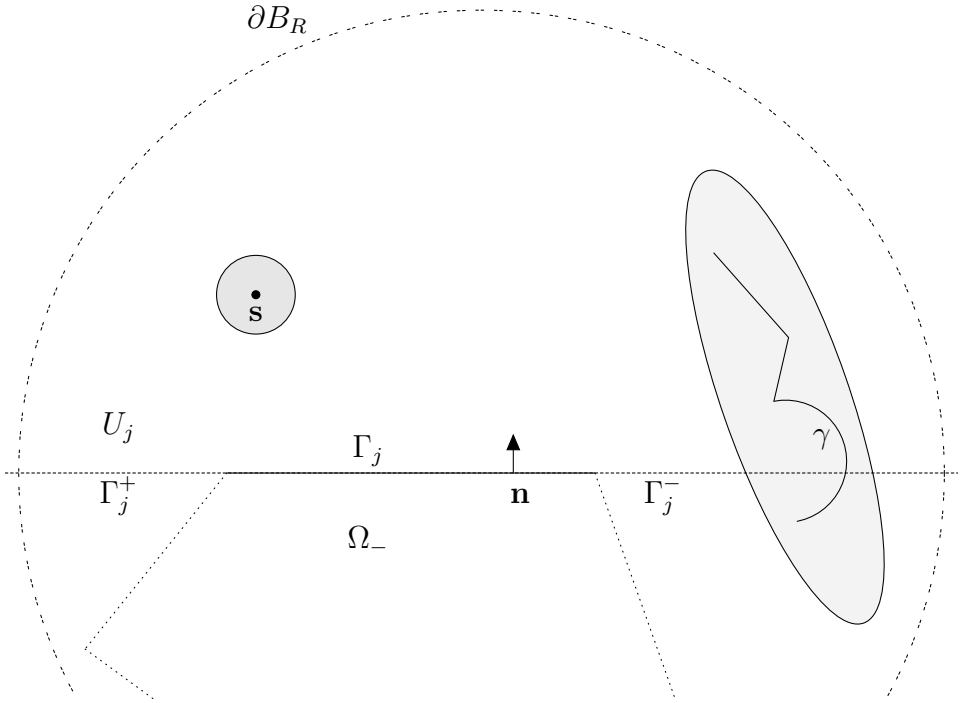

Figure 3.6: Example of components used for half-plane representation, in which the shaded region(s) denote(s) the choice of Z. This diagram may be used to explain the point source (at $\mathbf{s}$) or beam source (at γ) case, or the incident wave corresponding to the combination of both.

3.2.2 Regularity of $v_\pm$ for source-type terms

In the previous subsection we separated the leading order behaviour for a large class of source-type incidences, of the form stated in Definition 3.6. We now relax further, to the entire space $H_{\mathrm{src}}(\Omega_+; Z)$, inside of which we prove the required bounds on the diffracted waves.

THEOREM 3.10. *For incident field u^{inc}, if there exists Z such that $u^{inc} \in H_{\mathrm{src}}(\Omega_+; Z)$ (as in Definition 3.5), then Assumption 2.4 holds with $M(u) = M_Z(u)$, that is*

$$M_Z(u) := \|u^{inc}\|_{L^\infty(\Omega_+ \setminus Z)} + \|u^s\|_{L^\infty(\Omega_+)} + \sqrt{\frac{k}{8}} \|u^{inc}\|_{\mathcal{L}(Z)}. \tag{3.21}$$

Hence the functions $v_j^\pm$, for $j = 1, \ldots, n_\Gamma$, are analytic in the right half-plane $\mathrm{Re}[s] > 0$, where they satisfy the bounds

$$|v_j^\pm(s)| \leq \begin{cases} C_j^\pm M_Z(u) k |ks|^{-\delta_j^\pm}, & 0 < |s| \leq 1/k, \\ C_j^\pm M_Z(u) k |ks|^{-1/2}, & |s| > 1/k, \end{cases}$$

where $\delta_j^+, \delta_j^- \in (0, 1/2)$ are given by $\delta_j^+ := 1 - \pi/\omega_j$ and $\delta_j^- := 1 - \pi/\omega_{j+1}$. The

constant C_j^+ depends only on c_*, and ω_j, whilst the constant C_j^- depends only on c_*, and ω_{j+1}.

Proof. The analyticity of the functions $v_j^{\pm}(s)$ in $\mathrm{Re}[s] > 0$ follows from their definition (2.3) and the analyticity of $\mu(s)$ in the same set, which is shown in [35, Lemma 3.4].

Firstly we deal with the case of $|s| > 1/k$. It follows that $k(s+t) > 1$, hence the bound [35, (3.7)] can be simplified and we may write

$$|v_j^+(s)| \leq \frac{k^2}{2} \int_0^\infty |\mu\left(k(s+t)\right)|^{-3/2} \left| u\left(\mathbf{y}_j(\tilde{L}_{j-1} - t)\right)\right| \mathrm{d}t \tag{3.22}$$

$$\leq \frac{k^2}{2} \int_0^\infty k(|s|+t)^{-3/2} \left| u\left(\mathbf{y}_j(\tilde{L}_{j-1} - t)\right)\right| \mathrm{d}t. \tag{3.23}$$

We now split the integral, separating the set $Z' \subset (1/k, \infty)$ containing all t such that $\mathbf{y}_j(\tilde{L}_{j-1} - t) \in Z$. It follows that

$$\begin{aligned}
|v_j^+(s)| \leq & \frac{k^2}{2} \left[\int_{(0,\infty)\setminus Z'} + \int_{Z'}\right] k(|s|+t)^{-3/2} \left| u\left(\mathbf{y}_j(\tilde{L}_{j-1} - t)\right)\right| \mathrm{d}t, \\
\leq & \frac{k^2}{2} \left(\|u\|_{L^\infty(D\setminus Z)}\right) \int_{(0,\infty)\setminus Z'} k(|s|+t)\,\mathrm{d}t \\
& + \frac{k^2}{2} \int_{Z'} k(|s|+t)^{-3/2} \left| u\left(\mathbf{y}_j(\tilde{L}_{j-1} - t)\right)\right| \mathrm{d}t \\
\leq & \frac{k^2}{2} \left(\|u\|_{L^\infty(D\setminus Z)}\right) \int_{(0,\infty)\setminus Z'} k(|s|+t)\,\mathrm{d}t + \frac{k^2}{2} \|u^s\|_{L^\infty(Z)} \int_{Z'} k(|s|+t)^{-3/2}\,\mathrm{d}t \\
& + \frac{k^2}{2} \int_{Z'} (k(|s|+t))^{-3/2} \left| u^{\mathrm{inc}}\left(\mathbf{y}_j(\tilde{L}_{j-1} - t)\right)\right| \mathrm{d}t.
\end{aligned}$$

Since $|s| > 1/k$ and Z' is bounded, we can write

$$\int_0^\infty (k(|s|+t))^{-3/2}\,\mathrm{d}t \leq 2k^{-1}|ks|^{-1/2}$$

and

$$\left(\int_{Z'} |k(|s|+t)|^{-3}\,\mathrm{d}t\right)^{1/2} \leq \frac{k^{-1/2}}{\sqrt{2}}|ks|^{-1} \leq \frac{k^{-1/2}}{\sqrt{2}}|ks|^{-1/2},$$

hence by the Cauchy-Schwarz inequality

$$|v_j^+(s)| \leq M_Z(u) k |ks|^{-1/2} \quad \text{for } s > \frac{1}{k}.$$

For $|s| \leq 1/k$, the definition (2.3) of v_j^+ gives

$$|v_j^+(s)| \leq \frac{k^2}{2} \left[\int_0^{1/k} + \int_{1/k}^\infty\right] \left|\mu\big(k(s+t)\big)\right| \left|u\big(\mathbf{y}_j(\widetilde{L}_{j-1} - t)\big)\right| \mathrm{d}t$$

As $(0, 1/k) \not\subset Z'$, it follows from the Definition of $H_{\mathrm{src}}(\Omega_+; Z)$ that u^{inc} is infinitely differentiable in this region, and satisfies [35, Lemma 3.5], hence

$$u(\mathbf{x}) \leq C\|u\|_{L^\infty(\Omega_+\setminus Z)}(k|\mathbf{x}|)^{\pi/\omega_j}, \quad \text{for } |\mathbf{x}| < 1/k,$$

for C independent of k, and

$$u(\mathbf{x}) \leq CM_Z(u)(k|\mathbf{x}|)^{\pi/\omega_j}, \quad \text{for } |\mathbf{x}| < 1/k.$$

The first integral is bounded as in the proof of [35, Theorem 3.2], hence

$$\begin{aligned}\int_0^{1/k} \left|\mu\big(k(s+t)\big)\right|\left|u\big(\mathbf{y}_j(\widetilde{L}_{j-1}-t)\big)\right| \mathrm{d}t &\leq \|u\big(\mathbf{y}_j(\widetilde{L}_{j-1}-t)\big)\|_{L^\infty(0,1/k)} k|ks|^{-\delta_j^\pm} \\ &\leq k\left(\|u^{\mathrm{inc}}\|_{L^\infty(\Omega_+\setminus Z)} + \|u^s\|_{L^\infty(\Omega_+)}\right)|ks|^{-\delta_j^\pm} \\ &\leq k\left(\|u^{\mathrm{inc}}\|_{L^\infty(\Omega_+\setminus Z)} + \|u^s\|_{L^\infty(\Omega_+)}\right)|ks|^{-\delta_j^\pm},\end{aligned} \tag{3.24}$$

whilst the second integral is bounded as in the case $|s| > 1/k$. Combining all bounds proves the assertion.

□

Provided that $M_Z(u)$ has only algebraic growth in k, the conditions of Assumption 2.4 are satisfied, and a *hp* method as described in §2.3 converges exponentially. We note again that up to this point, the case $u^{\mathrm{inc}} \in C^\infty(\mathbb{R}^2)$ also fits inside of this framework, by choosing Z empty. We now seek fully explicit bounds on $M_Z(u)$ for the case of point source incidence.

THEOREM 3.11. *For point source incidence $u^{inc} = u^{inc}_{PS}(\cdot; \mathbf{s})$ with $\mathrm{dist}(\mathbf{s}, \Gamma) > 1/k$, it follows that $u^{inc}_{PS} \in H_{\mathrm{src}}(\Omega_+; Z)$ (of Definition 3.5) with $Z = B_r(\mathbf{s})$ and $r = \min(1, 1/(2k))$, moreover we have a k-explicit bound on the constant of Theorem 3.10*

$$M_Z(u) \leq$$
$$C_2 + \frac{C_1|\Gamma|^{1/2}}{2}\left[2\,\mathrm{diam}(\Omega_+) + \frac{1}{k}\right]\log^{1/2}(2+kL_*)\left(\sqrt{\frac{2}{\pi\,\mathrm{dist}(\mathbf{s},\Gamma)}} + \frac{1}{\pi\,\mathrm{dist}(\mathbf{s},\Gamma)\sqrt{k}}\right),$$

where C_1 and L_* are the constants from Theorem 3.1, and

$$C_2 = \frac{1}{2\sqrt{\pi}} + \frac{1}{\sqrt{2}}\left(1 + \frac{2}{\pi}(1 + \gamma_E + \mathrm{e}^{1/4})\right)(5 + \log^2 2 + \log 16)^{1/2}.$$

Hence Assumption 2.4(ii) holds.

Proof. Noting the definition (3.21) of $M_Z(u)$, we bound each of the three components separately.

(i) The bound on

$$\|u_{PS}^{\text{inc}}\|_{L^\infty(\Omega_+\setminus Z)} \leq \frac{1}{2\sqrt{\pi}}$$

follows immediately from (A.7); given the monotonicity of the absolute value of Hankel functions, the maximal value will occur at the boundary of Z.

(ii) Secondly we prove the bound on $\|u^s\|_{L^\infty(\Omega_+)}$. By Definition A.4 of the H_k^1 norm, we have

$$\|u_{PS}^{\text{inc}}\|_{H_k^1(\Gamma)} = \left(\int_\Gamma k^2|\Phi(\mathbf{y},\mathbf{s})|^2 + |\nabla_\Gamma\Phi(\mathbf{y},\mathbf{s})|^2\,\mathrm{d}s(\mathbf{y})\right)^{1/2},$$

which we can bound using $(a+b)^{1/2} \leq a+b$ for a and b non-negative, hence

$$\|u_{PS}^{\text{inc}}\|_{H_k^1(\Gamma)} = |\Gamma|^{1/2}\left(\sup_{\mathbf{y}\in\Gamma} k^2|\Phi(\mathbf{y},\mathbf{s})|^2 + \sup_{\mathbf{y}\in\Gamma}|\nabla_\Gamma\Phi(\mathbf{y},\mathbf{s})|^2\,\mathrm{d}s(\mathbf{y})\right)^{1/2}.$$

Given the definition of Φ, and that $H_0'^{(1)}(kz) = -kH_1^{(1)}(kz)$ for $z>0$, using (A.7) and (A.8) to bound these yields

$$\|u_{PS}^{\text{inc}}\|_{H_k^1(\Gamma)} \leq \frac{|\Gamma|^{1/2}}{2}\left(\sqrt{\frac{2k}{\pi\,\mathrm{dist}(\mathbf{s},\Omega_+)}} + \frac{1}{\pi\,\mathrm{dist}(\mathbf{s},\Omega_+)}\right).$$

Combining with Theorem 3.1, we obtain

$$\begin{aligned}&\|u^s\|_{L^\infty(\Omega_+)}\\ &\leq \frac{C_1|\Gamma|^{1/2}}{2}\left[2\,\mathrm{diam}(\Omega_+)+\frac{1}{k}\right]\log^{1/2}(2+kL_*)\left(\sqrt{\frac{2}{\pi\,\mathrm{dist}(\mathbf{s},\Gamma)}}+\frac{1}{\pi\,\mathrm{dist}(\mathbf{s},\Gamma)\sqrt{k}}\right)\end{aligned}$$

(iii) Thirdly we prove the bound on $\|u_{PS}^{\text{inc}}\|_{\mathcal{L}(Z)}$. We choose ℓ_* to be a line of the form (3.10) containing $\mathbf{s}$; given the monotonicity of $|\Phi(\cdot,\mathbf{s})|$, this line will maximise the norm. By definition of Φ and the L^2 norm,

$$\|u_{PS}^{\text{inc}}\|^2_{L^2(\ell_*\cap Z)} = 2\int_0^{\frac{1}{2k}}\left|\frac{1}{4}H_0^{(1)}(kt)\right|^2\mathrm{d}t.$$

Using (A.10) we can write

$$\|u_{PS}^{\text{inc}}\|^2_{L^2(\ell_*\cap Z)} \leq \frac{1}{8}\int_0^{\frac{1}{2k}}\hat{c}^2\left(1+|\log(kt)|\right)^2\mathrm{d}t$$

$$= \frac{1}{8k}\hat{c}^2(5 + \log^2 2 + \log 16),$$

hence

$$\|u_{PS}^{\text{inc}}\|_{L^2(\ell_* \cap Z)} \leq \frac{1}{2\sqrt{2k}}\hat{c}(5 + \log^2 2 + \log 16)^{1/2}.$$

Noting the definition (3.21), it follows from (i) and (iii) that

$$C_2 = \|u_{PS}^{\text{inc}}\|_{L^\infty(\Omega_+ \setminus Z)} + \sqrt{\frac{k}{8}}\|u_{PS}^{\text{inc}}\|_{L^2(\ell_* \cap Z)},$$

the result follows, with (ii) contributing the k-dependent components of the bound. □

Now we prove a similar result for the beam source case.

THEOREM 3.12. *Suppose u_{BS}^{inc} is a beam source incidence (in the sense of Definition 3.6(ii)) with density $\varphi \in L^2(\gamma)$, emanating from γ with $\operatorname{dist}(\gamma, \Omega_+) \geq 1/k$. If $M(u) = M_Z(u)$ where Z is a bounded open neighbourhood containing γ, or if $M(u) = M_\infty(u)$, then given $k_0 > 0$ we have the bound*

$$M(u) \lesssim \log^{1/2}(k)\|\varphi\|_{L^2(\gamma)}, \quad \text{for } k \geq k_0.$$

Hence if there exists a $\beta' > 0$ such that $\|\varphi\|_{L^2(\gamma)} \lesssim k^{\beta'}$, then Assumption 2.4(ii) holds.

Proof. Noting the Definition (3.21) of $M_Z(u)$, we bound each of the three components separately.

(i) Firstly, the bound on $\|u_{BS}^{\text{inc}}\|_{L^\infty(\Omega_+ \setminus Z)}$,

$$\|u_{BS}^{\text{inc}}\|_{L^\infty(\Omega_+ \setminus Z)} \leq \inf_{\mathbf{x} \in \Omega_+ \setminus Z} \int_\gamma |\Phi(\mathbf{x}, \mathbf{y})\varphi(\mathbf{y})| \, \mathrm{d}s(\mathbf{y})$$

and using (A.7) we can bound

$$\|u_{BS}^{\text{inc}}\|_{L^\infty(\Omega_+ \setminus Z)} \lesssim \inf_{\mathbf{x} \in \Omega_+ \setminus Z} \int_\gamma \left| \frac{1}{(k|\mathbf{x} - \mathbf{y}|)^{1/2}} \varphi(\mathbf{y}) \right| \mathrm{d}s(\mathbf{y}),$$

from which it follows that

$$\|u_{BS}^{\text{inc}}\|_{L^\infty(\Omega_+ \setminus Z)} \lesssim k^{-1/2}\|\varphi\|_{L^2(\gamma)}. \tag{3.25}$$

(ii) Secondly, the bound on $\|u^s\|_{L^\infty(\Omega_+)}$. We start by rewriting the k-weighted norm

$$\begin{aligned}\|u_{BS}^{\text{inc}}\|_{H_k^1(\Omega_+)} &= \left(\int_\Gamma k^2|u_{BS}^{\text{inc}}|^2 + |\nabla_\Gamma u_{BS}^{\text{inc}}|^2\,\mathrm{d}s\right)^{1/2} \\ &= \left(\int_\Gamma k^2|\mathcal{S}_{\gamma\to\Gamma}\varphi|^2 + |\mathcal{D}_{\gamma\to\Gamma}\varphi|^2\,\mathrm{d}s\right)^{1/2} \\ &\lesssim \left(k\|\mathcal{S}\|_{L^2(\gamma)\to L^2(\Gamma)} + \|\mathcal{D}\|_{L^2(\gamma)\to L^2(\Gamma)}\right)\|\varphi\|_{L^2(\gamma)}.\end{aligned}$$

We may bound further using Lemma 5.14(i) and (ii), to obtain

$$\|u_{BS}^{\text{inc}}\|_{H_k^1(\Omega_+)} \lesssim (k^{1/2}+1)\|\varphi\|_{L^2(\gamma)},$$

which when combined with Theorem 3.1(ii) yields

$$\|u^s\|_{L^\infty(\Omega_+)} \lesssim \log^{1/2} k\|\varphi\|_{L^2(\gamma)}, \tag{3.26}$$

for $k \geq k_0$.

(iii) Thirdly, the bound on $\|u_{BS}^{\text{inc}}\|_{\mathcal{L}(Z)}$. Using the definition (3.11) of the $\mathcal{L}(Z)$ norm, we may write

$$\begin{aligned}\sup_{c,\theta}\left(\int_{\ell_{c,\theta}\cap Z}|u_{BS}^{\text{inc}}|^2\,\mathrm{d}s\right)^{1/2} &= \sup_{c,\theta}\left(\int_{\ell_{c,\theta}\cap Z}\left|\int_\gamma \Phi(\mathbf{x},\mathbf{y})\varphi(\mathbf{y})\,\mathrm{d}s(\mathbf{y})\right|^2\mathrm{d}s(\mathbf{x})\right)^{1/2} \\ &\leq \sup_{c,\theta}\left(\int_{\ell_{c,\theta}\cap Z}\left(\int_\gamma \frac{1}{4}\sqrt{\frac{2}{k\pi|\mathbf{x}-\mathbf{y}|}}|\varphi(\mathbf{y})|\,\mathrm{d}s(\mathbf{y})\right)^2\mathrm{d}s(\mathbf{x})\right)^{1/2}\end{aligned}$$

using the bound on the Hankel function (A.7) once more. It then follows by [7, Lemma 3.2(a)] that

$$\|u_{BS}^{\text{inc}}\|_{\mathcal{L}(Z)} \lesssim k^{-1/2}\|\varphi\|_{L^2(\gamma)}. \tag{3.27}$$

Combining (3.25)-(3.27) with the definition (3.21) yields the result for $M_Z(u)$. The result for $M_\infty(u)$ follows by taking the limit as the region Z shrinks towards a set of measure zero. □

We note that Theorems 3.11 and 3.12 imply $M(u) = M_Z(u) \lesssim \log^{1/2} k$ for sufficiently large k, which is sharper in its k-dependence than the plane wave case of Remark 2.5, for which the corresponding bound is $M(u) = M_\infty(u) \lesssim k^{1/2}\log^{1/2} k$. It should be noted that this bound is not believed to be sharp, as numerical experiments suggest $M(u) = O(1)$ for for plane wave incidence (see [35, §6]). These theorems, coupled with Theorem 3.10 show that Assumption 2.4 holds for the point source and beam source incidence, therefore exponential convergence of the HNA method is predicted by Theorem 2.14.

3.2.3 Numerical experiments for the point source

We now demonstrate via numerical examples the effectiveness of the Hybrid Numerical Asymptotic method for the point source problem. Specifically we consider the problems where Ω_- is an equilateral triangle ($n_\Gamma = 3$) with $L_j = 2\pi$ for $j = 1, \ldots, n_\Gamma$, with incident field $u_{PS}^{\text{inc}}(\mathbf{x}; \mathbf{s})$ for a range of $\mathbf{s}$ which will be introduced shortly. Figure 3.10 plots the approximation u to both problems, whilst Figure 3.12 plots the boundary solution ν_p of §2.3 for the triangle and regular pentagon ($n_\Gamma = 5$). In both cases the absolute value of the boundary solution is largest at the point of the boundary which is closest to the source. This is largely accounted for by the geometrical optics component Ψ_{PS}.

We solve using the classical combined formulation (Definition 1.2) using the Galerkin method outlined in §2.3, on a single mesh, hence (referring to (2.11)) we seek $v_N \in \overline{V}_N^{\text{HNA}}(\Gamma)$ such that

$$(\mathcal{A}_{k,\eta} v_N, \varphi)_{L^2(\Gamma)} = \frac{1}{k} (f - \mathcal{A}_{k,\eta} \Psi_{\text{PS}}, \varphi)_{L^2(\Gamma)}, \quad \text{for all } \varphi \in \overline{V}_N^{\text{HNA}}(\Gamma), \tag{3.28}$$

where Ψ_{PS} is as in (3.13). For the mesh parameters of §2.2 we introduce some polynomial dependence on α_j (of (2.7)), choosing $\alpha_j = \min((1 + (\mathbf{p}_j)_i)/8, 2)$, where i corresponds to the ith mesh element on the jth side. The result of Theorem 2.9 still holds, given that α_j is bounded above by a constant independent of the polynomial degree. We choose $c_j = 2$ (of Theorem 2.9), and we choose the polynomial degree vectors $\mathbf{p}_j$ in accordance with Remark 2.10. We compute all inner products in the Galerkin method using the quadrature routines discussed in Appendix B. We note also that the set Z discussed throughout this section is not a parameter of the numerical method; we require only that such a Z exists. Convergence analysis was run for $k \in \{5, 10, 20, 40, 80, 160\}$ with $p \in \{1, \ldots, 7\}$, taking $p = 8$ as the reference solution. The approximation was also validated by means of comparison against a standard BEM solution, we do not give these results here. For the triangle, the vertices are

$$\mathbf{P}_1 = \begin{pmatrix} 2\pi/\sqrt{3} \\ 0 \end{pmatrix}, \quad \mathbf{P}_2 = \begin{pmatrix} -\pi/\sqrt{3} \\ \pi \end{pmatrix}, \quad \mathbf{P}_3 = \begin{pmatrix} -\pi/\sqrt{3} \\ -\pi \end{pmatrix},$$

whilst the point sources we consider are emanating from

$$\mathbf{s}_1 = \begin{pmatrix} 1 \\ 4 \end{pmatrix}, \quad \mathbf{s}_2 = \begin{pmatrix} 4 \\ 0 \end{pmatrix}, \quad \mathbf{s}_3 = \begin{pmatrix} -\pi/\sqrt{3} \\ -4 \end{pmatrix}.$$

Figures 3.8 and 3.9 show the convergence of the HNA Galerkin method for each of the three cases for the triangle, which are depicted in Figure (3.7). In each case

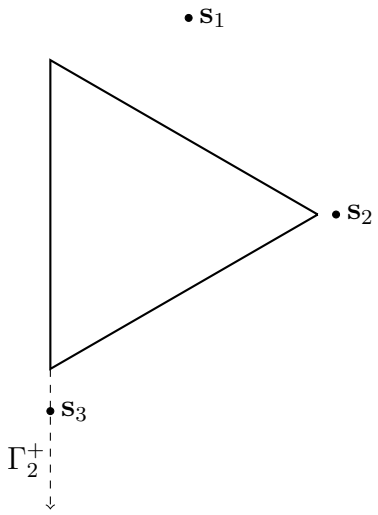

Figure 3.7: Schematic of triangular scatterer Ω_- with position of each source point

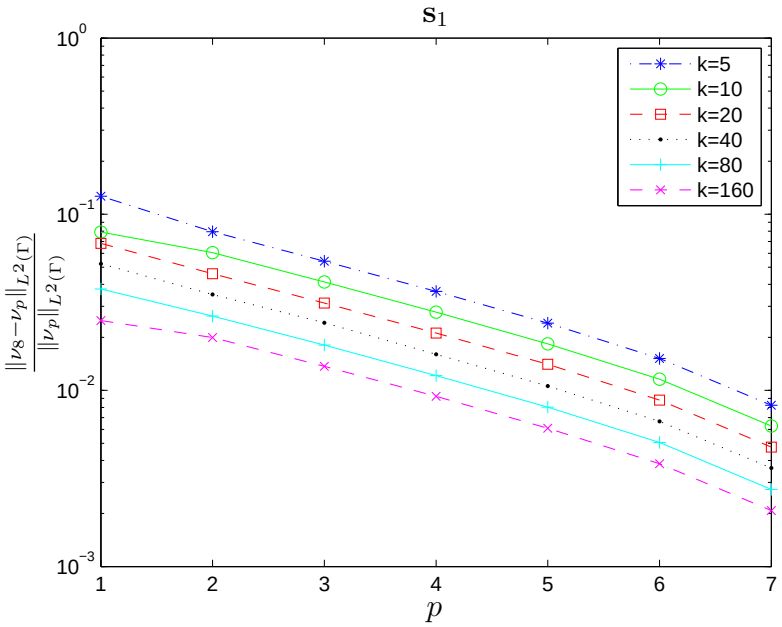

Figure 3.8: Relative $L^2(\Gamma)$ errors for the triangle, for source point $\mathbf{s}_1$.

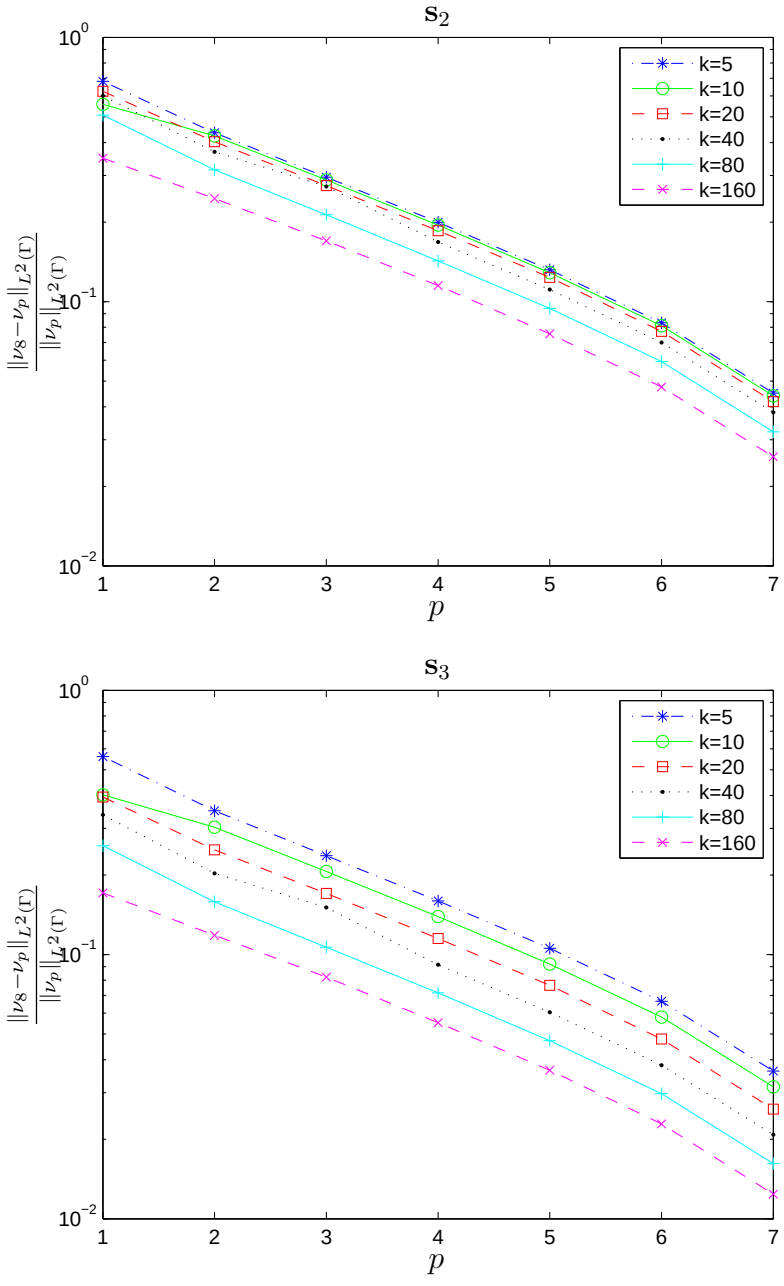

Figure 3.9: Relative $L^2(\Gamma)$ errors for the triangle, for source point $\mathbf{s}_2$ and $\mathbf{s}_3$.

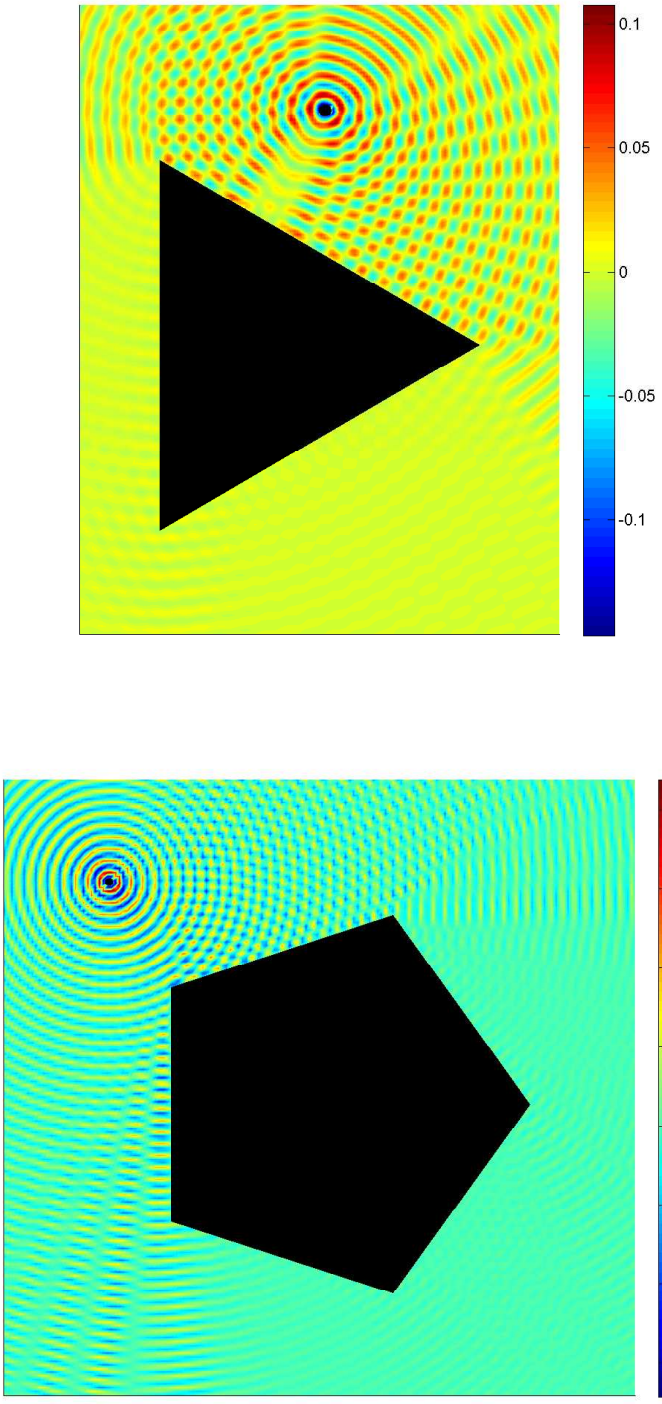

Figure 3.10: Real part of u_N for $p = 8$ in Ω_+ for the regular triangle and the pentagon, with wavenumber $k = 20$. The source point $\mathbf{s}$ is covered by a set $Z = B_{1/k}(\mathbf{s})$ inside which we do not evaluate u. This was done for aesthetic reasons; the colourbar scale would be skewed for large values of $\Phi(\mathbf{x}, \mathbf{s})$, when $\mathbf{x}$ is close to $\mathbf{s}$.

we observe similar rates of exponential convergence. Moreover, for fixed p the error does not increase with k, indeed it can be seen to decrease, which demonstrates the frequency independence of our approach. For a source point $\mathbf{s}_1$, we observe the lowest relative errors, which can be explained as the source is furthest away from Ω_- in this case. Theorem (3.11) suggests that $M_Z(u)$ of (3.21) grows with $1/\sqrt{\text{dist}(\mathbf{s}, \Omega_-)}$. The point $\mathbf{s}_2$ is closer to Ω_- than $\mathbf{s}_1$, with distance $|\mathbf{s}_2 - \mathbf{P}_1| \approx 0.372$, for which the rate of convergence appears to be shifted by a multiplicative constant which further justifies the hypothesis that convergence is weaker for source point closer to Γ. The point $\mathbf{s}_3$ was chosen to lie on the extended line Γ_2^+, such that the integrand of (3.2) is unbounded, as the path of integration contains a singularity. This confirms the theoretical result that the HNA method will converge exponentially, even if the solution u is unbounded on the extended line (as previous analyses of HNA methods would not explain this). The method can be seen to converge similarly for $\mathbf{s}_3$, which is to be expected given the distance is $|\mathbf{s}_3 - \mathbf{P}_3| \approx 0.858$, $\mathbf{s}_3$ is a similar distance from Ω_- as $\mathbf{s}_2$.

Figure 3.11 shows how the conditioning of the discrete system grows with p and k. Recall from §2.2 that the conditioning of the discrete system depends closely on the choice of α_j, which here is chosen to be $\min((1+(\mathbf{p}_j)_i)/8, 2)$. It is difficult to determine trends in the conditioning from this plot, for lower wavenumbers $k = 5, 20, 40$ the conditioning appears to peak, and then drop for higher p. If poor conditioning causes the system to become unstable, a larger value of α_j should be chosen, removing unnecessary basis elements. This can be done without computation of any further inner products; carefully selected rows and columns from the discrete system can be removed to achieve this.

Implementation of the beam source problem follows similarly, although we do not present any results here. In such a case, the right hand side will contain a triple integral $(\mathcal{A}\Psi_{\text{BS}}, \phi)_{L^2(\Gamma)}$ for basis function ϕ, as in this instance Ψ_{BS} itself contains an integral.

3.3 Conclusions and further work

In this chapter we have developed theory that proves the HNA method converges exponentially for Herglotz-type, point and beam source incidence. This was demonstrated by numerical examples for the case of the point source.

A key development for future work is to generalise the density of the beam source term to $H^{-1/2}(\gamma)$, rather than $H^{-1/2+\epsilon}(\gamma)$ for $\epsilon > 0$ that has been explored here. This would be essential for analysis of iterative HNA methods for multiple screen

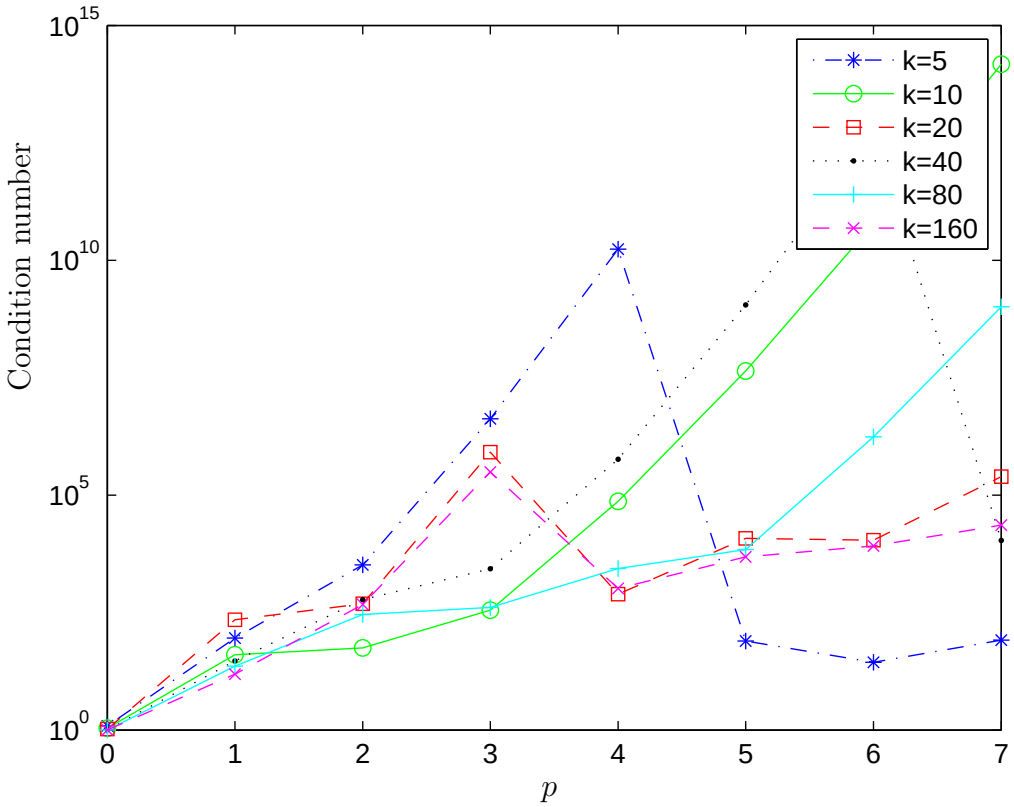

Figure 3.11: Plot of condition number of Galerkin matrices against k and p, for the triangle problem.

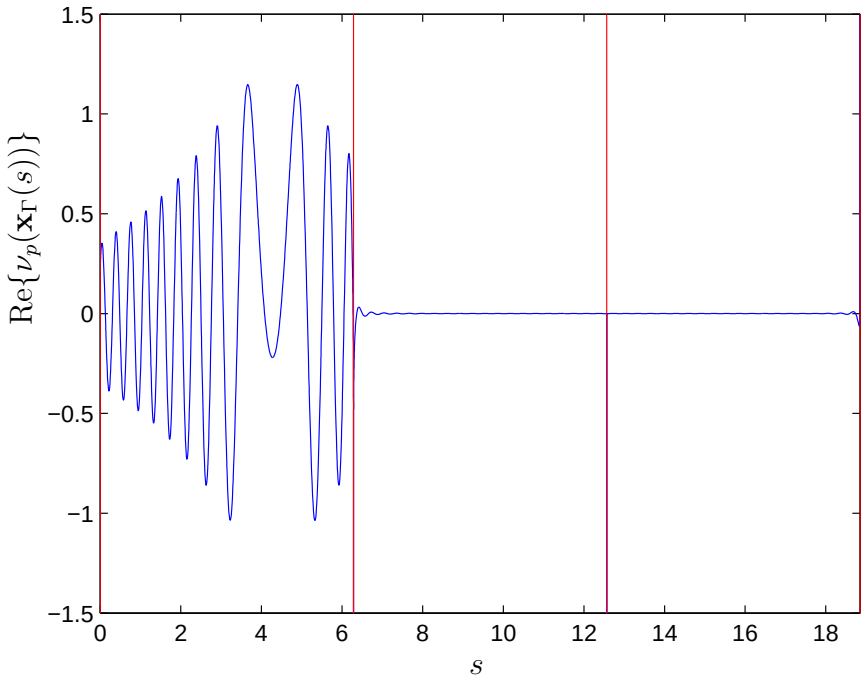

(a)

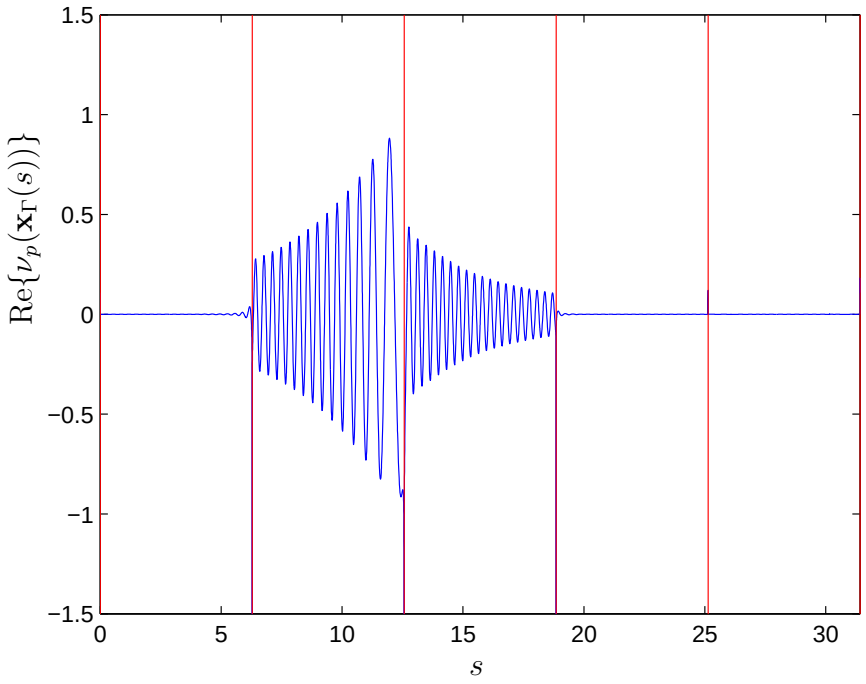

(b)

Figure 3.12: Plot of real part of boundary solution, for the problems depicted in Figure 3.10 (a) and (b).

problems, which we plan to address in future work (see Chapter 8). Alternatively, the methods in this Chapter may be combined with non-convex polygons of [15], or the penetrable obstacles of [31].

Chapter 4

HNA BEM for multiple scattering problems

The results produced in this chapter will appear in [27], and were summarised in [11].

The multiple scattering formulation that we will present in this chapter may be considered a natural extension of the beam source problem of Definition 3.6(ii). The key difference is that the density φ, which is a known parameter for the beam source single scattering problem, becomes the unknown $-(\partial_{\mathbf{n}}^{+}u)|_{\gamma}$, where the source γ becomes the boundary of the other scatterer(s) in the multiple obstacle scattering problem. This can be easily demonstrated via two alternate interpretations of the following example. Considering the BVP (1.4)–(1.6) of plane wave incidence, we let Γ denote the boundary of a bounded Lipschitz open set Ω_{Γ}. Now we extend this problem twice, to two different but related problems, and let γ be *either* the boundary of another Lipschitz open set disjoint from Ω_{Γ}, *or* the source line of a beam source, which is an additional source of incidence to the plane wave, hence the sum of both sources makes up the incident field. We consider the two problems,

(i) Single scattering by a sound-soft obstacle with Lipschitz boundary $\Gamma = \partial\Omega$ by a beam emanating from γ with density $\varphi \in L^2(\gamma)$ *and* a plane wave $\mathrm{e}^{\mathrm{i}k\mathbf{d}\cdot\mathbf{x}}$ with incident direction $\mathbf{d}$.

(ii) Multiple scattering by two sound soft obstacles, with Lipschitz boundaries Γ and γ, scattering by a plane wave with incident direction $\mathbf{d}$.

Taking note of the representation (1.10), which applies to either case, we have

$$u = u^{\mathrm{inc}} - S_k \partial_{\mathbf{n}}^{+} u, \quad \text{in } \Omega_{+},$$

where in problem (i) the integral operator S_k of (1.11) is over Γ, and in problem (ii) S_k is over $\Gamma \cup \gamma$. Writing the integrals in full illustrates the equivalence of these two

problems, we see that the equation is the same, but the meaning of its terms changes,

$$u(\mathbf{x}) = \overbrace{\mathrm{e}^{\mathrm{i}k\mathbf{x}\cdot\mathbf{d}}}^{=u^{\mathrm{inc}}(\mathbf{x}) \text{ for problem (i), } \varphi \text{ known}} \underbrace{+ \int_\gamma \Phi(\mathbf{x},\mathbf{y})\varphi(\mathbf{y})\,\mathrm{d}s(\mathbf{y}) - \int_\Gamma \Phi(\mathbf{x},\mathbf{y})\frac{\partial u}{\partial \mathbf{n}}(\mathbf{y})\,\mathrm{d}s(\mathbf{y})}_{=u^s(\mathbf{x})=-S_k\partial^+_{\mathbf{n}}u \text{ for problem (ii), with unknown } \varphi=-[\partial u/\partial \mathbf{n}]|_\gamma}, \quad \mathbf{x}\in\Omega_+, \qquad (4.1)$$

$$\overbrace{\qquad\qquad\qquad\qquad\qquad\qquad}^{=u^s=-S_k\partial^+_{\mathbf{n}}u \text{ for problem (i)}}$$

whilst the first right-hand side term $\mathrm{e}^{\mathrm{i}k\mathbf{x}\cdot\mathbf{d}}$ is the incident field for problem (ii). The interpretation depends on whether φ is a known or unknown density. It follows that every multiple scattering problem (ii) has an associated single obstacle beam source problem (i), with $\varphi = -(\partial^+_{\mathbf{n}}u)|_\gamma$.

In this chapter, we consider the problem of scattering by multiple sound-soft scatterers, at least one of which is a convex polygon. The aim is to use the HNA basis of §2.2 on the convex polygon, coupled with a standard basis on the other scatterers, to reduce the dimension of the approximation space that is required to solve the problem. To do this, in §4.3 we extend our ansatz (2.2), such that leading order behaviour from other obstacles is also accounted for. As was the requirement for extensions of the HNA method in Chapter 3, we show that the diffracted waves satisfy Assumption 2.4, to guarantee exponential convergence of our scheme. In §4.4 we outline the procedure for a Galerkin BEM, and present numerical results in §4.5.

4.1 Specific problem statement

Here we have more than one scattering obstacle, which we denote by $\Omega_- := \Omega_\Gamma \cup \Omega_\gamma$, where Ω_Γ is a convex polygon with boundary Γ, remaining consistent with other polygonal parameters of Definition 2.3. The other obstacle(s) $\Omega_\gamma := \bigcup_{i=1}^{N_\gamma} \Omega_i$ consist of $N_\gamma \in \mathbb{N}$ connected Lipschitz open sets Ω_i, each pairwise disjoint with piecewise C^1 boundary γ_i. Denote the interior of the convex polygon by $\Omega_\Gamma \subset \mathbb{R}^2$ and its boundary by $\Gamma := \partial\Omega_\Gamma$. We denote the combined Lipschitz boundary of Ω_γ by $\gamma := \partial\Omega_\gamma$. We assume that the distance between Γ and γ is positive, so that $\partial\Omega$ is Lipschitz.

Given the scattering obstacles Ω_-, we aim to solve the BVP (1.4)-(1.6) with the incident field

$$u^{\mathrm{inc}}(\mathbf{x}) = u^{\mathrm{inc}}_{PW}(\mathbf{x};\alpha) := \mathrm{e}^{\mathrm{i}k\mathbf{d}_\alpha\cdot\mathbf{x}}, \quad \text{where } \mathbf{d}_\alpha := (\cos\alpha, \sin\alpha),$$

$\mathbf{x}\in\mathbb{R}^2$ and $k>0$ is the wavenumber. Although plane wave incidence is considered in this chapter, we believe that it would be straightforward to combine the incident fields of Chapter 3 with the multiple obstacle configurations considered here. This is discussed further in Remark 4.6.

4.2 Boundary representation

The aim of this section is to extend the representation of [16, eq. (3.5)] for $\partial^+_{\mathbf{n}} u$ on Γ to account for the contribution from other scatterer(s) Ω_γ. Proceeding as in [16, §3], and in §3.2.1 and §3.1, extending a side Γ_j and solving the resulting half-plane problem, we can obtain an explicit representation for $\partial^+_{\mathbf{n}} u$ on Γ_j in terms of known oscillatory functions on Γ_j and $\partial^+_{\mathbf{n}} u$ on γ. This representation will form the ansatz used for the boundary element method. Although parallels were drawn at the start of this chapter between the beam source and the multiple scattering problem, a different derivation to the boundary representation of §3.2.1 is required to ensure the boundary conditions (1.5) are satisfied.

Considering a single side Γ_j of Ω_Γ, $1 \leq j \leq n_\Gamma$, we define Γ_j^+ and Γ_j^- as the infinite extensions of Γ_j in the clockwise and anti-clockwise directions (about the interior Ω_Γ) respectively (see Figure 4.1). As defined at the start of Chapter 3, for $j = 1, \ldots n_\Gamma$ we define $\Gamma_j^\infty := \Gamma_j^+ \cup \Gamma_j \cup \Gamma_j^-$ with U_j the half-plane with boundary Γ_j^∞, always chosen such that Ω_Γ does not lie inside U_j. In addition, when u or u^s is on $\Gamma \cup \gamma$, it is assumed that the exterior trace has been taken. We construct an open ball B_R of radius R centred at the origin, with R chosen sufficiently large that $U_j \cap \Omega_\gamma \subset B_R$, i.e. all the scatterers in the relative upper half-plane lie inside the ball.

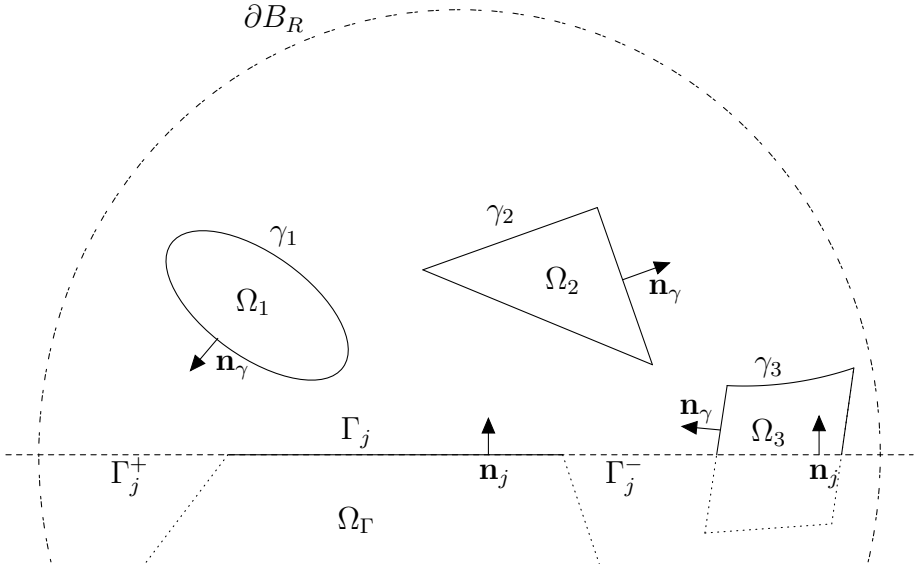

Figure 4.1: Configuration with (at least) four scatterers. The relative upper-half plane U_j is the area above the line $\Gamma_j^\infty = \Gamma_j^- \cup \Gamma_j \cup \Gamma_j^+$. Note the intersection of Ω_3 (the right-hand scatterer) with $\Gamma_j^- \subset \Gamma_j^\infty$; $\mathbf{n}_j$ points into $\Omega_3 \cap U_j$ whilst $\mathbf{n}_\gamma$ on γ_3 points out of $\Omega_3 \cap U_j$ and into $\Omega_+ \cap U_j$.

Green's second identity can now be applied to $G_j(\mathbf{x},\cdot)$ and u^s on $\Omega_+\cap U_j\cap B_R$ to obtain for $\mathbf{x}\in U_j$

$$\begin{aligned}u^s(\mathbf{x}) &= \int_{\partial(\Omega_+\cap U_j\cap B_R)}\left[\frac{\partial G_j(\mathbf{x},\mathbf{y})}{\partial \mathbf{n}(\mathbf{y})}u^s(\mathbf{y}) - G_j(\mathbf{x},\mathbf{y})\frac{\partial u^s}{\partial \mathbf{n}}(\mathbf{y})\right]\mathrm{d}s(\mathbf{y})\\ &= 2\int_{\Gamma_j^\infty\cap B_R\setminus\Omega_\gamma}\frac{\partial\Phi(\mathbf{x},\mathbf{y})}{\partial\mathbf{n}_j(\mathbf{y})}u^s(\mathbf{y})\,\mathrm{d}s(\mathbf{y})\\ &\quad+\int_{\gamma\cap U_j}\left[\frac{\partial G_j(\mathbf{x},\mathbf{y})}{\partial\mathbf{n}_\gamma(\mathbf{y})}u^s(\mathbf{y}) - G_j(\mathbf{x},\mathbf{y})\frac{\partial u^s(\mathbf{y})}{\partial\mathbf{n}_\gamma}\right]\mathrm{d}s(\mathbf{y})\\ &\quad-\int_{\partial B_R\cap U_j}\left[\frac{\partial G_j(\mathbf{x},\mathbf{y})}{\partial r}u^s(\mathbf{y}) - G_j(\mathbf{x},\mathbf{y})\frac{\partial u^s(\mathbf{y})}{\partial r}\right]\mathrm{d}s(\mathbf{y}).\end{aligned}\tag{4.2}$$

Throughout this derivation, we often replace $\partial/\partial\mathbf{n}$ by the more specific $\partial/\partial\mathbf{n}_j$ or $\partial/\partial\mathbf{n}_\gamma$, to make clearer which direction the normal derivative is being taken. Note that $\partial/\partial\mathbf{n}_j = \mathbf{n}_j\cdot\nabla$ and $\partial/\partial\mathbf{n}_\gamma = \mathbf{n}_\gamma\cdot\nabla$, where $\mathbf{n}_j$ and $\mathbf{n}_\gamma$ are the unit normal vector fields pointing into $\Omega_+\cap U_j\cap B_R$ from $\Gamma_j^\infty\cap B_R\setminus\Omega_\gamma$ and from $\gamma\cap U_j$, respectively, whilst $\partial/\partial r = \frac{\mathbf{y}}{|\mathbf{y}|}\cdot\nabla$ denotes the normal derivative on $\partial B_R\cap U_j$ pointing out of $\Omega_+\cap U_j\cap B_R$. We have used that $\partial G_j(\mathbf{x},\mathbf{y})/\partial\mathbf{n}_j(\mathbf{y}) = 2\partial\Phi(\mathbf{x},\mathbf{y})/\partial\mathbf{n}_j(\mathbf{y})$ and $G(\mathbf{x},\mathbf{y}) = 0$ for $\mathbf{y}\in\Gamma_j^\infty$. As $R\to\infty$, the third integral vanishes by the same reasoning as, e.g., [17, Theorem 2.4]. The representation (4.2) then becomes

$$u^s(\mathbf{x}) = 2\int_{\Gamma_j^\infty\setminus\Omega_\gamma}\frac{\partial\Phi(\mathbf{x},\mathbf{y})}{\partial\mathbf{n}_j(\mathbf{y})}u^s(\mathbf{y})\,\mathrm{d}s(\mathbf{y})\tag{4.3}$$

$$+\int_{\gamma\cap U_j}\left[\frac{\partial G_j(\mathbf{x},\mathbf{y})}{\partial\mathbf{n}_\gamma(\mathbf{y})}u^s(\mathbf{y}) - G_j(\mathbf{x},\mathbf{y})\frac{\partial u^s(\mathbf{y})}{\partial\mathbf{n}_\gamma}\right]\mathrm{d}s(\mathbf{y}),\tag{4.4}$$

for $\mathbf{x}\in U_j\setminus\Omega_\gamma$. We apply Green's second identity to u_{PW}^{inc} and $G_j(\mathbf{x},\mathbf{y})$ in $\Omega_\gamma\cap U_j$ and obtain, for $\mathbf{x}\in\Omega_+\cap U_j$,

$$\begin{aligned}&\left(\int_{\gamma\cap U_j} - \int_{\Gamma_j^\infty\cap\Omega_\gamma}\right)\left[\frac{\partial G_j(\mathbf{x},\mathbf{y})}{\partial\mathbf{n}(\mathbf{y})}u_{PW}^{\mathrm{inc}}(\mathbf{y}) - G_j(\mathbf{x},\mathbf{y})\frac{\partial u_{PW}^{\mathrm{inc}}}{\partial\mathbf{n}}(\mathbf{y})\right]\mathrm{d}s(\mathbf{y})\\ &\qquad=\int_{\Omega_\gamma\cap U_j}\left[\Delta G_j(\mathbf{x},\mathbf{y})u_{PW}^{\mathrm{inc}}(\mathbf{y}) - G_j(\mathbf{x},\mathbf{y})\Delta u_{PW}^{\mathrm{inc}}(\mathbf{y})\right]\mathrm{d}V(\mathbf{y}) = 0,\end{aligned}\tag{4.5}$$

as u_{PW}^{inc} and $\Phi(\mathbf{x},\cdot)$ satisfy the Helmholtz equation (1.4) in Ω_γ for $\mathbf{x}\in\Omega_+\cap U_j$. The sign of the boundary integral differs on the two parts of $\partial(\Omega_\gamma\cap U_j) = (\gamma\cap U_j)\cup(\Omega_\gamma\cap\Gamma_j^\infty)$ because the normal derivative $\partial/\partial\mathbf{n}$ involves the outward-pointing normal vector $\mathbf{n}_\gamma$ on $\gamma\cap U_j$ and the inward-pointing normal $\mathbf{n}_j$ on $\Omega_\gamma\cap\Gamma_j^\infty$, as depicted in Figure 4.1. We use $u^s = u - u_{PW}^{\mathrm{inc}}$ to expand the last term in (4.4): for $\mathbf{x}\in\Omega_+\cap U_j$

$$\int_{\gamma\cap U_j}\left[\frac{\partial G_j(\mathbf{x},\mathbf{y})}{\partial\mathbf{n}_\gamma(\mathbf{y})}u^s(\mathbf{y}) - G_j(\mathbf{x},\mathbf{y})\frac{\partial u^s}{\partial\mathbf{n}_\gamma}(\mathbf{y})\right]\mathrm{d}s(\mathbf{y})$$

$$= \int_{\gamma\cap U_j} \left[\frac{\partial G_j(\mathbf{x},\mathbf{y})}{\partial \mathbf{n}_\gamma(\mathbf{y})} \big(\underbrace{u(\mathbf{y})}_{=0} - u^{\rm inc}_{PW}(\mathbf{y}) \big) - G_j(\mathbf{x},\mathbf{y}) \frac{\partial (u - u^{\rm inc}_{PW})}{\partial \mathbf{n}_\gamma}(\mathbf{y}) \right] \mathrm{d}s(\mathbf{y})$$

$$\overset{(4.5)}{=} - \int_{\gamma\cap U_j} G_j(\mathbf{x},\mathbf{y}) \frac{\partial u}{\partial \mathbf{n}_\gamma}(\mathbf{y})\, \mathrm{d}s(\mathbf{y})$$

$$+ \int_{\Gamma_j^\infty\cap\Omega_\gamma} \left[-\frac{\partial G_j(\mathbf{x},\mathbf{y})}{\partial \mathbf{n}_j(\mathbf{y})} u^{\rm inc}_{PW}(\mathbf{y}) + G_j(\mathbf{x},\mathbf{y}) \frac{\partial u^{\rm inc}_{PW}}{\partial \mathbf{n}_\gamma}(\mathbf{y}) \right] \mathrm{d}s(\mathbf{y}).$$

Substituting this expression in (4.4) and using again

$$\frac{\partial G_j(\mathbf{x},\mathbf{y})}{\partial \mathbf{n}_j(\mathbf{y})} = 2 \frac{\partial \Phi(\mathbf{x},\mathbf{y})}{\partial \mathbf{n}_j(\mathbf{y})}$$

and $G_j(\mathbf{x},\mathbf{y}) = 0$ on Γ_j^∞ we obtain a representation for u^s,

$$u^s(\mathbf{x}) = 2 \int_{\Gamma_j^\infty\setminus\Omega_\gamma} \frac{\partial \Phi(\mathbf{x},\mathbf{y})}{\partial \mathbf{n}_j(\mathbf{y})} u^s(\mathbf{y})\, \mathrm{d}s(\mathbf{y}) - \int_{\gamma\cap U_j} G_j(\mathbf{x},\mathbf{y}) \frac{\partial u(\mathbf{y})}{\partial \mathbf{n}_\gamma}\, \mathrm{d}s(\mathbf{y})$$
$$- 2 \int_{\Gamma_j^\infty\cap\Omega_\gamma} \frac{\partial \Phi(\mathbf{x},\mathbf{y})}{\partial \mathbf{n}_j(\mathbf{y})} u^{\rm inc}_{PW}(\mathbf{y})\, \mathrm{d}s(\mathbf{y}), \qquad \mathbf{x} \in \Omega_+ \cap U_j. \tag{4.6}$$

The final term of (4.6) will be non-zero only if $\Gamma_j^\infty \cap \Omega_\gamma \neq \emptyset$, namely, in case one of the components of γ is aligned with one of the sides of Γ (see Figure 4.1).

This integral representation must be combined with one for $u^{\rm inc} = u^{\rm inc}_{PW}$ to construct a useful representation for $\partial^+_{\mathbf{n}} u$ on Γ_j. The half-plane representation of (3.1) can be applied to upward propagating plane waves (see [10, §3]). We consider first the case $\mathbf{n}_j \cdot \mathbf{d} \geq 0$, where Γ_j is in shadow: from [16, eq. (3.3)]

$$u^{\rm inc}_{PW}(\mathbf{x}) = 2 \int_{\Gamma_j^\infty} \frac{\partial \Phi(\mathbf{x},\mathbf{y})}{\partial \mathbf{n}_\gamma(\mathbf{y})} u^{\rm inc}_{PW}(\mathbf{y})\, \mathrm{d}s(\mathbf{y}), \quad \mathbf{x} \in U_j.$$

Adding this to (4.6) and taking the Neumann trace on Γ_j, we obtain a representation for the solution

$$\frac{\partial u}{\partial \mathbf{n}}(\mathbf{x}) = 2 \int_{\Gamma_j^\infty\setminus\Omega_\gamma} \frac{\partial^2 \Phi(\mathbf{x},\mathbf{y})}{\partial \mathbf{n}_j(\mathbf{x}) \partial \mathbf{n}_j(\mathbf{y})} u(\mathbf{y})\, \mathrm{d}s(\mathbf{y})$$
$$- 2 \int_{\gamma\cap U_j} \frac{\partial \Phi(\mathbf{x},\mathbf{y})}{\partial \mathbf{n}_j(\mathbf{x})} \frac{\partial u}{\partial \mathbf{n}_\gamma}(\mathbf{y})\, \mathrm{d}s(\mathbf{y}), \qquad \mathbf{x} \in \Gamma_j, \quad \mathbf{n}_j \cdot \mathbf{x} \geq 0. \tag{4.7}$$

For a downward-propagating wave $\mathbf{n}_j \cdot \mathbf{d} < 0$, we can apply the same result to the lower half-plane $\mathbb{R}^2 \setminus \overline{U}_j$ (where the direction of the normal is reversed)

$$u^{\rm inc}_{PW}(\mathbf{x}) = -2 \int_{\Gamma_j^\infty} \frac{\partial \Phi(\mathbf{x},\mathbf{y})}{\partial \mathbf{n}_j(\mathbf{y})} u^{\rm inc}_{PW}(\mathbf{y})\, \mathrm{d}s(\mathbf{y}), \quad \mathbf{x} \in \mathbb{R}^2 \setminus \overline{U}_j.$$

Now define $u^r(\mathbf{x}) := -u^{\rm inc}_{PW}(\widetilde{\mathbf{x}}^j)$ for $\mathbf{x} \in U_j$. Intuitively, u^r may be considered the reflection of $u^{\rm inc}_{PW}$ by a sound-soft line at Γ_j^∞. It follows that

$$u^r(\mathbf{x}) = 2\int_{\Gamma_j^\infty} \frac{\partial\Phi(\widetilde{\mathbf{x}}^j,\mathbf{y})}{\partial\mathbf{n}_j(\mathbf{y})} u^{\rm inc}_{PW}(\mathbf{y})\,{\rm d}s(\mathbf{y}) = -2\int_{\Gamma_j^\infty} \frac{\partial\Phi(\mathbf{x},\mathbf{y})}{\partial\mathbf{n}_j(\mathbf{y})} u^{\rm inc}_{PW}(\mathbf{y})\,{\rm d}s(\mathbf{y}),$$

rearranging this and adding $u^{\rm inc}_{PW}$ gives

$$u^{\rm inc}_{PW}(\mathbf{x}) = u^{\rm inc}_{PW}(\mathbf{x}) + u^r(\mathbf{x}) + 2\int_{\Gamma_j^\infty} \frac{\partial\Phi(\mathbf{x},\mathbf{y})}{\partial\mathbf{n}_j(\mathbf{y})} u^{\rm inc}_{PW}(\mathbf{y})\,{\rm d}s(\mathbf{y}).$$

Summing with (4.6) and taking the Neumann trace gives the representation for $\partial^+_{\mathbf{n}} u$ on Γ_j:

$$\begin{aligned}\frac{\partial u}{\partial\mathbf{n}}(\mathbf{x}) = 2\frac{\partial u^{\rm inc}_{PW}}{\partial\mathbf{n}}(\mathbf{x}) &+ 2\int_{\Gamma_j^\infty\setminus\Omega_\gamma} \frac{\partial^2\Phi(\mathbf{x},\mathbf{y})}{\partial\mathbf{n}_j(\mathbf{x})\partial\mathbf{n}_j(\mathbf{y})} u(\mathbf{y})\,{\rm d}s(\mathbf{y}) \\ &- 2\int_{\gamma\cap U_j} \frac{\partial\Phi(\mathbf{x},\mathbf{y})}{\partial\mathbf{n}_j(\mathbf{x})}\frac{\partial u}{\partial\mathbf{n}_\gamma}(\mathbf{y})\,{\rm d}s(\mathbf{y}), \qquad \mathbf{x}\in\Gamma_j, \quad \mathbf{n}_j\cdot\mathbf{x} < 0. \end{aligned} \tag{4.8}$$

It is interesting to compare (4.7) and (4.8) with the single scattering representation (3.2). Here we have an extra term, arising from the presence of additional scatterers Ω_γ inside U_j.

We now write more explicitly the integral representation (4.7)–(4.8) in terms of the parametrisations of the segments Γ_j and of their extensions Γ_j^∞. We use (4.7)–(4.8) to represent the solution on a single side Γ_j, extending the ansatz (2.2) to multiple scattering problems

$$\boxed{\frac{\partial u}{\partial\mathbf{n}}\big(\mathbf{x}_\Gamma(s)\big) = \Psi_{\rm PW}\big(\mathbf{x}_\Gamma(s)\big) + v_j^+(s-\widetilde{L}_{j-1})\mathrm{e}^{\mathrm{i}ks} + v_j^-(\widetilde{L}_j - s)\mathrm{e}^{-\mathrm{i}ks} + \mathcal{G}_{\gamma\to\Gamma_j}\left.\frac{\partial u}{\partial\mathbf{n}}\right|_\gamma(\mathbf{x}_\Gamma(s)),}$$

$$\text{for} \quad s\in\left[\widetilde{L}_{j-1},\widetilde{L}_j\right],\ j=1,\ldots,n_\Gamma. \tag{4.9}$$

Here $\Psi_{\rm PW}$ is the Geometrical Optics Approximation (of §2.1) for a plane wave and a single scatterer,

$$\Psi_{\rm PW}(\mathbf{x}) = \begin{cases} 2\mathrm{i}k\mathbf{n}(\mathbf{x})\cdot\mathbf{d}\mathrm{e}^{\mathrm{i}k\mathbf{x}\cdot\mathbf{d}}, & \mathbf{d}\cdot\mathbf{n}(\mathbf{x}) < 0, \\ 0, & \mathbf{d}\cdot\mathbf{n}(\mathbf{x}) \geq 0, \end{cases} \tag{4.10}$$

for $\mathbf{x}\in\Gamma$. In (4.9), the envelopes of the diffracted waves on each side are defined (slightly differently to (2.3)) by

$$v_j^+(s) := \frac{\mathrm{i}k^2}{2}\int_{(0,\infty)\setminus Z_j^+} \mu\big(k(s+t)\big)\mathrm{e}^{\mathrm{i}k(t-\widetilde{L}_{j-1})} u\big(\mathbf{y}_j(\widetilde{L}_{j-1}-t)\big)\,{\rm d}t, \qquad s\in[0,L_j],$$

$$v_j^-(s) := \frac{\mathrm{i}k^2}{2} \int_{(0,\infty)\setminus Z_j^-} \mu\big(k(s+t)\big) \mathrm{e}^{\mathrm{i}k(\widetilde{L}_j+t)} u\big(\mathbf{y}_j(\widetilde{L}_j+t)\big)\,\mathrm{d}t, \qquad s \in [0, L_j], \tag{4.11}$$

where $Z_j^+ := \{t \in \mathbb{R} : \mathbf{y}_j(\widetilde{L}_{j-1} - t) \in \Omega_\gamma\}$ and $Z_j^- := \{t \in \mathbb{R} : \mathbf{y}_j(\widetilde{L}_j + t) \in \Omega_\gamma\}$ are used to exclude the points inside γ from the integral, to remain consistent with (4.7)–(4.8). The interaction operator $\mathcal{G}_{\gamma\to\Gamma_j} : L^2(\gamma) \to H^1(\Gamma_j)$ is defined by

$$\mathcal{G}_{\gamma\to\Gamma_j}\varphi(\mathbf{x}) := -2\int_{\gamma\cap U_j} \frac{\partial\Phi(\mathbf{x},\mathbf{y})}{\partial\mathbf{n}_j(\mathbf{x})}\varphi(\mathbf{y})\,\mathrm{d}s(\mathbf{y}), \quad \mathbf{x} \in \Gamma_j \subset \Gamma, \tag{4.12}$$

for $\varphi \in L^2(\gamma)$ (see Theorem 5.16(ii) for a bound on this mapping). We extend this definition to $\mathcal{G}_{\gamma\to\Gamma} : L^2(\gamma) \to L^2(\Gamma)$ as $(\mathcal{G}_{\gamma\to\Gamma}\varphi)|_{\Gamma_j} := \mathcal{G}_{\gamma\to\Gamma_j}\varphi$ for $j = 1, \ldots, n_\Gamma$ and $\varphi \in L^2(\gamma)$. Bounds on this map are given in Lemma 4.2.

If γ is taken to be empty, this reduces to the single scattering case (2.2) as $Z_j^\pm$ are empty so the representation (2.3) is equivalent to (4.11), also $\mathcal{G}_{\gamma\to\Gamma}\varphi = 0$ if γ is of measure zero.

REMARK 4.1. *The ansatz* (4.9) *is an extension of [16], [35], with an additional term which relates the solution on* Γ *to the solution on* γ*. It is important to note that this additional term is not the only term influenced by* γ *and that one cannot solve for* $v_\pm$ *on a single scatterer and then add the* $\mathcal{G}_{\gamma\to\Gamma}[\partial u/\partial n|_\gamma]$ *term. The reason for this is clear from* (4.11)*: even if* $Z_j^\pm$ *were of measure zero, so that the equation for the diffracted envelope* (4.11) *is identical to the case of a single scatterer, the integral contains* u*, which depends on the configuration* $\partial\Omega$*. Intuitively this makes sense as diffracted waves emanating from the corners of* Γ *will also be influenced by the presence of additional scatterers.*

Some of the error estimates in §4.4 require the following bound on the operator $\mathcal{G}_{\gamma\to\Gamma}$.

LEMMA 4.2 (Bounds on the interaction operator $\mathcal{G}_{\gamma\to\Gamma}$)**.** *For* $\partial\Omega = \Gamma \cup \gamma$ *with* Γ *and* γ *disjoint, we have the following bound on the interaction operator* $\mathcal{G}_{\gamma\to\Gamma}$ *defined in* (4.12)*:*

$$\|\mathcal{G}_{\gamma\to\Gamma}\|_{L^2(\gamma)\to L^2(\Gamma)} \le \sqrt{L_\Gamma L_\gamma}\left(\sqrt{\frac{k}{2\pi\,\mathrm{dist}(\Gamma,\gamma)}} + \frac{1}{\pi\,\mathrm{dist}(\Gamma,\gamma)}\right), \tag{4.13}$$

where L_Γ *and* L_γ *are the perimeter of* Ω_Γ *and* Ω_γ *respectively.*

Proof. For $0 \neq \varphi \in L^2(\gamma)$, using the Cauchy–Schwarz inequality, we can write

$$\begin{aligned}
\frac{\|\mathcal{G}_{\gamma\to\Gamma}\varphi\|_{L^2(\Gamma)}}{\|\varphi\|_{L^2(\gamma)}} &= \frac{1}{\|\varphi\|_{L^2(\gamma)}} \left(\sum_{j=1}^{n_\Gamma} \int_{\Gamma_j} \left| 2 \int_{\gamma\cap U_j} \frac{\partial\Phi(\mathbf{x},\mathbf{y})}{\partial\mathbf{n}(\mathbf{x})} \varphi(\mathbf{y})\,\mathrm{d}s(\mathbf{y}) \right|^2 \mathrm{d}s(\mathbf{x}) \right)^{1/2} \\
&\leq \frac{2}{\|\varphi\|_{L^2(\gamma)}} \left(\int_\Gamma \left\| \frac{\partial\Phi(\mathbf{x},\cdot)}{\partial\mathbf{n}(\mathbf{x})} \right\|^2_{L^2(\gamma)} \|\varphi\|^2_{L^2(\gamma)}\,\mathrm{d}s(\mathbf{x}) \right)^{1/2} \\
&= 2 \left(\int_\Gamma \int_\gamma \left| \frac{\partial\Phi(\mathbf{x},\mathbf{y})}{\partial\mathbf{n}(\mathbf{x})} \right|^2 \mathrm{d}s(\mathbf{y})\,\mathrm{d}s(\mathbf{x}) \right)^{1/2} \\
&\leq 2 \left(\int_\Gamma \mathrm{d}s \int_\gamma \mathrm{d}s \right)^{1/2} \sup_{\mathbf{x}\in\Gamma,\mathbf{y}\in\gamma} \left| \frac{\partial\Phi(\mathbf{x},\mathbf{y})}{\partial\mathbf{n}(\mathbf{x})} \right|.
\end{aligned}$$

The result follows from $H_0^{(1)\prime}(z) = -H_1^{(1)}(z)$ and (A.7), which states that $|H_1^{(1)}(z)| \leq \sqrt{2/(\pi z)} + 2/(\pi z)$ for $z > 0$. □

We remark that the above proof of Lemma 4.2 is a special case of the more general Lemma 5.13 of Chapter 5.

4.3 Regularity estimates

Notational definitions for the parameters of the convex polygon Ω_Γ which are used in this section can be found in Definition 2.3, and remain the same as the single scattering case. As in previous HNA methods for scattering by a plane wave, we choose our constant $M(u)$ of Assumption 2.4 to be

$$M(u) = M_\infty(u) := \sup_{\mathbf{x}\in\Omega_+} |u(\mathbf{x})| \tag{4.14}$$

and as in Chapter 3, we are primarily interested in how $M_\infty(u)$ depends on k, and this is shown in Corollary 4.7.

We now aim to show, as in [16,35] and Chapter 3 (where no additional scatterers were present), that the functions $v_j^\pm$ are complex-analytic, and can be approximated much more efficiently than $\partial_{\mathbf{n}}^+ u|_\Gamma$. This is a key result of [35] for scattering by a single convex polygon, which we update to our multiple scattering formulation by adapting the intermediate results of [35, §3]. We first consider the solution behaviour near the corners.

LEMMA 4.3. *Suppose that $\mathbf{x} \in \Omega_+$ satisfies $r := |\mathbf{x} - \mathbf{P}_j| \in (0, 1/k]$, and $r < \mathrm{dist}(\mathbf{P}_j, \gamma)$. Then there exists a constant $C > 0$, depending only on $\partial\Omega$ and c_* of Definition 2.3, such that (with $M_\infty(u)$ as in (4.14)),*

$$|u(\mathbf{x})| \leq C(kr)^{\pi/\omega_j} M_\infty(u).$$

Proof. Follows exactly the same arguments as [35, Lemma 3.5], with the slight modification to the definition $R_j := \min\{L_{j-1}, L_j, \pi/(2k), \mathrm{dist}(\mathbf{P}_j, \gamma)\}$, which ensures only areas close to the corner $\mathbf{P}_j$ inside Ω_+ are considered. □

THEOREM 4.4. *Assume that $c_r \in (0,1]$ is chosen such that*

$$\mathrm{dist}(\{\mathbf{P}_j, j = 1, \ldots, n_\Gamma\}, \gamma) > c_r/k,$$

and that $u^{inc} \in C^\infty(\mathbb{R}^2)$. Then the functions $v_j^\pm$, for $j = 1, \ldots, n_\Gamma$, are analytic in the right half-plane $\mathrm{Re}[s] > 0$, where they satisfy the bounds

$$|v_j^\pm(s)| \leq \begin{cases} C_j^\pm M_\infty(u)\big(k|ks|^{-\delta_j^\pm} + k(k|s| + c_r)^{-1}\big), & 0 < |s| \leq 1/k, \\ C_j^\pm M_\infty(u) k|ks|^{-1/2}, & |s| > 1/k, \end{cases} \tag{4.15}$$

where $M_\infty(u)$ is as in (4.14), $\delta_j^+, \delta_j^- \in (0, 1/2)$ are given by $\delta_j^+ := 1 - \pi/\omega_j$ and $\delta_j^- := 1 - \pi/\omega_{j+1}$. The constant C_j^+ depends only on c_*, c_r and ω_j, whilst the constant C_j^- depends only on c_*, c_r and ω_{j+1}.

Proof. The analyticity of the functions $v_j^\pm(s)$ in $\mathrm{Re}[s] > 0$ follows from their definition (2.3) and the analyticity of $\mu(s)$ in the same set, which is shown in [35, Lemma 3.4]. The estimate of $|v_j^\pm(s)|$ for $|s| > 1/k$ follows as in the proof of [35, Theorem 3.2]. For $|s| \leq 1/k$, the definition (2.3) of v^+ gives

$$\begin{aligned} |v_j^+(s)| \leq \frac{k^2}{2} \int_{(0, c_r/k)} &\big|\mu\big(k(s+t)\big)\big|\big|u\big(\mathbf{y}_j(\widetilde{L}_{j-1} - t)\big)\big| \,\mathrm{d}t \\ &+ \frac{k^2}{2} \int_{(c_r/k, \infty)\setminus Z_j^+} \big|\mu\big(k(s+t)\big)\big|\big|u\big(\mathbf{y}_j(\widetilde{L}_{j-1} - t)\big)\big| \,\mathrm{d}t. \end{aligned}$$

Since $c_r \leq 1$ and thanks to Lemma 4.3, the first integral is bounded as in the proof of [35, Theorem 3.2], leading to the term $M_\infty(u)k|ks|^{-\delta_j^\pm}$ in the assertion. Using the bound on μ from [35, Lemma 3.4], we control the second integral as

$$\begin{aligned} \frac{k^2}{2} &\int_{(c_r/k, \infty)\setminus Z_j^+} \big|\mu\big(k(s+t)\big)\big|\big|u\big(\mathbf{y}_j(\widetilde{L}_{j-1} - t)\big)\big| \,\mathrm{d}t \\ &\leq C M_\infty(u) k^2 \int_{c_r/k}^\infty \big|k(s+t)\big|^{-3/2} \Big(\big|k(s+t)\big|^{-1/2} + (\pi/2)^{1/2}\Big) \,\mathrm{d}t \\ &\leq C M_\infty(u) k^2 \Big(k^{-2}(|s| + c_r/k)^{-1} + k^{-3/2}(|s| + c_r/k)^{-1/2}\Big) \\ &= C M_\infty(u) k \Big((k|s| + c_r)^{-1} + (k|s| + c_r)^{-1/2}\Big). \end{aligned}$$

The bound in the assertion follows by noting that $k|s| + c_r < 2$ and proving a similar estimate for v^-. □

The constant c_r is small when the scatterers are close together, relative to the wavelength of the problem. Thus the terms containing c_r in the bound of Theorem 4.4 control the effect of the separation between Γ and γ on the singular behaviour of $v_j^{\pm}$. However, the method we present is designed for high-frequency problems, and to maintain $c_r = O(1)$ as k increases, the separation of the scatterers is allowed to decrease inversely proportional to k. Hence, for the configurations that we consider of practical interest in the high-frequency regime, the condition (4.16) of the following corollary will hold.

COROLLARY 4.5. *Suppose that*

$$\operatorname{dist}(\Omega_\Gamma, \gamma) \geq 1/k \tag{4.16}$$

and $u^{inc} \in C^\infty(\mathbb{R}^2)$. It follows that Assumption 2.4(i) holds with $M(u) = M_\infty(u)$.

Proof. Due to the geometrical constraint, we can choose $c_r = 1$ in Theorem 4.4, and thus the second bound of (4.15) can be simplified to

$$|v_j^{\pm}(s)| \leq C_j^{\pm} M_\infty(u) k |ks|^{-\delta_j^{\pm}}, \quad \text{for } 0 < |s| \leq 1/k, \quad j = 1, \ldots, n_\Gamma,$$

thus aligning the bounds of Theorem 4.4 with those of those of Assumption 2.4. □

It follows immediately that the best approximation estimates of Corollary 2.11 hold for the diffracted waves emanating from Γ even if other obstacles Ω_γ are present, provided that they are sufficiently far away from Γ that (4.16) holds.

REMARK 4.6. *The approach of Theorem 4.4 could be extended to any source-type $u^{inc} \in H_{src}(\Omega_+; Z)$, provided that Z does not intersect Ω_γ, by combining with the proof of Theorem 3.10. This would enable us to develop multiple scattering HNA for a broader class of incident fields. For the remainder of this section, we focus on the simpler plane wave case.*

We now aim to understand how the constant $M_\infty(u)$ depends on k, which is key for Assumption 2.4 to hold and for exponential convergence of our HNA method, via Theorem 2.14. Unlike the case for star shaped Ω_-, we do not provide a fully explicit bound on $M_\infty(u)$, as the following corollary is sufficient for our needs.

COROLLARY 4.7 (Bound on $M_\infty(u)$ for non-trapping polygon)**.** *Suppose that Ω_- is a non-trapping polygon (in the sense of Definition 2.2), with plane wave incidence $u^{inc} = u^{inc}_{PW}$. Then given $k_0 > 0$, we have that*

$$M_\infty(u) \lesssim k^{1/2} \log^{1/2} k, \quad \textit{for } k \geq k_0,$$

where $M_\infty(u)$ is defined as in (4.14)*. Hence Assumption 2.4(ii) holds.*

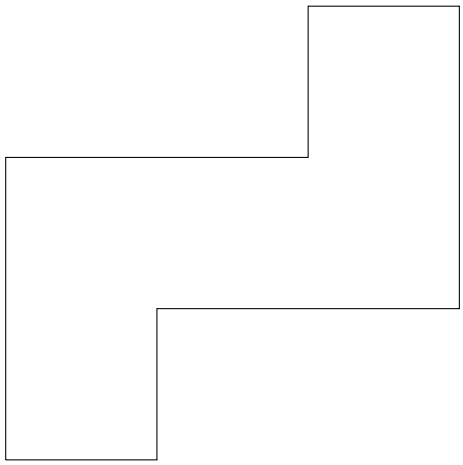

Figure 4.2: An example of a non-convex, non-star-shaped, non-trapping polygon as in [15] for which corollary 4.7 provides a k-explicit bound on $M_\infty(u)$.

Proof. Follows immediately from Theorem 3.1 and the definition (2.5) of u^{inc}_{PW}. □

We have now shown (via Corollary 4.5 and 4.7) that for polygonal multiple scattering configurations with plane wave incidence, both components of Assumption 2.4 hold, hence exponential convergence of our HNA approximation of the diffracted waves on Γ is predicted by Theorem 2.14.

To the best knowledge of the author, Corollary 4.7 represents the only available k-explicit bound on $M_\infty(u)$ for multiple scatterers. We do not expect such a bound to hold for the most general configurations and incident fields, since it was shown in [7, Theorem 2.8] that there exist trapping configurations for which $\|(\mathcal{A}'_{k,\eta})^{-1}\|_{L^2(\partial\Omega)\to L^2(\partial\Omega)}$ is bounded below by a term which grows exponentially with k, suggesting there exist incident fields for which $M_\infty(u)$ may grow similarly. In particular, Theorem 4.7 is immediately applicable to the case of polygons which are non-convex, non-star-shaped and non-trapping, considered in [15] (see Definition 3.1 therein, or Figure 4.2), for which the stronger result $M_\infty(u) = \mathcal{O}(1)$ for $k \to \infty$ was conjectured, in the (then) absence of any available algebraic bounds. The bound of Corollary 4.7 is sufficient to guarantee exponential convergence of such polygons without this conjecture.

4.4 Galerkin method

In what follows, using the parametrisation of Γ and γ we make the obvious identification between $L^2(\Gamma_j)$ and $L^2(0, L_j)$, and between $L^2(\gamma)$ and $L^2(0, L_\gamma)$, when no confusion can arise.

We first choose an N_Γ-dimensional approximation space $V_{N_\Gamma}^{\mathrm{HNA}}(\Gamma)$ to be either $\overline{V}_{N_\Gamma}^{\mathrm{HNA}}(\Gamma)$ or $\overline{\overline{V}}_{N_\Gamma}^{\mathrm{HNA}}(\Gamma)$ from §2.2 to approximate

$$v_\Gamma(s) := \frac{1}{k}\left(v_j^+(s-\widetilde{L}_{j-1})\mathrm{e}^{\mathrm{i}ks} + v_j^-(\widetilde{L}_j - s)\mathrm{e}^{-\mathrm{i}ks}\right), \quad s \in \left[\widetilde{L}_{j-1}, \widetilde{L}_j\right],\ j = 1, \ldots, n_\Gamma.$$

To account for the contribution from γ, we parametrise $\mathbf{x}_\gamma : [0, L_\gamma] \to \gamma$ and construct an appropriate N_γ-dimensional approximation space $V_{N_\gamma}^{hp}(\gamma) \subset L^2(0, L_\gamma)$ for

$$v_\gamma(s) := \frac{1}{k}\left.\frac{\partial u}{\partial \mathbf{n}}\right|_\gamma \big(\mathbf{x}_\gamma(s)\big), \quad s \in [0, L_\gamma]. \tag{4.17}$$

Whilst a representation analogous to (4.9) on γ holds when Ω_γ is a convex polygon, this approach is not suitable for our multiple scattering approximation. If such a representation is used on multiple polygons, the system to solve must be written as a Neumann series before it can be solved, and other difficulties arise from such a formulation. This alternative approach is outlined briefly in 4.4.1. Hence we approximate the entire solution v_γ, rather than any of its individual components as listed in (4.9). An advantage of this approach is that the only restriction imposed on γ is that it must be Lipschitz and piecewise analytic. For $V_{N_\gamma}^{hp}(\gamma)$ we use a standard *hp*-BEM approximation space consisting of piecewise polynomials to approximate v_γ, where the mesh and degree vector chosen will depend on the geometry of Ω_γ. If Ω_γ is a convex polygon (as in the examples of §4.5), the same geometric grading is used as for Γ. For the remainder of the chapter, we make the following assumption about the rate of convergence on γ.

ASSUMPTION 4.8. *The sequence of nested sequence of approximation spaces*

$$\left(V_{N_\gamma}^{hp}(\gamma)\right)_{N_\gamma \in \mathbb{N}}$$

is such that

$$\inf_{w_{N_\gamma} \in V_{N_\gamma}^{hp}(\gamma)} \|v_\gamma - w_{N_\gamma}\|_{L^2(\gamma)} \leq C_\gamma \mathrm{e}^{-\tau_\gamma p_\gamma},$$

where the constants $C_\gamma, \tau_\gamma > 0$ may depend on k.

Now we outline a procedure for implementation of the key ideas discussed up to this point. It follows the same principles as the single scattering Galerkin method of §2.3, we solve using a BIE of the form (1.14) with either choice of $\mathcal{A}$ discussed in §1.1.2. We will also use the notation introduced in Definition 1.6 to split the behaviour of the operator $\mathcal{A}$ to individual obstacles. However, due to the combination

of approximation spaces on different scatterers, the method is more complex, so we describe it in full. We simplify the notation by writing $\|\mathcal{G}_{\gamma\to\Gamma}\| := \|\mathcal{G}_{\gamma\to\Gamma}\|_{L^2(\gamma)\to L^2(\Gamma)}$.

Our approximation space V_N is based on the representation of the Neumann trace

$$\partial^+_{\mathbf{n}} u = \begin{cases} \Psi_{\mathrm{PW}} + kv_\Gamma + k\mathcal{G}_{\gamma\to\Gamma} v_\gamma, & \text{on } \Gamma, \\ kv_\gamma, & \text{on } \gamma, \end{cases} \tag{4.18}$$

where v_Γ and v_γ are the unknowns we solve for.

Inserting (4.18) into the BIE (1.14), we can write the problem to solve in block form: Find $v \in L^2(\Gamma) \times L^2(\gamma)$ such that

$$\mathcal{A}_\square \mathcal{G}_\square v = \begin{bmatrix} f|_\Gamma - \mathcal{A}_{\Gamma\to\Gamma}\Psi_{\mathrm{PW}} \\ f|_\gamma - \mathcal{A}_{\Gamma\to\gamma}\Psi_{\mathrm{PW}} \end{bmatrix}, \quad \text{where} \quad \mathcal{A}_\square := \begin{bmatrix} \mathcal{A}_{\Gamma\to\Gamma} & \mathcal{A}_{\gamma\to\Gamma} \\ \mathcal{A}_{\Gamma\to\gamma} & \mathcal{A}_{\gamma\to\gamma} \end{bmatrix}$$
$$\text{and} \quad \mathcal{G}_\square := k \begin{bmatrix} \mathcal{I}_\Gamma & \mathcal{G}_{\gamma\to\Gamma} \\ 0 & \mathcal{I}_\gamma \end{bmatrix}, \tag{4.19}$$

$f|_\Gamma$ and $f|_\gamma$ denote the restriction of f to Γ and γ respectively. From the invertibility of $\mathcal{A}_\square$ (equivalent to invertibility of $\mathcal{A}$) and invertibility of $\mathcal{G}_\square$ (which follows from the triangular structure of $\mathcal{G}_\square$), it is clear that (4.19) has a unique solution. Our approximation is designed to approximate the unknown components of the solution on Γ and γ, that is

$$v_N := \begin{pmatrix} v_\Gamma^{N_\Gamma} \\ v_\gamma^{N_\gamma} \end{pmatrix} \approx \begin{pmatrix} v_\Gamma \\ v_\gamma \end{pmatrix} = v, \tag{4.20}$$

where v is the solution to (4.19). Recall that we use an HNA approximation space $V^{\mathrm{HNA}}_{N_\Gamma}(\Gamma)$ (single- or overlapping- mesh) on Γ, with a standard *hp*-approximation space $V^{hp}_{N_\gamma}(\gamma)$ on γ. The solution v_N to the discrete problem therefore lies inside of the space

$$V_N^{\mathrm{HNA}^*}(\Gamma,\gamma) := V^{\mathrm{HNA}}_{N_\Gamma}(\Gamma) \times V^{hp}_{N_\gamma}(\gamma),$$

where the total number of degrees of freedom is $N = N_\gamma + N_\Gamma$. In the theory that follows we make use of the norm

$$\|(\cdot,\cdot)\|_{L^2(\Gamma)\times L^2(\gamma)} := \left(\|\cdot\|^2_{L^2(\Gamma)} + \|\cdot\|^2_{L^2(\gamma)} \right)^{1/2}. \tag{4.21}$$

We will make the obvious identification between $\|\cdot\|_{L^2(\Gamma)\times L^2(\gamma)}$ and $\|\cdot\|_{L^2(\partial\Omega)}$. Our discrete problem to solve is: find $v_N \in V_N^{\mathrm{HNA}^*}(\Gamma,\gamma)$ such that

$$\begin{aligned} \left(\mathcal{A}_{\Gamma\to\Gamma} v_\Gamma^{N_\Gamma}, w_N\right)_{L^2(\Gamma)} + \left([\mathcal{A}_{\gamma\to\Gamma} + \mathcal{A}_{\Gamma\to\Gamma}\mathcal{G}_{\gamma\to\Gamma}] v_\gamma^{N_\gamma}, w_N\right)_{L^2(\Gamma)} &= \frac{1}{k}\left(f - \mathcal{A}_{\Gamma\to\Gamma}\Psi_{\mathrm{PW}}, w_N\right)_{L^2(\Gamma)}, \\ \left(\mathcal{A}_{\Gamma\to\gamma} v_\Gamma^{N_\Gamma}, w_N\right)_{L^2(\gamma)} + \left([\mathcal{A}_{\gamma\to\gamma} + \mathcal{A}_{\Gamma\to\gamma}\mathcal{G}_{\gamma\to\Gamma}] v_\gamma^{N_\gamma}, w_N\right)_{L^2(\gamma)} &= \frac{1}{k}\left(f - \mathcal{A}_{\Gamma\to\gamma}\Psi_{\mathrm{PW}}, w_N\right)_{L^2(\gamma)}, \end{aligned} \tag{4.22}$$

for all $w_N \in V_N^{\mathrm{HNA}^*}(\Gamma, \gamma)$.

Concerning the stability of the discrete problem (4.22), we now present a lemma which may be applied to Galerkin or collocation BEM. We use the positive constants C_q and N_0, which are analogous to their use single scattering Galerkin method discussed in §2.3.

LEMMA 4.9 (Quasi-optimality of projection methods)**.** *There exist positive constants C_q and N_0 such that v_N exists, for $N \geq N_0$*

$$\|v - v_N\|_{L^2(\partial\Omega)} \leq C_q \min_{w_N \in V_N^{\mathrm{HNA}^*}(\Gamma,\gamma)} \|v - w_N\|_{L^2(\partial\Omega)},$$

where both C_q and N_0 may depend on k.

Proof. It can be shown that $\mathcal{A}_\square$ is a compact perturbation of a coercive operator, for either choice of $\mathcal{A}$. We have from [16, p620] that $\mathcal{A} = \mathcal{A}_{\Gamma\to\Gamma}$ is a compact perturbation of a coercive operator (namely the identity), and the same arguments can be applied to each $\mathcal{A}_{\gamma_i\to\gamma_i}$ for $i = 1, \ldots n_\gamma$. As the kernels of $\mathcal{A}_{\Gamma\to\gamma_i}$ and $\mathcal{A}_{\gamma_i\to\Gamma}$ are continuous for $i = 1, \ldots, n_\gamma$, these operators are also compact, hence $\mathcal{A}_{k,\eta}$ is a compact perturbation. Similar arguments can be made for $\mathcal{A} = \mathcal{A}_k$.

Let $\mathcal{P}_N$ be an orthogonal projection operator from $L^2(\Gamma)\times L^2(\gamma)$ onto $V_N^{\mathrm{HNA}^*}(\Gamma, \gamma)$. Applying [16, Theorem 5.1] separately to v_Γ and v_γ shows convergence in $L^2(\partial\Omega)$. Then [16, Theorem 5.2] shows existence of a solution via a bound on

$$\|(\mathcal{I} + \mathcal{P}_N K)^{-1}\|_{L^2(\partial\Omega)\to L^2(\partial\Omega)} =: C_q < \infty, \tag{4.23}$$

where

$$K := \mathcal{A}_\square \mathcal{G}_\square - \mathcal{I} \quad \text{with} \quad \mathcal{I} := \begin{bmatrix} \mathcal{I}_\Gamma & 0 \\ 0 & \mathcal{I}_\gamma \end{bmatrix}.$$

We also note that

$$\mathcal{P}_N(\mathcal{I} + K)v = \mathcal{P}_N \begin{bmatrix} f|_\Gamma - \mathcal{A}_{\Gamma\to\Gamma}\Psi_{\mathrm{PW}} \\ f|_\gamma - \mathcal{A}_{\Gamma\to\gamma}\Psi_{\mathrm{PW}} \end{bmatrix},$$

which we combine with (4.19) to obtain

$$v_N + \mathcal{P}_N K v_N = \mathcal{P}_N(\mathcal{I} + K)v,$$

rearranging and adding v to both sides yields

$$(\mathcal{I} + \mathcal{P}_N K)(v - v_N) = (\mathcal{I} - \mathcal{P}_N)v,$$

hence we can bound

$$\|v - v_N\|_{L^2(\partial\Omega)\to L^2(\partial\Omega)} \leq \left\|(\mathcal{I} + \mathcal{P}_N K)^{-1}\right\|_{L^2(\partial\Omega)\to L^2(\partial\Omega)} \|v - \mathcal{P}_N v\|_{L^2(\partial\Omega)\to L^2(\partial\Omega)}$$

and the bound follows from the definition of $\mathcal{P}_N$ and (4.23). □

Recalling that we are actually approximating the (dimensionless) diffracted waves on Γ and the (dimensionless) Neumann trace of the solution on γ; the full approximation to the Neumann trace follows by inserting v_N into (4.18), and is denoted

$$\nu_N := \begin{cases} \Psi_{\mathrm{PW}} + k v_\Gamma^{N_\Gamma} + k\mathcal{G}_{\gamma\to\Gamma} v_\gamma^{N_\gamma}, & \text{on } \Gamma, \\ k v_\gamma^{N_\gamma}, & \text{on } \gamma, \end{cases} \tag{4.24}$$

and the following theorem can be used to determine the error in the full approximation.

THEOREM 4.10. *Suppose* (4.16) *and Assumption 4.8 hold. For $N \geq N_0$ (of Lemma 4.9), we have the bound*

$$\left\|\partial_{\mathbf{n}}^+ u - \nu_N\right\|_{L^2(\partial\Omega)} \leq C_q k \left(1 + \|\mathcal{G}_{\gamma\to\Gamma}\|^2\right)^{1/2} \left(\left(C_\Gamma M_\infty(u) k^{-1/2} J(k) \mathrm{e}^{-\tau_\Gamma p_\Gamma}\right)^2 + \left(C_\gamma \mathrm{e}^{-\tau_\gamma p_\gamma}\right)^2\right)^{1/2},$$

where C_Γ and τ_Γ are is as in Corollary 2.11, $M_\infty(u)$ is as in Theorem 2.4 with τ_γ and C_γ as in Assumption 4.8.

Proof. From the definition (4.24) we can split the norm over $\partial\Omega$ and rewrite in terms of v_N of (4.20),

$$\begin{aligned}
&\left\|\partial_{\mathbf{n}}^+ u - \nu_N\right\|_{L^2(\partial\Omega)} \\
&\leq k \left(\|v_\Gamma - v_\Gamma^{N_\Gamma}\|_{L^2(\Gamma)}^2 + (\|\mathcal{G}_{\gamma\to\Gamma}\|^2 + 1)\|v_\gamma - v_\gamma^{N_\gamma}\|_{L^2(\gamma)}^2\right)^{1/2} \\
&\leq k(\|\mathcal{G}_{\gamma\to\Gamma}\|^2 + 1)^{1/2} \|v - v_N\|_{L^2(\partial\Omega)}, \\
&\leq k(\|\mathcal{G}_{\gamma\to\Gamma}\|^2 + 1)^{1/2} C_q \inf_{w_N \in V_N^{\mathrm{HNA}^*}(\Gamma,\gamma)} \|v - w_N\|_{L^2(\partial\Omega)} \\
&= k(\|\mathcal{G}_{\gamma\to\Gamma}\|^2 + 1)^{1/2} C_q \left(\inf_{w_\Gamma^N \in V_{N_\Gamma}^{\mathrm{HNA}}(\Gamma)} \|v_\Gamma - w_\Gamma^{N_\Gamma}\|_{L^2(\Gamma)}^2 + \inf_{w_\gamma^{N_\gamma} \in V_{N_\gamma}^{hp}(\gamma)} \|v_\gamma - w_\gamma^{N_\gamma}\|_{L^2(\gamma)}^2 \right)^{1/2},
\end{aligned}$$

where the penultimate step follows from Lemma 4.9. The result then follows from Corollary 2.11 and Assumption 4.8. □

REMARK 4.11 (The constants of Theorem 4.10)**.** *There may seem to be a certain amount of ambiguity about the value or k-dependence of the constants of 4.10 in practice, as these depend on Assumption 4.8 and 2.4(ii). Here we summarise the cases where each constant is known.*

(i) In Chapter 5 we will see that if the constellation combined operator $\mathcal{A}_k$ is used with a configuration for which the conditions of Theorem 5.7 are satisfied, we have that $C_q \leq \|\mathcal{A}_k\|_{L^2(\partial\Omega)\to L^2(\partial\Omega)}/\zeta$ and $N_0 = 1$, where ζ is the coercivity constant from Theorem 5.7.

(ii) If Ω is a non-trapping polygon (in the sense of Definition 2.2), then we may obtain a k-explicit bound on $M_\infty(u)$, by Corollary 4.7.

(iii) Theorem 5.10 shows that an h-BEM approximation on γ will result in the constants $\tau_\gamma = 0$ and $C_\gamma \lesssim (k/N_\gamma) + hk^{3/2}$, where h is the largest element of a suitably graded mesh, with N_γ elements. As $\tau_\gamma = 0$, we cannot guarantee exponential convergence of the scheme if an h-BEM discretisation is used on γ. Whilst we expect that it may be possible to obtain a bound on C_γ and $\tau_\gamma > 0$ for an hp-BEM using techniques of [41], this would be considerably more complex and we do not investigate this here.

In summary, if an h-BEM approximation were used on γ, for non-trapping polygonal constellation shaped Ω_-, with each star-shaped obstacle sufficiently far apart, then we have k-explicit bounds on the error in our solution.

Our approximation ν_N can be used to obtain estimates for quantities of practical interest, such as the total field u and the far-field pattern of (1.16). The approximation u_N to the solution u of the BVP (1.4)–(1.5) is obtained by combining ν_N with (1.10),

$$u_N(\mathbf{x}) := u^{\mathrm{inc}}(\mathbf{x}) - \int_0^{L_\Gamma} \Phi\left(\mathbf{x}, \mathbf{y}_\Gamma(s)\right) \left(k v_\Gamma^{N_\Gamma}(s) + \Psi_{\mathrm{PW}}\left(\mathbf{y}_\Gamma(s)\right) + k[\mathcal{G}_{\gamma\to\Gamma} v_\gamma^{N_\gamma}](s)\right) \mathrm{d}s$$
$$- k \int_0^{L_\gamma} \Phi\left(\mathbf{x}, \mathbf{y}_\gamma(s)\right) v_\gamma^{N_\gamma}(s)\, \mathrm{d}s, \quad \text{for } \mathbf{x} \in \Omega_+.$$

Here the parametrisation $\mathbf{y}_\Gamma$ is defined exactly as in (2.1), whilst $\mathbf{y}_\gamma$ is the analogous parametrisation of γ, as was defined for (4.17). Expanding further, we can extend our definition of $\mathcal{G}_{\gamma\to\Gamma}$ to a parametrised form by

$$\mathcal{G}_{\gamma\to\Gamma} v_\gamma^{N_\gamma}(s) := \int_0^{L_\gamma} \chi_j(t) \frac{\partial \Phi(\mathbf{y}_\Gamma(s), \mathbf{y}_\gamma(t))}{\partial \mathbf{n}(\mathbf{y}_\Gamma(s))} v_\gamma^{N_\gamma}(t)\, \mathrm{d}t, \quad \mathbf{y} \in \Gamma_j, \tag{4.25}$$

where the indicator function

$$\chi_j(t) := \begin{cases} 1, & \mathbf{y}_\gamma(t) \in U_j, \\ 0, & \text{otherwise}, \end{cases}$$

is used to ensure the path of integration remains inside the upper half-plane U_j.

COROLLARY 4.12. *Suppose* (4.16) *and Assumption 4.8 hold. Using the constants of these assumptions, Lemma 4.9 and Theorem 4.10,*

$$\|u - u_N\|_{L^\infty(\Omega_+)}$$
$$\leq \|S_k\|_{L^2(\partial\Omega)\to L^\infty(\Omega_+)} k \left(1 + \|\mathcal{G}_{\gamma\to\Gamma}\|^2\right)^{1/2} \left(\left(C_\Gamma M_\infty(u) k^{-1/2} J(k) \mathrm{e}^{-\tau_\Gamma p}\right)^2 + \left(C_\gamma \mathrm{e}^{-\tau_\gamma p}\right)^2\right)^{1/2},$$

for $N \geq N_0$.

Proof. The result follows from the bounds on $\|S_k\|_{L^2(\partial\Omega)\to L^\infty(\Omega_+)}$ given by Lemma [35, Lemma 4.1], Theorem 4.10, and

$$\|u-u_N\|_{L^\infty(\Omega_+)} = \left\|S_k\left(\partial_{\mathbf{n}}^+ u-\nu_N\right)\right\|_{L^\infty(\Omega_+)} \le \|S_k\|_{L^2(\partial\Omega)\to L^\infty(\Omega_+)}\left\|\partial_{\mathbf{n}}^+ u-\nu_N\right\|_{L^2(\partial\Omega)}$$

□

Similarly, we may approximate the far-field pattern by inserting ν_N into (1.16).

COROLLARY 4.13. *Suppose* (4.16) *and Assumption 4.8 hold. Using the constants of these assumptions, Lemma 4.9 and Theorem 4.10, we have the following bound on the far-field approximation*

$$\begin{aligned}&\|u^\infty-u_N^\infty\|_{L^\infty(0,2\pi)}\\ &\le C_q k\left(1+\|\mathcal{G}_{\gamma\to\Gamma}\|^2\right)^{1/2}(L_\Gamma+L_\gamma)^{1/2}\left(\left(C_\Gamma M_\infty(u)k^{-1/2}J(k)\mathrm{e}^{-\tau_\Gamma p}\right)^2+\left(C_\gamma \mathrm{e}^{-\tau_\gamma p}\right)^2\right)^{1/2},\end{aligned}$$

for $N\ge N_0$.

Proof. By the Cauchy–Schwarz inequality

$$\begin{aligned}|u^\infty(\theta)-u_N^\infty(\theta)| &\le k\int_{\partial\Omega}\left|\partial_{\mathbf{n}}^+ u-\nu_N\right|\mathrm{d}s\\ &\le\quad k(L_\Gamma+L_\gamma)^{1/2}\left\|\partial_{\mathbf{n}}^+ u-\nu_N\right\|_{L^2(\partial\Omega)},\end{aligned}$$

and the result follows by Theorem 4.10. □

Now we briefly outline the implementation of the Galerkin method which is used to produce the results in §4.5.

We choose suitable bases Λ_Γ and Λ_γ, with

$$\operatorname{span}\Lambda_\Gamma = V_\Gamma \quad\text{and}\quad \operatorname{span}\Lambda_\gamma = V_\gamma.$$

To determine v_N we seek $\mathbf{a}\in\mathbb{C}^N$ which solves the block matrix system $B\mathbf{a}=\mathbf{b}$, where

$$B := \left[\begin{array}{c|c} \overset{\varphi\in\Lambda_\Gamma}{(\mathcal{A}_{\Gamma\to\Gamma}\varphi,\phi)_{L^2(\Gamma)}} & \overset{\varphi\in\Lambda_\gamma}{([\mathcal{A}_{\gamma\to\Gamma}+\mathcal{A}_{\Gamma\to\Gamma}\mathcal{G}_{\gamma\to\Gamma}]\varphi,\phi)_{L^2(\Gamma)}} \\ \hline (\mathcal{A}_{\Gamma\to\gamma}\varphi,\phi)_{L^2(\gamma)} & ([\mathcal{A}_{\gamma\to\gamma}+\mathcal{A}_{\Gamma\to\gamma}\mathcal{G}_{\gamma\to\Gamma}]\varphi,\phi)_{L^2(\gamma)}\end{array}\right]\begin{array}{l}\phi\in\Lambda_\Gamma\\ \phi\in\Lambda_\gamma\end{array} \tag{4.26}$$

and

$$\mathbf{b} := \frac{1}{k}\left[\begin{array}{c}(f-\mathcal{A}_{\Gamma\to\Gamma}\Psi_{\mathrm{PW}},\phi)_{L^2(\Gamma)}\\ \hline (f-\mathcal{A}_{\Gamma\to\gamma}\Psi_{\mathrm{PW}},\phi)_{L^2(\gamma)}\end{array}\right]\begin{array}{l}\phi\in\Lambda_\Gamma\\ \phi\in\Lambda_\gamma\end{array}. \tag{4.27}$$

4.4.1 An alternative Galerkin method

Here we briefly outline the formulation which follows if the HNA representation (4.9) is used on two convex scatterers, hence for this example we assume that both Ω_Γ and Ω_γ are convex polygons. This method has not been implemented, and despite the seemingly intuitive approach of using the HNA representation (4.9) on multiple obstacles, this leads to less intuitive issues with implementation, which will become evident shortly. Define $\mathcal{G}_{\Gamma\to\gamma}$ in the obvious way, which is the analogous interaction operator from Γ to γ, such that the position of Γ and γ in (4.12) are swapped. For consistency, we define $\Psi_\Gamma := \Psi_{\mathrm{PW}}$ of (4.10), whilst Ψ_γ is as (4.10) with Γ replaced by γ. For simplicity, we define the diffracted waves on Γ and γ to be w_Γ and w_γ respectively, as in the definition (2.6) (it follows that $kw_\Gamma = v_\Gamma$ of Definition (2.6)).

Writing the HNA representation (4.9) on both scatterers, we obtain

$$\begin{bmatrix} \left.\dfrac{\partial u}{\partial \mathbf{n}}\right|_\Gamma \\ \left.\dfrac{\partial u}{\partial \mathbf{n}}\right|_\gamma \end{bmatrix} = \begin{bmatrix} \Psi_\Gamma + w_\Gamma + \mathcal{G}_{\gamma\to\Gamma} \left.\dfrac{\partial u}{\partial \mathbf{n}}\right|_\gamma \\ \Psi_\gamma + w_\gamma + \mathcal{G}_{\Gamma\to\gamma} \left.\dfrac{\partial u}{\partial \mathbf{n}}\right|_\Gamma \end{bmatrix},$$

which we may re-arrange to

$$\begin{bmatrix} \mathcal{I} & -\mathcal{G}_{\gamma\to\Gamma} \\ -\mathcal{G}_{\Gamma\to\gamma} & \mathcal{I} \end{bmatrix} \begin{bmatrix} \left.\dfrac{\partial u}{\partial \mathbf{n}}\right|_\Gamma \\ \left.\dfrac{\partial u}{\partial \mathbf{n}}\right|_\gamma \end{bmatrix} = \begin{bmatrix} \Psi_\Gamma + w_\Gamma \\ \Psi_\gamma + w_\gamma \end{bmatrix}. \tag{4.28}$$

Assuming the inverse of the 2×2 operator matrix of (4.28) can be written as a convergent Neumann series, we obtain the representation

$$\begin{bmatrix} \left.\dfrac{\partial u}{\partial \mathbf{n}}\right|_\Gamma \\ \left.\dfrac{\partial u}{\partial \mathbf{n}}\right|_\gamma \end{bmatrix} = \sum_{n=0}^{\infty} \begin{bmatrix} 0 & \mathcal{G}_{\gamma\to\Gamma} \\ \mathcal{G}_{\Gamma\to\gamma} & 0 \end{bmatrix}^n \begin{bmatrix} \Psi_\Gamma + w_\Gamma \\ \Psi_\gamma + w_\gamma \end{bmatrix}. \tag{4.29}$$

By (1.14) we may write

$$\mathcal{A} \sum_{n=0}^{\infty} \begin{bmatrix} 0 & \mathcal{G}_{\gamma\to\Gamma} \\ \mathcal{G}_{\Gamma\to\gamma} & 0 \end{bmatrix}^n \begin{bmatrix} \Psi_\Gamma + w_\Gamma \\ \Psi_\gamma + w_\gamma \end{bmatrix} = \begin{bmatrix} f|_\Gamma \\ f|_\gamma \end{bmatrix} \tag{4.30}$$

and moving all known data to the right-hand side, we obtain an equation to solve where the unknown is just the diffracted waves w_Γ and w_γ

$$\mathcal{A} \sum_{n=0}^{\infty} \begin{bmatrix} 0 & \mathcal{G}_{\gamma\to\Gamma} \\ \mathcal{G}_{\Gamma\to\gamma} & 0 \end{bmatrix}^n \begin{bmatrix} w_\Gamma \\ w_\gamma \end{bmatrix} = \begin{bmatrix} f|_\Gamma \\ f|_\gamma \end{bmatrix} - \mathcal{A} \sum_{n=0}^{\infty} \begin{bmatrix} 0 & \mathcal{G}_{\gamma\to\Gamma} \\ \mathcal{G}_{\Gamma\to\gamma} & 0 \end{bmatrix}^n \begin{bmatrix} \Psi_\Gamma \\ \Psi_\gamma \end{bmatrix}. \tag{4.31}$$

Now we may approximate the unknown diffracted waves w_Γ and w_γ. We define an alternative approximation space

$$V_N^{\mathrm{HNA}^\dagger}(\Gamma,\gamma) := V_{N_\Gamma}^{\mathrm{HNA}}(\Gamma) \times V_{N_\gamma}^{\mathrm{HNA}}(\gamma),$$

Where $N = N_\gamma + N_\Gamma$. Applying the BIE representation (1.14), truncating the Neumann series after T terms and moving known data to the right-hand side, we can write an alternative discrete problem: find $v_N \in V_N^{\mathrm{HNA}^\dagger}(\Gamma,\gamma)$ such that

$$\begin{aligned}
&\alpha_m \left(\mathcal{A} \sum_{n=0}^{T} \begin{bmatrix} 0 & \mathcal{G}_{\gamma\to\Gamma} \\ \mathcal{G}_{\Gamma\to\gamma} & 0 \end{bmatrix}^n v_N,\ \varphi \right)_{L^2(\Gamma)\times L^2(\gamma)} \\
&= \left(\begin{bmatrix} f|_\Gamma \\ f|_\gamma \end{bmatrix} - \mathcal{A} \sum_{n=0}^{T} \begin{bmatrix} 0 & \mathcal{G}_{\gamma\to\Gamma} \\ \mathcal{G}_{\Gamma\to\gamma} & 0 \end{bmatrix}^n \begin{bmatrix} \Psi_\Gamma \\ \Psi_\gamma \end{bmatrix}, \varphi \right)_{L^2(\Gamma)\times L^2(\gamma)},
\end{aligned}$$

for all $\varphi \in V_N^{\mathrm{HNA}^\dagger}(\Gamma,\gamma)$. Intuitively this method may be interpreted as tracing repeated reflections and diffractions of each basis function, up to T reflections. Hence we are not just approximating the diffracted waves, but every subsequent reflection of the diffracted waves. We do not present numerical results or analysis for this method, largely because it is significantly more difficult to implement and analyse than the main method we present. This is due to the repeated application of the interaction operators, resulting in $(T+2)$-dimensional integrals. Moreover, convergence of the Neumann series (4.29) is not guaranteed. The condition $\|\mathcal{G}\|_{\gamma\to\Gamma} < 1$ is sufficient for convergence of the Neumann series, although given that the bound (4.13) grows like $O(\sqrt{k})$, we have no guarantee of convergence for problems beyond a certain frequency range.

This method should not be considered *iterative* in the same sense as traditional iterative methods, such as those in [25]. Whilst it does contain a Neumann series, only one linear system must be solved unlike classical iterative approaches which requires a solve at each iteration, for each term in the truncated Neumann series.

4.5 Numerical results

Here we present numerical results for the solution of the problem (4.22), with the classical combined layer formulation $\mathcal{A} = \mathcal{A}_{k,\eta}$. The configuration tested consists of two equilateral triangles, separated by $\mathrm{dist}(\Gamma,\gamma) = \sqrt{3}\pi/5$, with $L_\Gamma = 6\pi$ and $L_\gamma = 3\pi/5$ (as in Figure 4.3). It follows that there are exactly k wavelengths on each side of Γ and $k/10$ on each side of γ. Experiments were run for $k \in \{5, 10, 20, 40, 80, 160\}$ for a range of incident directions $\mathbf{d}$. In terms of observed error, each $\mathbf{d}$ gave very similar

results. Here we focus on the example $\mathbf{d} = (1,1)/\sqrt{2}$, which has some re-reflection, partial illumination and is asymmetric, (see Figure 4.3). Our error analysis examines convergence on the boundary $\partial\Omega = \Gamma \cup \gamma$. To construct our approximation space, we first choose $V_{N_\Gamma}^{\mathrm{HNA}}(\Gamma) = \overline{V}_{N_\Gamma}^{\mathrm{HNA}}(\Gamma)$, the single-mesh approximation space of §2.2, with $p_j = p$ for each side $j = 1, \ldots, n_\Gamma = 3$, and choose the degree vector $\mathbf{p}$ in accordance with Remark 2.10. A grading parameter of $\sigma = 0.15$ is used, with $c_j = 2$ (where c_j is the constant from Theorem 2.9), for $j = 1, \ldots, n_\Gamma$. We choose $\alpha_j = \min\{(\mathbf{p}_j)_i)/4, 2\}$, introducing some dependence on the polynomial degree on the ith mesh element of the jth side. This ensures that α_j is bounded independently of p_j. We will see shortly that the method converges exponentially, despite this dependence on $(\mathbf{p}_j)_i$ requiring that fewer elements of the approximation space are used, than as required for Theorem 2.9, which predicted exponential convergence.

For the standard hp-BEM space $V_{N_\gamma}^{hp}(\gamma)$, we use the same parameters $\mathbf{p}$, σ and c_j to grade towards the corners of γ, so the construction of the mesh on γ is much the same as on Γ. The key difference is the inclusion of meshpoints distributed evenly between each x_{n-1} and x_n; ensuring that no mesh element is longer than $N_\lambda \in \mathbb{N}$ wavelengths. The intention here is to resolve the oscillations on γ, by increasing the degrees of freedom linearly with k. The maximum polynomial degree p remains the same across every such subdivision. Therefore, the degrees of freedom N_γ for a general polygon γ is given by

$$N_\gamma = \sum_{j=1}^{N_\gamma} 2 \left((\mathbf{p}_j)_{n_j} \left\lceil N_\lambda \frac{x_{n_j+1}^j - x_{n_j}^j}{2\pi/k} \right\rceil + \sum_{\ell=1}^{n_j-1} (\mathbf{p}_j)_\ell \left\lceil N_\lambda \frac{x_{\ell+1}^j - x_\ell^j}{2\pi/k} \right\rceil \right)$$

where $n_{\gamma,s}$ is the number of sides of γ (for these examples $n_{\gamma,s} = 3$), x_ℓ^j is the ℓth meshpoint of the jth side of γ, and N_λ is the minimum number of wavelengths per mesh element.

The integrals (4.26) and (4.27), and the L^2 norms used to estimate the error in Figure 4.4 are computed using the quadrature rules discussed in Appendix B. Many of these consist of double or triple integrals, which are difficult to compute. The markers correspond to the increasing polynomial degree $p = 0, \ldots, 8$, whilst the horizontal axis represents the total degrees of freedom N, which depends on both p and k. These are compared against a reference solution, which is taken to be the $p = 8$ approximation, in which case we write $N = N^*$. Additional checks were performed against a high order standard BEM approximation to validate the reference solution, although we do not give the results of this here. The increased number of oscillations appear to be handled by the increase in N_γ for each k, (here N_Γ remains fixed as k increases, whilst

N_γ increases linearly) with exponential convergence observed in each case (see Figure 4.4(a)), as is predicted by Theorem 4.10. Figure (4.3) depicts the domain solution u_{N^*}, whilst Figure 4.5 plots ν_{N^*} on Γ and γ.

We note that for $k = 20$ the rate of convergence is not as consistent as for other wavenumbers. Following this unexpected result, we adjusted the value of α_j and N_λ (details above each plot in Figure 4.4). This resulted in a larger number of basis functions included in the space $V_N^{\mathrm{HNA}^*}(\Gamma, \gamma)$, as it can be seen from Figure 4.4(a) that the region of inconsistent convergence of $k = 10$ has the same number of degrees of freedom as for $k = 5$, however this should be slightly higher to account for the increased oscillations. This adjustment appears to have fixed the problem, as is visible from Figure 4.4(b), however this suggests that the choice of α_j for the single-mesh space has a sensitive effect on the convergence of the method.

In summary, assuming a suitable choice of parameters, for fixed k we observe exponential convergence of the method with respect to p. The error does not increase significantly as k increases, if the degrees of freedom N remains fixed. We note also that we have chosen $N_\Gamma = O(1)$ and $N_\gamma = O(k)$, but N_γ is relatively small compared to $N = N_\Gamma + N_\gamma$ for the examples considered here. However as $k \to \infty$ we have $N = O(k)$. This is why the method is particularly well suited to the type of example we present here, with one large polygon (for which the high frequency asymptotics are well understood), and one (or many) small polygon(s) on which the high frequency asymptotics do not need to be known.

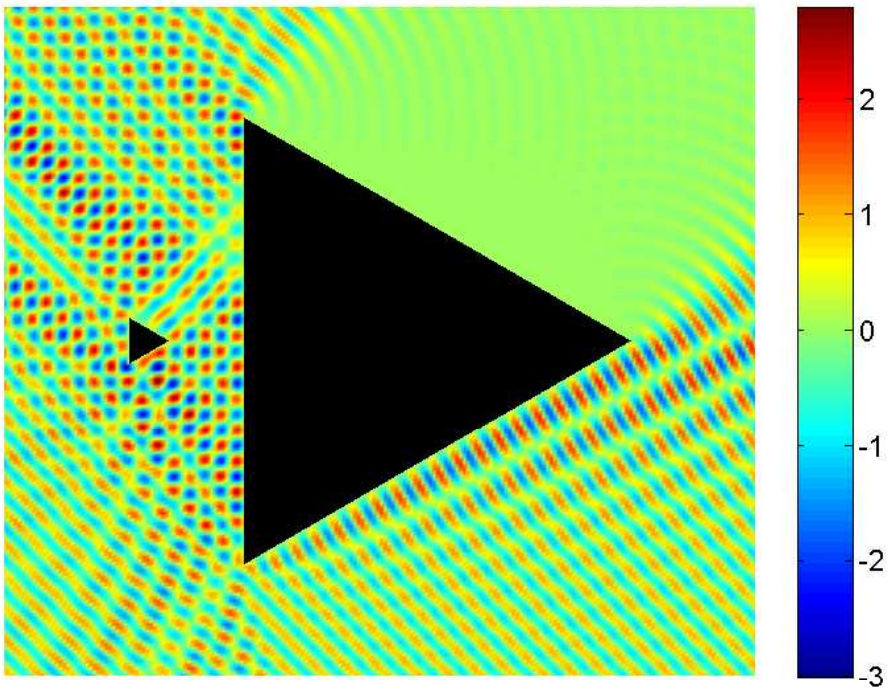

Figure 4.3: $\mathrm{Re}(u)$ in Ω_+, scattering by two triangles. $L_\Gamma = 6\pi$, $L_\gamma = 3\pi/5$, $k = 10$, $\mathbf{d} = (1,1)/\sqrt{2}$.

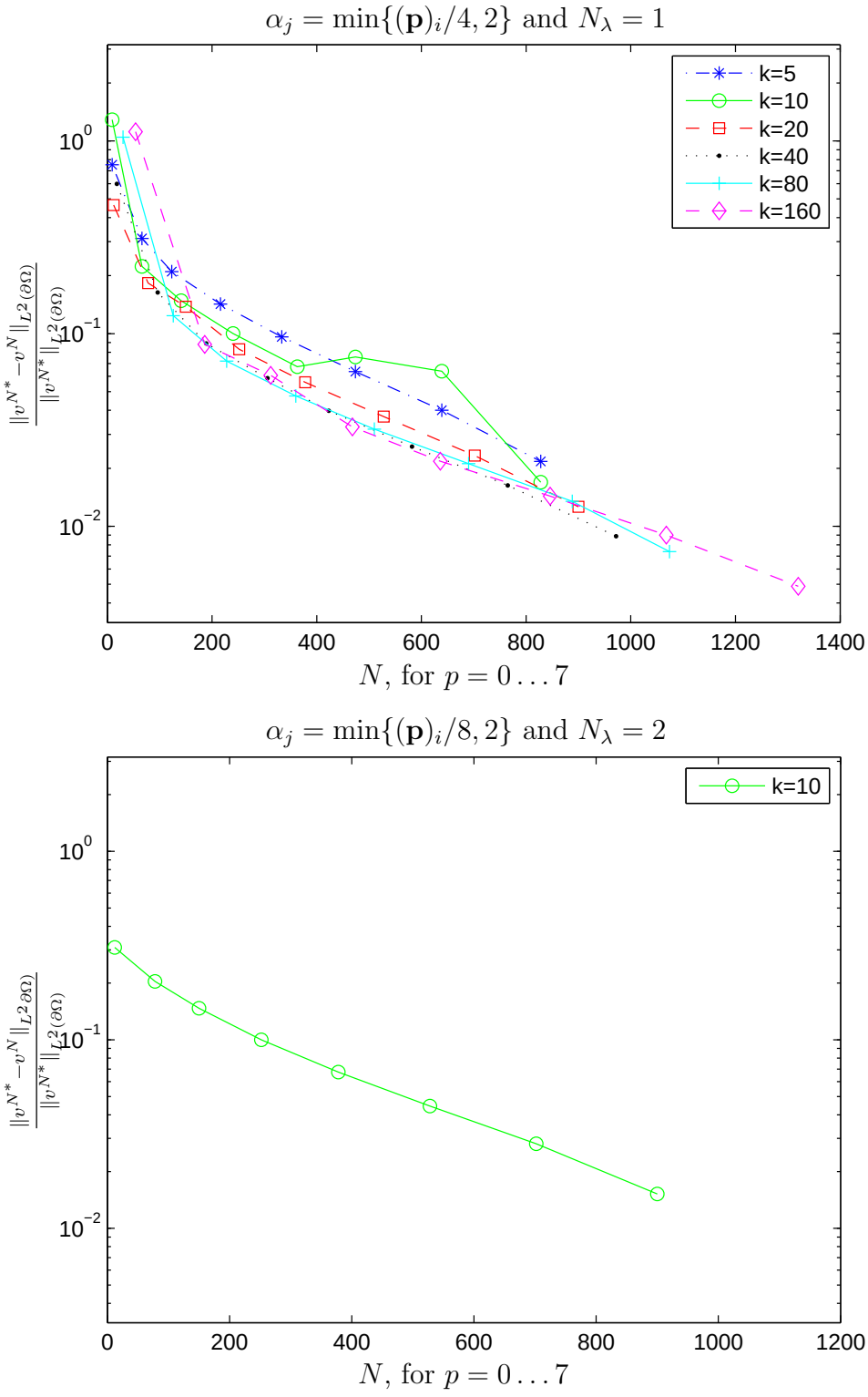

Figure 4.4: Convergence plots for varying choices of α_j, suggesting that the convergence depends sensitively on this choice.

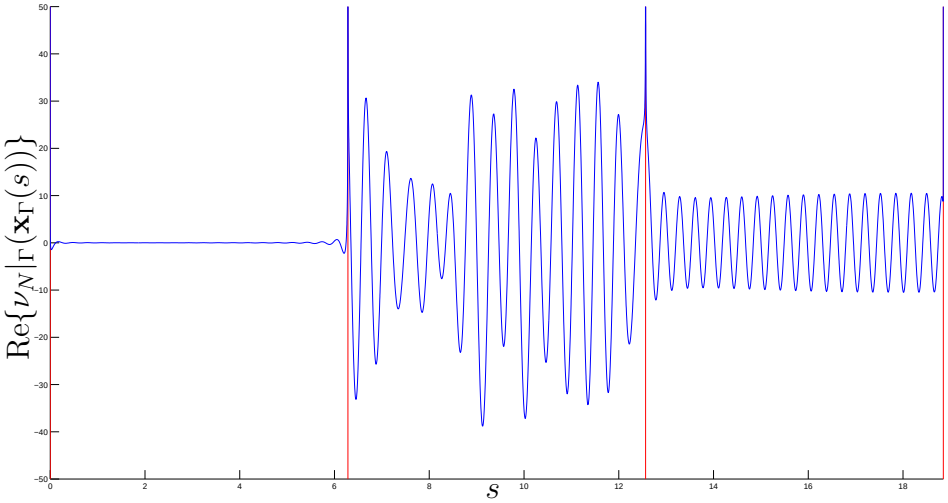

(a)

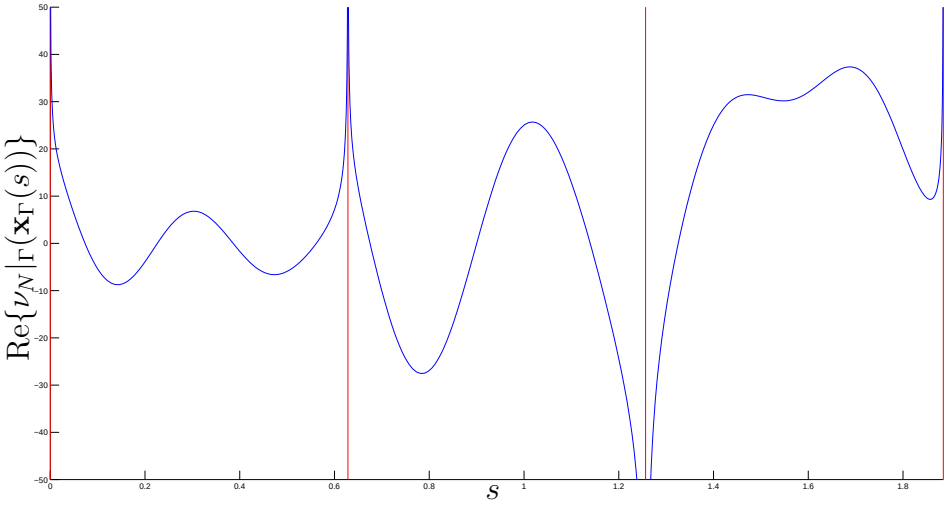

(b)

Figure 4.5: Plots of real component of the boundary solution on Γ (a) and γ (b), for $k = 20$ problem depicted in Figure 4.3.

4.6 Further work

Whilst the composite quadrature approach (discussed in §B.3) used for these results is sufficient to demonstrate the effectiveness of our method, it becomes expensive as k grows, in particular for the triple integral $(\mathcal{A}_{\Gamma\to\gamma}\mathcal{G}_{\gamma\to\Gamma}v, w)_{L^2(\gamma)}$, which contains a singular integrand in certain cases, care must be taken to ensure enough memory is available to compute this. Practical implementations of the method should instead incorporate oscillatory quadrature and further generalised Gaussian quadrature to handle the near singularities (see for e.g. [38] and [37] respectively) with a computational cost which does not increase with k. Such quadrature routines can be difficult to implement for double or triple integrals, however the dimension of integration may be reduced by one if a collocation approach (1.19), is used. Indeed, a key advantage of a Galerkin method is that it can (sometimes) provide more information about the error of the approximation. However, when the problem to be solved is not one listed in Remark 4.11, we cannot obtain k-explicit bounds on our approximation, so there is no advantage of using the Galerkin method, and the Collocation method (with one fewer dimension per integral, as discussed in Remark 2.12) may be preferable, if stability issues observed in the investigation into collocation HNA of [47] can be avoided.

As demonstrated by this example, our method is best suited to cases where γ has a size parameter no larger than one wavelength, in which case there is no need to increase N_γ to resolve the oscillations. We re-emphasise that our choice of Ω_γ could be generalised considerably, to any two-dimensional bounded Lipschitz obstacle (provided a suitable mesh is chosen), although we have not exploited this generalisation in this particular example. Furthermore, Ω_γ may comprise of many such objects. Similarly, γ and Γ may be connected, such that $\Gamma \cup \gamma$ is the boundary of a single connected obstacle. This would require more sophisticated bounds on $\|\mathcal{G}_{\gamma\to\Gamma}\|$, and would result in even more computationally demanding triple integrals, which may contain an integrand which is the product of two singular kernels. Likewise, Γ may be generalised to any surface for which the high frequency asymptotics are understood, and so may be penetrable (using theory of [31]) or non-convex (using [15]). In the case of penetrable Ω_Γ, this extension would not be trivial, and would require the beam tracing algorithm to incorporate the leading order behaviour emanating from γ. A more trivial extension would be to generalise the incident field to any of the types considered in Chapter 3, as discussed in Remark 4.6.

Chapter 5

Well-posedness of Galerkin BEM for high frequency multiple obstacle problems

The results produced in this chapter will appear in [29].

Previous HNA methods (Chapter 3, [35], and [15]) have utilised the coercivity of the star-combined operator to construct a k-independent Galerkin method with a unique solution for any approximation space, with k-explicit bounds on the quasi-optimality constant. However in Chapter 4, we are generally (aside from the cases discussed in Remark 4.11, some of which are proved in this chapter) forced to assume that $N \geq N_0$ without knowledge of N_0, and have no bounds on our stability constant C_q. In this case, we cannot predict how accurate our Galerkin method is, or even if a solution exists for a given N. More generally, the question of k-, h- or p- explicit conditions for uniqueness of the Galerkin equations and quasi-optimality estimates for any multiple scattering BEM is very much unanswered. In this chapter, we answer this question for two classes of multiple scattering domains. Given the complexity of hp-error analysis (investigated for single obstacles in, for example, [41]), we restrict our attention to h-BEM approximations.

The main result of this chapter (Theorem 5.5) is a condition for uniqueness of the Galerkin equations and bound on the stability constant for a mildly trapping (see Definition 5.4) multiple scattering configuration, which we believe to be the first result of its type for multiple scattering problems. We also provide new h-BEM best approximation estimates for polygonal configurations (Theorem 5.9) and show that the constellation combined operator of Definition 1.3 is coercive for a certain class of multiple scattering configurations (Theorem 5.7). Moreover, we prove fully explicit bounds on its coercivity constant.

Due to the lengthy proofs that follow, this chapter is structured differently to the others in this thesis, so we outline this structure here. In §5.1 we specify the type of problem considered in this chapter. In §5.2 we summarise the main results, which are subsequently proved in §5.3–§5.5. Further work is summarised in §5.6.

5.1 Specific problem statement

In this chapter we will consider the more general configuration of n_γ pairwise disjoint obstacles Ω_i with boundary γ_i, for $i = 1, \ldots, n_\gamma$. The majority of results hold for any incidence field (in the sense of Definition 1.1) and do not require polygonal obstacles, indeed some are for multiple smooth obstacles. In terms of the notation of the general problem statement §1.1.1, we have $\Omega_- = \bigcup_{i=1}^{n_\gamma} \Omega_i$ with boundary $\partial\Omega = \gamma = \bigcup_{i=1}^{n_\gamma} \gamma_i$. Additional restrictions on the geometry shall be specified as they are required.

Reformulating as a BIE (1.14), we will consider approximations on the following type of space.

DEFINITION 5.1 (h-refined spaces)**.** *For Lipschitz boundary γ we denote by $V_N^h(\gamma)$ the h-refined space of piecewise constant functions defined over a one-dimensional mesh*

$$\mathcal{M}_h(\gamma) := (x_i)_{i=0}^N \text{ on } [0, |\gamma|),$$

with $x_N = x_0$ (the parametrisation of the boundary is periodic), and $x_i > x_{i-1}$ for $i = 1, \ldots, N$. We also define the mesh width on the ith element to be $h_i := x_i - x_{i-1}$, and the parameter

$$h := \max_{i=1,\ldots,N} \{h_i\}.$$

We say that a mesh $\mathcal{M}_h(\gamma)$ is quasi-regular if there exists a $t \in (0, 1]$ such that

$$\frac{h}{t} \leq h_i \leq h, \quad \text{for } i = 1, \ldots, N.$$

The above definition implies that $h \to 0$ as $N \to \infty$. The Galerkin h-BEM problem we seek to solve is the following: Find v_h in $V_N^h(\gamma)$ such that

$$(\mathcal{A}v_h, \varphi)_{L^2(\gamma)} = (f, \varphi)_{L^2(\gamma)}, \quad \text{for all } \varphi \in V_N^h(\gamma), \tag{5.1}$$

where $\mathcal{A}$ and f may be of either formulation, Definition 1.2 or 1.3.

In this chapter, we seek $N_0 > 0$ such that v_h exists and is unique for all $N \geq N_0$. Given existence and uniqueness of v_h, we are also interested in k- and h- explicit bounds on the quasi-optimality constant $C_q \geq 1$, for which

$$\|\partial_{\mathbf{n}}^+ u - v_h\|_{L^2(\gamma)} \leq C_q \min_{w_h \in V_N^h(\gamma)} \|\partial_{\mathbf{n}}^+ u - w_h\|_{L^2(\gamma)}, \quad \text{for } N(h) \geq N_0 \tag{5.2}$$

Bounds on the stability constant C_q and N_0 are guaranteed by the following property.

DEFINITION 5.2 (Coercivity)**.** *We say $\mathcal{A}$ is coercive if there exists a constant $\zeta > 0$ such that*

$$\left|(\mathcal{A}\varphi, \varphi)_{L^2(\gamma)}\right| \geq \zeta \|\varphi\|^2_{L^2(\gamma)}, \quad \text{for all } \varphi \in L^2(\gamma),$$

and we call ζ the 'coercivity constant' of $\mathcal{A}$. We note that equivalent definitions of coercivity exist, see [49, Remark 2.1.55]

When the operator $\mathcal{A}$ is coercive, it follows from Cea's Lemma and the Lax–Milgram Theorem that (5.1) has a unique solution on any subspace $V_N^h(\gamma) \subset L^2(\gamma)$, i.e. $N_0 = 1$, with quasi-optimality constant $C_q = \|\mathcal{A}\|_{L^2(\gamma)\to L^2(\gamma)}/\zeta$.

REMARK 5.3 (Known coercive formulations for single scattering configurations)**.** *To the best knowledge of the authors, there currently exist no coercive formulations for the boundary element formulation of multiple scattering problems (excluding Theorem 5.7, which we present shortly). However, there have been a handful of results for single scattering ($n_\gamma = 1$) problems.*

(i) In the case of a single star-shaped obstacle (see Definition 1.3) γ, the star-combined operator of Definition 1.4 is coercive ([52]), with coercivity constant

$$\zeta = \operatorname*{ess\,inf}_{\mathbf{x}\in\gamma}\{\mathbf{n}(\mathbf{x}) \cdot (\mathbf{x} - \mathbf{x}_i^c)\}.$$

(ii) It is shown in [53] that the standard combined operator is coercive for sufficiently large k when γ is piecewise analytic and C^3 with strictly positive curvature, with $\zeta = 1 - O(k^{-1/2})$, for $k \geq k_0$.

(iii) The problem of scattering by a screen (and more generally, a fractal screen) is uniquely solvable (in the continuous case) with $\mathcal{A} = \mathcal{S}_k$, which is shown to be coercive with $\zeta = 1/(2\sqrt{2})$ in [14, Theorem 5.3].

(iv) For sufficiently large k, the standard combined-layer operator has been shown to be coercive for a range of obstacles, via an investigation of the numerical range in [8].

There are a range of other results available regarding the quasi-optimality constant C_q for h-BEM in the single scattering case, these can be found in [30] and [20], and are not stated here. The coercivity results we list above are more relevant in what follows, as we extend these to obtain bounds on C_q for multiple scattering cases.

It should be noted that the above remark is closely related to Remark 2.13, in which stability constants were discussed for single scattering problems.

5.2 Summary of main results

The ideas behind the two key results of this chapter, Theorems 5.5 and 5.7, share the same starting point. This is to take an operator $\mathcal{A}$ defined over multiple obstacles with combined boundary γ, and separate the coercive components corresponding to the single scattering cases. To do this and more generally focus on the interactions between individual pairs of scatterers, the following construction will be necessary.

Given $\mathcal{A}$ of (1.14), we are interested in cases where $\mathcal{A}_{\gamma_i \to \gamma_i}$ is coercive, with coercivity constant ζ_i for $i = 1, \ldots, n_\gamma$. This is equivalent to the operator $\mathcal{A}$ being coercive for the single scattering cases (as discussed in Remark 5.3), i.e. with $\gamma = \partial\Omega$ replaced by γ_i in (1.14). To handle the non-diagonal terms separately, we define the operator of cross terms $\mathcal{A}_\times : L^2(\gamma) \to L^2(\gamma)$,

$$\mathcal{A}_\times \varphi := \sum_{\ell=1, \ell \neq i}^{n_\gamma} \mathcal{A}_{\gamma_\ell \to \gamma_i} \varphi, \quad \text{on } \gamma_i, \quad \text{for } i = 1, \ldots, n_\gamma. \tag{5.3}$$

We now define the operator of diagonal terms $\mathcal{A}_D : L^2(\gamma) \to L^2(\gamma)$

$$\mathcal{A}_D \varphi := \sum_{i=1}^{n_\gamma} \mathcal{A}_{\gamma_i \to \gamma_i} \varphi, \quad \text{on } \gamma_i, \quad \text{for } i = 1, \ldots, n_\gamma. \tag{5.4}$$

Hence we have split the operator

$$\mathcal{A} = \underbrace{\qquad\qquad}_{n_\gamma \text{ single scattering components,}} \mathcal{A}_D + \underbrace{\qquad\qquad}_{n_\gamma(n_\gamma - 1) \text{ multiple obstacle interactions.}} \mathcal{A}_\times .$$

If each single scattering component $\mathcal{A}_{\gamma_i \to \gamma_i}$ is coercive, then $\mathcal{A}_D$ is coercive, and we may write

$$\left| (\mathcal{A}\varphi, \varphi)_{L^2(\gamma)} \right| \geq \sum_{i=1}^{n_\gamma} \zeta_i \|\varphi\|^2_{L^2(\gamma_i)} - \left| (\mathcal{A}_\times \varphi, \varphi)_{L^2(\gamma)} \right|, \quad \text{for } \varphi \in L^2(\gamma).$$

For the cases we are interested in, the kernel of the operator $\mathcal{A}_\times$ is smooth, and we shall see in Theorem 5.16 that $\mathcal{A}_\times$ has useful regularising properties. Under the assumption that $\mathcal{A}_\times : H^{-s}(\gamma) \mapsto H^s(\gamma)$ for $s \in [0, 1/2]$, we may write

$$\left| (\mathcal{A}\varphi, \varphi)_{L^2(\gamma)} \right| \geq \min_{i=1,\ldots,n_\gamma} \{\zeta_i\} \|\varphi\|^2_{L^2(\gamma)} - \left| \langle \mathcal{A}_\times \varphi, \varphi \rangle_{H^s(\gamma) \times H^{-s}(\gamma)} \right|, \quad \text{for } \varphi \in L^2(\gamma), \tag{5.5}$$

where we have appealed to the duality of the spaces $H^s(\gamma)$ and $H^{-s}(\gamma)$, for $s \geq 0$. Theorem 5.5 takes (5.5) with $\mathcal{A} = \mathcal{A}'_{k,\eta}$ (of Definition 1.2, constants ζ_i discussed in Remark 5.3(i)) with $\mathcal{A}_\times : H^{-1/2}(\gamma) \to H^{1/2}(\gamma)$ to construct a Gårding inequality, from which k- and h- explicit estimates can be obtained. Theorem 5.7 takes (5.5) and chooses $\mathcal{A} = \mathcal{A}_k$ (see Definition 1.4, constants ζ_i discussed in 5.3(ii)) with $\mathcal{A}_\times : L^2(\gamma) \to L^2(\gamma)$, from which we obtain a fully explicit condition for coercivity.

5.2.1 Well posedness and quasi-optimality

Before we can state our first condition for quasi-optimality (5.2), we specify the type of configuration to which it applies.

DEFINITION 5.4 (Mild trapping)**.** *We say a configuration Ω_- is 'mild trapping' [57, §2] if*

(i) each γ_i is C^∞ with strictly positive curvature,

(ii) for any γ_i and γ_j, there exists a convex set containing $\gamma_i \cup \gamma_j$ that does not intersect $\gamma \setminus (\gamma_i \cup \gamma_j)$.

The result that follows is based on the properties of the Dirichlet to Neumann map for mildly trapping configurations, which depends intimately on the resonances of the resolvent operator $(\Delta + k^2)^{-1}$. The proof is quite lengthy and is given in §5.4.

THEOREM 5.5. *If γ is mild trapping (in the sense of Definition 5.4) with $n_\gamma = 2$, then given $k_0 \geq \mathrm{e}$ there exist positive constants C and η_0, both independent of k and h, such that if η is chosen with*

$$\eta_0 k \leq \eta \lesssim k$$

and N is chosen such that

$$h \leq \frac{C}{k^2(1 + k^{7/6}\log k)^2(1 + k\log k)^2}, \quad \text{for } k \geq k_0, \tag{5.6}$$

the Galerkin equations (5.1) *with the standard combined operator (of Definition 1.2) $\mathcal{A} = \mathcal{A}'_{k,\eta}$ have a unique solution $v_h \in V_N^h(\gamma)$ defined on a uniform mesh (in the sense of Definition 5.1), which satisfies the stability condition*

$$\|\partial_{\mathbf{n}}^+ u - v_h\|_{L^2(\gamma)} \lesssim (1 + k^{7/6}\log k) \inf_{w_h \in V_N^h(\gamma)} \|\partial_{\mathbf{n}}^+ u - w_h\|_{L^2(\gamma)}, \tag{5.7}$$

for all $k \geq k_0$.

Hence in terms of the quasi-optimality condition (5.2), by Theorem 5.5 we have a condition (5.6) on h such that $N \geq N_0$ (recalling that h is inversely proportional to N), and a bound (5.7) on the stability constant C_q. We emphasise that there is no condition on the separation of the obstacles, the only restriction is on the smoothness and convexity of the boundary of each obstacle γ_i. To the best knowledge of the author, this is the first k-explicit stability result for multiple scattering BEM, and is one of the more general results of this thesis.

5.2.2 Results concerning the constellation combined operator

As discussed in Remark 5.3, the star combined operator of [52] is coercive for star-shaped obstacles. Harnessing the coercive properties of the single obstacle problem, we are able to construct geometries such that the interaction between the obstacles is sufficiently small that the coercivity property still holds. The results that follow apply to any operator which is coercive on a singe scatterer, although here we focus on the example of our extension of the star-combined of [52], as this is the only operator coercive on L^2 for which we have an explicit bound on the coercivity constants in the single scattering case.

We now collect some fundamental results about the constellation combined operator.

THEOREM 5.6. *For constellation-shaped (in the sense of Definition 1.3) γ, the constellation-combined operator $\mathcal{A}_k$ of Definition 1.4 is bounded and invertible on $L^2(\gamma)$, and there exists a $k_0 > \mathrm{e}$ such that*

$$\|\mathcal{A}_k\|_{L^2(\gamma)\to L^2(\gamma)} \lesssim k^{1/2}, \quad \textit{for } k \geq k_0$$

and

$$\|\mathcal{A}_k^{-1}\|_{L^2(\gamma)\to L^2(\gamma)} \lesssim \begin{cases} k^{3/2}\log k, & \textit{for } \gamma \textit{ a non-trapping polygon,} \\ k^{2/3}\log k, & \textit{for } \gamma \textit{ mild trapping,} \end{cases} \qquad \textit{for } k \geq k_0.$$

Proof. Invertibility: Using the notation of Definition 1.4, by [13, Theorem 2.41] the n_γ (homogeneous) oblique impedance problems on each γ_i have only the trivial solution. It then follows from [13, Corollary 2.40] that $\mathcal{A}_k$ is invertible.

Bound on $\|\mathcal{A}_k\|_{L^2(\gamma)\to L^2(\gamma)}$: Follows immediately from [52, Theorem 4.2].

Bound on $\|\mathcal{A}_k^{-1}\|_{L^2(\gamma)\to L^2(\gamma)}$: Proved in §5.5. □

We now state a restriction on the geometry of γ for which the constellation combined operator $\mathcal{A}_k$ is coercive. The proof relies on a series of intermediate results, which are in §5.3.

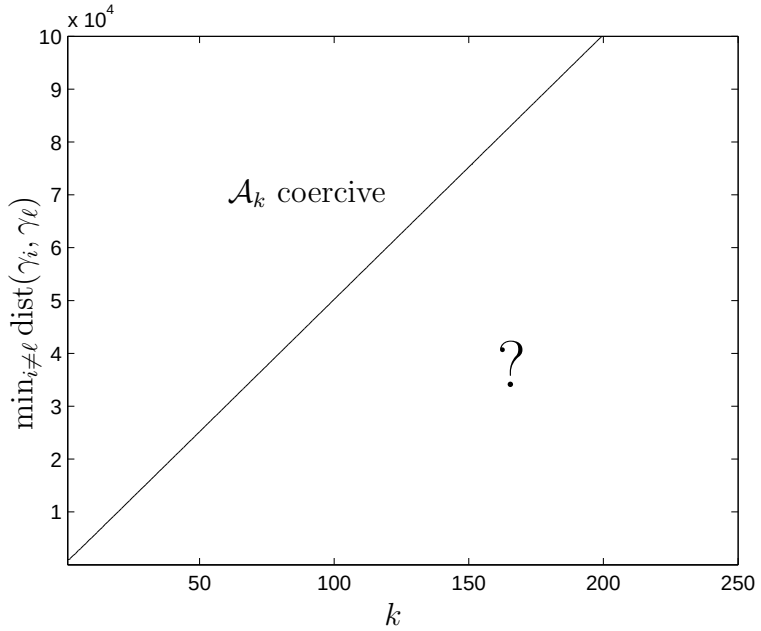

Figure 5.1: Separation required to ensure coercivity of a configuration of $N_\gamma \geq 2$ circles of radius 1, against wavenumber k. The upper-left region indicates the configurations for which a coercive formulation is possible using Theorem 5.7.

THEOREM 5.7 (Condition for coercivity of constellation-combined operator)**.** *Suppose γ is constellation-shaped (in the sense of Definition 1.3), with the separation of each obstacle γ_i large enough that $\zeta > 0$, where*

$$\zeta := \operatorname*{ess\,inf}_{\mathbf{x}\in\gamma} \{\mathbf{Z}(\mathbf{x}) \cdot \mathbf{n}(\mathbf{x})\} - \sum_{i=1}^{n_\gamma} \sqrt{\frac{|\gamma_i|(|\gamma| - |\gamma_i|)}{\pi \operatorname{dist}(\gamma_i, \gamma \setminus \gamma_i)}} \left[3 \max_{\ell\neq i} \{\operatorname{diam}(\gamma_\ell)\} \left(\sqrt{2k} + \frac{1}{\sqrt{\pi \operatorname{dist}(\gamma_i, \gamma \setminus \gamma_i)}} \right) + \frac{1}{\sqrt{8k}} \right]$$

holds, then the constellation-combined operator $\mathcal{A}_k$ (of Definition 1.4) is coercive (in the sense of Definition 5.2) with coercivity constant ζ. Here $|\cdot|$ represents the one-dimensional Hausdorff measure.

Whilst Theorem 5.7 represents the first coercive formulation for any class of multiple scattering configurations, it is important that we illustrate the extent of the above restriction. Suppose we consider the problem of scattering by N_γ circles of radius 1, Figure 5.1 represents the required minimal distance of the circles to ensure that the condition of Theorem 5.7 is satisfied.

5.2.3 Best approximation error for h-BEM

To complement the quasi-optimality results, we now present some best approximation results for the h-BEM case. We do not expect these estimates to be sharp, but they

are required for a complete analysis of the h-BEM method. Best approximation estimates depend on the incident wave, those we present in this section §5.2.3 are for plane waves, hence $u^{\text{inc}} = u^{\text{inc}}_{PW}$ of (2.5). The first best approximation result is not new, but is complementary to the problem of Theorem 5.5, so is included here.

THEOREM 5.8. *For a mildly trapping (in the sense of Definition 5.4) domain Ω_- with plane wave incidence* (2.5)*, given $k_0 > 0$, a uniform (in the sense of Definition 5.1) h-BEM enjoys the following best approximation property:*

$$\inf_{w_h \in V_N^h(\gamma)} \|v - w_h\|_{L^2(\gamma)} \lesssim hk^{7/6} \log k \|v\|_{L^2(\gamma)}, \quad \text{for } k \geq k_0.$$

Proof. Follows immediately from [20, Theorem 1.14(b)], as mild trapping domains can be written as a finite union of compact subsets of curved C^∞ hypersurfaces. □

We will shortly present the following best approximation result for configurations of multiple convex polygons, which is an extension of the single scattering case of [30, Theorem 1.2].

DEFINITION 5.9 ($V_N^h(\gamma)$ on a graded mesh)**.** *Suppose that Γ_j is a single side of length L_j of a polygonal obstacle. We define a* quasi-regular *(in the sense of Definition 5.1) graded mesh $(s_{\ell,j})_{\ell=1}^{2N_j}$ by*

$$s_{\ell,j} = \frac{L_j}{2}\left(\frac{\ell}{N_j}\right)^{q_j}, \quad \text{and} \quad s_{N_j+\ell,j} := L_j - \frac{L_j}{2}\left(\frac{N_j-\ell}{N_j}\right)^{q_j}, \quad \text{for } \ell = 0, \ldots, N_j,$$

where q_j is the grading parameter, chosen such that

$$q_j > \frac{2\omega_j^*}{2\pi - \omega_j^*}, \tag{5.8}$$

where $\omega_j^* = \max\{\omega_j, \omega_{j+1}\}$, with ω_j the internal angle of the jth corner, as in Definition 2.3. It follows that the diameter of the largest mesh element (of Definition 5.1) is

$$h = \max_j \max_{\ell=1,\ldots,2N_j-1} \{s_{\ell,j+1} - s_{\ell,j}\}.$$

We note that the definition of the graded mesh we consider here is different to that of §4.4 used for the HNA methods.

THEOREM 5.10. *Suppose we have plane wave incidence, with a multiple scattering configuration with combined boundary γ containing at least one convex polygon with boundary Γ. Suppose further that the condition* (4.16) *holds, with*

$$M_\infty(u) := \sup_{\mathbf{x} \in \Omega_+} |u(\mathbf{x})| \lesssim 1,$$

where u is the solution to the BVP (1.4)–(1.6). *Suppose further that a quasi-regular graded mesh (of Definitions 5.1(i) and 5.9) is used with $O(N)$ mesh points. Then given $k_0 > 0$ we have*

$$\inf_{w_h \in V_N^h(\gamma)} \|v - w_h\|_{L^2(\Gamma)} \lesssim \frac{k}{N}\|v\|_{L^2(\Gamma)} + hk^{3/2}\|v\|_{L^2(\gamma)}, \quad \text{for all } k > k_0,$$

where h is as in Definition 5.9. If Ω_γ consists entirely of convex polygons, then the same result applies with Γ replaced by γ on the left-hand side.

Proof. Recall we have the representation (4.9) on Γ_j,

$$v(s) = \Psi_{\mathrm{PW}}(\mathbf{x}_\Gamma(s)) + v_+(s - \tilde{L}_{j-1})\mathrm{e}^{\mathrm{i}ks} + v_+(\tilde{L}_j - s)\mathrm{e}^{\mathrm{i}-ks} + \mathcal{G}_{\gamma'\to\Gamma_j} v|_{\gamma'}(\mathbf{x}_\Gamma(s)), \quad (5.9)$$

for $s \in [\tilde{L}_{j-1}, \tilde{L}_j]$, where $\gamma' := \gamma \setminus \Gamma$ denotes the union of all other scatterers. We begin by bounding the final term of (5.9).

$$\inf_{w_h \in V_N^h(\gamma)} \left\|\mathcal{G}_{\gamma'\to\Gamma_j} v - w_h\right\|_{L^2(\Gamma_j)} \lesssim h \left\|\mathcal{G}_{\gamma'\to\Gamma_j} v\right\|_{H^1(\Gamma_j)},$$

from classical results on h-approximation theory (see e.g. [49, Theorem 4.3.22(b)]). Looking ahead to Theorem 5.16(ii) we obtain $\|\mathcal{G}_{\gamma'\to\Gamma_j}\|_{L^2(\gamma')\to H^1(\Gamma_j)} \lesssim k^{-1/2} + k^{3/2}$, choosing $k_0 \geq 1$ yields

$$\inf_{w_h \in V_N^h(\gamma)} \left\|\mathcal{G}_{\gamma'\to\Gamma_j} v - w_h\right\|_{L^2(\Gamma_j)} \lesssim hk^{3/2} \|v\|_{L^2(\gamma')} \lesssim hk^{3/2} \|v\|_{L^2(\gamma)}. \quad (5.10)$$

It is shown in §4.3 that the diffracted waves $v_\pm$ of (2.3) satisfy bounds analogous to the single scattering problem when (4.16) holds, which is the case provided that we choose $k_0 \geq 1/\mathrm{dist}(\Gamma, \gamma')$, hence the best approximation of the first three terms of (5.9) satisfy the same bounds as [30, Theorem 1.2], and are thus asymptotically bounded by k/N. □

We remark briefly that the above requirement does not require the polygons to be non-trapping (in the sense of Definition 2.2), only that the individual polygons are convex. Any trapping will be reflected in the size of $\|v\|_{L^2(\gamma)}$. Moreover, we hypothesise that the constraint may be relaxed to any polygonal domain, provided that similar bounds on $\|\mathcal{G}_{\gamma\to\Gamma_j}\|_{L^2(\gamma)\to H^1(\Gamma_j)}$ for non-convex Γ can be obtained, though this would require further work. The key difference is that neighbouring sides of Γ_j may lie in the relative upper half plane U_j of Γ_j, in which case the integrand of $\|\mathcal{G}_{\gamma\to\Gamma_j}\|_{L^2(\gamma)\to H^1(\Gamma_j)}$ is singular at the corner point between the two sides.

5.3 Proof of Theorem 5.7, conditions for coercivity of $\mathcal{A}_k$

If the separation between the obstacles increases, the interaction between them and therefore $\mathcal{A}_\times$ tends to zero. Here we aim to find a finite threshold beyond which the interaction between the obstacles is insufficient to beat the coercivity property. This idea is captured by the following lemma, which may be applied to operators other than the constellation-combined.

LEMMA 5.11. *Suppose an operator $\mathcal{A} : L^2(\gamma) \to L^2(\gamma)$ is such that the restriction (in the sense of Definition 1.6) $\mathcal{A}_{\gamma_i \to \gamma_i}$ is coercive (in the sense of Definition 5.2) with coercivity constant ζ_i for $i = 1, \ldots, N_\gamma$. If*

$$\zeta := \min_{i=1,\ldots,N_\gamma} \{\zeta_i\} - \sum_{i=1}^{n_\gamma} \|\mathcal{A}\|_{L^2(\gamma_i)\to(\gamma\setminus\gamma_i)} > 0, \tag{5.11}$$

then the operator $\mathcal{A}$ is coercive with

$$\left|(\mathcal{A}\varphi, \varphi)_{L^2(\gamma)}\right| \geq \zeta \|\varphi\|^2_{L^2(\gamma)}, \quad \text{for all } \varphi \in L^2(\gamma).$$

Proof. For $\varphi \in L^2(\gamma)$ we may split the operator $\mathcal{A}_\times$ into obstacle-wise components using Definition 5.3

$$(\mathcal{A}_\times \varphi, \varphi)_{L^2(\gamma)} = \sum_{i=1}^{n_\gamma} (\mathcal{A}_\times \varphi_i, \varphi)_{L^2(\gamma\setminus\gamma_i)},$$

which we can bound using the continuity of $\mathcal{A}$ and the triangle inequality

$$\left|(\mathcal{A}_\times \varphi, \varphi)_{L^2(\gamma)}\right| \leq \sum_{i=1}^{n_\gamma} \|\mathcal{A}\|_{L^2(\gamma_i)\to L^2(\gamma\setminus\gamma_i)} \|\varphi\|_{L^2(\gamma_i)} \|\varphi\|_{L^2(\gamma\setminus\gamma_i)}.$$

Noting that both $\|\varphi\|_{L^2(\gamma_i)}$ and $\|\varphi\|_{L^2(\gamma\setminus\gamma_i)} \leq \|\varphi\|_{L^2(\gamma)}$, we may bound further

$$\left|(\mathcal{A}_\times \varphi, \varphi)_{L^2(\gamma)}\right| \leq \|\varphi\|^2_{L^2(\gamma)} \sum_{i=1}^{n_\gamma} \|\mathcal{A}\|_{L^2(\gamma_i)\to L^2(\gamma\setminus\gamma_i)}.$$

The result follows immediately from (5.5), choosing $s = 0$.

□

REMARK 5.12 (Positive-definiteness analogy)**.** *When comparing integral operators with matrices, coercivity is often interpreted as a generalisation of positive-definiteness. In the same way Lemma 5.11 may be interpreted as a generalisation of strict diagonal dominance; the restriction* (5.11) *ensures that the off-diagonal terms of $\mathcal{A}_\times$ are sufficiently small when compared with the diagonal terms of $\mathcal{A}_D$ that the matrix of operators remains coercive. This is analogous to the case with square matrices, for which strict diagonal dominance ensures positive definiteness.*

For constellation-shaped (in the sense of Definition 1.3) γ, if we choose $\mathcal{A} = \mathcal{A}_k$ then $(\mathcal{A}_k)_{\gamma_i \to \gamma_i}$ is coercive (in the sense of Definition 5.2) with coercivity constant $\zeta_i = \operatorname*{ess\,inf}_{\mathbf{x} \in \gamma_i} \{(\mathbf{x} - \mathbf{x}_i) \cdot \mathbf{n}(\mathbf{x})\}$ for $i = 1, \ldots, N_\gamma$. Our aim now is to bound explicitly the constant ζ of (5.11) in this case, motivating the following lemma. For simplicity, we will use the shorthand of Definition 1.6 in this lemma, and for much of this chapter.

LEMMA 5.13. *For $X, Y \subset \gamma$ with relatively open X and Y with disjoint closure, if $\mathcal{T} : L^2(\gamma) \to L^2(\gamma)$ is an integral operator with kernel $\kappa(\mathbf{x}, \mathbf{y})$ essentially bounded for $\mathbf{x} \neq \mathbf{y}$, then*

$$\|\mathcal{T}\|_{L^2(Y) \to L^2(X)} \leq \sqrt{|X||Y|} \operatorname*{ess\,sup}_{\mathbf{x} \in X, \mathbf{y} \in Y} |\kappa(\mathbf{x}, \mathbf{y})| < \infty,$$

where $|\cdot|$ denotes the one-dimensional Hausdorff measure.

Proof. For $0 \neq \varphi \in L^2(Y)$,

$$\frac{\|\mathcal{T}\varphi\|_{L^2(X)}}{\|\varphi\|_{L^2(Y)}} = \frac{1}{\|\varphi\|_{L^2(Y)}} \left(\int_X \left| \int_Y \kappa(\mathbf{x}, \mathbf{y}) \varphi(\mathbf{y}) \, \mathrm{d}s(\mathbf{y}) \right|^2 \mathrm{d}s(\mathbf{x}) \right)^{1/2}. \tag{5.12}$$

Using the Cauchy–Schwarz inequality, we can write

$$\left| \int_Y \kappa(\mathbf{x}, \mathbf{y}) \varphi(\mathbf{y}) \, \mathrm{d}s(\mathbf{y}) \right| \leq \int_Y |\kappa(\mathbf{x}, \mathbf{y}) \varphi(\mathbf{y})| \, \mathrm{d}s(\mathbf{y}) \leq \|\kappa(\mathbf{x}, \cdot)\|_{L^2(Y)} \|\varphi\|_{L^2(Y)},$$

for $\mathbf{x} \in X$. Combining this with (5.13),

$$\begin{aligned} \frac{\|\mathcal{T}\varphi\|_{L^2(X)}}{\|\varphi\|_{L^2(Y)}} &\leq \frac{1}{\|\varphi\|_{L^2(Y)}} \left(\int_X \|\kappa(\mathbf{x}, \cdot)\|^2_{L^2(Y)} \|\varphi\|^2_{L^2(Y)} \, \mathrm{d}s(\mathbf{x}) \right)^{1/2} \\ &= \left(\int_X \int_Y |\kappa(\mathbf{x}, \mathbf{y})|^2 \, \mathrm{d}s(\mathbf{y}) \, \mathrm{d}s(\mathbf{x}) \right)^{1/2} \\ &\leq \left(\int_X \mathrm{d}s \int_Y \mathrm{d}s \right)^{1/2} \sup_{\mathbf{x} \in X, \mathbf{y} \in Y} |\kappa(\mathbf{x}, \mathbf{y})| \end{aligned}$$

and the result follows. □

This result can now be used to derive bounds on cross terms of integral operators.

LEMMA 5.14. *For $X, Y \subset \gamma$ with X and Y disjoint, we have the following bounds on*

(i) the single layer operator $\mathcal{S}_k$

$$\|\mathcal{S}_k\|_{L^2(Y) \to L^2(X)} \leq \sqrt{\frac{|X||Y|}{2\pi k \operatorname{dist}(X, Y)}},$$

(ii) the double layer operator $\mathcal{D}_k$ and its adjoint $\mathcal{D}'_k$

$$\left.\begin{matrix}\|\mathcal{D}_k\|_{L^2(Y)\to L^2(X)}\\ \|\mathcal{D}'_k\|_{L^2(Y)\to L^2(X)}\end{matrix}\right\} \leq \sqrt{|X||Y|}\left(\sqrt{\frac{k}{2\pi\,\mathrm{dist}(X,Y)}}+\frac{1}{\pi\,\mathrm{dist}(X,Y)}\right),$$

(iii) the product of $\mathbf{z}\in(L^\infty(X))^2$ with the surface gradient operator $\nabla_\gamma\mathcal{S}_k$

$$\|\mathbf{z}\cdot\nabla_\gamma\mathcal{S}_k\|_{L^2(Y)\to L^2(X)} \leq \operatorname*{ess\,sup}_{\mathbf{x}\in X}|\mathbf{z}(\mathbf{x})|\sqrt{|X||Y|}\left(\sqrt{\frac{2k}{\pi\,\mathrm{dist}(X,Y)}}+\frac{2}{\pi\,\mathrm{dist}(X,Y)}\right),$$

(iv) the Standard Combined operator

$$\|\mathcal{A}'_{k,\eta}\|_{L^2(Y)\to L^2(X)} \leq \sqrt{|X||Y|}\left[\sqrt{\frac{k}{2\pi\,\mathrm{dist}(X,Y)}}+\frac{1}{\pi\,\mathrm{dist}(X,Y)}+\frac{|\eta|}{\sqrt{2\pi\,\mathrm{dist}(X,Y)}}\right],$$

(v) the Constellation Combined operator with X and Y the boundaries of star-shaped obstacles,

$$\|\mathcal{A}_k\|_{L^2(Y)\to L^2(X)} \leq \sqrt{\frac{|X||Y|}{\pi\,\mathrm{dist}(X,Y)}}\left[3\max_{\mathbf{x}\in X}\{|\mathbf{Z}(\mathbf{x})|\}\left(\sqrt{2k}+\sqrt{\frac{1}{\pi\,\mathrm{dist}(X,Y)}}\right)+\sqrt{\frac{1}{8k}}\right].$$

Here $\mathbf{z}$ may be any $\mathbf{z}\in(L^\infty(X))^2$, whilst $\mathbf{Z}$ refers specifically to the vector $\mathbf{Z}$ of Definition 1.4.

Proof. (i): Single-layer
We take $\kappa(\mathbf{x},\mathbf{y}) = \frac{\mathrm{i}}{2}\Phi(\mathbf{x},\mathbf{y}) = \frac{\mathrm{i}}{2}H_0^{(1)}(k|\mathbf{x}-\mathbf{y}|)$ in the statement of Lemma 5.13. From A.7 we have that $|H_0^{(1)}(z)| \leq \sqrt{2/(\pi z)}$ for $z>0$, from which it follows that $|\kappa(\mathbf{x},\mathbf{y})| \leq \sqrt{1/(2\pi k|\mathbf{x}-\mathbf{y}|)}$, whilst from the disjointedness of X and Y, we have $|\kappa(\mathbf{x},\mathbf{y})| \leq \sqrt{1/(2\pi k\,\mathrm{dist}(X,Y))}$, and the result follows.

(ii): Double-layer
We prove only the bound on $\mathcal{D}_k$. For this case $\kappa(\mathbf{x},\mathbf{y}) = \frac{\mathrm{i}}{2}\partial\Phi(\mathbf{x},\mathbf{y})/\partial n(\mathbf{y}) = \frac{\mathrm{i}k}{2}H_1^{(1)}(k|\mathbf{x}-\mathbf{y}|)\mathbf{n}(\mathbf{x})\cdot(\mathbf{x}-\mathbf{y})/|\mathbf{x}-\mathbf{y}|$, we combine with A.8, which states that $|H_1^{(1)}(z)| \leq \sqrt{2/(\pi z)}+2/(\pi z)$ for $z>0$, and the result follows.

(iii): Surface gradient of single-layer
In this case we have the kernel $\kappa(\mathbf{x},\mathbf{y}) = 2\mathbf{z}(\mathbf{x})\cdot\nabla\Phi(\mathbf{x},\mathbf{y})-2(\mathbf{z}(\mathbf{x})\cdot\mathbf{n}(\mathbf{x}))\partial\Phi(\mathbf{x},\mathbf{y})/\mathbf{n}(\mathbf{x})$. By applying the triangle inequality and the discrete Cauchy Schwarz inequality to $\mathbf{z}$, we obtain $|\kappa(\mathbf{x},\mathbf{y})| \leq |\mathbf{z}(\mathbf{x})||H_1^{(1)}(k|\mathbf{x}-\mathbf{y}|)|$, and the result follows by the same

reasoning as the previous cases.

(iv): Standard combined
Combine (i) and (ii), follows by the definition of $\mathcal{A}'_{k,\eta}$ (see Definition 1.2).

(v): Constellation-combined
All notation is as in Definition 1.4. We first note that

$$\operatorname*{ess\,sup}_{\mathbf{x}\in X}|\mathbf{Z}(\mathbf{x})\cdot\mathbf{n}(\mathbf{x})| \le \sup_{\mathbf{x}\in X}|\mathbf{Z}(x)| \le \operatorname{diam}(X) \quad \text{and} \quad \|\hat{\eta}\|_{L^\infty(X)} \le k\operatorname{diam}(X)+\frac{1}{2},$$

since X is star shaped. Applying the triangle inequality yields

$$\begin{aligned}&\|\mathcal{A}_k\|_{L^2(Y)\to L^2(X)}\\ &\quad\le \operatorname{diam}(X)\|\mathcal{D}'_k\|_{L^2(Y)\to L^2(X)} + \|\mathbf{Z}\cdot\nabla_\gamma\mathcal{S}_k\|_{L^2(Y)\to L^2(X)} + \|\hat{\eta}\|_{L^\infty(X)}\|\mathcal{S}_k\|_{L^2(Y)\to L^2(X)}.\end{aligned}$$

Combining this with the above bounds on $\mathcal{S}_k$, $\mathcal{D}'_k$ and $\mathbf{z}\cdot\nabla_\gamma\mathcal{S}_k$ choosing $\mathbf{z}=\mathbf{Z}$,

$$\begin{aligned}\|\mathcal{A}_k\|_{L^2(Y)\to L^2(X)} \;\le\;& \operatorname{diam}(X)\sqrt{|X||Y|}\left(\sqrt{\frac{k}{2\pi\operatorname{dist}(X,Y)}}+\frac{1}{\pi\operatorname{dist}(X,Y)}\right)\\ &+2\operatorname{diam}(X)\sqrt{|X||Y|}\left(\sqrt{\frac{k}{2\pi\operatorname{dist}(X,y)}}+\frac{1}{\pi\operatorname{dist}(X,Y)}\right)\\ &+\sqrt{|X||Y|}\left(k\operatorname{diam}(X)+\frac{1}{2}\right)\sqrt{\frac{1}{2\pi k\operatorname{dist}(X,Y)}},\end{aligned}$$

the bound follows. □

Lemma 5.14 suggests that there exist configurations $\gamma\subset\mathbb{R}^2$ with wavenumbers k such that $\|\mathcal{A}_k\|_{L^2(\gamma_i)\to L^2(\gamma_j)}$ is small enough to satisfy the conditions of Lemma 5.11 for γ_i and γ_j two disjoint obstcales of the configuration γ, and the result of Theorem 5.7 follows.

Proof of Theorem 5.7. We apply Theorem 5.11 to $\mathcal{A}=\mathcal{A}_k$ on γ. The diagonal terms are coercive by [52] and the first term on the right-hand side of (5.5) simplifies since

$$\zeta_i := \operatorname*{ess\,inf}_{\mathbf{x}\in\gamma_i}\{\mathbf{n}(\mathbf{x})\cdot(\mathbf{x}-\mathbf{x}_i)\}, \qquad \text{hence} \qquad \min_i\{\zeta_i\} = \operatorname*{ess\,inf}_{\mathbf{x}\in\gamma}\{\mathbf{Z}(\mathbf{x})\cdot\mathbf{n}(\mathbf{x})\},$$

by the definition of $\mathbf{Z}$. The cross terms $\|\mathcal{A}\|_{L^2(\gamma_i)\to(\gamma\setminus\gamma_i)}$ can be bounded using Lemma 5.14(v), and the result follows from Lemma 5.11. □

5.4 Proof of Theorem 5.5, stability for multiple smooth obstacles

This proof depends on the fact that if γ is the combined boundary of multiple $C^{1,1}$ obstacles, then the regularity of $\mathcal{A}_\times : \gamma \to \gamma$ is stronger than that of $\mathcal{A} : \gamma \to \gamma$, from which it can be shown that $\mathcal{A}$ satisfies a Gårding inequality. Whilst it is a standard result (see, e.g., [13]) that for $|s| \leq 1/2$, $\mathcal{A} : H^{s-1/2}(\gamma) \to H^{s-1/2}(\gamma)$, we show here (for γ consisting of C^1 obstacles) that $\mathcal{A}_\times : H^{s-1/2}(\gamma) \to H^{s+1/2}(\gamma)$. Here, the improved regularity is a consequence of the smooth kernel of either choice of $\mathcal{A}_\times$, a property not enjoyed by $\mathcal{A}$, and a bound on $\|\mathcal{A}_\times\|_{H^{-1/2}(\gamma)\to H^{1/2}(\gamma)}$ enables us to write (5.5) as a Gårding inequality. As norms in $H^{s-1/2}(\gamma)$ and $H^{s+1/2}(\gamma)$ are difficult to compute, we interpolate via the following Lemma, which enables us to work in Sobolev spaces of integer order. We parametrise X by $\mathbf{x}(t_X)$ and Y by $\mathbf{y}(t_Y)$ in the natural way, with a piecewise continuous vector valued map, such that $|\dot{\mathbf{x}}| = 1$ for $t_X \in [0, |X|)$ and $|\dot{\mathbf{y}}| = 1$ for $t_Y \in [0, |Y|)$. This will simplify the integrals which must be computed to bound the operator norms we are interested in. Indeed, we will make use of the norm

$$\begin{aligned}&\|\kappa\|_{H^1(X\times Y)}\\ &:= \left(\int_0^{|X|}\int_0^{|Y|} |\kappa(\mathbf{x}(t_X),\mathbf{y}(t_Y))| + \left|\frac{\partial\kappa(\mathbf{x}(t_X),\mathbf{y}(t_Y))}{\partial t_X}\right| + \left|\frac{\partial\kappa(\mathbf{x}(t_X),\mathbf{y}(t_Y))}{\partial t_Y}\right|\right)^{1/2}\end{aligned} \tag{5.13}$$

LEMMA 5.15. *For relatively open $X, Y \subset \partial D$ with disjoint closures, if $\mathcal{T}$ is an integral operator with kernel $\kappa \in H^1(X\times Y)$ then the following mappings are bounded:*

(i)

$$\|\mathcal{T}_{Y\to X}\|_{H^{-1}(Y)\to L^2(X)} \leq \left(\int_0^{|X|} \|\kappa(\mathbf{x}(t_X),\cdot)\|^2_{H^1(Y)}\,\mathrm{d}t_X\right)^{1/2}.$$

(ii)

$$\|\mathcal{T}_{Y\to X}\|_{L^2(Y)\to H^1(X)} \leq \left(\int_0^{|X|} \|\kappa(\mathbf{x}(t_X),\cdot)\|^2_{L^2(Y)} + \left\|\frac{\mathrm{d}\kappa\,(\mathbf{x}(t_X),\cdot)}{\mathrm{d}t_X}\right\|^2_{L^2(Y)}\mathrm{d}t_X\right)^{1/2}.$$

(iii) For $s \in [-1/2, 1/2]$,

$$\|\mathcal{T}_{Y\to X}\|_{H^{-1/2+s}(Y)\to H^{1/2+s}(X)} \leq \|\kappa\|_{H^1(X\times Y)}.$$

Proof. (i): The definition of the operator norm states:

$$\|\mathcal{T}\|^2_{H^{-1}(Y)\to L^2(X)} := \sup_{\substack{\varphi_n\in H^{-1}(Y)\\ \varphi\neq 0}} \frac{\|T\varphi\|_{L^2(X)}}{\|\varphi\|_{H^{-1}(Y)}} \tag{5.14}$$

As φ may not be integrable, we instead consider the sequence $(\varphi_n)_{n\in\mathbb{N}}$ in $C^\infty(Y)$, such that

$$\lim_{n\to\infty} \|\varphi_n\|_{H^{-1}(Y)} = \|\varphi\|_{H^{-1}(Y)}.$$

We may now write

$$\begin{aligned}
\|\mathcal{T}\varphi_n\|^2_{L^2(X)} &:= \sup_{\substack{\varphi_n\in H^{-1}(Y)\\ \varphi\neq 0}} \int_0^{|X|} |\mathcal{T}_{Y\to X}\varphi_n(t_X)|^2 \,\mathrm{d}t_X, \\
&\leq \left(\int_0^{|Y|} |\kappa(\mathbf{x}(t_X),\mathbf{y}(t_Y))\varphi_n(\mathbf{y}(t_Y))|\right)^2 \mathrm{d}t_X, \\
&\leq \int_0^{|X|} \|\kappa(\mathbf{x}(t_X),\cdot)\|^2_{H^1(Y)} \,\|\varphi_n\|^2_{H^{-1}(Y)} \,\mathrm{d}t_X,
\end{aligned}$$

hence considering the limit as $n\to\infty$, noting the density of $C^\infty(Y)$ in $H^{-1}(Y)$, we obtain

$$\|\mathcal{T}\varphi\|^2_{L^2(X)} \leq \|\varphi\|^2_{H^{-1}(Y)} \int_0^{|X|} \|\kappa(\mathbf{x}(t_X),\cdot)\|^2_{H^1(Y)} \,\mathrm{d}t_X, \quad \text{for all } \varphi\in H^{-1}(Y). \tag{5.15}$$

The result follows by combining (5.14) with (5.15).

(ii) Similarly,

$$\begin{aligned}
&\|\mathcal{T}\|^2_{L^2(Y)\to H^1(X)} \\
= &\sup_{\substack{\varphi\in L^2(Y)\\ \varphi\neq 0}} \int_0^{|X|} \left[|\mathcal{T}_{Y\to X}\varphi(\mathbf{x}(t_X))|^2 + \left|\frac{\mathrm{d}}{\mathrm{d}t_X}\mathcal{T}_{Y\to X}\varphi(\mathbf{x}(t_X))\right|^2\right] \mathrm{d}t_X / \|\varphi\|_{L^2(Y)} \\
\leq &\sup_{\substack{\varphi\in L^2(Y)\\ \varphi\neq 0}} \int_0^{|X|} \left[\left(\int_0^{2\pi} \left|\kappa\big(\mathbf{x}(t_X),\mathbf{y}(t_Y)\big)\varphi\big(\mathbf{y}(t_Y)\big)\right| \mathrm{d}t_Y\right)^2\right. \\
&\left. + \left(\int_0^{|X|} \left|\frac{\partial\kappa}{\partial t_X}(\mathbf{x}(t_X),\mathbf{y})\varphi(\mathbf{y}(t_Y))\,\mathrm{d}t_Y\right|\right)^2\right] \mathrm{d}t_X \,/\, \|\varphi\|_{L^2(Y)} \\
\leq &\sup_{\substack{\varphi\in L^2(Y)\\ \varphi\neq 0}} \int_0^{|X|} \left[\left\|\kappa(\mathbf{x}(t_X),\cdot)\right\|^2_{L^2(Y)} \|\varphi\|^2_{L^2(Y)} + \left\|\frac{\partial\kappa}{\partial t_X}(\mathbf{x}(t_X),\cdot)\right\|^2_{L^2(Y)} \|\varphi\|^2_{L^2(Y)}\right] \mathrm{d}t_X \,/\, \|\varphi\|_{L^2(Y)},
\end{aligned}$$

again, the result follows immediately.

(iii) Taking the maximum of (i) and (ii) and interpolating (see for example [49, §2.1.7]) for $s\in(-1/2,1/2)$

$$\|\mathcal{T}_{Y\to X}\|^2_{H^{-1/2+s}(Y)\to H^{1/2+s}(X)} \leq \max\left\{\|\mathcal{T}_{Y\to X}\|^2_{H^{-1}(Y)\to L^2(X)}, \|\mathcal{T}_{Y\to X}\|^2_{L^2(Y)\to H^1(X)}\right\}$$

$$\begin{aligned} &\leq \|\kappa\|^2_{L^2(X\times Y)} + \left\|\frac{\partial\kappa}{\partial t_X}\right\|^2_{L^2(X\times Y)} + \left\|\frac{\partial\kappa}{\partial t_Y}\right\|^2_{L^2(X\times Y)} \\ &= \|\kappa\|^2_{H^1(X\times Y)}, \end{aligned}$$

by definition (5.13) of the $H^1(X \times Y)$ norm. □

The following theorem applies Lemma 5.15 to integral operators of interest, concerning bounds on the individual elements of $\mathcal{A}_\times$. As is the case throughout this thesis, the bounds in the following Lemma are of the form $a \lesssim b$, to denote $a \leq cb$, where c depends only on the geometry of the problem. In each case, the dependence of c on the geometry is clear from the proof, although the results of the theorem state only the k-dependence, which is all that is required for what follows.

THEOREM 5.16. *For $X, Y \subset \partial D$ disjoint with $X \in C^{1,1}$, there exist the following bounds on $H^{-1/2+s}(Y) \to H^{1/2+s}(X)$, for $s \in [-1/2, 1/2]$:*

(i) For the single-layer operator $\mathcal{S}_k$,

$$\|\mathcal{S}_k\|_{H^{s-1/2}(Y)\to H^{s+1/2}(X)} \lesssim k^{-1/2} + k.$$

(ii) For the adjoint double-layer operator $\mathcal{D}'_k$,

$$\|\mathcal{D}'_k\|_{H^{s-1/2}(Y)\to H^{s+1/2}(X)} \lesssim k^{-1/2} + k^{3/2}.$$

Moreover, if X is a straight line segment, we have a bound on the interaction operator (4.12)

$$\|\mathcal{G}_{Y\to X}\|_{H^{s-1/2}(Y)\to H^{s+1/2}(X)} \lesssim k^{-1/2} + k^{3/2}.$$

(iii) For the product of $\mathbf{Z}$ (as in Definition 1.4) with the surface gradient operator $\nabla_\gamma \mathcal{S}_k$,

$$\|\mathbf{Z}\cdot\nabla_\gamma \mathcal{S}_k\|_{H^{s-1/2}(Y)\to H^{s+1/2}(X)} \lesssim k^{-1/2} + k^{3/2}.$$

(iv) For the Standard Combined operator $\mathcal{A}'_{k,\eta}$

$$\|\mathcal{A}'_{k,\eta}\|_{H^{s-1/2}(Y)\to H^{s+1/2}(X)} \lesssim k^{-1/2} + k^{3/2} + |\eta|(k^{-1/2} + k).$$

(v) For the Constellation Combined operator $\mathcal{A}_k$

$$\|\mathcal{A}_k\|_{H^{s-1/2}(Y)\to H^{s+1/2}(X)} \lesssim k^{-1/2} + k^2.$$

Proof. In this proof, a bound on the derivative of the gradient of the fundamental solution is required, so we derive it here:

$$\begin{aligned}\frac{\partial}{\partial t_X}\left[\nabla_\gamma \Phi(\mathbf{x}(t_X),\mathbf{y})\right] &= -\frac{\mathrm{i}k}{4}\left(\frac{\dot{\mathbf{x}}}{|\mathbf{x}-\mathbf{y}|}+(\mathbf{x}-\mathbf{y})\frac{\dot{\mathbf{x}}\cdot(\mathbf{y}-\mathbf{x})}{|\mathbf{x}-\mathbf{y}|^3}\right)H_1^{(1)}(k|\mathbf{x}-\mathbf{y}|)\\ &\quad -\frac{\mathrm{i}k^2}{4}\dot{\mathbf{x}}\cdot\frac{(\mathbf{y}-\mathbf{x})}{|\mathbf{x}-\mathbf{y}|}\frac{(\mathbf{x}-\mathbf{y})}{|\mathbf{x}-\mathbf{y}|}H_1^{(1)'}(k|\mathbf{x}-\mathbf{y}|),\end{aligned}$$

namely

$$\left|\frac{\partial}{\partial t_X}\left[\nabla_\gamma \Phi(\mathbf{x}(t_X),\mathbf{y})\right]\right| \le \frac{k}{2\,\mathrm{dist}(X,Y)}\left|H_1^{(1)}(k|\mathbf{x}-\mathbf{y}|)\right|+\frac{k^2}{4}\left|H_1^{(1)'}(k|\mathbf{x}-\mathbf{y}|)\right|, \quad (5.16)$$

and by symmetry, we have the same bound for the derivative in t_Y,

$$\left|\frac{\partial}{\partial t_Y}\left[\nabla_\gamma \Phi(\mathbf{x},\mathbf{y}(t_Y))\right]\right| \le \frac{k}{2\,\mathrm{dist}(X,Y)}\left|H_1^{(1)}(k|\mathbf{x}-\mathbf{y}|)\right|+\frac{k^2}{4}\left|H_1^{(1)'}(k|\mathbf{x}-\mathbf{y}|)\right|. \quad (5.17)$$

Each of the bounds *(i)-(iii)* seeks to obtain an upper bound on $\|\kappa\|^2_{H^1(X\times Y)}$ for the kernel κ of the given integral operator $\mathcal{T}$, from which a bound on $\|\mathcal{T}_k\|_{H^{s-1/2}(Y)\to H^{s+1/2}(X)}$ follows immediately by Lemma 5.15 part *(iii)*.

(i): The single-layer operator $\mathcal{S}_k$ has kernel

$$\kappa_1(\mathbf{x},\mathbf{y}) := \Phi(\mathbf{x},\mathbf{y}) = \frac{\mathrm{i}}{4}H_0^{(1)}(k|\mathbf{x}-\mathbf{y}|). \quad (5.18)$$

Bounding the derivatives, we obtain

$$\left|\frac{\partial \kappa_1}{\partial t_X}(\mathbf{x}(t_X),\mathbf{y})\right| = \left|\frac{\mathrm{i}k}{4}\frac{\dot{\mathbf{x}}\cdot(\mathbf{x}-\mathbf{y})}{|\mathbf{x}-\mathbf{y}|}H_1^{(1)}(k\,|\mathbf{x}-\mathbf{y}|)\right| \le \frac{k}{4}\left|H_1^{(1)}(k|\mathbf{x}-\mathbf{y}|)\right| \quad (5.19)$$

and

$$\left|\frac{\partial \kappa_1}{\partial t_Y}(\mathbf{x},\mathbf{y}(t_Y))\right| = \frac{k}{4}\left|H_1^{(1)}(k\,|\mathbf{x}-\mathbf{y}|)\right|. \quad (5.20)$$

Bounding (5.18) using (A.7), and bounding (5.19) and (5.20) using (A.8), then integrating yields,

$$\begin{aligned}&\|\mathcal{S}_k\|^2_{H^{s-1/2}(Y)\to H^{s+1/2}(X)}\\ \le\ & \int_X\int_Y\left[\frac{1}{16k\,\mathrm{dist}(X,Y)}+\frac{k^2}{8}\left(\sqrt{\frac{2}{\pi k\,\mathrm{dist}(X,Y)}}+\frac{2}{\pi k\,\mathrm{dist}(X,Y)}\right)^2\right]\mathrm{d}s\,\mathrm{d}s\\ \le\ & \frac{|X||Y|}{16k\,\mathrm{dist}(X,Y)}+\frac{k^2}{8}|X||Y|\left(\sqrt{\frac{2k}{\pi\,\mathrm{dist}(X,Y)}}+\frac{2}{\pi\,\mathrm{dist}(X,Y)}\right)^2\end{aligned}$$

$$\lesssim \quad k^{-1} + k^2,$$

from which the result follows.

(ii): The adjoint double-layer operator $\mathcal{D}_k'$ has kernel

$$\kappa_2(\mathbf{x},\mathbf{y}) := \frac{\partial \Phi(\mathbf{x},\mathbf{y})}{\partial n(\mathbf{x})} = -\frac{\mathrm{i}k}{4}\frac{\mathbf{n}\cdot(\mathbf{x}-\mathbf{y})}{|\mathbf{x}-\mathbf{y}|}H_1^{(1)}(k|\mathbf{x}-\mathbf{y}|),$$

which is straightforward to bound using (A.7)

$$|\kappa_2(\mathbf{x},\mathbf{y})| \leq \frac{k}{4}\left|H_1^{(1)}(k|\mathbf{x}-\mathbf{y}|)\right| \leq \frac{k}{4}\sqrt{\frac{2}{\pi k \operatorname{dist}(X,Y)}} \lesssim k^{1/2}. \tag{5.21}$$

To bound the t_X derivative, we use the identity,

$$\left|\frac{\mathrm{d}\mathbf{n}}{\mathrm{d}t_X}(\mathbf{x}(t_X))\right| = \left|\frac{\mathrm{d}}{\mathrm{d}t_X}\begin{bmatrix}\dot{x}_2(t_X)\\ -\dot{x}_1(t_X)\end{bmatrix}\right| = \left|\begin{bmatrix}\ddot{x}_2(t_X)\\ -\ddot{x}_1(t_X)\end{bmatrix}\right| = |\ddot{\mathbf{x}}|, \tag{5.22}$$

in a distributional sense, justifying the requirement that the first derivative of $\mathbf{x}$ must be Lipschitz. To bound the derivative of the product, using (5.21), (5.22) and (5.16),

$$\begin{aligned}\left|\frac{\partial \kappa_2}{\partial t_X}(\mathbf{x}(t_X),\mathbf{y})\right| &\leq \left|\frac{\mathrm{d}\mathbf{n}(\mathbf{x}(t_X))}{\mathrm{d}t_X}\right|\left|\nabla_\gamma \Phi(\mathbf{x}(t_X),\mathbf{y})\right| + \left|\mathbf{n}(\mathbf{x}(t_X))\right|\left|\frac{\partial}{\partial t_X}\left[\nabla_\gamma \Phi(\mathbf{x}(t_X),\mathbf{y})\right]\right|,\\ &\leq k\left(\frac{|\ddot{\mathbf{x}}|}{4} + \frac{1}{2\operatorname{dist}(X,Y)}\right)\left|H_1^{(1)}(k|\mathbf{x}-\mathbf{y}|)\right| + \frac{k^2}{4}\left|H_1^{(1)'}(k|\mathbf{x}-\mathbf{y}|)\right|,\end{aligned}$$

and from this,

$$\begin{aligned}&\int_X\int_Y \left|\frac{\partial \kappa_2}{\partial t_X}\right|^2 \mathrm{d}s\,\mathrm{d}s\\ &\quad\leq k^2|Y|\left(\frac{\|\ddot{\mathbf{x}}\|_{L^2(X)}^2}{16} + \frac{|X|}{4\operatorname{dist}(X,Y)^2} + \frac{|X|\|\ddot{\mathbf{x}}\|_{L^2(X)}}{4\operatorname{dist}(X,Y)}\right)|H_1^{(1)}(k\operatorname{dist}(X,Y))|^2\\ &\qquad + \frac{|X||Y|k^3}{4}\left(\frac{\|\ddot{\mathbf{x}}\|_{L^2(X)}}{4} + \frac{1}{2\operatorname{dist}(X,Y)}\right)|H_1^{(1)}(k\operatorname{dist}(X,Y))||H_1^{(1)'}(k\operatorname{dist}(X,Y))|\\ &\qquad + \frac{|X||Y|k^4}{16}|H_1^{(1)'}(k\operatorname{dist}(X,Y))|^2.\end{aligned}$$

We can bound using (A.8) and (A.9), focusing on the k dependence,

$$\begin{aligned}&\int_X\int_Y \left|\frac{\partial \kappa_2}{\partial t_X}\right|^2 \mathrm{d}s\,\mathrm{d}s\\ &\quad\leq k^2|Y|\left(\frac{\|\ddot{\mathbf{x}}\|_{L^2(X)}^2}{16} + \frac{|X|}{4\operatorname{dist}(X,Y)^2} + \frac{|X|\|\ddot{\mathbf{x}}\|_{L^2(X)}}{4\operatorname{dist}(X,Y)}\right)\end{aligned}$$

$$
\begin{aligned}
&\times \left(\sqrt{\frac{2}{\pi k \operatorname{dist}(X,Y)}} + \frac{4}{\pi k \operatorname{dist}(X,Y)} \right)^2 \\
&+ \frac{|X||Y|k^3}{4} \left(\frac{\|\ddot{\mathbf{x}}\|_{L^2(X)}}{4} + \frac{1}{2\operatorname{dist}(X,Y)} \right) \left(\sqrt{\frac{2}{\pi k \operatorname{dist}(X,Y)}} + \frac{4}{\pi k \operatorname{dist}(X,Y)} \right) \\
&\quad \times \left(\sqrt{\frac{2}{\pi k \operatorname{dist}(X,Y)}} + \frac{4}{\pi k \operatorname{dist}(X,Y)} + \frac{2}{\pi k^2 \operatorname{dist}(X,Y)^2} \right) \\
&+ \frac{|X||Y|k^4}{16} \left(\sqrt{\frac{2}{\pi k \operatorname{dist}(X,Y)}} + \frac{4}{\pi k \operatorname{dist}(X,Y)} + \frac{2}{\pi k^2 \operatorname{dist}(X,Y)^2} \right)^2 \\
&\lesssim k^{-1} + k^3. \qquad (5.23)
\end{aligned}
$$

The terms involving derivatives of $\mathbf{x}$ are properties of the geometry of X, and so are absorbed into the constant. Similar but simpler calculations using (A.8) and (A.9) to bound (5.17) show

$$\int_X \int_Y \left| \frac{\partial \kappa_2}{\partial t_Y} \right|^2 \mathrm{d}s \, \mathrm{d}s \lesssim k^{-1} + k^3. \qquad (5.24)$$

Combining (5.21), (5.23) and (5.24) yields

$$\|\mathcal{D}'_k\|_{H^{s-1/2}(Y) \to H^{s+1/2}(X)} \lesssim k^{-1/2} + k^{3/2},$$

as required. The special case for the operator $\mathcal{G}_{Y \to X}$, where X is a subset of a straight line segment, follows identical arguments as the kernel is either zero, or the equal to κ_2.

(iii): Here for simplicity we assume that X is star shaped. This is sufficient for every immediate use of this Theorem, although the asymptotic result is unaffected. The kernel for the surface potential operator is

$$
\begin{aligned}
\kappa_3(\mathbf{x}, \mathbf{y}) &:= \mathbf{Z}(\mathbf{x}) \cdot \left(\nabla_\gamma \Phi_k(\mathbf{x}, \mathbf{y}) - \mathbf{n}(\mathbf{x}) \frac{\partial \Phi_k(\mathbf{x}, \mathbf{y})}{\partial \mathbf{n}(\mathbf{x})} \right) \\
&= (\mathbf{Z}(\mathbf{x}) - (\mathbf{Z}(\mathbf{x}) \cdot \mathbf{n}(\mathbf{x}))\mathbf{n}(\mathbf{x})) \cdot \nabla_\gamma \Phi_k(\mathbf{x}, \mathbf{y}) \qquad (5.25)
\end{aligned}
$$

and it is straightforward to show that

$$|\mathbf{Z}(\mathbf{x}) - (\mathbf{Z}(\mathbf{x}) \cdot \mathbf{n}(\mathbf{x}))\mathbf{n}(\mathbf{x})| \leq \operatorname{diam}(X). \qquad (5.26)$$

Hence we can bound (5.25) using (5.26),

$$|\kappa_3(\mathbf{x}, \mathbf{y})| \leq \frac{k \operatorname{diam}(X)}{2} \left| H_1^{(1)}(k|\mathbf{x} - \mathbf{y}|) \right| \leq \frac{k \operatorname{diam}(X)}{2} \sqrt{\frac{2}{\pi k \operatorname{dist}(X,Y)}} \lesssim k^{1/2}. \qquad (5.27)$$

Before the t_X derivative can be bounded, an intermediate bound is required. We begin by differentiating the vector components of the operator,

$$\begin{aligned}&\tfrac{\mathrm{d}}{\mathrm{d}t_X}\left[\mathbf{Z}(\mathbf{x}) - (\mathbf{Z}(\mathbf{x})\cdot\mathbf{n}(\mathbf{x}))\mathbf{n}(\mathbf{x})\right]\\ &= \dot{\mathbf{x}} - \left(\dot{\mathbf{x}}\cdot\mathbf{n}(\mathbf{x}) + \mathbf{Z}(\mathbf{x})\cdot\begin{bmatrix}\dot{x}_2\\ -\dot{x}_1\end{bmatrix}\right)\mathbf{n}(\mathbf{x}) - (\mathbf{Z}(\mathbf{x})\cdot\mathbf{n}(\mathbf{x}))\begin{bmatrix}\ddot{x}_2\\ -\ddot{x}_1\end{bmatrix}.\end{aligned}$$

This can be bounded in terms of geometric parameters,

$$\left|\frac{\mathrm{d}}{\mathrm{d}t_X}\left[\mathbf{Z}(\mathbf{x}) - (\mathbf{Z}(\mathbf{x})\cdot\mathbf{n}(\mathbf{x}))\mathbf{n}(\mathbf{x})\right]\right| \leq 1 + \left(1 + |\ddot{\mathbf{x}}|\right)\operatorname{diam}(X). \tag{5.28}$$

By the product rule

$$\begin{aligned}\left|\frac{\partial\kappa_3}{\partial t_X}(\mathbf{x},\mathbf{y})\right| &\leq \left|\frac{\partial}{\partial t_X}\left[\Big(\mathbf{Z}(\mathbf{x}) - \Big(\mathbf{Z}(\mathbf{x}(t_X))\cdot\mathbf{n}(\mathbf{x}(t_X))\Big)\mathbf{n}(\mathbf{x}(t_X))\Big)\cdot\nabla_\gamma\Phi(\mathbf{x}(t_X),\mathbf{y})\right]\right|\\
&\leq \left|\frac{\mathrm{d}}{\mathrm{d}t_X}\left[\mathbf{Z}(\mathbf{x}(t_X)) - \Big(\mathbf{Z}(\mathbf{x}(t_X))\cdot\mathbf{n}(\mathbf{x}(t_X))\Big)\mathbf{n}(\mathbf{x}(t_X))\right]\cdot\nabla_\gamma\Phi(\mathbf{x}(t_X),\mathbf{y})\right|\\
&\quad + \left|\Big(\mathbf{Z}(\mathbf{x}) - \Big(\mathbf{Z}(\mathbf{x})\cdot\mathbf{n}(\mathbf{x})\Big)\mathbf{n}(\mathbf{x})\Big)\cdot\frac{\partial}{\partial t_X}\Big[\nabla_\gamma\Phi(\mathbf{x}(t_X),\mathbf{y})\Big]\right|\\
&\leq \operatorname{diam}(X)\left(\frac{k}{\operatorname{dist}(X,Y)}\left|H_1^{(1)}(k|\mathbf{x}-\mathbf{y}|)\right| + \frac{k^2}{2}\left|H_1^{(1)'}(k|\mathbf{x}-\mathbf{y}|)\right|\right)\\
&\quad + \frac{k}{4}\Big(1 + \left(1 + |\ddot{\mathbf{x}}|\right)\operatorname{diam}(X)\Big)\left|H_1^{(1)}(k|\mathbf{x}-\mathbf{y}|)\right|,\end{aligned}$$

using the bounds (5.26), (5.28) and (5.16). We can therefore bound

$$\begin{aligned}&\int_X\int_Y\left|\frac{\partial\kappa_3}{\partial t_X}\right|^2\mathrm{d}s\,\mathrm{d}s\\
&\leq |X||Y|\operatorname{diam}(X)^2\left(\frac{k}{\operatorname{dist}(X,Y)}\left|H_1^{(1)}(k|\mathbf{x}-\mathbf{y}|)\right| + \frac{k^2}{2}\left|H_1^{(1)'}(k|\mathbf{x}-\mathbf{y}|)\right|\right)^2\\
&\quad + |Y||H_1^{(1)}(k|\mathbf{x}-\mathbf{y}|)\\
&\quad \times|\operatorname{diam}(X)\left(\frac{k}{\operatorname{dist}(X,Y)}|H_1^{(1)}(k|\mathbf{x}-\mathbf{y}|)| + \frac{k^2}{2}|H_1^{(1)'}(k|\mathbf{x}-\mathbf{y}|)|\right)\\
&\quad\quad\times\frac{k|X|}{2}\left(1 + \frac{\operatorname{diam}(X)}{2}\left(1 + \operatorname{diam}(X)\|\ddot{\mathbf{x}}\|_{L^2(\gamma)}\right)\right)\\
&\quad + \frac{k^2|Y|}{16}\left(4|X| + \operatorname{diam}(X)\left(|X| + \|\ddot{\mathbf{x}}\|_{L^2(X)}^2 + |X|(1 + \|\mathbf{x}\|_{L^2(X)})\right)\right)\\
&\quad\times\left|H_1^{(1)}(k|\mathbf{x}-\mathbf{y}|)\right|^2\\
&\leq |X||Y|\operatorname{diam}(X)^2\left(\frac{k}{\operatorname{dist}(X,Y)}\left(\sqrt{\frac{2}{\pi k\operatorname{dist}(X,Y)}} + \frac{4}{\pi k\operatorname{dist}(X,Y)}\right)\right.\end{aligned}$$

$$
\begin{aligned}
&+ \frac{k^2}{2}\left(\sqrt{\frac{2}{\pi k\,\mathrm{dist}(X,Y)}} + \frac{4}{\pi k\,\mathrm{dist}(X,Y)} + \frac{2}{\pi k^2\,\mathrm{dist}(X,Y)^2}\right)\Bigg)^2 \\
&+ |Y|\left(\sqrt{\frac{2}{\pi k\,\mathrm{dist}(X,Y)}} + \frac{4}{\pi k\,\mathrm{dist}(X,Y)}\right) \\
&\quad \times \mathrm{diam}(X)\Bigg(\frac{k}{\mathrm{dist}(X,Y)}\left(\sqrt{\frac{2}{\pi k\,\mathrm{dist}(X,Y)}} + \frac{4}{\pi k\,\mathrm{dist}(X,Y)}\right) \\
&+ \frac{k^2}{2}\left(\sqrt{\frac{2}{\pi k\,\mathrm{dist}(X,Y)}} + \frac{4}{\pi k\,\mathrm{dist}(X,Y)} + \frac{2}{\pi k^2\,\mathrm{dist}(X,Y)^2}\right)\Bigg) \\
&\quad \times \frac{k|X|}{2}\left(1 + \frac{\mathrm{diam}(X)}{2}\left(1 + \mathrm{diam}(X)\|\ddot{\mathbf{x}}\|_{L^2(\gamma)}\right)\right) \\
&+ \frac{k^2|Y|}{16}\left(4|X| + \mathrm{diam}(X)\left(|X| + \|\ddot{\mathbf{x}}\|^2_{L^2(X)} + |X|(1 + \|\mathbf{x}\|_{L^2(X)})\right)\right) \\
&\quad \times \left(\sqrt{\frac{2}{\pi k\,\mathrm{dist}(X,Y)}} + \frac{4}{\pi k\,\mathrm{dist}(X,Y)}\right)^2 \\
&\lesssim 1 + k^{3/2}. \qquad (5.29)
\end{aligned}
$$

The bound on the derivative in t_Y is simpler to compute, following from (5.17) and (5.26),

$$
\begin{aligned}
&\left|\frac{\partial \kappa_3}{\partial t_Y}(\mathbf{x}, \mathbf{y}(t_Y))\right| \leq \\
&\mathrm{diam}(Y)\left(\frac{k}{\mathrm{dist}(X,Y)} H_1^{(1)}(k|\mathbf{x}-\mathbf{y}|) + \frac{k^2}{2} H_1^{(1)'}(k|\mathbf{x}-\mathbf{y}|)\right) \\
&\leq \mathrm{diam}(Y)\left(\frac{k}{\mathrm{dist}(X,Y)}\left(\sqrt{\frac{2}{\pi k\,\mathrm{dist}(X,Y)}} + \frac{4}{\pi k\,\mathrm{dist}(X,Y)}\right)\right) \\
&\quad + \mathrm{diam}(Y)\frac{k^2}{2}\left(\left(\sqrt{\frac{2}{\pi k\,\mathrm{dist}(X,Y)}} + \frac{4}{\pi k\,\mathrm{dist}(X,Y)} + \frac{2}{\pi k^2\,\mathrm{dist}(X,Y)^2}\right)\right) \\
&\lesssim 1 + k^{3/2}. \qquad (5.30)
\end{aligned}
$$

Combining (5.27), (5.29) and (5.30) proves the claim. The bounds *(iv)* and *(v)* follow directly from the bounds *(i)-(iii)*. □

Although the previous bound is for multiple $C^{1,1}$ obstacles, we could apply the single obstacle coercivity result of Remark 5.3(ii) to the diagonal operator $(\mathcal{A}_{k,\eta})_D$, to rewrite (5.5) as the following Gårding inequality for C^3 obstacles,

$$
\langle \mathcal{A}\varphi, \varphi\rangle_{L^2(\gamma)\times L^2(\gamma)} \geq \zeta_D \|\varphi\|^2_{L^2(\gamma)} - \zeta_\times \|\varphi\|^2_{H^{-1/2}(\gamma)}, \quad \text{for all } \varphi \in L^2(\gamma), \qquad (5.31)
$$

where $\mathcal{A} = \mathcal{A}'_{k,\eta}$ or $\mathcal{A}_k$, with $\zeta_\times = \|\mathcal{A}_\times\|_{H^{-1/2}(\gamma)\to H^{1/2}(\gamma)}$ and $\zeta_D = \min_i\{\zeta_i\}$, whilst ζ_i are the coercivity constants from the corresponding single scattering cases (discussed in Remark 5.3). At this stage, one may apply standard results for Gårding inequalities of (for example), [51, Theorem 5.21], to obtain a condition on h which will guarantee there exists a unique solution of (5.2) and provide a bound on the constant C_q. However, this condition is in terms of quantities which we cannot bound using results in the current literature, so we will require a slightly different approach if we are to use best approximation bounds currently available to us. In particular, we will restrict our attention to the case $\mathcal{A} = \mathcal{A}'_{k,\eta}$ for multiple C^∞ obstacles, as we shall require results regarding the adjoint of $\mathcal{A}$, which has not been studied for the constellation combined operator. Hereafter we use the notation

$$\langle \cdot, \cdot \rangle_\gamma := \langle \cdot, \cdot \rangle_{H^s(\gamma)\times H^{-s}(\gamma)}, \quad \text{for } s \in [-1, 1],$$

justified by the duality pairing between $H^{-s}(\gamma)$ and $H^s(\gamma)$. Denote by $\mathcal{S}_0 : H^{-1/2}(\gamma) \to H^{1/2}(\gamma)$ the single-layer operator for the Laplace problem,

$$\mathcal{S}_0\varphi(\mathbf{x}) := \frac{-1}{2\pi}\int_\gamma \log|\mathbf{x}-\mathbf{y}|\varphi(\mathbf{y})\,\mathrm{d}s(\mathbf{y}), \quad \text{for } \varphi \in H^{-1/2}(\gamma).$$

It is well known that $\mathcal{S}_0$ is coercive (see for example [51, (9.15)]);

$$\langle \mathcal{S}_0\varphi, \varphi\rangle_\gamma \geq \zeta_0\|\varphi\|^2_{H^{-1/2}(\gamma)}, \quad \text{for all } \varphi \in H^{-1/2}(\gamma), \tag{5.32}$$

for some $\zeta_0 > 0$. We shall now adapt the classical quasi-optimality result which follows from a Gårding inequality, using quantities associated with $\mathcal{S}_0$.

THEOREM 5.17 (Modified Gårding inequality)**.** *Let $a : L^2(\gamma)\times L^2(\gamma)$ be a continuous, injective bilinear form satisfying a Gårding inequality, i.e. there exist positive constants ζ_D and $\zeta_\times$ such that*

$$|a(\varphi,\varphi)| \geq \zeta_D\|\varphi\|^2_{L^2(\gamma)} - \zeta_\times\|\varphi\|^2_{H^{-1/2}(\gamma)}, \quad \textit{for all } \varphi \in L^2(\gamma). \tag{5.33}$$

Given $f \in H^{-1/2}(\gamma)$, define $\mathcal{A}^*f \in L^2(\gamma)$ as the solution to the variational problem

$$a(\varphi, \mathcal{A}^*f) = \langle \varphi, \mathcal{S}_0 f\rangle_\gamma, \quad \textit{for all } \varphi \in L^2(\gamma), \tag{5.34}$$

where $\mathcal{S}_0 : H^{-1/2}(\gamma) \to H^{1/2}(\gamma)$ denotes the single-layer operator for the Laplace problem. Let $(V_N)_{N\in\mathbb{N}}$ be a dense sequence of finite-dimensional nested subspaces of $L^2(\gamma)$, and let

$$\mathcal{E}(V_N) := \sup_{f\in H^{-1/2}(\gamma)} \min_{v_h\in V_N} \frac{\|\mathcal{A}^*f - v_h\|_{L^2(\gamma)}}{\|f\|_{H^{-1/2}(\gamma)}}. \tag{5.35}$$

If

$$\mathcal{E}(V_N) \leq \frac{\zeta_0}{C_a}\left(\frac{\zeta_D\zeta_0}{2\zeta_\times\|\mathcal{S}_0\|_{H^{-1/2}(\gamma)\to H^{1/2}(\gamma)}}\right)^{1/2}, \tag{5.36}$$

where C_a is the continuity constant of a, then the Galerkin equations (5.1) *have a unique solution v_h, which satisfies*

$$\|v - v_h\|_{L^2(\gamma)} \leq \frac{2C_a}{\zeta_D}\min_{w_h\in V_N}\|v - w_h\|_{L^2(\gamma)}. \tag{5.37}$$

Proof. We begin by assuming the solution v_h exists. Given that a satisfies a Gårding inequality (5.33), we can use the coercivity result (5.32) to write

$$\zeta_D\|\varphi\|^2_{L^2(\gamma)} - \frac{\zeta_\times}{\zeta_0}\langle\mathcal{S}_0\varphi,\varphi\rangle_\gamma \leq |a(\varphi,\varphi)|, \quad \text{for all } \varphi\in L^2(\gamma). \tag{5.38}$$

The modified Gårding inequality (5.38) applied to $\varphi = v - v_h$ implies that

$$\zeta_D\|v - v_h\|^2_{L^2(\gamma)} - \frac{\zeta_\times}{\zeta_0}\|\mathcal{S}_0\|_{H^{-1/2}(\gamma)\to H^{1/2}(\gamma)}\|v - v_h\|^2_{H^{-1/2}(\gamma)} \leq |a(v - v_h, v - v_h)|.$$

By Galerkin Orthogonality, the right-hand side of this inequality can be replaced by $|a(v - v_h, v - w_h)|$ for any $w_h \in V_N$ Using this along with continuity constant C_a of $a(\cdot,\cdot)$, we find that

$$\zeta_D\|v-v_h\|^2_{L^2(\gamma)}-\frac{\zeta_\times}{\zeta_0}\|\mathcal{S}_0\|_{H^{-1/2}(\gamma)\to H^{1/2}(\gamma)}\|v-v_h\|^2_{H^{-1/2}(\gamma)} \leq C_a\|v-v_h\|_{L^2(\gamma)}\|v-w_h\|_{L^2(\gamma)}, \tag{5.39}$$

for all $v_h \in V_N$. Therefore, quasi-optimality (5.37) follows if we can show

$$\left(\frac{\zeta_\times}{\zeta_0}\|\mathcal{S}_0\|_{H^{-1/2}(\gamma)\to H^{1/2}(\gamma)}\right)^{1/2}\|v - v_h\|_{H^{-1/2}(\gamma)} \leq \left(\frac{\zeta_D}{2}\right)^{1/2}\|v - v_h\|_{L^2(\gamma)}, \tag{5.40}$$

by squaring both sides, substituting into (5.39) and dividing by $\|v - v_h\|_{L^2(\gamma)}$.

Choosing $f = v - v_h$ in the definition of $\mathcal{A}^*$ (5.34), by Galerkin orthogonality and continuity of a, we can write

$$\begin{aligned}\langle\mathcal{S}_0(v - v_h), v - v_h\rangle_\gamma &= a\left(v - v_h, \mathcal{A}^*(v - v_h)\right)\\ &= a\left(v - v_h, \mathcal{A}^*(v - v_h) - w_h\right)\\ &\leq C_a\|v - v_h\|_{L^2(\gamma)}\|\mathcal{A}^*(v - v_h) - w_h\|_{L^2(\gamma)}.\end{aligned} \tag{5.41}$$

Now the definition of $\mathcal{E}(V_N)$ (5.35) implies that there exists a $w_h \in V_N$ such that

$$\|\mathcal{A}^*(v - v_h) - w_h\|_{L^2(\gamma)} \leq \mathcal{E}(V_N)\|v - v_h\|_{H^{-1/2}(\gamma)}.$$

Using this to bound the right-hand side of (5.41) and the coercivity (5.32) to bound the left-hand side of (5.41), we divide through by $\|v - v_h\|_{H^{-1/2}(\gamma)}$ to obtain

$$\|v - v_h\|_{H^{-1/2}(\gamma)} \leq \frac{C_a}{\zeta_0} \mathcal{E}(V_N) \|v - v_h\|_{L^2(\gamma)}.$$

Therefore (5.36) implies that (5.40) and thus also (5.37) holds.

Existence of v_h follows identical arguments to the proof of [51, Theorem 5.21]. □

We will use this Theorem with $a(\cdot, \cdot) = (\mathcal{A}'_{k,\eta}[\cdot], \cdot)_{L^2(\gamma)}$. We note that the operator $\mathcal{A}^*$ is closely related to an adjoint problem, and we will thus require bounds on the adjoint of the Standard Combined Formulation (1.2)

$$\mathcal{A}_{k,\eta} := \mathcal{I} + \mathcal{D}'_k - \mathrm{i}\eta \mathcal{S}_k. \tag{5.42}$$

In particular we will require $\|\mathcal{A}^{-1}_{k,\eta}\|_{H^{1/2}(\gamma) \to H^{1/2}(\gamma)}$ for a mildly trapping domain, in order to bound the solution of the adjoint problem (5.34). To do this, we will first bound the DtN map of Definition 1.7. This uses the result of [57] for mild trapping domains, which provides a resonance free strip in the complex plane for the operator $\chi(\Delta + k^2)^{-1}\chi$, where χ is a compactly supported $C^\infty(\Omega_+)$ function.

LEMMA 5.18. *For a mildly trapping (in the sense of Definition 5.4) domain Ω_- with boundary γ consisting of $n_\gamma = 2$ obstacles, and u^s the scattered field of the solution to the BVP (1.4)–(1.6), given $k_0 \geq \mathrm{e}$ we have the following bound on the Dirichlet to Neumann map*

$$\|\partial^+_{\mathbf{n}} u^s\|_{L^2(\gamma)} \lesssim k \log k \|\tau_+ u^s\|_{H^1(\gamma)}, \quad \textit{for } k \geq k_0.$$

Proof. Define the cut-off function χ to be smooth with compact support, such that $\chi = 1$ in a neighbourhood of γ. We have the mild trapping result from [57], if $\tilde{u} \in H^1_{\mathrm{loc}}(\Omega_+)$ satisfies $(\Delta + k^2)\tilde{u} = f$ in Ω_+, where $f \in L^2(\Omega_+)$ has compact support, and $\tilde{u}$ satisfies the radiation condition (1.6) and boundary condition $\tau_+ \tilde{u} = 0$, then we have the resolvent estimate

$$\|\chi \tilde{u}\|_{H^1_k(\Omega_+)} \lesssim \log k \|f\|_{L^2(\Omega_+)}, \quad \text{for } k \geq k_0. \tag{5.43}$$

For $g_D \in H^1(\gamma)$, we define

(i) u^s such that $(\Delta + k^2)u^s = 0$ in Ω_+ with $\tau_+ u^s = g_D$ on γ, also u^s satisfies the radiation condition (1.6). This term is intended to represent the scattered field of the problem (1.4)-(1.6).

(ii) w such that $(\Delta + k^2 + \mathrm{i}|k|)w = 0$ in Ω_+ with $\tau_+ w = g_D$ on γ, also w satisfies the radiation condition (1.6).

(iii) $v := \tilde{u} - \chi w$

(iv) $h := \mathrm{i}|k|\chi w - w\Delta\chi - 2\nabla w \cdot \nabla\chi$

It follows from these definitions that $v \in H^1_{\mathrm{loc}}(\Omega_+)$, satisfies the Sommerfeld radiation condition and $(\Delta + k^2)v = h$ in Ω_+ and $\tau_+ v = 0$ on γ. Since h has compact support, we can use (5.43) to write

$$\|\chi v\|_{H^1_k(\Omega_+)} \lesssim \log k \|h\|_{L^2(\Omega_+)}, \quad \text{for } k \geq k_0. \tag{5.44}$$

By the definition (iv) of h we can write

$$\|h\|_{L^2(\Omega_+)} \lesssim \|w\|_{H^1_k(\Omega_+)}, \quad \text{for } k \geq k_0, \tag{5.45}$$

hence we can bound (5.44) using (5.45) to write

$$\|\chi v\|_{H^1_k(\Omega_+)} \lesssim \log k \|w\|_{H^1_k(\Omega_+)}, \quad \text{for } k \geq k_0. \tag{5.46}$$

It follows from the definition (iii) of v that

$$\|\chi\tilde{u}\|_{H^1_k(\Omega_+)} \lesssim \|\chi v\|_{H^1_k(\Omega_+)} + \|\chi w\|_{H^1_k(\Omega_+)}, \tag{5.47}$$

hence combining with (5.46) with (5.47) we can write for $k \geq k_0$

$$\begin{aligned} \|\chi\tilde{u}\|_{H^1_k(\Omega_+)} &\lesssim \log k \|w\|_{H^1_k(\Omega_+)} + \|\chi w\|_{H^1_k(\Omega_+)} \\ &\lesssim \log k \|w\|_{H^1_k(\Omega_+)}, \end{aligned} \tag{5.48}$$

where we have combined the norms under the assumption that $k_0 \geq \mathrm{e}$, to force $\log k \geq 1$. We now collect two further results from [6] which will enable us to obtain the result as claimed. Firstly, [6, Lemma 3.3] gives the result

$$\|w\|_{H^1_k(\Omega_+)} \lesssim \|g_D\|_{H^1_k(\gamma)}, \quad \text{for } k \geq k_0, \tag{5.49}$$

combining the above (5.49) with (5.48) gives

$$\|\chi\tilde{u}\|_{H^1_k(\Omega_+)} \lesssim \log k \|g_D\|_{H^1_k(\gamma)}, \quad \text{for } k \geq k_0. \tag{5.50}$$

Secondly, applying [6, Lemma 2.3(i)] to u^s gives us

$$\|\partial^+_{\mathbf{n}} u^s\|_{L^2(\gamma)} \lesssim \|\nabla_\gamma \tau_+ u^s\|_{L^2(\gamma)} + \|\chi u^s\|_{H^1_k(\Omega_+)}, \quad \text{for } k \geq k_0. \tag{5.51}$$

Now we piece everything together. Applying (5.50) choosing $\tilde{u} = \chi u^s$ and adding $\|\nabla_\gamma \tau_+ u^s\|_{L^2(\gamma)}$ to both sides yields for $k \geq k_0$

$$\begin{aligned}\|\nabla_\gamma \tau_+ u^s\|_{L^2(\gamma)} + \|\chi u^s\|_{H^1_k(\Omega_+)} &\lesssim \|\nabla_\gamma \tau_+ u^s\|_{L^2(\gamma)} + \log k \|u^s\|_{H^1_k(\gamma)} \\ &\lesssim \log k \|u^s\|_{H^1_k(\gamma)}, \end{aligned} \tag{5.52}$$

where we have again combined the norms under the assumption that $k_0 \geq \mathrm{e}$, and we have written $\tau_+ u^s$ instead of g_D (they are equal by the definition (i)). Bounding (5.52) below using (5.51) yields

$$\|\partial^+_{\mathbf{n}} u^s\|_{L^2(\gamma)} \lesssim \log k \|\tau_+ u^s\|_{H^1_k(\gamma)}, \quad \text{for } k \geq k_0,$$

from which the result follows by the definition (A.4) of the $H^1_k(\gamma)$ norm. □

Lemma 5.18 may be interpreted as the following bound on the Dirichlet to Neumann operator of §1.7: given k_0, for mild trapping domains (in the sense of Definition 5.4) of two obstacles with boundary γ we have

$$\|P^+_{\mathrm{DtN}}\|_{L^2(\gamma) \to H^1(\gamma)} \lesssim k \log k, \quad \text{for } k \geq k_0.$$

Despite being closely related to our problem, the bound on the Dirichlet to Neumann map of Lemma 5.18 is not sufficient to bound $\mathcal{A}^{-1}$. We must consider also the *interior impedance problem*, which is:

Given $\psi \in H^{-1/2}(\gamma)$ and $\eta \in \mathbb{R} \setminus \{0\}$, find $u^- \in C^2(\Omega_-) \cap H^1(\Omega_-)$ such that $(\Delta + k^2)u^- = 0$ holds in Ω_- and $\partial^-_n u^- - \mathrm{i}\eta \tau_- u_- = \psi$ on γ.

We will also make use of bounds on the interior impedance to Dirichlet map $P^{-,\eta}_{\mathrm{ItD}} : H^{1/2}(\gamma) \to H^{-1/2}(\gamma)$ which takes interior impedance data ψ to the interior Dirichlet trace of the solution $\tau_- u^-$. Further details can be found in [13, §2.7].

THEOREM 5.19. *For a mild trapping (in the sense of Definition 5.4) two obstacle domain, given $k_0 \geq \mathrm{e}$ we have a bound on the inverse of the adjoint of the Standard Combined Layer Operator:*

$$\|\mathcal{A}^{-1}_{k,\eta}\|_{H^{1/2}(\gamma) \to H^{1/2}(\gamma)} \lesssim 1 + |\eta| + k \log k, \quad \textit{for } k \geq k_0.$$

Proof. We use the representation [13, (2.89)] to write

$$\mathcal{A}^{-1}_{k,\eta} = \mathcal{I} - P^{-,\eta}_{ItD}(P^+_{DtN} - \mathrm{i}\eta), \tag{5.53}$$

which we can bound

$$\begin{aligned}&\|\mathcal{A}_{k,\eta}^{-1}\|_{H^{1/2}(\gamma)\to H^{1/2}(\gamma)}\\&\leq 1+\|P_{ItD}^{-,\eta}\|_{H^{-1/2}(\gamma)\to H^{1/2}(\gamma)}\|P_{DtN}^{+}\|_{H^{1/2}(\gamma)\to H^{-1/2}(\gamma)}+|\eta|\|P_{ItD}^{-,\eta}\|_{H^{1/2}(\gamma)\to H^{1/2}(\gamma)}.\end{aligned}\tag{5.54}$$

Combining Lemma 5.18 with [50, Lemma 2.3] we obtain

$$\|P_{DtN}^{+}\|_{H^{1/2}(\gamma)\to H^{-1/2}(\gamma)}\leq k\log k,\quad \text{for } k\geq k_0.\tag{5.55}$$

We now consider two separate interior impedance problems, for data φ and $\psi\in H^{1/2}(\gamma)$,

$$(\Delta+k^2)v=0 \text{ in } \Omega_-,\quad \text{with}\quad (\partial_n^- - \mathrm{i}\eta)v=\varphi \text{ on } \gamma\tag{5.56}$$

and

$$(\Delta+k^2)w=0 \text{ in } \Omega_-,\quad \text{with}\quad (\partial_n^- - \mathrm{i}\eta)w=\psi \text{ on } \gamma.\tag{5.57}$$

By application of Green's second identity to v and w in Ω_- we can write

$$\int_\gamma v(\partial_n^- - \mathrm{i}\eta)w=\int_\gamma w(\partial_n^- - \mathrm{i}\eta)v,$$

and from the condition on γ of (5.56) and (5.57)

$$\int_\gamma v\psi=\int_\gamma w\varphi.$$

Since the choice of φ and ψ in $H^{1/2}(\gamma)$ was arbitrary, we may write

$$\langle P_{ItD}\varphi,\psi\rangle_\gamma'=\langle\varphi,P_{ItD}\psi\rangle_\gamma',\quad \text{for all } \varphi,\psi\in H^{1/2}(\gamma),$$

where $\langle\cdot,\cdot\rangle_\gamma'$ denotes the real L^2 inner product. Hence by the same arguments as [50, Lemma 2.3] we can write

$$\|P_{ItD}^{-,\eta}\|_{H^{-1/2}(\gamma)\to H^{1/2}(\gamma)}\leq\|P_{ItD}^{-,\eta}\|_{L^2(\gamma)\to H^1(\gamma)},\quad \text{for } k\geq k_0,$$

which may be combined with [6, Corollary 1.9] to obtain

$$\|P_{ItD}^{-,\eta}\|_{H^{-1/2}(\gamma)\to H^{1/2}(\gamma)}\lesssim 1.\tag{5.58}$$

Finally we note, since $H^{1/2}(\gamma)\subset H^{-1/2}(\gamma)$, that

$$\|P_{ItD}^{-,\eta}\|_{H^{1/2}(\gamma)\to H^{1/2}(\gamma)}\leq\|P_{ItD}^{-,\eta}\|_{H^{-1/2}(\gamma)\to H^{1/2}(\gamma)}.\tag{5.59}$$

Combining (5.54), (5.55), (5.58) and (5.59) proves the assertion. □

This bound on $\mathcal{A}_{k,\eta}^{-1}$ enables us to prove the main result of this section, Theorem 5.5.

Proof of Theorem 5.5. It follows immediately from (5.5) with $s = 1/2$ that $\mathcal{A}'_{k,\eta}$ satisfies a Gårding inequality (5.33), choosing ζ_D to be the minimum of the coercivity constant for the single scattering problems on γ_1 and γ_2 (these follow from [53, Theorem 1.2], conditions are explained in (5.64)), separating the diagonal terms as before with $\zeta_\times = \|(\mathcal{A}'_{k,\eta})_\times\|_{H^{1/2}(\gamma)\to H^{-1/2}(\gamma)}$. Hence Theorem 5.17 can provide us with conditions to prove the assertion, but we must bound each constant of Theorem 5.17 appropriately, given the context in which we are applying it. We choose the bilinear form of Theorem 5.17 to be $a(\phi,\varphi) = \left(\mathcal{A}'_{k,\eta}\phi,\varphi\right)_{L^2(\gamma)}$, with approximation space $V_N = V_N^h(\gamma)$ of Definition 5.1. The problem (5.34) to solve becomes

$$\left(\mathcal{A}'_{k,\eta}\phi, \mathcal{A}^* f\right)_{L^2(\gamma)} = \langle \phi, \mathcal{S}_0 f\rangle_{H^{-1/2}(\gamma)\times H^{1/2}(\gamma)}, \quad \text{for } \phi \in L^2(\gamma), \tag{5.60}$$

hence

$$(\phi, \mathcal{A}_{k,\eta}\mathcal{A}^* f)_{L^2(\gamma)} = \langle \phi, \mathcal{S}_0 f\rangle_{H^{-1/2}(\gamma)\times H^{1/2}(\gamma)}, \quad \text{for } \phi \in L^2(\gamma),$$

and thus a solution to (5.60) is

$$\mathcal{A}^* f = \mathcal{A}_{k,\eta}^{-1}\mathcal{S}_0 f, \tag{5.61}$$

so we choose $\mathcal{A}^* = \mathcal{A}_{k,\eta}^{-1}\mathcal{S}_0$. Standard h-space approximation theory from, for example, [54, Theorem 10.4] tells us that

$$\min_{v_h\in V_N^h(\gamma)} \|\mathcal{A}^* f - v_h\|_{L^2(\gamma)} \leq h^{1/2}\|\mathcal{A}^* f\|_{H^{1/2}(\gamma)}. \tag{5.62}$$

Combining (5.62) with (5.61) and bounding the right-hand side yields

$$\min_{v_h\in V_N^h(\gamma)} \|\mathcal{A}^* f - v_h\|_{L^2(\gamma)} \leq h^{1/2}\left\|\mathcal{A}_{k,\eta}^{-1}\right\|_{H^{1/2}(\gamma)\to H^{1/2}(\gamma)}\|\mathcal{S}_0\|_{H^{-1/2}(\gamma)\to H^{1/2}(\gamma)}\|f\|_{H^{-1/2}(\gamma)},$$

and hence by (5.35) we may write

$$\mathcal{E}(V_N^h(\gamma)) \leq h^{1/2}\left\|\mathcal{A}_{k,\eta}^{-1}\right\|_{H^{1/2}(\gamma)\to H^{1/2}(\gamma)}\|\mathcal{S}_0\|_{H^{-1/2}(\gamma)\to H^{1/2}(\gamma)}.$$

Substituting the relevant parameters into (5.35), it follows that a sufficient condition for (5.36) to hold is

$$h \leq \left(\frac{\zeta_0}{\left\|\mathcal{A}_{k,\eta}^{-1}\right\|_{H^{1/2}(\gamma)\to H^{1/2}(\gamma)}\|\mathcal{A}'_{k,\eta}\|_{L^2(\gamma)\to L^2(\gamma)}}\right)^2 \frac{\zeta_D\zeta_0}{2\|(\mathcal{A}'_{k,\eta})_\times\|_{H^{-1/2}(\gamma)\to H^{1/2}(\gamma)}\|\mathcal{S}_0\|^3_{H^{-1/2}(\gamma)\to H^{1/2}(\gamma)}}. \tag{5.63}$$

To obtain the condition (5.6) on the mesh width h, we now bound each term on the right-hand side of (5.63) below, to ensure that h is chosen sufficiently small such that this bound holds. It is therefore equivalent to bound above the terms in the denominator of (5.63). The Laplacian single layer operator does not depend on k, hence

$$\zeta_0 = O(1), \quad \text{and } \|\mathcal{S}_0\|_{H^{-1/2}(\gamma)\to H^{1/2}(\gamma)} = O(1).$$

From [53, Theorem 1.2] and [53, (1.15a)] we know that given $\delta > 0$, there exists a $k_0 > 0$ and an $\eta_0 > 0$ such that

$$1 - \delta \lesssim \zeta_D, \quad \text{for } k \geq k_0, \tag{5.64}$$

for $\eta_0 k \lesssim \eta$, (noting the scaling adjustment discussed in Remark 1.5) where ζ_D the coercivity constant for the single scattering case. Henceforth we assume this condition on η holds, and we can write $1 \lesssim \zeta_D$ for $k \geq k_0$.

Now we focus on the remaining operator norms contained in (5.63).

- We have $\|(\mathcal{A}'_{k,\eta})_\times\|_{H^{-1/2}(\gamma)\to H^{1/2}(\gamma)} \lesssim k^2$ for $k \geq k_0$, from Theorem 5.16(iv), choosing $\eta = O(k)$.
- We have $\|\mathcal{A}_{k,\eta}^{-1}\|_{H^{1/2}(\gamma)\to H^{1/2}(\gamma)} \lesssim 1 + k\log k$ for $k \geq k_0$, from Theorem 5.19, choosing $\eta = O(k)$.
- Applying the triangle inequality to the definition of $\|\mathcal{A}'_{k,\eta}\|_{L^2(\gamma)\to L^2(\gamma)}$, we may bound using [20, (1.32)], to obtain $\|\mathcal{A}'_{k,\eta}\|_{L^2(\gamma)\to L^2(\gamma)} \lesssim 1 + k^{7/6}\log k$ for $k \geq k_0$, choosing $\eta = O(k)$.

For the bound on the quasi-optimality constant (5.37), we must bound (5.7) above, first we use (5.64) to write $\zeta_D^{-1} \lesssim 1$, which combined with the above bound on $\|\mathcal{A}'_{k,\eta}\|_{L^2(\gamma)\to L^2(\gamma)}$, gives us the bound

$$2\frac{C_\alpha}{\zeta_D} \lesssim 1 + k^{7/6}\log k, \quad \text{for } k \geq k_0,$$

completing the proof. □

With further work, this proof may be extended to configurations of $n_\gamma \geq 3$ obstacles. The key component is the bound (5.43), which may be extended to mild trapping domains of an arbitrary number of obstacles, provided that Definition 5.4 still holds, using results of [40] and [46] on trapping for several convex bodies.

5.5 Proof of Theorem 5.6, bounds on inverse of constellation combined

We now turn our attention to the bounds on $\mathcal{A}_k^{-1}$ of Theorem 5.6. A further construction is required to do this. Our interior oblique impedance problem [13, (2.6)] is:

Given $\psi \in L^2(\gamma)$ with $\mathbf{Z}$ and $\hat{\eta}$ as in Definition 1.4, find $u^- \in C^2(\Omega_-) \cap H^1(\Omega_-)$ with $\tau_- u^- \in H^1(\gamma)$, such that $(\Delta + k^2)u^- = 0$ holds in Ω_- and $\mathbf{n} \cdot \mathbf{Z}\partial_n^- u^- + \mathbf{Z} \cdot \nabla_\gamma \tau_- u^- \mathrm{i}\hat{\eta}\tau_- u^- = \psi$ on γ.

We denote the corresponding oblique impedance to Dirichlet map by $P_{\mathrm{ItD}}^{-,\hat{\eta},\mathbf{Z}}$.

LEMMA 5.20. *We have the following bound on the oblique interior impedance to Dirichlet map, for $k > k_0$*

$$\|P_{ItD}^{-,\hat{\eta},\mathbf{x}}\|_{L^2(\gamma_i)\to H_k^1(\gamma_i)} \lesssim \begin{cases} k^{1/2}\log k, & \gamma_i \text{ star-shaped and piecewise smooth,} \\ k^{1/3}, & \gamma_i \in C^\infty \text{ with strictly positive curvature.} \end{cases}$$

Proof. The interior oblique impedance problem may be split into n_γ disjoint problems, as there is no interaction between the obstacles. Without loss of generality, we consider the problem on one obstacle with boundary γ_i, and translate the obstacle such that $\mathbf{x}_i^c = 0$, where $\mathbf{x}_i^c$ is the central point of Definition 1.4. Hence we consider an arbitrary Ω_i, inside which $\tilde{u}$ is the solution to the interior oblique impedance problem, such that

$$\begin{aligned} (\Delta + k^2)\tilde{u} = 0, &\quad \text{inside } \Omega_i, \\ (\mathbf{x}\cdot\nabla - \mathrm{i}\hat{\eta})\tilde{u} = w, &\quad \text{on } \gamma_i. \end{aligned}$$

By [13, Corollary 2.41], for $\hat{\eta}$ defined as in Definition 1.3, this has a unique solution with

$$\tau_-\tilde{u} = \mathcal{S}_k\phi = P_{\mathrm{ItD}}^{-,\hat{\eta},\mathbf{x}} w, \tag{5.65}$$

where $\phi := \mathcal{A}_k^{-1} w$. additionally we have that

$$\|\phi\|_{L^2(\gamma_i)} \leq \frac{2}{\operatorname{ess\,inf}_{\mathbf{x}\in\gamma_i}\{\mathbf{x}\cdot\mathbf{n}(\mathbf{x})\}} \|w\|_{L^2(\gamma_i)}. \tag{5.66}$$

By the definition of the operator norm, we can write

$$\|P_{\mathrm{ItD}}^{-,\hat{\eta},\mathbf{x}}\|_{L^2(\gamma_i)\to H_k^1(\gamma_i)} \leq \sup_{w\in L^2(\gamma_i)} \frac{\|P_{\mathrm{ItD}}^{-,\hat{\eta},\mathbf{x}} w\|_{H_k^1(\gamma_i)}}{\|w\|_{L^2(\gamma_i)}},$$

by (5.65) we have that

$$\|P_{\mathrm{ItD}}^{-,\hat{\eta},\mathbf{x}}\|_{L^2(\gamma_i)\to H_k^1(\gamma_i)} \leq \sup_{w\in L^2(\gamma_i)} \frac{\|\mathcal{S}_k\phi\|_{H_k^1(\gamma_i)}}{\|w\|_{L^2(\gamma_i)}},$$

and by (5.66) it follows that

$$\|P_{\mathrm{ItD}}^{-,\hat{\eta},\mathbf{x}}\|_{L^2(\gamma_i)\to H_k^1(\gamma_i)} \leq \sup_{w\in L^2(\gamma_i)} \frac{\|\mathcal{S}_k\phi\|_{H_k^1(\gamma_i)}}{\|\phi\|_{L^2(\gamma_i)}},$$

hence

$$\|P_{\mathrm{ItD}}^{-,\hat{\eta},\mathbf{x}}\|_{L^2(\gamma_i)\to H_k^1(\gamma_i)} \leq \|\mathcal{S}_k\|_{L^2(\gamma_i)\to H_k^1(\gamma_i)}.$$

The result then follows from the bounds on the single layer operator given in [20, Theorem 1.4]. □

We are now ready to prove the bounds on $\mathcal{A}_k^{-1}$.

Proof of Theorem 5.6. If γ is constellation shaped, it follows immediately from [13, Theorem 2.42] that

$$\begin{aligned}\|\mathcal{A}_k^{-1}\|_{L^2(\gamma)\to L^2(\gamma)} \leq & \frac{1}{\operatorname*{ess\,inf}_{\mathbf{x}\in\gamma}\{\mathbf{Z}(\mathbf{x})\cdot\mathbf{n}(\mathbf{x})\}}\left[1+\frac{\|\hat{\eta}\|_{L^\infty(\gamma)}}{k}+\|\mathbf{Z}\|_{L^\infty(\gamma)}\right]\|P_{\mathrm{ItD}}^{-,\hat{\eta},\mathbf{Z}}\|_{L^2(\gamma)\to H_k^1(\gamma)} \\ & + \|P_{\mathrm{DtN}}^{+}P_{\mathrm{ItD}}^{-,\hat{\eta},\mathbf{Z}}\|_{L^2(\gamma)\to L^2(\gamma)},\end{aligned}$$

which we can simplify further using Definition 1.4 of $\mathbf{Z}$ and $\hat{\eta}$, and splitting the second norm

$$\|\mathcal{A}_k^{-1}\|_{L^2(\gamma)\to L^2(\gamma)} \lesssim \left(1+\|P_{\mathrm{DtN}}^{+}\|_{H_k^1(\gamma)\to L^2(\gamma)}\right)\|P_{\mathrm{ItD}}^{-,\hat{\eta},\mathbf{Z}}\|_{L^2(\gamma)\to H_k^1(\gamma)},$$

as $\hat{\eta}/k \sim 1$. For star-shaped and piecewise smooth polygons, the result follows after bounding the DtN map using [6, Theorem 1.4(6)] and bounding the ItD map using Lemma 5.20. □

5.6 Further work

In this chapter we have presented two key theorems on the stability of high frequency multiple scattering BEM. They appear to be the first of their kind, hence there are many areas in which they could be developed further. It does not appear difficult to extend both theorems to three-dimensional obstacles, as the underlying coercivity results for single scattering problems have three dimensional analogues.

Moreover, the result of Theorem 5.5 may be extended to $n_\gamma \in \mathbb{N}$ obstacles, as discussed at the end of §5.4. Extension of Theorem 5.5 to non-trapping polygonal

constellation-shaped domains may be possible, via the Constellation Combined operator, because in the single scattering case the Star Combined operator is coercive for star-shaped domains, whereas the Standard Combined operator is (known to be) coercive only when the domain to has a C^3 boundary. This would require a representation of the adjoint of the Constellation Combined operator that is analogous to (5.53), written in terms of Dirichlet-to-Neumann and Interior Impedance-to-Dirichlet maps (following similar steps to [13, Theorem 2.33]), which could then be bounded using the results for non-trapping polygons of [6]. This may then be used with Theorem 5.17 to provide a result analogous to Theorem 5.19, where the (stronger) coercivity result for star-shaped obstacles of [52] may be used to bound ζ_D.

Chapter 6

Numerically stable implementation of Embedding Formulae

The results produced in this chapter will appear in [28], and were summarised in [27].

For problems of time harmonic scattering by polygonal obstacles, Embedding Formulae provide a useful means of computing the far-field pattern (of (1.16)) of any incident wave for which the Herglotz kernel (in the sense of Definition 1.8) is known, given the far-field pattern of a set of *canonical problems*. The number of such problems to be solved depends only on the geometry of the scatterer. The motivation for this chapter comes from the Tmatrom method for multiple scattering problems, described in the next chapter. The Tmatrom method requires $O(k)$ single scattering problems to be solved, each with a different incident field, however the Herglotz kernel is known for each of these incidences. Using the Embedding Formulae, we aim to reduce the number of problems to be solved to $O(1)$, as we can obtain the solution of many problems using the solution of a small number (as few as eight), depending only on the geometry of Ω_Γ. Given an approximation to the far-field pattern of the canonical problems, it is possible to implement the Embedding Formulae (as are stated in [9]) in just four or five lines of additional code, yet little research has been published which applies the Embedding Formulae in a practical sense. Whilst the formulae themselves are in principle exact, any implementation will inherit numerical error from the method used to solve the canonical problems. This error can lead to numerical instabilities. Here, we present a method to regulate these instabilities, via a careful combination of three methods, two of which use a Taylor expansion of the far-field pattern of the canonical problems. Estimates of the truncation error in this expansion are derived.

An outline of this chapter is as follows. In §6.1, we introduce Embedding Formulae, and the problems to which they apply. We also explain why and where numerical

instabilities can occur when the formulae are implemented in practice. In §6.2 we derive an alternative formulation of the Embedding Formulae which are numerically stable, and in §6.3 we analyse the error in this alternative formulation. Finally, in §6.4 we extend the Embedding Formulae to Herglotz-type incidence (previously these formulae had only been applied to problems of plane wave incidence).

6.1 Specific problem statement

We seek the solution of the BVP (1.4)–(1.6) a quasi-regular n_Γ-sided polygon Ω_Γ with boundary $\partial\Omega = \Gamma$, where quasi-regular means that all external angles $\omega_j = Q\pi$ for $j = 1, \dots n_\Gamma$ for some $Q \in \mathbb{Q}_+$, i.e. all angles are equal to the same rational multiple of π. In such a case we have the elementary formula

$$\omega_j = \pi \frac{n_\Gamma + 2}{n_\Gamma}. \tag{6.1}$$

In [9], this is extended to all rational polygons (for which each angle is a rational multiple of π, but the angles need not be equal), hence similar extensions may be in principle applied to the techniques we present here. In terms of the notation of the general problem statement §1.1, $\Omega_- = \Omega_\Gamma$, and $\Omega_+ = \mathbb{R}^2 \setminus \overline{\Omega_\Gamma}$. We choose our coordinate system so that at least one side of Γ is aligned with the horizontal x_1-axis, and that the origin lies inside Ω_Γ.

For an incident plane wave approaching from angle α (measured anti-clockwise from the horizontal axis), the incident direction vector is $\mathbf{d}_\alpha := (\cos\alpha, -\sin\alpha)$,

$$u^{\text{inc}}(\mathbf{x}) = u^{\text{inc}}_{PW}(\mathbf{x}; \alpha) := \mathrm{e}^{\mathrm{i}k\mathbf{x}\cdot\mathbf{d}_\alpha}, \quad \mathbf{x} \in \mathbb{R}^2.$$

We use the following notation to denote the far-field pattern induced by $u^{\text{inc}}_{PW}(\cdot;\alpha)$ at observation angle θ

$$D(\theta, \alpha) := \mathcal{F}_\infty u^{\text{inc}}_{PW}(\theta). \tag{6.2}$$

In this Chapter, we denote the total solution for plane wave scattering by $u_\alpha := u^{\text{inc}}_{PW}(\cdot;\alpha) + u^s_\alpha$, where u^s_α denotes the scattered field. We are primarily interested in efficient and numerically stable approximation of $D(\theta, \alpha)$ over a large range of points $(\theta, \alpha) \in [0, 2\pi)^2$. We will make use of the following representation of the far-field coefficient,

$$D(\theta, \alpha) = -\int_\Gamma \mathrm{e}^{-\mathrm{i}k[y_1\cos(\theta)+y_2\sin(\theta)]} \frac{\partial u_\alpha}{\partial \mathbf{n}}(\mathbf{y})\, \mathrm{d}s(\mathbf{y}), \tag{6.3}$$

which is nothing more than the far-field coefficient of (1.16) written in our new notation (6.2).

Throughout the Chapter, some Greek letters are to be interpreted as a point on the unit circle, so for example θ identifies with $\theta + 2\pi$, whilst we say that θ_1 is *close to* θ_2 if $|e^{i\theta_1} - e^{i\theta_2}| < \epsilon$ for some $\epsilon > 0$ small.

6.1.1 Embedding Formulae

Suppose we want to compute the far-field coefficient $D(\theta, \alpha)$ for a range of $\alpha \in [0, 2\pi)$. The Embedding Formulae of [9, (3.4)] can do this for quasi-regular polygons, given the solution for a relatively small number of canonical problems. We choose parameters p and q to be the smallest integers such that $q/p = (n_\Gamma + 2)/n_\Gamma$ and solve (1.4)-(1.6) and compute (6.3) for canonical incident angles $\{\alpha_1, \ldots, \alpha_{M_\omega}\} =: A_{M_\omega}$ (the parameter M_ω depends on q, and is discussed in Remark 6.1 below). We note that in previous Chapters p was used to describe polynomial degree, which is not a quantity of interest in this Chapter. However, p has been used to describe this parameter in wider literature on Embedding Formulae, with which we are aiming to be notationally consistent. It follows from [9, (3.4)] that.

$$D(\theta, \alpha) = \frac{\sum_{m=1}^{M_\omega} B_m(\alpha)\Lambda(\theta, \alpha_m)D(\theta, \alpha_m)}{\Lambda(\theta, \alpha)}, \quad \text{for } (\theta, \alpha) \in [0, \pi)^2, \tag{6.4}$$

where

$$\Lambda(\theta, \alpha) := \cos(p\theta) - (-1)^p \cos(p\alpha) \tag{6.5}$$

and $[B_m]_{m=1}^{M_\omega} \in \mathbb{C}^{M_\omega}$ solves the system of equations

$$\sum_{m=1}^{M_\omega} B_m(\alpha)\Lambda(\alpha_n, \alpha_m)D(\alpha_n, \alpha_m) = (-1)^{p+1}\Lambda(\alpha, \alpha_n)D(\alpha, \alpha_n), \tag{6.6}$$

for $n = 1, \ldots, M_\omega$. For $(\theta, \alpha) \in [0, 2\pi)^2$ such that $\Lambda(\theta, \alpha) \neq 0$, the representation (6.4) can be evaluated explicitly to obtain the far-field coefficient $D(\theta, \alpha)$. As explained in [9], for the case $\Lambda(\theta, \alpha) = 0$, L'Hopitâl's rule may be applied to obtain $D(\theta, \alpha)$, with a second application in the sub-case $[\partial\Lambda/\partial\theta](\theta, \alpha) = 0$. Put formally, (at least) one application of L'Hopitâl's rule is required for θ in the set

$$\begin{aligned} \Theta_\alpha &:= \{\theta \in [0, 2\pi) : \Lambda(\theta, \alpha) = 0\} \\ &= \begin{cases} \{\theta \in [0, 2\pi) : \theta = \pm\alpha + (2n+1)\pi/p, & n \in \mathbb{Z}\}, \quad p \text{ odd}, \\ \{\theta \in [0, 2\pi) : \theta = \pm\alpha + 2n\pi/p, & n \in \mathbb{Z}\}, \quad p \text{ even}, \end{cases} \end{aligned} \tag{6.7}$$

with a second application if $[\partial\Lambda/\partial\theta](\theta, \alpha) = \cos(p\theta) = 0$, i.e. if

$$\theta \in \Theta_* := \pi(2\mathbb{N} - 1)/(2p) \tag{6.8}$$

also. The set Θ_α usually contains $2p$ elements, except for p special values of α where $\alpha \in (2\mathbb{N}+1)\pi/p$ for p odd and $\alpha \in 2\pi\mathbb{N}/p$ for p even, for which Θ_α contains p elements (in such a case these elements are also in Θ_*). We will also make use of a closely related set A_*, consisting of all α_* such that $\Theta_{\alpha_*} \subset \Theta_*$. It follows for even p that $A_* = \Theta_*$ and for odd p that $A_* = \Theta_* + \pi/p = \Theta_*$; hereafter we shall just refer to Θ_* instead of A_*, as they are equal. Note that this does not imply that $\Lambda(\theta_*, \alpha_*) = 0$ for all $(\theta_*, \alpha_*) \in \Theta_* \times A_*$.

We now summarise the process of implementing Embedding Formulae.

(i) Given the geometry of the obstacle Ω_Γ, compute p, q and M_ω (details in Remark 6.1).

(ii) Compute the far-field coefficient $D(\cdot, \alpha_m)$ for M_ω distinct incident angles α_m.

(iii) Given an incident angle α, solve the $M_\omega \times M_\omega$ system (6.6) to determine the coefficients $B_m(\alpha)$.

(iv) Obtain $D(\theta, \alpha)$ using (6.4), using (6.7) and (6.8) to determine if application(s) of L'Hopitâl's rule is/are required.

(v) For a different incident angle α, steps (i) and (ii) need not be repeated.

REMARK 6.1. *In [9, §3] the number of distinct incident angles required for quasi-regular polygons is stated as $M_\omega = n_\Gamma(n_\Gamma + 1)$. This is based on the idea that $q-1$ canonical solutions are needed for each corner of the polygon, hence if we take the obvious choice (considering* (6.1)*) of $q = n_\Gamma + 2$, this yields the choice.*

$$M_\omega = n_\Gamma(q-1) = n_\Gamma(n_\Gamma + 1) \tag{6.9}$$

However, the obvious *choice of $q = n_\Gamma + 2$ may not be the best choice. Noting* (6.1) *for even n_Γ, we may instead choose $q = (n_\Gamma + 2)/2$ and $p = n_\Gamma/2$ and thus* (6.9) *becomes*

$$M_\omega = n_\Gamma(q-1) = n_\Gamma\left(\frac{n_\Gamma + 2}{2} - 1\right) = \frac{{n_\Gamma}^2}{2}.$$

This sharpens the choice of [9, (3.3)], reducing the number of solves required by more than half, for even n_Γ. Although the choice suggested by [9] still holds, the system (6.1.1) *may become under-determined when implemented numerically. Moreover, in [9], no constraint is placed on the incident angles A_{M_ω}, other than that they are distinct. Numerical experiments have shown that close clustering of these incident angles may cause the Embedding Formulae to become inaccurate. Given that the*

Embedding Formulae for polygons extend naturally from those of a rational wedge, one would expect that if at least $q-1$ incident angles can 'see' any given corner of Γ that is $\mathbf{n}(\mathbf{x}) \cdot (\cos(\alpha), \cos(\theta)) > 0$, then the Embedding Formulae would hold. Numerical experiments suggest that this is sufficient, and we will assume that this constraint holds for the remainder of the Thesis.

Example

We briefly demonstrate the power of Embedding Formulae with the simple geometry of a square ($n_\Gamma = 4$), fixing the wavenumber $k = 1$. It follows by Remark 6.1 that $q = 3$, $p = 2$ and hence $M_\omega := n_\Gamma(q-1) = 8$, which is the smallest M for any polygon. We solve for $M_\omega = 8$ randomly chosen (in accordance with Remark 6.1) incident angles, as depicted in Figure 6.1. These angles $A_{M_\omega} = \{\alpha_1, \ldots, \alpha_8\}$ correspond to the canonical problems.

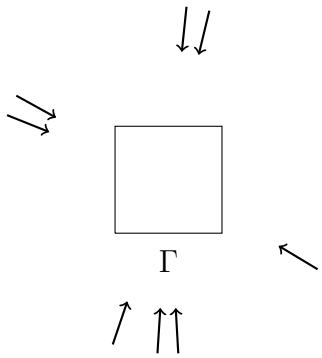

Figure 6.1: Schematic diagram of the randomly selected incident angles used for the Embedding Formulae.

We solve these using MPSpack (developed in [4], although here we use the version adapted for Tmatrom [23] which can output the far field pattern) with 60 degrees of freedom, to obtain an approximation to $D(\theta, \alpha)$ for $(\theta, \alpha) \in [0, 2\pi) \times A_{M_\omega}$ (two of the far-field patterns are plotted in Figure 6.2). A few extra lines of code can be used to implement the embedding formula (6.4) and we obtain (an approximation to) $D(\theta, \alpha)$ for all $(\theta, \alpha) \in [0, 2\pi)^2$, (as in Figure 6.3).

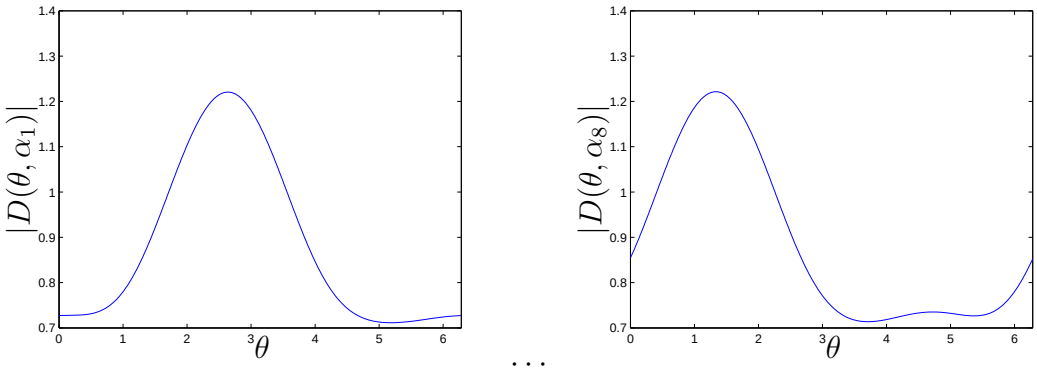

(a) (b)

Figure 6.2: Example of two of eight far-field patterns required for embedding formula: α_1 and α_8.

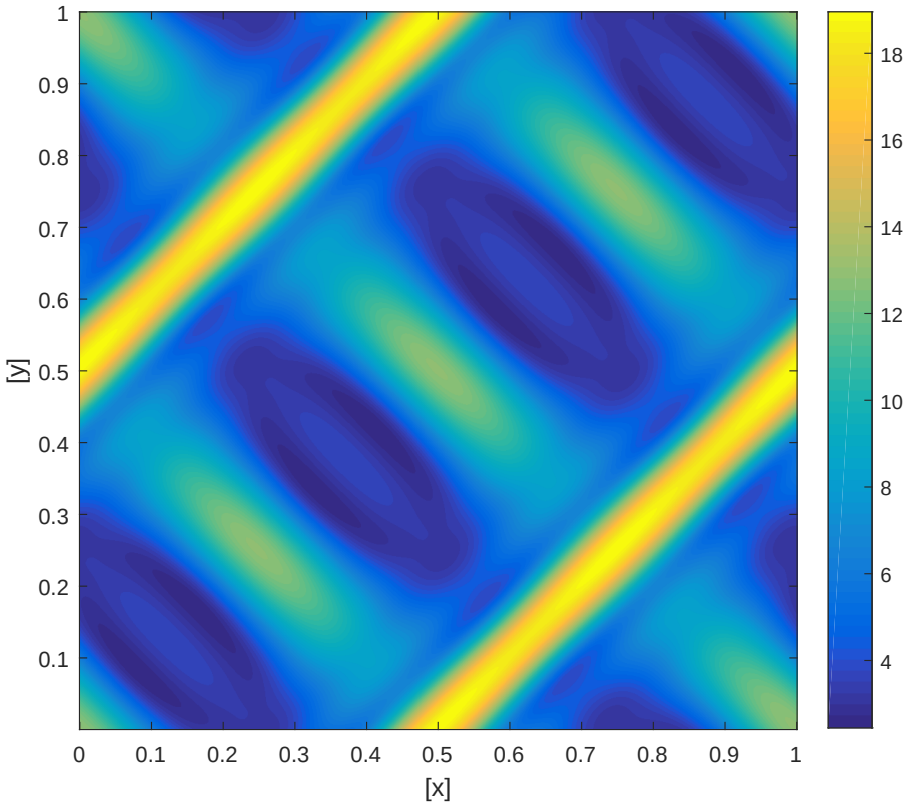

Figure 6.3: Full range of values of $D(\theta, \alpha)$ obtained from embedding formula.

6.1.2 Naive implementation of Embedding Formulae

Henceforth, we shall simplify the notation via $\hat{D}(\theta,\alpha) := \Lambda(\theta,\alpha)D(\theta,\alpha)$. This chapter is primarily concerned with efficient and stable approximation of the far-field coefficient $D(\theta,\alpha)$. We now motivate this by demonstrating cases when a naive implementation of (6.4) can become unstable. Any numerical approximation to u_α will not be exact, and this can cause significant numerical instabilities close to Θ_α. To see why, we denote by $\mathcal{P}_F D(\theta,\alpha)$ some numerical approximation to $D(\theta,\alpha)$, adopting the notational convention $\mathcal{P}_F\hat{D} := \Lambda\mathcal{P}_F D$, and define the embedding formula coupled with our numerical solver as

$$D(\theta,\alpha) \approx \mathcal{E}_{\mathcal{P}_F} D(\theta,\alpha) := \frac{\sum_{m=1}^{M_\omega} b_m(\alpha)\mathcal{P}_F\hat{D}(\theta,\alpha_m)}{\Lambda(\theta,\alpha)}, \tag{6.10}$$

where $[b_m]_{m=1}^{M_\omega} \approx [B_m]_{m=1}^{M_\omega}$ solves the system of equations

$$\sum_{m=1}^{M_\omega} b_m(\alpha)\mathcal{P}_F\hat{D}(\alpha_n,\alpha_m) = (-1)^{p+1}\mathcal{P}_F\hat{D}(\alpha,\alpha_n), \quad \text{for } n = 1,\dots,M_\omega. \tag{6.11}$$

A key component of implementation rests on the following assumption.

ASSUMPTION 6.2 (Unisolvence for modified far-field basis)**.** *We assume both of the following:*

(i) The system (6.6) *is uniquely solvable for any* $\alpha \in [0,2\pi)$*, hence the coefficients* $B_m(\alpha)$ *exist, are unique and satisfy*

$$B_{\max} := \max_{\substack{\alpha\in[0,2\pi)\\ m\in\{1,\dots,M_\omega\}}} |B_m(\alpha)| < \infty.$$

(ii) The system (6.11) *is uniquely solvable for any* $\alpha \in [0,2\pi)$*, hence the coefficients* $b_m(\alpha)$ *exist, are unique and satisfy*

$$b_{\max} := \max_{\substack{\alpha\in[0,2\pi)\\ m\in\{1,\dots,M_\omega\}}} |b_m(\alpha)| < \infty.$$

To the best knowledge of the author, the question of Assumption 6.2(i), and hence the more difficult question Assumption 6.2(ii), are still open. We do not specify the projection operator $\mathcal{P}_F$ here, the choice of $\mathcal{P}_F$ makes no difference to the points at which the Embedding Formulae become numerically unstable. An example of a suitable choice would be the HNA approximation to the far-field (2.13), however for the majority of this Chapter we use MPSpack, a MATLAB package introduced in [5].

It then follows that the error in the embedding formula is

$$|D(\theta,\alpha) - \mathcal{E}_{\mathcal{P}_F} D(\theta,\alpha)| = \frac{1}{|\Lambda(\theta,\alpha)|} \left| \sum_{m=1}^{M_\omega} \left[B_m(\alpha) \hat{D}(\theta,\alpha_m) - b_m(\alpha) \mathcal{P}_F \hat{D}(\theta,\alpha_m) \right] \right| \tag{6.12}$$

It is clear from (6.12) that for any amount of numerical error, a naive implementation of the embedding formula can lead to arbitrarily large error at points (θ,α) such that $\Lambda(\theta,\alpha) \approx 0$. In the context of Embedding Formulae, this is what is meant by numerical instability: if a solver $\mathcal{P}_F$ has a relatively small amount of numerical error, we observe a relatively large amount of error when coupled with the corresponding Embedding Formula $\mathcal{E}_{\mathcal{P}_F} D$. The following lemma bounds the scaling of this error in terms of known parameters. A simple interpretation of the lemma is that $1/\Lambda(\theta,\alpha) \sim |\theta - \theta_0|^{-1}$ when θ_0 is far from θ_*, but $1/\Lambda(\theta,\alpha) \sim |\theta - \theta_0|^{-2}$ when $|\theta_0 - \theta_*| \sim |\theta - \theta_0|$.

LEMMA 6.3. *The following bounds hold for all* $(\theta,\alpha) \in [0,2\pi)^2$*:*

$$\frac{p^2}{8} |\theta - \theta_0||\theta_0 - \theta_*| \leq |\Lambda(\theta,\alpha)| \leq p^2 |\theta - \theta_0| \left(\frac{1}{2}|\theta - \theta_0| + |\theta_0 - \theta_*| \right),$$

for $p \in \mathbb{N}$ *and* Λ *as in* (6.5)*, where* θ_0 *is the element of* Θ_α *closest to* θ*, and* θ_* *is the element of* Θ_* *closest to* θ_0*.*

Proof. Firstly, by the definition (6.7) of Θ_α we have

$$\Lambda(\theta,\alpha) = \cos(p\theta) - \cos(p\theta_0), \quad \text{for } \theta_0 \in \Theta_\alpha, \tag{6.13}$$

(for p even or odd) and from standard trigonometric identities it follows that

$$|\Lambda(\theta,\alpha)| = |\Lambda(\theta,\theta_0)| = 2\,|\sin\left(p(\theta - \theta_0)/2\right)| \cdot |\sin\left(p(\theta + \theta_0)/2\right)|. \tag{6.14}$$

We focus on the lower bound. Due to the distribution of Θ_α and Θ_*, if θ_0 is the element of Θ_α closest to θ, we can be certain that $|\theta + \theta_0|/2 \leq |\theta + \theta_0|/2$, hence

$$\begin{aligned}
|\Lambda(\theta,\alpha)| &\geq 2\,|\sin\left(p(\theta - \theta_0)/2\right)| \cdot |\sin\left(p(\theta_* + \theta_0)/2\right)| \\
&= 2\,|\sin\left(p(\theta - \theta_0)/2\right)| \cdot |\sin\left(p(2\theta_* + (\theta_0 - \theta_*))/2\right)| \\
&= 2\,|\sin\left(p(\theta - \theta_0)/2\right)| \cdot |\sin(p\theta_*)\cos(p(\theta_0 - \theta_*)/2) + \sin(p(\theta_0 - \theta_*)/2)\cos(p\theta_*)|.
\end{aligned}$$

By the definition (6.8) of Θ_*, we have that $\sin(p\theta_*) = 0$ and $|\cos(p\theta_*)| = 1$, hence

$$|\Lambda(\theta,\alpha)| \geq 2\,|\sin\left(p(\theta - \theta_0)/2\right)| \cdot |\sin(p(\theta_0 - \theta_*)/2)|. \tag{6.15}$$

From the definitions of Θ_α (6.7) and Θ_* (6.8), it follows that the furthest θ can be from the nearest θ_0 or θ_* is $\pi/(2p)$. Hence the argument of both sines of (6.15) is at

most $\pi/4$, so we may use the identity $|\sin(x)| \geq |x/2|$ for $0 \leq |x| \leq \pi/4$ (twice) to obtain the lower bound on $|\Lambda(\theta, \alpha)|$ as claimed.

Now we focus on the upper bound. Writing $\theta + \theta_0 = (\theta + \theta_*) + (\theta_0 - \theta_*)$ and applying elementary trigonometric addition formulae gives

$$\sin\left(\frac{p}{2}(\theta + \theta_0)\right) = \sin\left(\frac{p}{2}(\theta + \theta_*)\right)\cos\left(\frac{p}{2}(\theta_0 - \theta_*)\right) + \sin\left(\frac{p}{2}(\theta_0 - \theta_*)\right)\cos\left(\frac{p}{2}(\theta + \theta_*)\right)$$

which we can bound using the triangle inequality and $\cos(x) \leq 1$ to obtain

$$\left|\sin\left(\frac{p}{2}(\theta + \theta_0)\right)\right| \leq \left|\sin\left(\frac{p}{2}(\theta + \theta_*)\right)\right| + \left|\sin\left(\frac{p}{2}(\theta_0 - \theta_*)\right)\right|$$

Since $|\sin(px/2)|$ is symmetric about the points $x \in \Theta_*$, it follows that $|\sin(p(\theta_* + \theta)/2)| = |\sin(p(\theta_* - \theta)/2)|$, hence

$$\left|\sin\left(\frac{p}{2}(\theta + \theta_0)\right)\right| \leq \left|\sin\left(\frac{p}{2}(\theta - \theta_*)\right)\right| + \left|\sin\left(\frac{p}{2}(\theta_0 - \theta_*)\right)\right|.$$

We may use this to bound (6.14), at which point the identity $|\sin(x)| \leq |x|$ may be used to obtain

$$|\Lambda(\theta, \alpha)| \leq 2\frac{p}{2}|\theta - \theta_*|\frac{p}{2}\left(|\theta - \theta_*| + |\theta_0 - \theta_*|\right),$$

finally we use the triangle inequality to write $|\theta - \theta_*| \leq |\theta - \theta_0| + |\theta_0 - \theta_*|$ and obtain the lower bound as claimed. □

The upper bound of Lemma 6.3 can be used to identify and quantify cases where the error from the solver $\mathcal{P}_F$ becomes significantly exaggerated by the term $1/\Lambda(\theta, \alpha)$. Conversely, we observe $|\theta_0 - \theta_*| \ll 1$ is not a sufficient condition for instability, but when coupled with the additional condition of $|\theta - \theta_0| \ll 1$ we observe a stronger instability than before, as demonstrated by Figure 6.4. The lower bound of Lemma 6.3 will be used in §6.3 for error analysis. It is also clear from Figure 6.4 that increasing the number of degrees of freedom (DOFs) of the solver $\mathcal{P}_F$ will reduce the region of instability. However, for any degree of accuracy there will always be θ at which the error is arbitrarily large, and as we shall see, increasing DOFs may be an unnecessarily expensive approach to reducing width of the unstable region.

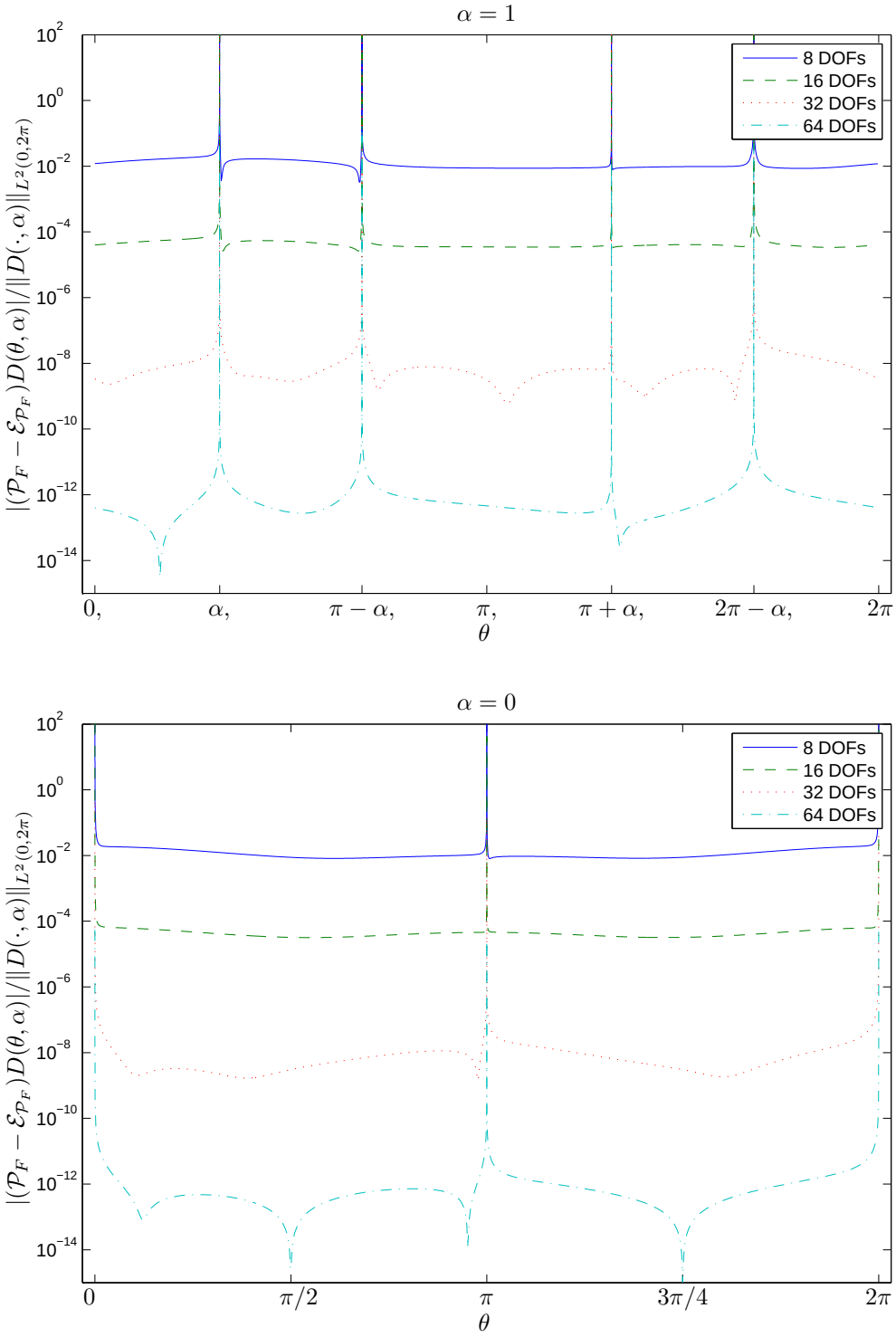

Figure 6.4: Two plots showing relative error in the naive embedding approximation (6.10), with $\alpha = 1$ (not close to $\theta_* \in \Theta_*$) depicted in (a), and $\alpha = 0 \in \Theta_*$ depicted in (b). Note that there are half as many unstable points in (b), as $\alpha = 0 \in \Theta_*$.

6.2 Numerically stable implementation

We now begin to reformulate the naive implementation (6.10), and develop a numerically stable approximation for any $(\theta, \alpha) \in [0, 2\pi)^2$.

6.2.1 Single variable Taylor expansion

A large portion of the instability can be overcome by Taylor expanding around the $\theta_0 \in \Theta_\alpha$ to which θ is closest. This point is special, because although we do not know the exact values of $D(\theta_0, \alpha_m)$, we know that

$$\sum_{m=1}^{M_\omega} B_m(\alpha)\hat{D}(\theta_0, \alpha_m) = 0, \quad \text{despite} \quad \sum_{m=1}^{M_\omega} b_m(\alpha)\mathcal{P}_F\hat{D}(\theta_0, \alpha_m) \neq 0,$$

due to approximation error of the solver $\mathcal{P}_F$. Hence we can remove the first ($n = 0$) term from the Taylor expansion, the exact representation becomes

$$D(\theta, \alpha) = \frac{\theta - \theta_0}{\Lambda(\theta, \alpha)} \sum_{m=1}^{M_\omega} B_m(\alpha) \sum_{n=1}^{\infty} \frac{(\theta - \theta_0)^{n-1}}{n!} \frac{\partial^n \hat{D}}{\partial \theta^n}(\theta_0, \alpha_m), \quad \text{for } \theta \text{ close to } \theta_0 \in \Theta_\alpha \tag{6.16}$$

and truncating after N_T terms in the Taylor expansion, we can define a second approximation

$$D(\theta, \alpha) \approx \mathcal{E}^0_{\mathcal{P}_F} D(\theta, \alpha; \theta_0, N_T) := \frac{\theta - \theta_0}{\Lambda(\theta, \alpha)} \sum_{m=1}^{M_\omega} b_m(\alpha) \sum_{n=1}^{N_T} \frac{(\theta - \theta_0)^{n-1}}{n!} \frac{\partial^n}{\partial \theta^n} \mathcal{P}_F \hat{D}(\theta, \alpha_m). \tag{6.17}$$

Whilst we have added an additional source of error in the form of the Taylor remainder, the Taylor coefficients regulate the numerical instability present in (6.12). It follows immediately from Lemma 6.3 that the singular behaviour of (6.17) is bounded by

$$\frac{|\theta - \theta_0|}{|\Lambda(\theta, \alpha)|} \leq \frac{8}{p^2 |\theta_* - \theta_0|}, \quad \text{for } \theta_* \notin \Theta_*,$$

hence we now have stability when θ is close to $\theta_0 \in \Theta_\alpha$, provided that θ_0 is sufficiently far from any $\theta_* \in \Theta_*$. Figure 6.5 provides visual representation of this. Here the error measured on the colourbar in plots (a) and (b) is

$$\frac{|\mathcal{P}_F D(\theta, \alpha) - \mathcal{E}_{\mathcal{P}_F} D(\theta, \alpha)|}{\|\mathcal{P}_F D\|_{L^2([0,2\pi)^2)}} \quad \text{and} \quad \frac{\left|\mathcal{P}_F D(\theta, \alpha) - \mathcal{E}^0_{\mathcal{P}_F} D(\theta, \alpha; \theta_0, 10)\right|}{\|\mathcal{P}_F D\|_{L^2([0,2\pi)^2)}} \tag{6.18}$$

respectively, choosing $N_T = 10$, where the threshold for *close* is any point such that $|\theta - \theta_0| < 0.25$, for $\theta_0 \in \Theta_\alpha$. For the far-field solver $\mathcal{P}_F$, a modified version of MPSpack

of [5] has been used, such that derivatives of the far-field pattern may be computed (see §C.1 for more details of how this can be done). Whilst the relative error in both cases appears to peak below 10^{-8}, this is only due to a lack of granularity; these plots contain 1000×1000 points but close to the unstable points the relative error is observed to become arbitrarily large in Figure 6.6(a), which focuses on an unstable point from Figure 6.5(b). We observe that whilst most of the instabilities are handled in Figure 6.5(b) using (6.17), there are points at which instabilities still exist. However, it is important to note that with a naive implementation (6.10), for every $\alpha \in [0, 2\pi)$ there are at least two $\theta_0 \in \Theta_\alpha$ for which the approximation is unstable, totalling an infinite number of unstable points (θ, α) in $[0, 2\pi)^2$ (these form the unstable lines in Figure 6.5(a)). In contrast when using the approximation (6.17), instabilities occur only close to $\theta \in \Theta_*$ for each $\alpha \in \Theta_*$, so (6.17) reduces the instabilities to a finite set of points, also in $\Theta_* \times \Theta_*$ (these are the unstable points in Figure 6.5(b)).

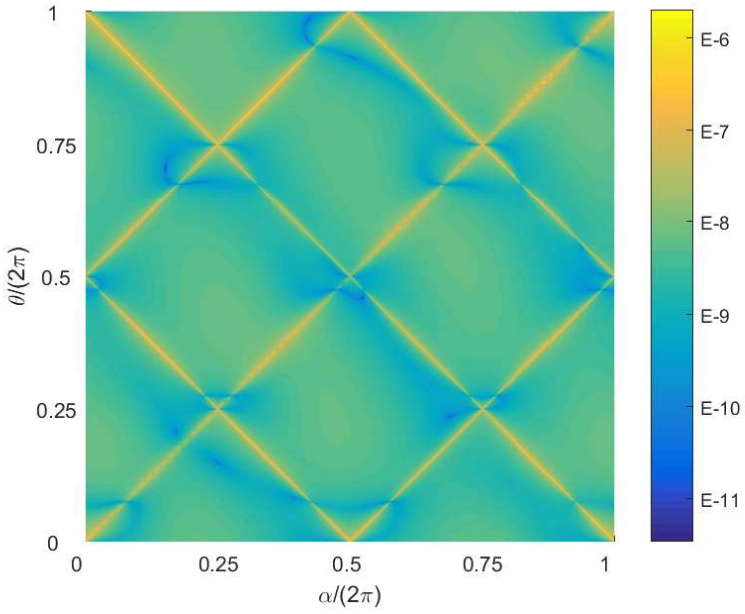

(a)

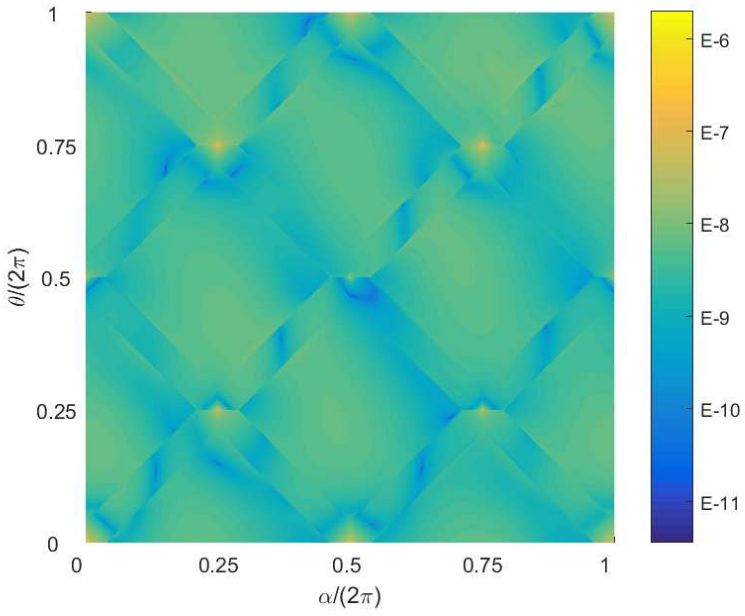

(b)

Figure 6.5: Two plots of relative error for different implementation of Embedding Formulae for scattering by a regular four sided square by incident waves with wavenumber $k = 1$. Plot (a) depicts accuracy for a naive implementation (6.10), whilst Plot (b) depicts accuracy using an $N_T = 10$ degree Taylor expansion approximation (6.17).

6.2.2 Multivariate expansion - first order

This approach will require the following result (see e.g. [17, Theorem 3.15]):

THEOREM 6.4 (Reciprocity Relation)**.** *For a plane wave incidence approaching from angle α, and a sound-soft obstacle Ω_Γ, we have the identity*

$$D(\theta, \alpha) = D(\alpha, \theta).$$

Until now, we have been able to choose the canonical incident angles A_{M_ω} relatively freely (as discussed in Remark 6.1). Contrary to the approach for standard Embedding Formulae, it can be advantageous to choose these such that $A_{M_\omega} \subset \Theta_*$. Supposing we are close to a source of instability (θ_*, α_*), which as suggested by Figure 6.5(b) is not regulated by (6.17), and that the canonical incident waves have been chosen such that $\theta_* =: \alpha_{m_1} \in A_{M_\omega}$ and $\alpha_* =: \alpha_{m_2} \in A_{M_\omega}$ (see Figure 6.8). We can then use the Reciprocity Relation (Theorem 6.4) to obtain a first order multi-variate Taylor series approximation in terms of quantities that require only the canonical solutions,

$$\begin{aligned} D(\theta, \alpha) &\approx D(\theta_*, \alpha_*) + (\theta - \theta_*)\frac{\partial D}{\partial \theta}(\theta_*, \alpha_*) + (\alpha - \alpha_*)\frac{\partial D}{\partial \alpha}(\theta_*, \alpha_*) \\ &= D(\theta_*, \alpha_{m_2}) + (\theta - \theta_*)\frac{\partial D}{\partial \theta}(\theta_*, \alpha_{m_2}) + (\alpha - \alpha_*)\frac{\partial D}{\partial \theta}(\alpha_*, \alpha_{m_1}) \\ &\approx \mathcal{P}_F D(\theta_*, \alpha_{m_2}) + (\theta - \theta_*)\frac{\partial \mathcal{P}_F D}{\partial \theta}(\theta_*, \alpha_{m_2}) + (\alpha - \alpha_*)\frac{\partial \mathcal{P}_F D}{\partial \theta}(\alpha_*, \alpha_{m_1}) \\ &=: \mathcal{E}^*_{\mathcal{P}_F} D(\theta, \alpha; \theta_*, \alpha_*), \end{aligned} \tag{6.19}$$

where the derivative of each far-field pattern follows from the representation (6.3). Figure 6.6 shows that the error in (6.17) is unbounded close to $(0, 0)$. We have relative error measured by

$$\frac{\left|\mathcal{P}_F D(\theta, \alpha) - \mathcal{E}^0_{\mathcal{P}_F} D(\theta, \alpha; 10)\right|}{\|\mathcal{P}_F D\|_{L^2([0,2\pi)^2)}} \quad \text{and} \quad \frac{\left|\mathcal{P}_F D(\theta, \alpha) - \mathcal{E}^*_{\mathcal{P}_F} D(\theta, \alpha)\right|}{\|\mathcal{P}_F D\|_{L^2([0,2\pi)^2)}} \tag{6.20}$$

for Figure 6.6 and 6.7 respectively. To implement the approximation (6.19), we choose $\alpha_{m_1} = 0$, and for $\|(\theta, \alpha) - (0, 0)\|_\infty < 7.5 \times 10^{-4}$; replacing the single variable Taylor expansion (6.17) with the first order two-variable Taylor expansion (6.19), which is observed to stabilise the error at around 10^{-5}. To improve on this, a higher order Taylor expansion is required, which is discussed in Remark 6.5. The diagonal region of high accuracy in Figure 6.6(a) is along the line $\theta = \theta_0 \in \Theta_\alpha$, where L'Hopital's rule is used, hence there is no amplified error term due to $1/\Lambda$ featuring in the representation.

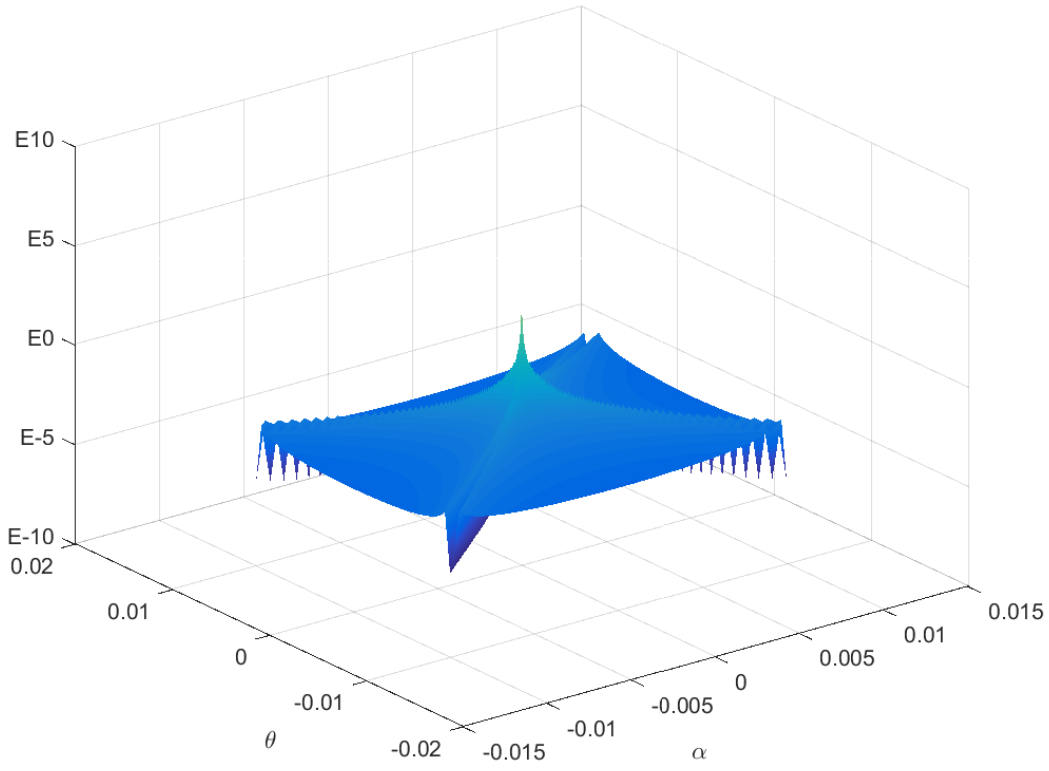

Figure 6.6: Image focusing on Figure 6.5(b) at an unstable point $(\theta, \alpha) = (0, 0)$.

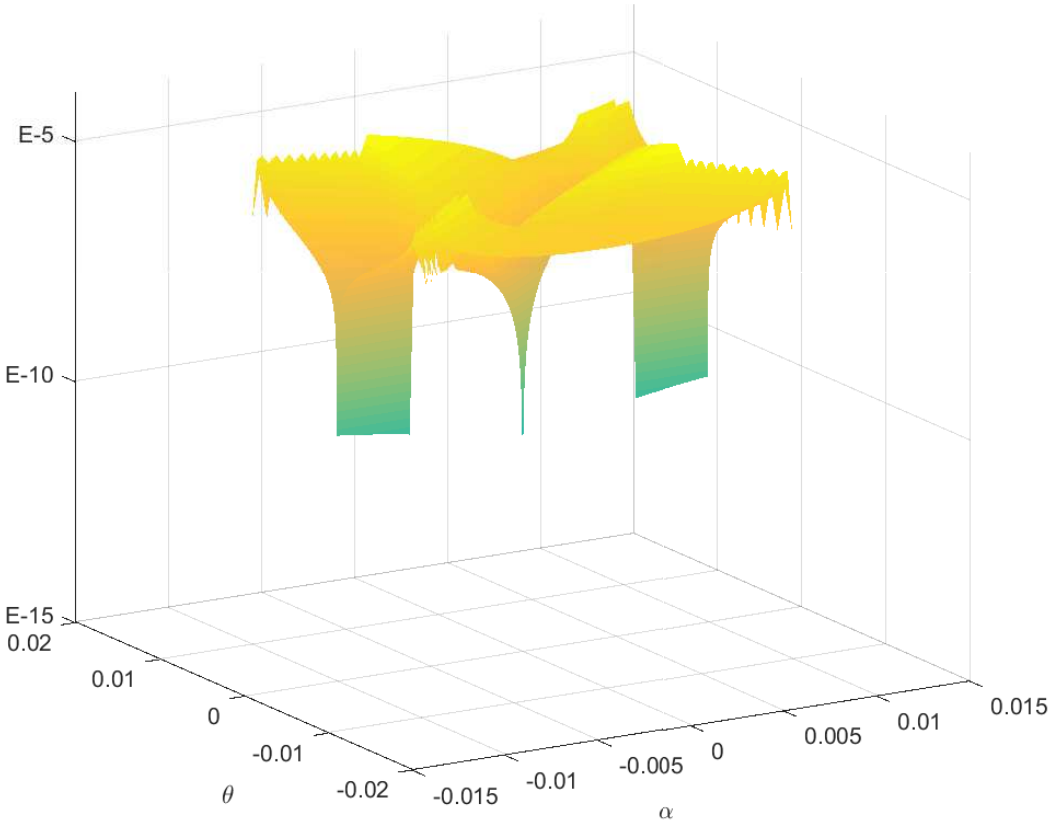

Figure 6.7: Image focusing on the an unstable point $(\theta, \alpha) = (0, 0)$ of Figure 6.5(b) and 6.6, having chosen incident angles in accordance with Figure 6.8 and used the approximation (6.19)

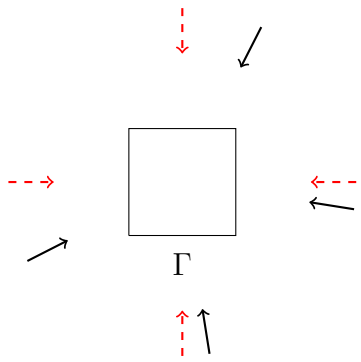

Figure 6.8: Diagram of incident angles chosen for a square, when implementing (6.19). Incident angles $\alpha_m \in A_{M_\omega} \cap \Theta_*$ are dashed, whilst other incident angles $\alpha_m \in A_{M_\omega} \setminus \Theta_*$ are chosen randomly, in accordance with the conditions suggested in Remark 6.1.

REMARK 6.5. *The key reason that* (6.19) *cannot be easily extended to even a*

second order approximation for all $(\theta, \alpha) \in [0, 2\pi)^2$ is that the cross derivative terms are very difficult to compute. Considering the far-field representation (6.3)*, it is not clear how to compute mixed derivatives in both α and θ. Derivatives purely in θ follow by taking the derivative inside the integral sign, whilst differentiation purely in α may then be obtained via the Reciprocity Relation (Theorem 6.4). We propose that higher order cross derivatives may be computed using the embedding representation 6.4, for which derivatives in α require derivatives of the right hand side of 6.6. This gets messy very quickly, and for most practical applications would not be necessary, given the error observed in Figures 6.9(b) and 6.6(b). Further details are given in Appendix C.3.*

6.2.3 Combined approach

We are now able to construct a numerically stable (over all $[0, 2\pi)^2$ method using an appropriate combination of the approximations (6.10), (6.17) and (6.19).

DEFINITION 6.6 (Combined Embedding Approximation)**.** *Given thresholds $T_0 > 0$ and $T_* > 0$, we choose the parameters of our approximation $\mathcal{P}_F$ to ensure Assumption 6.2 holds and that the canonical set of incident waves A_{M_ω} is chosen such that $\Theta_* \subset A_{M_\omega}$. We define the Combined Embedding Approximation by*

$$\mathcal{E}^{\circledast}_{\mathcal{P}_F} D(\theta, \alpha; N_T) := \tag{6.21}$$

$$\begin{cases} \left[\sum_{m=1}^{M_\omega} b_m(\alpha) \dfrac{\partial \mathcal{P}_F \hat{D}}{\partial \theta}(\theta, \alpha_m)\right] \Big/ \left[\dfrac{\partial \Lambda}{\partial \theta}(\theta, \alpha)\right], & \text{for } \theta \in \Theta_\alpha \text{ and } \min\limits_{\theta_* \in \Theta_*} |\theta - \theta_*| > T_*, \\ \left[\sum_{m=1}^{M_\omega} b_m(\alpha) \dfrac{\partial^2 \mathcal{P}_F \hat{D}}{\partial \theta^2}(\theta, \alpha_m)\right] \Big/ \left[\dfrac{\partial^2 \Lambda}{\partial \theta^2}(\theta, \alpha)\right], & \text{for } \theta \in \Theta_\alpha \text{ and } \theta \in \Theta_*, \\ \mathcal{E}^0_{\mathcal{P}_F} D(\theta, \alpha; \theta_0, N_T), & \text{for } \theta_0 \in \Theta_\alpha : 0 < |\theta - \theta_0| \le T_0 \text{ and } \min\limits_{\theta_* \in \Theta_*} |\theta - \theta_*| > T_*, \\ \mathcal{E}^*_{\mathcal{P}_F} D(\theta, \alpha; \theta_*, \alpha_*), & \text{for } |\theta - \theta_0| < T_* \text{ and } |\theta_0 - \theta_*| < T_*, \text{ for some } \theta_* \text{ and } \alpha_* \in \Theta_* \\ \mathcal{E}_{\mathcal{P}_F} D(\theta, \alpha), & \text{otherwise,} \end{cases} \tag{6.22}$$

for $(\theta, \alpha) \in [0, 2\pi)^2$, where θ_0 is chosen to be the element of Θ_α closest to θ, and θ_* is chosen to be the element of Θ_* closest to θ_0 with $\alpha_* \in \Theta_*$ such that $\theta_* \in \Theta_{\alpha_*}$.

Results for the combined approach are depicted in Figure 6.9. The relative error is determined by comparing against the MPSpack approximation to the far-field, $\mathcal{P}_F D$. The error for this is greater in Figures 6.9(b) and 6.10 (which is a close-up version of 6.9(b)) than for 6.9(a). This is due to the use of the first order expansion (6.19)

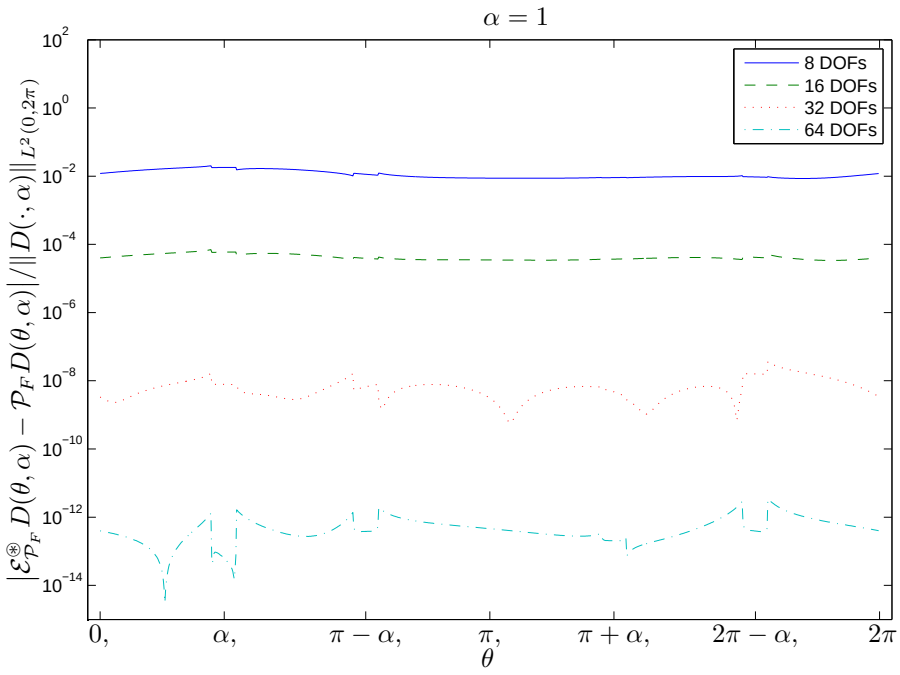

(a)

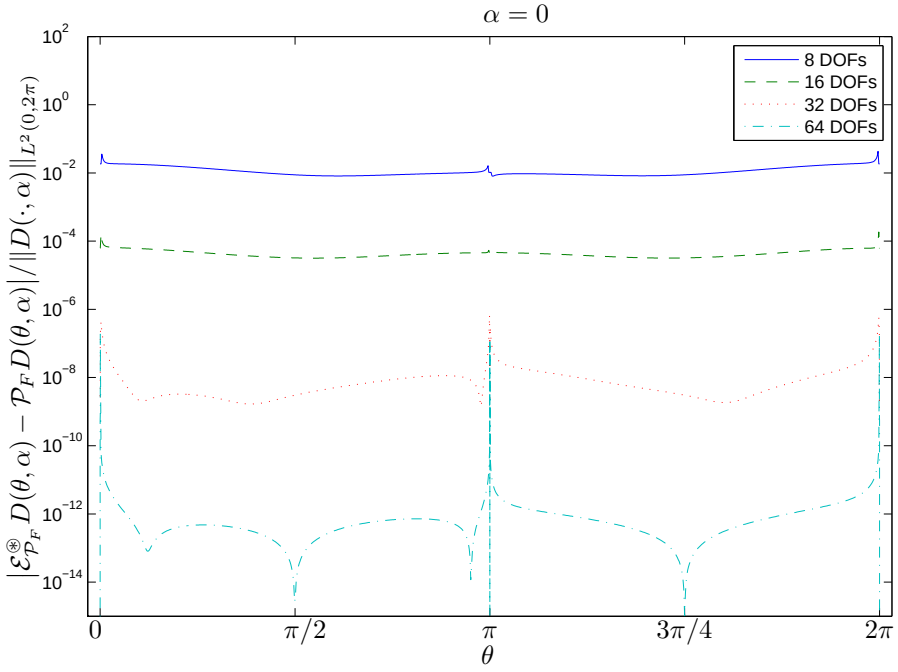

(b)

Figure 6.9: Two plots showing relative error when using the Combined Embedding Approximation, with $\alpha = 1$ (not close to $\theta_* \in \Theta_*$) depicted in (a), and $\alpha = 0 \in \Theta_*$ depicted in (b). Figure 6.10 is a close-up of the spike in the centre of Figure (b), demonstrating that the unbounded error observed in Figure 6.4 is no longer present.

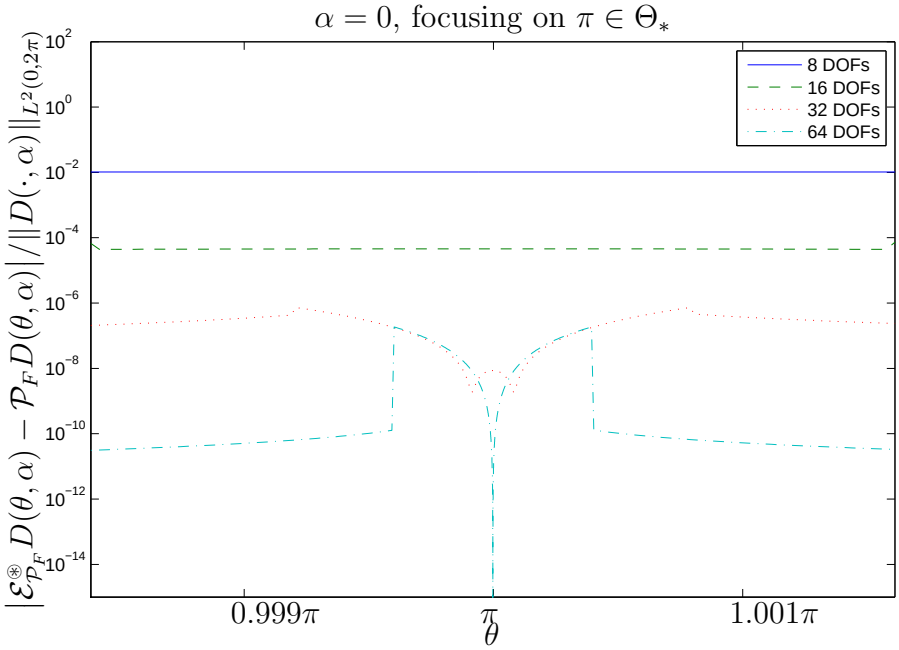

Figure 6.10: A close up of the spike of Figure 6.9(b).

instead of the tenth order expansion used for 6.9(a). When compared against the results of Figure 6.4, a significant improvement is visible.

There are a few developments which may improve the accuracy and efficiency of the Combined Embedding Approximation. We present one here in Remark 6.7, the others can be found in Appendix C.

REMARK 6.7. *In the special case where*

$$(\theta, \alpha) \in (\Theta_* \times [0, 2\pi)) \cup ([0, 2\pi) \times \Theta_*)\,,$$

it is possible to easily compute higher order terms in the multi-variate Taylor expansion (contrary to the general case discussed in Remark 6.5). The multivariate expansion reduces to a single variable expansion since $(\alpha - \alpha_*) = 0$*, and we have the representation*

$$D(\theta, \alpha_*) = \sum_{n=0}^{\infty} \frac{(\theta - \theta_*)^n}{n!} D(\theta_*, \alpha_*),$$

which can be easily computed in terms of known terms if we choose $\theta_*, \alpha_* \in A_{M_\omega}$*. A similar representation holds if* $(\theta - \theta_*) = 0$*. We do not absorb this into our method, as it only fixes the error for a small number of special cases. The error in Figures 6.9(b) and 6.10 could be reduced via these Taylor expansions, as* $\alpha \in \Theta_*$ *in this case.*

However, the error displayed in this plot is more representative of the general (and much more common) case of points in a small neighbourhood of Θ_*.

6.3 Error analysis

In this section we assume that an approximation to the Neumann trace $\partial^+_{\mathbf{n}} u_\alpha$ is available. The Neumann trace approximation $\mathcal{P}_N[\partial u_\alpha/\partial \mathbf{n}]$ is related to the far-field approximation via

$$\mathcal{P}_F D(\theta,\alpha) = -\int_\Gamma \mathrm{e}^{-\mathrm{i}k(y_1\cos\theta+y_2\sin\theta)}\mathcal{P}_N\left[\frac{\partial u_\alpha}{\partial \mathbf{n}}\right](\mathbf{y})\,\mathrm{d}s(\mathbf{y}), \tag{6.23}$$

and we denote the error in this approximation by

$$\epsilon_N := \|(\mathcal{I}-\mathcal{P}_N)\partial^+_{\mathbf{n}} u_\alpha\|_{L^2(\Gamma)} \tag{6.24}$$

We now bound the error of the Combined Embedding Approximation, given the choice of thresholds T_0 and T_* (of Definition 6.6). We do this by bounding the error of five terms: the naive embedding (6.4), single L'Hopitâl's rule, double L'Hopitâl's rule, single variable Taylor expansion of §6.2.1 and first order multi-variate Taylor expansion of §6.5.

THEOREM 6.8. *The Combined Embedding Approximation of Definition 6.6*

$$\mathcal{E}^{\circledast}_{\mathcal{P}_F} D(\theta,\alpha;N_T) \approx D(\theta,\alpha)$$

is numerically stable for all (θ,α) *in* $[0,2\pi)^2$. *Moreover, we have the global error bound*

$$\left|\mathcal{E}^{\circledast}_{\mathcal{P}_F} D(\theta,\alpha;N_T,{N_T}^*) - D(\theta,\alpha)\right| \le \max\left\{I_0,I_1,I_2,I_3,I_4\right\},$$

where each I_i *is bounded and corresponds to a different component of the Combined Embedding Approximation* (6.21)

$$\begin{aligned}
I_0 :=& 8\epsilon^{(0)}_{\circledast}/(p^2T_0T_*),\\
I_1 :=& \epsilon^{(1)}_{\circledast}/(p^2T_*),\\
I_2 :=& \epsilon^{(2)}_{\circledast}/p^2,\\
I_3 :=& \frac{32}{p^2T_*}\left[\sum_{n=1}^{N_T}\frac{T_0^{n-1}}{n!}\epsilon^{(n)}_{\circledast}\right],\\
&+ M_\omega B_{\max}\frac{32}{p^2T_*}\frac{T_0^{N_T+1}}{(N_T+1)!}\left\|\frac{\partial^{N_T+1}\hat{D}}{\partial\theta^{N_T+1}}\right\|_{L^\infty([0,2\pi)^2)},
\end{aligned}$$

$$I_4 := \|(\mathcal{I} - \mathcal{P}_F)D\|_{L^\infty([0,2\pi)^2)} + 2T_* \left\| (\mathcal{I} - \mathcal{P}_F)\frac{\partial D}{\partial \theta} \right\|_{L^\infty([0,2\pi)^2)} + \max_{n_\theta + n_\alpha = 2} \frac{T_*^2}{2} \left\| \frac{\partial^2 D}{\partial \theta^{n_\theta} \partial \alpha^{n_\alpha}} \right\|_{L^\infty([0,2\pi)^2)},$$

for θ_0, T_0, α_* and T_* chosen as in (6.21)*, with*

$$\epsilon_{\circledast}^{(n)} := M_\omega \left[(B_{\max} + \epsilon_b) \left\| \frac{\partial^n}{\partial \theta^n}(\mathcal{P}_F - \mathcal{I})\hat{D} \right\|_{L^\infty([0,2\pi)^2)} + \epsilon_b \left\| \frac{\partial^n}{\partial \theta^n}\hat{D} \right\|_{L^\infty([0,2\pi)^2)} \right],$$

where $B_{\max}$ is the constant from Assumption 6.2 and

$$\epsilon_b := \max_{\substack{\alpha \in [0,2\pi) \\ m \in \{1,\dots,M_\omega\}}} |B_m(\alpha) - b_m(\alpha)|. \tag{6.25}$$

Proof. Proof of the global error bound is sufficient to show numerical stability. We split the proof into five parts, based on the five conditions of (6.21). We do not prove these bounds in the order they appear in the set (6.21).

On multiple occasions we will require the bound

$$\begin{aligned}
&\Big| \sum_{m=1}^{M_\omega} \Big[B_m \frac{\partial^n \hat{D}}{\partial \theta^n}(\theta,\alpha) - b_m \frac{\partial^n \mathcal{P}_F \hat{D}}{\partial \theta^n}(\theta,\alpha) \Big] \Big| \\
&= \left| \sum_{m=1}^{M_\omega} \left[B_m \frac{\partial^n \hat{D}}{\partial \theta^n}(\theta,\alpha) - [B_m + (b_m - B_m)] \frac{\partial^n}{\partial \theta^n} \left[\mathcal{I} + (\mathcal{P}_F - \mathcal{I}) \right] \hat{D}(\theta,\alpha) \right] \right| \\
&\leq M_\omega \left[(B_{\max} + \epsilon_b) \left\| \frac{\partial^n}{\partial \theta^n} (\mathcal{P}_F - \mathcal{I}) \hat{D} \right\|_{L^\infty([0,2\pi)^2)} + \epsilon_b \left\| \frac{\partial^n}{\partial \theta^n} \hat{D} \right\|_{L^\infty([0,2\pi)^2)} \right]
\end{aligned} \tag{6.26}$$

which is precisely the definition $\epsilon_{\circledast}^{(n)}$.

(i)

We combine the bound (6.26) (taking $n = 0$) and the representation (6.23) to obtain

$$|\mathcal{E}_{\mathcal{P}_F} D(\theta,\alpha) - D(\theta,\alpha)| \leq \frac{M_\omega \left[(B_{\max} + \epsilon_b)\epsilon_N |\Gamma| + \epsilon_b \|D\|_{L^\infty([0,2\pi)^2)} \right]}{|\Lambda(\theta,\alpha)|}, \tag{6.27}$$

by Lemma 6.3 and (6.26) we obtain

$$|\mathcal{E}_{\mathcal{P}_F} D(\theta,\alpha) - D(\theta,\alpha)| \leq \frac{8\epsilon_{\circledast}^{(0)}}{p^2 |\theta - \theta_0||\theta_0 - \theta_*|},$$

and since $|\theta - \theta_0| > T_0$ and $|\theta_0 - \theta_*| > T_*$ we have

$$|\mathcal{E}_{\mathcal{P}_F} D(\theta, \alpha) - D(\theta, \alpha)| \leq \frac{8\epsilon_{\circledast}^{(0)}}{p^2 T_0 T_*}.$$

(ii)

Following the same ideas as *(i)*, we obtain

$$\left| D(\theta_0, \alpha) - \frac{\sum_{m=1}^{M_\omega} b_m(\alpha) \frac{\partial \mathcal{P}_F \hat{D}}{\partial \theta}(\theta_0, \alpha_m)}{\frac{\partial \Lambda}{\partial \theta}(\theta_0, \alpha)} \right| \leq \frac{\epsilon_{\circledast}^{(1)}}{|p \sin(p\theta_0)|}.$$

From the condition $|\theta_0 - \theta_*| > T_*$ we can write

$$\begin{aligned} |p \sin(p\theta_0)| \geq & p |\sin(p(\theta_* \pm T_*))| \\ = & p |\sin(p\theta_*)\cos(pT_*) \pm \sin(pT_*)\cos(p\theta_*)| \\ = & p |\sin(pT_*)| \geq \frac{p^2 T_*}{2}, \end{aligned}$$

and the bound follows immediately.

(iii)

Again, following the ideas of *(i)* and *(ii)*, we are in the simpler case where

$$\left| \frac{\partial^2 \Lambda(\theta_*, \alpha)}{\partial \theta^2} \right| = p^2 |\cos(p\theta_*)| = p^2,$$

hence

$$\left| D(\theta_*, \alpha) - \frac{\sum_{m=1}^{M_\omega} b_m(\alpha) \frac{\partial^2 \mathcal{P}_F \hat{D}}{\partial \theta^2}(\theta_0, \alpha_m)}{\frac{\partial^2 \Lambda}{\partial \theta^2}(\theta_0, \alpha)} \right| \leq M_\omega \frac{(B_{\max} + \epsilon_b)\epsilon_N |\Gamma| + \epsilon_b \|D\|_{L^\infty([0,2\pi)^2)}}{p^2},$$

and the result follows from (6.26).

(iv) From Lemma 6.3,

$$\left| \frac{\theta - \theta_0}{\Lambda(\theta, \alpha)} \right| \leq \frac{8|\theta - \theta_0|}{p^2 |\theta - \theta_0||\theta_0 - \theta_*|} \leq \frac{8}{p^2 T_*}.$$

where we have used $T_* < |\theta_0 - \theta_*|$. Bounding the Taylor coefficients using the threshold $T_0 \geq |\theta - \theta_0|$,

$$\begin{aligned} & \left| D(\theta, \alpha) - \mathcal{E}^0_{\mathcal{P}_F} D(\theta, \alpha; \theta_0, N_T) \right| \\ & \leq \frac{8}{p^2 T_*} M_\omega \sum_{n=1}^{N_T} \frac{T_0^{n-1}}{n!} \left[(B_{\max} + \epsilon_b) \left\| \frac{\partial^n}{\partial \theta^n} (\mathcal{P}_F - \mathcal{I}) D \right\|_{L^\infty([0,2\pi)^2)} + \epsilon_b \left\| \frac{\partial^n}{\partial \theta^n} D \right\|_{L^\infty([0,2\pi)^2)} \right] \\ & \quad + M_\omega B_{\max} \frac{8}{p^2 T_*} \frac{T_0^{N_T}}{(N_T+1)!} \left\| \frac{\partial^{N_T+1} \hat{D}}{\partial \theta^{N_T+1}} \right\|_{L^\infty([0,2\pi)^2)} \end{aligned}$$

(v) Taking maximal values of the representation of (6.19)

$$
\begin{aligned}
&|D(\theta,\alpha) - \mathcal{E}^*_{\mathcal{P}_F} D(\theta,\alpha;\theta_*,\alpha_*,{N_T}^*)| \leq \\
&\|(\mathcal{I}-\mathcal{P}_F)D\|_{L^\infty([0,2\pi)^\infty)} + 2T_* \left\| (\mathcal{I}-\mathcal{P}_F)\frac{\partial D}{\partial\theta}\right\|_{L^\infty([0,2\pi)^\infty)} \\
&+ \max_{n_\theta+n_\alpha={N_T}^*+1} \frac{T_*^{{N_T}^*+1}}{({N_T}^*+1)!} \left\| \frac{\partial^{{N_T}^*+1} D}{\partial\theta^{n_\theta}\partial\alpha^{n_\alpha}}\right\|_{L^\infty([0,2\pi)^2)}
\end{aligned}
$$

□

The error bound in the above theorem contains a few components which we have not yet bounded. For the remainder of this section, we supplement the above error bound by bounding the terms using known data. Bounding the derivatives of the far-field pattern provides a gauge on the truncation error of the Taylor expansion.

LEMMA 6.9. *For $n_\theta, n_\alpha \in \mathbb{N}_0$ and $n = n_\theta + n_\alpha$, we have the following bound on the derivatives of the far-field pattern*

(i)

$$
\left\| \frac{\partial^n \hat{D}}{\partial\theta^n}\right\|_{L^\infty([0,2\pi)^2)} \leq |\Gamma| k \left[\frac{1+4\operatorname{diam}(\Gamma)}{\operatorname*{ess\,inf}_{\mathbf{x}\in\Gamma}(\mathbf{x}\cdot\mathbf{n}(\mathbf{x}))}\right] \sum_{n'=0}^{n} \left[\begin{pmatrix} n \\ n' \end{pmatrix} \max\{2, p^{n-n'}\}\xi_{n'}\right],
$$

(ii)

$$
\left\| \frac{\partial^n D}{\partial\theta^{n_\theta}\partial\alpha^{n_\alpha}}\right\|_{L^\infty([0,2\pi)^2)} \leq \frac{2|\Gamma|}{\operatorname*{ess\,inf}_{\mathbf{x}\in\Gamma}(\mathbf{x}\cdot\mathbf{n}(\mathbf{x}))} \xi_{n_\theta} \sum_{n'_\alpha=0}^{n_\alpha} \begin{pmatrix} n_\alpha \\ n'_\alpha \end{pmatrix} \zeta_{n_\alpha - n'_\alpha}\xi_{n'_\alpha},
$$

where

$$
\zeta_i = \begin{cases} \left(4k^2\operatorname{diam}(\Gamma)^2 + \frac{1}{4}\right)^{1/2}, & \text{for } i=0, \\ k\operatorname{diam}(\Gamma), & \text{otherwise.} \end{cases}
$$

and $\xi_i := \prod_{\ell=0}^{i}(\ell + k\operatorname{diam}(\Gamma))$. Similarly, there is a bound on the approximation error

(iii)

$$
\left\| \frac{\partial^n (\mathcal{I}-\mathcal{P}_F)\hat{D}}{\partial\theta^n}\right\|_{L^\infty([0,2\pi)^2)} \leq |\Gamma|\epsilon_N \sum_{n'=0}^{n} \left[\begin{pmatrix} n \\ n' \end{pmatrix} \max\{2, p^{n-n'}\}\xi_{n'}\right].
$$

(iv)

$$
\left\| \frac{\partial^n (\mathcal{I}-\mathcal{P}_F) D}{\partial\theta^n}\right\|_{L^\infty([0,2\pi)^2)} \leq |\Gamma|\epsilon_N \xi_n
$$

Proof. We are interested in derivatives of the kernel $K(\theta, \mathbf{y}) := \mathrm{e}^{-\mathrm{i}k(y_1\cos\theta + y_2\cos\theta)}$ of the integral far-field representation (6.3), in terms of the observation angle θ. This kernel is a plane wave, and so we seek the nth derivative in θ of the plane wave $K(\theta, \mathbf{y})$, which can be written as $\partial^n K/\partial\theta^n = g_n \cdot K$ where g_n can be defined iteratively,

$$g_1(\theta, \mathbf{y}) := -\mathrm{i}k[-y_1\sin(\theta) + y_2\cos(\theta)], \tag{6.28}$$

and

$$g_n(\theta, \mathbf{y}) = g_{n-1}(\theta, \mathbf{y})g_1(\theta, \mathbf{y}) + \frac{\partial g_{n-1}}{\partial\theta}(\theta, \mathbf{y}), \quad \text{for } n \geq 2$$

by repeated application of the product and chain rules. We can then write a general formula for g_n,

$$g_n(\theta, \mathbf{y}) = \Big(g_1(\theta, \mathbf{y}) + \frac{\partial}{\partial\theta}\Big)^n [g_1](\theta, \mathbf{y}), \quad \text{for } n \geq 2$$

Hence, for $\mathbf{y} \in \Gamma$

$$|g_n(\theta, \mathbf{y})| \leq \prod_{\ell=0}^{i}(\ell + k|\mathbf{y}|) \leq \prod_{\ell=0}^{i}(\ell + k\,\mathrm{diam}(\Gamma)) =: \xi_i. \tag{6.29}$$

The ℓ arises from each differentiation, and the $k|\mathbf{y}|$ comes from multiplication by g_1. *(i)* Writing the generalised product of the derivative

$$\frac{\partial^{N_T+1}\hat{D}}{\partial\theta^{N_T+1}}(\theta, \alpha) = \sum_{i=0}^{N_T+1} \begin{pmatrix} N_T+1 \\ i \end{pmatrix} \left[\frac{\partial^{N_T+1-i}\Lambda}{\partial\theta^{N_T+1-i}}(\theta, \alpha)\right] \left[\frac{\partial^i}{\partial\theta^i}\int_\Gamma K(\theta, \mathbf{y})\mathcal{P}_N \frac{\partial u_{\alpha_m}}{\partial\mathbf{n}}(\mathbf{y})\,\mathrm{d}s(\mathbf{y})\right],$$

recalling that $K(\theta, \mathbf{y}) := \mathrm{e}^{-\mathrm{i}k(y_1\cos\theta + y_2\cos\theta)}$. We use Cauchy–Schwarz to bound the integral representation for the far-field pattern, combining (6.29) with [35, Lemma 4.2] (which provides a bound on $\|\partial^+_{\mathbf{n}} u_{\alpha_m}\|_{L^2(\Gamma)}$), to obtain

$$\left|\frac{\partial^{N_T+1}\hat{D}}{\partial\theta^{N_T+1}}(\theta, \alpha)\right| \leq |\Gamma| \left[\frac{1 + 4\,\mathrm{diam}(\Gamma)}{\operatorname{ess\,inf}_{\mathbf{x}\in\Gamma}(\mathbf{x}\cdot\mathbf{n}(\mathbf{x}))}\right] \sum_{i=0}^{N_T+1} \left[\begin{pmatrix} N_T+1 \\ i \end{pmatrix} \max\{2, p^{N_T+1-i}\}\xi_i\right].$$

(ii) We now make use of the coercive star-combined operator of Definition 1.4, and denote by

$$f_k(\mathbf{x}; \alpha) := 2\left[\mathbf{x}\cdot\nabla - \mathrm{i}(k|\mathbf{x}| + \mathrm{i}/2)\right]\mathrm{e}^{\mathrm{i}k(x_1\cos\alpha - x_2\sin\alpha)}$$

the corresponding data for an incident plane wave of angle α, such that $\mathcal{A}_k[\partial u_\alpha/\partial\mathbf{n}](\mathbf{x}) = f_k(\mathbf{x}; \alpha)$ for almost all $\mathbf{x}$ on Γ, noting that the operator $\mathcal{A}_k$ is independent of α. Using the generalised product rule once more, we can write

$$\left\|\frac{\partial^{n_\alpha} f_k(\mathbf{x}; \alpha)}{\partial\alpha^{n_\alpha}}\right\|^2_{L^2(\Gamma)} \leq$$

$$\int_\Gamma \left| \sum_{n_\alpha=0}^{n'_\alpha} \left(\begin{array}{c} n_\alpha \\ n'_\alpha \end{array} \right) \frac{\partial^{n_\alpha - n'_\alpha}}{\partial \alpha^{n_\alpha - n'_\alpha}} \left[\mathrm{i}k(-x_1 \sin\alpha + x_2 \cos\alpha) - \mathrm{i}(k|\mathbf{x}| + \mathrm{i}/2) \right] \frac{\partial^{n'_\alpha}}{\partial \alpha^{n'_\alpha}} \mathrm{e}^{-\mathrm{i}k(x_1\cos\alpha + x_2 \sin\alpha)} \right|^2 \mathrm{d}s(\mathbf{y}).$$

We may make a second use of (6.29) for the plane wave $u^{\mathrm{inc}}_{PW}(\cdot;\alpha)$, whilst it is straightforward to show that the other derivatives are bounded by $\zeta_{n'_\alpha - n_\alpha}$, hence

$$\left\| \frac{\partial^{n_\alpha} f_k(\cdot;\alpha)}{\partial \alpha^{n_\alpha}} \right\|_{L^2(\Gamma)} \leq |\Gamma|^{1/2} \sum_{n_\alpha=0}^{n'_\alpha} \left(\begin{array}{c} n_\alpha \\ n'_\alpha \end{array} \right) \zeta_{n_\alpha - n'_\alpha} \xi_{n'_\alpha}. \tag{6.30}$$

We may write

$$\frac{\partial^n D(\theta,\alpha)}{\partial \theta^{n_\theta} \partial \alpha^{n_\alpha}} = -\int_\Gamma \frac{\partial^{n_\theta} K(\theta,\mathbf{y})}{\partial \theta^{n_\theta}} \left[\mathcal{A}_k^{-1} \frac{\partial^{n_\alpha} f_k}{\partial \alpha^{n_\alpha}} \right] (\mathbf{y};\alpha)\, \mathrm{d}s(\mathbf{y}),$$

and we can bound via Cauchy–Schwarz to obtain

$$\left| \frac{\partial^n D(\theta,\alpha)}{\partial \theta^{n_\theta} \partial \alpha^{n_\alpha}} \right| \leq \|g_n(\theta,\cdot)\|_{L^2(\Gamma)} \left\| \mathcal{A}_k^{-1} \right\|_{L^2(\Gamma)\to L^2(\Gamma)} \left\| \frac{\partial^{n_\alpha} f_k(\cdot;\alpha)}{\partial \alpha^{n_\alpha}} \right\|_{L^2(\Gamma)}$$

The coercivity constant [52, (1.17)] gives a bound on $\mathcal{A}_k^{-1} : L^2(\Gamma) \to L^2(\Gamma)$. Combining this with (6.30) and (6.29) we obtain the result.

The bound *(iii)* follows the same reasoning as *(i)* and *(ii)* respectively, we simply replace

$$\left\| \frac{\partial u_\alpha}{\partial \mathbf{n}} \right\|_{L^2(\Gamma)} \quad \text{with} \quad \left\| (\mathcal{I} - \mathcal{P}_N) \frac{\partial u_\alpha}{\partial \mathbf{n}} \right\|_{L^2(\Gamma)} \leq \epsilon_N.$$

The bound *(iv)* follows the same logic as *(iii)*, without the term $\Lambda(\theta,\alpha)$. □

In order to make the bounds of Theorem 6.8 fully explicit, bounds on ϵ_b of (6.25) are required. These depend on the stability of the system (6.1.1), which is closely related to the open question of Assumption 6.2(i).

6.4 More general incident waves

We now demonstrate how Embedding Formulae may be used to approximate the far-field pattern of a far broader class of incident waves than just plane waves, by means of a general formula, followed by some numerical examples.

Suppose that the Herglotz kernel (see Definition 1.8) $g_{\mathrm{Herg}} \in L^2(0,2\pi)$ is known for an incident field u^{inc}, hence we can write

$$u^{\mathrm{inc}}(\mathbf{x}) = u^{\mathrm{inc}}_{\mathrm{Herg}}(\mathbf{x}; g_{\mathrm{Herg}}) = \int_0^{2\pi} g_{\mathrm{Herg}}(\alpha) u^{\mathrm{inc}}_{PW}(\mathbf{x};\alpha)\, \mathrm{d}\alpha, \quad \text{for all } \mathbf{x} \in \mathbb{R}^2,$$

for $g_{\text{Herg}} \in L^2(0, 2\pi)$ and u_{PW}^{inc} as in (2.5). For Herglotz $u_{\text{Herg}}^{\text{inc}}$, we define

$$Hg_{\text{Herg}}(\theta) := \mathcal{F}_\infty[u_{\text{Herg}}^{\text{inc}}(\cdot; g_{\text{Herg}})](\theta),$$

hence we can write the far-field pattern of the corresponding scattered field as

$$Hg_{\text{Herg}}(\theta) := \int_0^{2\pi} g_{\text{Herg}}(\alpha) D(\theta, \alpha)\, \mathrm{d}\alpha \approx \int_0^{2\pi} g_{\text{Herg}}(\alpha) \mathcal{E}^{\circledast}_{\mathcal{P}_F} D\left(\theta, \alpha; N_T\right) \mathrm{d}\alpha. \tag{6.31}$$

In practice, the integral may be approximated by a quadrature rule, in which $[w_i]_{i=1}^{N_Q}$ and $[\alpha_i]_{i=1}^{N_Q}$ are $N_Q \in \mathbb{N}$ suitably chosen weights and nodes (see Appendix B for a summary of relevant quadrature rules), sufficient to resolve oscillations and singularities of the integrand to any desired accuracy. We may now generalise our Combined Expansion approximation to any Herglotz type functions, via

$$Hg_{\text{Herg}}(\theta) \approx \mathcal{E}^{\circledast}_{\mathcal{P}_F} Hg_{\text{Herg}}\left(\theta, g_{\text{Herg}}; N_T, (w_i)_{i=1}^{N_Q}, (\tilde{\alpha}_i)_{i=1}^{N_Q}\right) := \sum_{i=1}^{N_Q} w_i g_{\text{Herg}}(\tilde{\alpha}_i) \mathcal{E}^{\circledast}_{\mathcal{P}_F} D(\theta, \tilde{\alpha}_i).$$

where $\mathcal{E}^{\circledast}_{\mathcal{P}_F} D$ denotes the Combined Emebdding Approximation (6.2.3).

6.4.1 Numerical example: Regular Wavefunctions

We now compute numerical results for the particular example of a *Regular Wavefunction*, defined as

$$u^{\text{inc}}(\mathbf{x}) = \psi_\ell^{\text{inc}}(\mathbf{x}) := J_{|\ell|}(k|\mathbf{x}|)\mathrm{e}^{\mathrm{i}\ell\theta_{\mathbf{x}}}, \tag{6.32}$$

where J_n corresponds to the nth Bessel function of the first kind and $\theta_{\mathbf{x}}$ is the angle that $\mathbf{x}$ makes with the x_1-axis. The function ψ_{10} for $k = 40$ is depicted in Figure 3.2(b). The Herglotz kernel for (6.32), which follows by the Jacobi-Anger expansion (e.g. [17, (3.89)]) is given by

$$g_\ell(\alpha) := \begin{cases} \mathrm{e}^{-\mathrm{i}\ell\alpha}/(2\pi\mathrm{i}^\ell), & \ell \geq 0, \\ (-1)^\ell \mathrm{e}^{-\mathrm{i}\ell\alpha}/(2\pi\mathrm{i}^\ell), & \ell < 0, \end{cases} \tag{6.33}$$

hence we have $\psi_\ell^{\text{inc}} = u_{\text{Herg}}^{\text{inc}}(\cdot; g_\ell)$. We now consider the case in which Γ is a regular hexagon, with wavenumber $k = 1$. In our approximation we choose $N_Q = 20 \times \max(k, \ell)$ equally spaced quadrature points, to ensure there are 10 quadrature points per wavelength of the integrand of Hg_ℓ of (6.31), over the integral $[0, 2\pi)$. These are positioned such that

$$\min_{\substack{\alpha_* \in \Theta_* \\ i \in \{1, \ldots, N_Q\}}} |\tilde{\alpha}_i - \alpha_*| \tag{6.34}$$

is maximised, to avoid points where the error in the far field approximation is significantly amplified (as observed in the peaks of Figure 6.9(c), and quantified by Lemma 6.3).

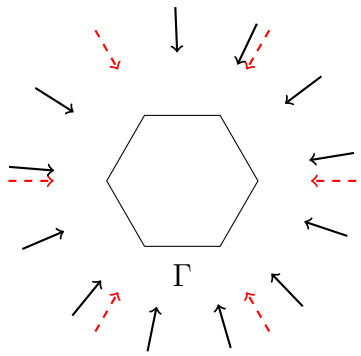

Figure 6.11: Schematic diagram of Hexagonal scatterer used for this section. For the Hexagon, it follows that $p = 3$ and $q = 4$, hence $M_\omega = n_\Gamma(q-1) = 18$. The incident angles A_{18} of canonical plane waves are shown, whilst those chosen to coincide with Θ_* are dashed. Each side length is 1.

Whilst the DOFs per side of the scatterer is the same as for the smallest errors observed in Figure 6.9(b), in Figure 6.13 we observe global errors lower than were seen in the peaks of Figure 6.9(c). This is most likely because of the careful choice (6.34). Figure 6.14 demonstrates how a naive approach is less stable, with much larger errors. Even in the semi-naive case of Figure 6.15, where the quadrature points are chosen far from points of Θ_* (in accordance with (6.34)), there is no improvement. This suggests that the method we present here is not only a means of removing numerical instability at certain points, but is essential for this generalised implementation of Embedding Formulae, which can compute the far-field coefficient for Herglotz-type incident fields. Naturally as k grows, the quadrature rule will require more points, and it will become harder to avoid the regions in which the error is largest.

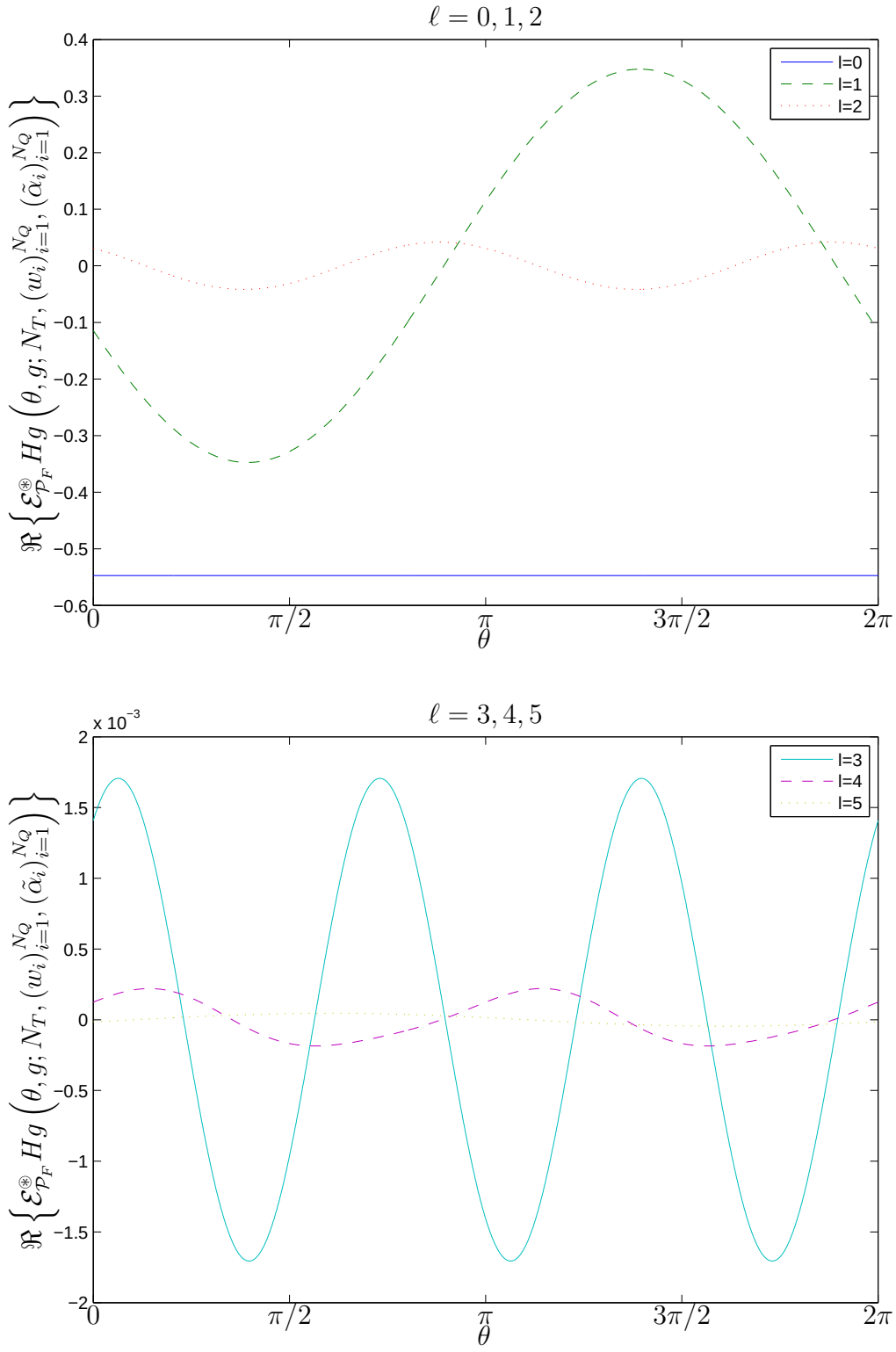

Figure 6.12: Far-field approximation of different Regular Wavefunctions, indexed by ℓ.

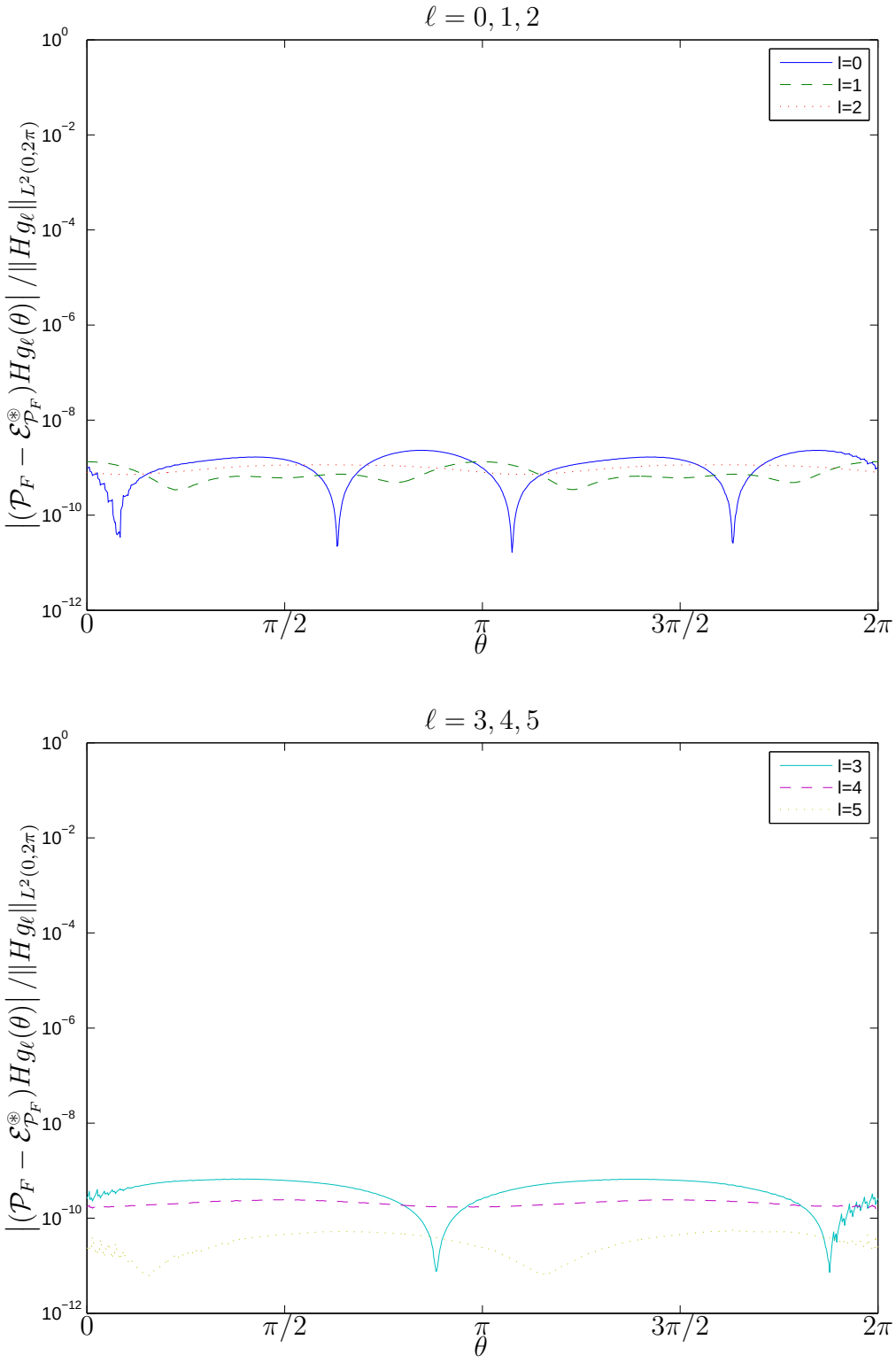

Figure 6.13: Error estimates using MPSpack with 90 DOFs as a reference solution, taking same DOFs per wavelength as for the square examples.

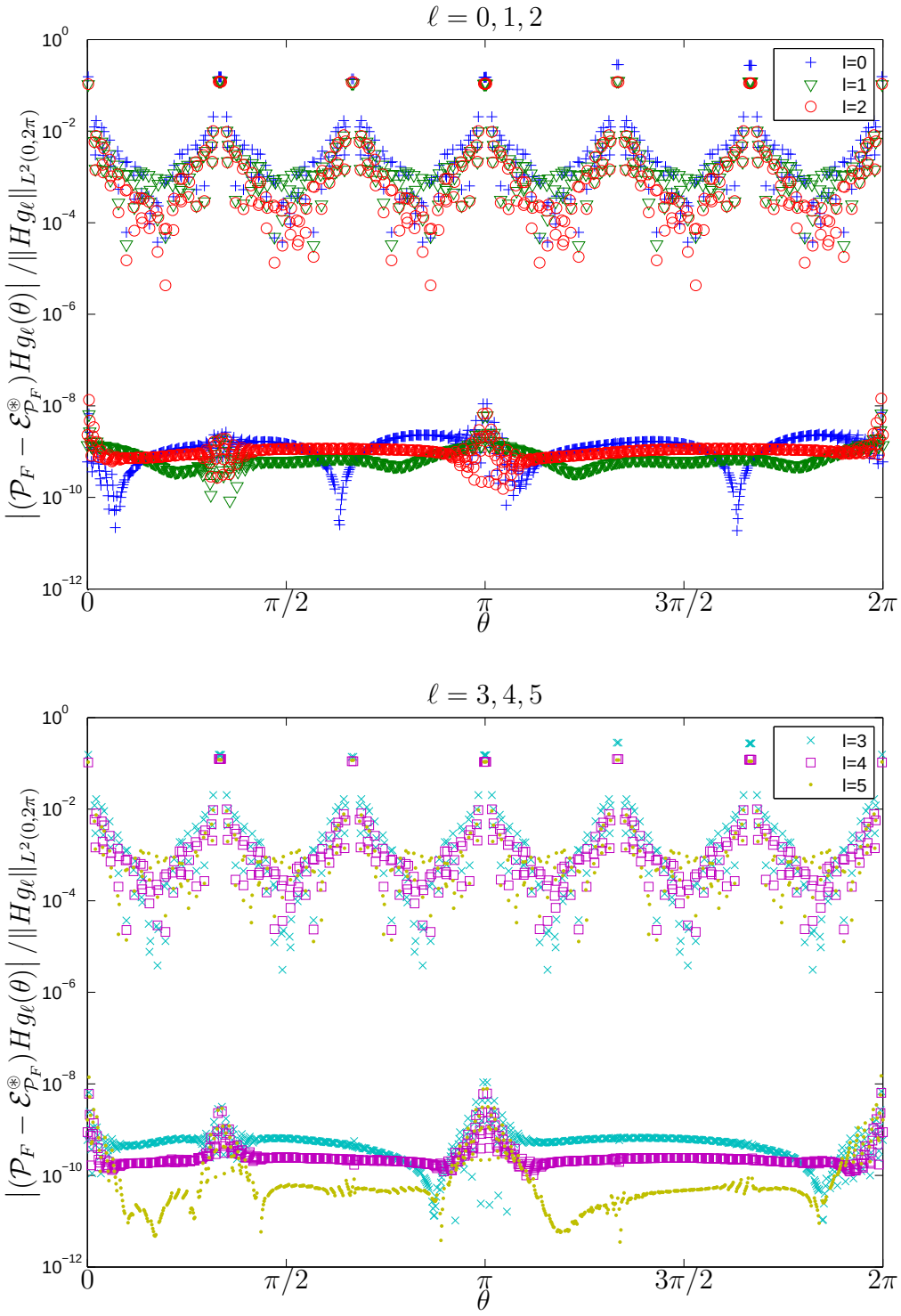

Figure 6.14: A completely naive embedding approach, with no careful selection of A_{M_ω} or weights and nodes for the integral, and no Taylor expansion.

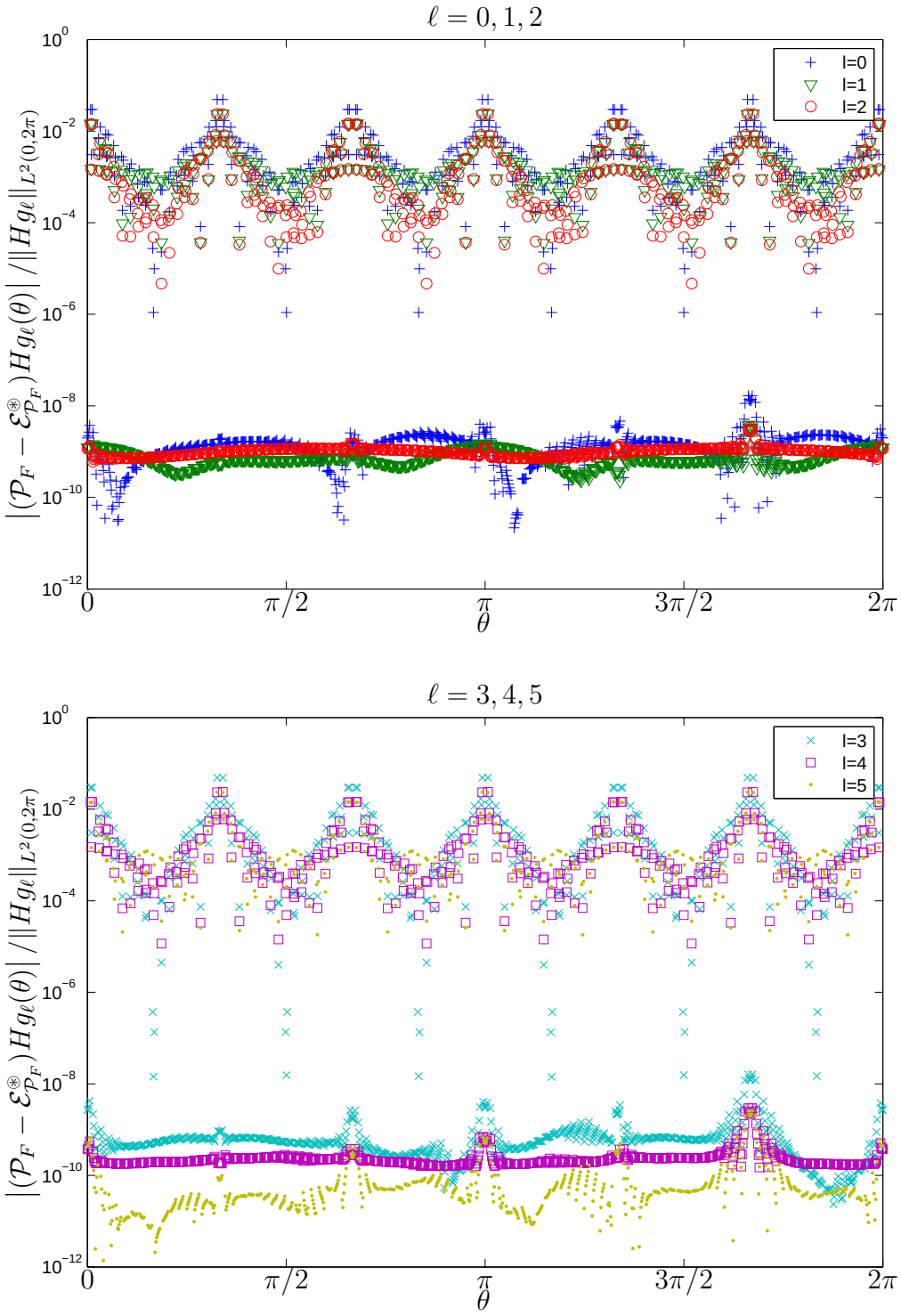

Figure 6.15: A semi-naive approach, in which quadrature weights are chosen as in Figure 6.13 to avoid Θ_*, at which the instability is largest.

This example demonstrates how, once the canonical problems have been solved,

and certain derivatives of the far-field solutions are obtained, that the far-field pattern of any Herglotz-type incident field can be computed relatively easily. Moreover, in certain cases, the global error can be reduced as part of this process.

6.5 Conclusions and extensions

We have demonstrated for a certain class of polygons, that the ideas of [9] can be implemented efficiently in a numerically stable manner for all $(\theta, \alpha) \in [0, 2\pi)^2$. Moreover, if an approximation to Neumann boundary data is known, bounds on the error can be obtained. These bounds could be made explicit with bounds on ϵ_b of (6.25), which would require an answer to the more general open question of Assumption 6.2(i).

Extension to the broader class of polygons with rational angles would be the next logical development of this method. As explained in [9, §3.2], for a general polygon Γ with rational angles, we instead require p and q to be integers such that $p\pi/q$ divides exactly $p_j\pi/q_j = \omega_j$ for each corner j. Then we choose $M_\omega = \sum_{j=1}^{n_\Gamma}(q_j - 1)$. It appears that extension to such polygons would be straightforward.

There may also be further possible refinements to the theory. Numerical results suggest that $M_\omega = n_\Gamma(q-1)$ becomes more than is required for certain n_Γ. For example, the system (6.1.1) becomes ill-conditioned for such a choice when $n_\Gamma = 8$, and numerical experiments suggest that in fact $M_\omega = 16 < n_\Gamma(q-1) = 32$ is sufficient in this case. Currently there is no theoretical explanation for this. But a poorly conditioned system could be another source of instability; understanding the reasoning behind this unexpected behaviour is key if the methods of this Chapter are to be applied to all rational geometries.

Alternative approaches to remedy the numerical instabilities may also be explored. Given that we know exactly where these instabilities occur, rather than approximating the unstable region with a Taylor expansion which converges to the exact value, it might be more efficient to use an alternative approximation over the unstable region.

Chapter 7

A numerically robust T-matrix method for multiple polygons

Here we introduce the Transmission Matrix (T-matrix) T-matrix methods for single (§7.1) and multiple obstacles (§7.2), for which the results and derivations are based on [22–24, 55]. We focus in particular on a relatively recent approach (of [23]). The novel contribution of this chapter is the combination with the Embedding Formulae of Chapter 6, in §7.3, which significantly reduces the computational cost required. Hence, it should be noted that the derivations and results of §7.1–7.2 are not new.

7.1 T-matrix methods for single scattering

Initially we focus on the T-matrix method for single obstacles. The construction of the T-matrix will be identical for the multiple scattering formulation of the problem of §7.2, in which each obstacle will have a single T-matrix, independent of the incident field. We are interested in the T-matrix because it extends easily to multiple scattering problems. The single scattering method has other applications, in particular for modelling moving obstacles. We do not explore this here.

7.1.1 Specific problem statement

Here we assume that the origin lies inside of a bounded open set $\Omega_- \subset \mathbb{R}^2$ with boundary $\partial\Omega$, such that the ball B_{R_-} with radius $R_- \geq \text{diam}(\Omega_-)/2$, is centred at the origin and contains Ω_-. We do not impose the requirement that Ω_- is connected, i.e., this obstacle can consist of many obstacles, and all of the following will still hold, provided a method to approximate the problem on Ω_- is available. For the purpose of understanding the T-matrix method, it is simpler to consider Ω_- as a single connected set. We consider the expansion of the incident field in terms of *regular wavefunctions*

ψ_ℓ^{inc}, that is

$$u^{\text{inc}}(\mathbf{x}) = \sum_\ell b_\ell \psi_\ell^{\text{inc}}(\mathbf{x}) \quad \text{in } B_-, \quad \text{where } \psi_\ell^{\text{inc}}(\mathbf{x}) := J_{|\ell|}(k|\mathbf{x}|)\mathrm{e}^{\mathrm{i}\ell\theta_{\mathbf{x}}}, \tag{7.1}$$

where J_n is the Bessel function of the first kind order n and $\theta_{\mathbf{x}} \in [0, 2\pi)$ is the angle that $\mathbf{x} \in \mathbb{R}^2$ makes with the x_1-axis. We expand the scattered field in terms of *radiating wavefunctions* ψ_ℓ^s, that is

$$u^s(\mathbf{x}) = \sum_\ell a_\ell \psi_\ell^s(\mathbf{x}) \quad \text{in } \mathbb{R}^2 \setminus B_- \quad \text{where } \psi_\ell^s(\mathbf{x}) := H_{|\ell|}^{(1)}(k|\mathbf{x}|)\mathrm{e}^{\mathrm{i}\ell\theta_{\mathbf{x}}}, \tag{7.2}$$

where $H_n^{(1)}$ is the Hankel function of the first kind, order n. At this stage, we consider the infinite dimensional case, for which both sums (7.1) and (7.2) are over all $\ell \in \mathbb{Z}$. The T-matrix is the matrix T that maps $\mathbf{a} := (a_\ell)_\ell$ to $\mathbf{b} := (b_\ell)_\ell$, hence

$$T\mathbf{a} = \mathbf{b}. \tag{7.3}$$

For incident fields such as plane wave and point source incidence, the coefficients b_ℓ are known and can be written explicitly (see [24]).

7.1.2 Computing the entries of the T-matrix

Given (7.3) and the coefficients $\mathbf{a}$, if we can compute (and invert) T then we have a representation for the scattered field from (7.2). The original formulation of T-matrix of [55] contains two methods to compute T, via the representation

$$T = -BA^{-1}. \tag{7.4}$$

The first method requires

$$(A)_{mn} = \frac{\mathrm{i}}{4}\left(\partial_{\mathbf{n}}^+ \psi_n^{\text{inc}}, \psi_m^s\right)_{L^2(\partial\Omega)}, \quad \text{and} \quad (B)_{mn} = \frac{\mathrm{i}}{4}\left(\partial_{\mathbf{n}}^+ \psi_n^{\text{inc}}, \psi_m^{\text{inc}}\right)_{L^2(\partial\Omega)}, \tag{7.5}$$

whilst the second approach takes

$$(A)_{mn} = \frac{\mathrm{i}}{4}\left(\psi_n^{\text{inc}}, \partial_{\mathbf{n}}^+ \psi_m^s\right)_{L^2(\partial\Omega)}, \quad \text{and} \quad (B)_{mn} = \frac{\mathrm{i}}{4}\left(\psi_n^{\text{inc}}, \partial_{\mathbf{n}}^+ \psi_m^{\text{inc}}\right)_{L^2(\partial\Omega)}. \tag{7.6}$$

Both approaches are commonly referred to as the *Null Field Method*, which along with other approaches (not mentioned here), can become numerically unstable for certain geometries Ω_- due to the singular nature of the Hankel functions (for more details see [23, §3]). This motivated the Tmatrom method of [21], for which

$$T_{mn} = \frac{1}{4}\frac{k}{\pi}\mathrm{i}^{|m|}(1+\mathrm{i})\int_0^{2\pi} [\mathcal{F}_\infty \psi_n^{\text{inc}}](\theta)\mathrm{e}^{-\mathrm{i}m\theta}\,\mathrm{d}\theta, \tag{7.7}$$

where $\mathcal{F}_\infty$ denotes the far-field map of (1.16). It follows that the Tmatrom method does not suffer from the same stability issues as other T-matrix methods, since the integrand of (7.7) is smooth. Tmatrom has the additional requirement that a *solver*, by which we loosely mean a numerical method which maps the Regular Wavefunction ψ_n^{inc} to an approximation of the far-field pattern $\mathcal{F}_\infty \psi_n^{\text{inc}}$, must be incorporated into the Tmatrom method. A suitable solver may involve the space $V_N^{\text{HNA}}(\partial\Omega)$ as introduced in Chapter 2, although there are many suitable choices. In the numerical example that follows we use MPSpack of [4].

7.1.3 Truncation of the T-matrix

In practice, we must truncate the T-matrix so that it is finite dimensional, summing over indices $\ell = -\hat{N}$ to $\ell = \hat{N}$, for $\hat{N} \in \mathbb{N}_0$. The finite dimensional case with truncated T results in an approximation to u^s via (7.2) and (7.3), and as $\hat{N}$ increases, this approximation improves. We define the truncated T-matrix as

$$\hat{T} := (T)_{n,m=-\hat{N}}^{\hat{N}} \in \mathbb{C}^{(2\hat{N}+1)\times(2\hat{N}+1)}, \quad \text{for } \hat{N} \in \mathbb{N}_0.$$

The number of dimensions $\hat{N}$ is typically chosen to satisfy the condition of [56]:

$$\hat{N} = \left\lceil kR_- + 4(kR_-)^{1/3} + 5 \right\rceil, \tag{7.8}$$

which is justified for the case (7.7) with point source or plane wave incidence in [24, Theorems 3.6 and 3.7]. This is another advantage over the null field method, which does not have this theoretical validation. Given that we sum over negative and positive indices of the wavefunctions, we require the far-field pattern and hence the solution, of $2\hat{N}+1$ problems with different radiating wavefunction incidence. It is clear from (7.8) that $k \lesssim \hat{N}$ as $k \to \infty$, hence the number of solves required by the Tmatrom method grows more than linearly with the wavenumber k, posing potential difficulties at large wavenumbers.

Given the truncated vector of coefficients

$$\hat{\mathbf{a}} := \hat{T}^{-1}(b_\ell)_{\ell=-\hat{N}}^{\hat{N}},$$

we can construct an approximation to the far-field pattern (1.16), by expanding each term in the truncated series (7.2) as $r \to \infty$ using [18, (10.2.5)],

$$u^\infty(\theta) \approx \hat{u}_{\hat{N}}^\infty(\theta) := \sum_{\ell=-\hat{N}}^{\hat{N}} \mathrm{i}^{-|\ell|-1} \hat{a}_\ell \mathrm{e}^{\mathrm{i}(\ell\theta)}. \tag{7.9}$$

We have the following error estimate from [24, Theorem 3.9].

THEOREM 7.1. *For scattering of a plane wave by a single obstacle Ω_-, if $\hat{N} > kR_-/2 + 1$ then the following error bound holds:*

$$\|u^\infty - u^\infty_{\hat{N}}\|^2_{L^2(0,2\pi)} \leq C\hat{N}^2 \left(\frac{R_- k\mathrm{e}}{2\hat{N}}\right)^{2\hat{N}} + C'\epsilon_F^2, \tag{7.10}$$

where C and C' are positive constants independent of k and $\hat{N}$, ϵ_F denotes the error in the far-field approximation of the solver used, and $\hat{u}^\infty_{\hat{N}}$ is the approximation (7.9) *to the far-field pattern u^∞ of* (1.16)*.*

7.2 T-matrices for multiple scattering

In this section we outline the procedure to extend any T-matrix method to multiple obstacles, which is based on the derivation of [22, §2.2]. Everything in this section holds for the infinite dimensional or truncated T-matrix case. Suppose now that Ω_- consists of n_γ pairwise disjoint obstacles, which we denote Ω_i for $i = 1, \ldots, n_\gamma$, hence $\Omega_- = \cup_{i=1}^{n_\gamma} \Omega_i$. For each obstacle, we denote by $\mathbf{x}_i^c$ a point inside of Ω_i, and denote by $T_{(i)}$ the T-matrix corresponding to the obstacle Ω_i with a coordinate system translated by $-\mathbf{x}_i^c$ in each case, so that the origin is inside of the obstacle. We impose the additional constraint that there exists a collection of pairwise disjoint balls $B_{R_i}(\mathbf{x}_i^c) \supset \Omega_i$, $R_i > 0$ for $i = 1, \ldots, n_\gamma$. Recalling the example (4.1), we now formulate the multiple scattering T-matrix method by considering a single scattering problem on each obstacle, where the sum of the scattered fields emanating from all other obstacles is absorbed into the incident field of a single scattering T-matrix problem on the ith obstacle Ω_i:

$$u_i^{\mathrm{inc}} := u^{\mathrm{inc}} + \sum_{i' \neq i} u^s_{i'}, \quad \text{in } B_i \tag{7.11}$$

where $u^s_{i'}$ is the (also unknown at this stage) contribution to the scattered field from the obstacle i'. Recalling that each single scattering problem requires the origin to be positioned inside of the scatterer, we will make use of the *Translation Addition Theorem* of [19] to translate $\mathbf{x}_{i'}^c$ to $\mathbf{x}_i^c$. Proceeding as in [22, §2.2], we define the two-dimensional analogue of translation addition matrix of [19, (51)] as

$$(S^{(i' \to i)})_{\ell,\ell'} := w_{\ell,\ell'} \rho^{(i')}_{\ell,\ell'} \mathrm{e}^{\mathrm{i}(\ell-\ell')\theta(\mathbf{x}_{i'}^c - \mathbf{x}_i^c)} H^{(1)}_{|\ell-\ell'|}(k|\mathbf{x}_{i'}^c - \mathbf{x}_i^c|) w_{\ell',\ell}$$

where

$$\rho^{(i')}_{\ell,\ell'} := \frac{\sqrt{\pi k}}{(-\mathrm{i})^{|\ell|(1-\mathrm{i})} H^{(1)}_{\ell'}(kR_{i'})}$$

and

$$w_{\ell',\ell} := \frac{1}{\sqrt{2\pi}}(-\mathrm{i})^{|\ell|-|\ell'|-|\ell-\ell'|}\int_0^{2\pi} \mathrm{e}^{\mathrm{i}(|\ell|-|\ell'|-|\ell-\ell'|)\theta}\,\mathrm{d}\theta.$$

Denote by $\mathbf{a}_{(i)}$ the vector $\mathbf{a}$ of (7.1), corresponding to the solution to the single obstacle problem (7.1.1) on Ω_i. We seek to determine the vector $\mathbf{b}_{(i)}$, which corresponds to the field scattered by Ω_i, given that additional terms have been absorbed into the incident field (7.11), emanating from the other scatterers. We may expand the terms in (7.11) to obtain a representation for the incidence

$$u_i^{\mathrm{inc}}(\mathbf{x}) = \sum_\ell (\mathbf{b}_{(i)})_\ell \psi_\ell^{\mathrm{inc}}(\mathbf{x}) + \sum_{i'\neq i}\sum_\ell (S_{(i'\to i)}\mathbf{a}_{(i')})_\ell \psi_\ell^s(\mathbf{x}-\mathbf{x}_{i'}^c), \quad \mathbf{x}\in B_i. \tag{7.12}$$

Now multiplying (7.12) by $T_{(i)}$, the T-matrix for the obstacle Ω_i, we obtain the contribution to the scattered field from Ω_i,

$$u_{(i)}^s(\mathbf{x}) = \sum_\ell (T_{(i)}\mathbf{b}_{(i)})_\ell \psi_\ell^s(\mathbf{x}) + \sum_{i'\neq i}\sum_\ell (T_{(i)}S_{(i'\to i)}\mathbf{a}_{(i')})_\ell \psi_\ell^s(\mathbf{x}-\mathbf{x}_{i'}^c), \quad \mathbf{x} \text{ in } \mathbb{R}^2\setminus B_i, \tag{7.13}$$

hence to determine the coefficients $\mathbf{b}_{(i)}$ of the scattered field for each Ω_i, the system to solve is

$$\mathbf{a}_{(i)} - \sum_{i\neq i'} T_{(i)}S_{(i'\to i)}\mathbf{a}_{(i')} = T_{(i)}\mathbf{b}_{(i')}, \quad \text{for } i = 1,\ldots,n_\gamma. \tag{7.14}$$

As in the single scattering case, in practice each T-matrix (and consequently each translation addition matrix $S_{(i'\to i)}$) must be truncated in accordance with (7.8).

7.3 Reducing the number of solves required

Here we extend the Tmatrom method by combining it with the Embedding Formulae used in Chapter 6. The theory here is for a single obstacle, but is equally adaptable to multiple obstacles using the ideas discussed in §7.2. We suppose now that our obstacle Ω_- is a rational (in the sense of §6.1) polygon. First we introduce the Herglotz kernel (of Definition 1.8) for the far-field pattern of the ℓth Regular Wavefunction ψ_ℓ^{inc}, which follows by the Jacobi-Anger expansion (e.g. [17, (3.89)]) and the definition (7.1):

$$g_\ell(\theta) := \begin{cases} \mathrm{e}^{-\mathrm{i}\ell\theta}/(2\pi\mathrm{i}^\ell), & \ell\geq 0,\\ (-1)^\ell \mathrm{e}^{-\mathrm{i}\ell\theta}/(2\pi\mathrm{i}^\ell), & \ell<0,\end{cases} \tag{7.15}$$

hence we can write (as in §6.4.1)

$$\psi_\ell^{\mathrm{inc}}(\mathbf{x}) = \int_0^{2\pi} g_\ell(\alpha)u_{PW}^{\mathrm{inc}}(\mathbf{x};\alpha)\,\mathrm{d}\alpha.$$

Using this, we may use our HNA method for Herglotz type incidence of §3.1 with Herglotz kernel g_ℓ, and solve for $\ell = -M_T, \ldots, M_T$. Using results computed in this thesis, we can determine the error in the approximation.

COROLLARY 7.2. *Suppose the conditions of Theorem 7.1 are satisfied, and the Herglotz-type HNA method of §3.1 is chosen as the solver to be used in conjunction with Tmatrom. Then the constant ϵ_F of Theorem 7.10 is bounded by*

$$\epsilon_F \leq Ck^{-1/2} C_q(k) M_\infty(u) J(k) \mathrm{e}^{-p\tau_\Gamma},$$

where C, J, p and τ_Γ are the constants from Corollary 2.11, C_q is the stability constant from Remark 2.13, whilst

$$M_\infty(u) \leq \left(\sqrt{2\pi} + 2C_1\sqrt{\pi}|\Gamma|^{1/2} \left[2\,\mathrm{diam}(\Omega_-) + \frac{1}{2k} \right] k^{1/2} \log^{1/2}(2 + kL_*) \right),$$

where C_1 and L^* are as in Theorem 3.1.

Proof. Follows immediately from (2.12), whilst the bound on $M_\infty(u)$ follows from Theorem 3.3, noting that the required bound on the Herglotz kernel is $\|g_\ell\|_{L^2(0,2\pi)} = 1$, by (7.15). □

When solving high frequency problems, Tmatrom with Herglotz-type HNA clearly provides a numerically robust approximation, with explicit error bounds available in the specific case of single scattering by a plane wave. The key advantage is that once the T-matrix has been computed, it can be re-used for different incident waves, and problems can be solved very quickly, as the coefficients are given explicitly. This is exactly the same benefit of using the Embedding Formulae in Chapter 6; once the canonical problems were solved, we can solve easily for any incident angle, and bound the error in doing so. We do not compare the efficiency of the two methods here, instead we combine them.

We now provide a brief example to motivate integration of the Embedding Formulae with a numerical solver, before incorporating with Tmatrom. Suppose that we are solving the problem of scattering of a plane wave with wavenumber $k = 1000$ by multiple (identical) squares, of identical orientation. The same T-matrix may be used for each square. Given that the total number of solves is $2M_T + 1$, and we must satisfy the condition (7.8), we must solve for $\ell \in \{-1045, \ldots, 1045\}$ incident fields, a total of 2091 solves. Although it is only necessary to recompute the right-hand side of the Galerkin system (2.11) in each instance, as k grows the number of solves grows faster than $2k$, clearly introducing a k-dependence to the method. However, from

Remark 6.1, one can implement an embedding formula for a square by solving for only eight plane waves, after which we can use the Embedding Formulae to produce the far-field pattern for Herglotz kernel g_ℓ of 7.15 for $\ell \in \{-1045, \dots, 1045\}$, enabling us to compute the T-matrix without the need for further solves. This number does not increase with frequency, and depends only on the geometry of the obstacle.

We may write this idea generally for any rational (in the sense of §6.1) polygonal obstacle Ω_-. Using embedding theory

$$\begin{aligned}\mathcal{F}_\infty \psi_\ell^{\text{inc}}(\theta) &= \int_0^{2\pi} g_\ell(\alpha) \mathcal{F}_\infty \left[\mathrm{e}^{\mathrm{i}k(\cdot)\cdot \mathbf{d}_\alpha}\right](\theta)\,\mathrm{d}\alpha, \quad \text{where } \mathbf{d}_\alpha := (\cos\alpha, -\sin\alpha) \\ &= \int_0^{2\pi} g_\ell(\theta) D(\theta,\alpha)\,\mathrm{d}\alpha,\end{aligned}$$

where $\mathcal{F}_\infty$ is the far-field map (1.17). Inserting into (7.7) and substituting (6.4) we obtain an extension to the Tmatrom method, for which the entries are computed via

$$T_{j\ell} = \frac{1}{4}\frac{k}{\pi}\mathrm{i}^{|j|}(1+\mathrm{i})\int_0^{2\pi}\int_0^{2\pi} g_\ell(\alpha)\frac{\sum_{m=1}^{M_\omega} B_m(\alpha)\Lambda(\theta,\alpha_m)D(\theta,\alpha_m)}{\Lambda(\theta,\alpha)}\mathrm{e}^{-\mathrm{i}j\theta}\,\mathrm{d}\alpha\,\mathrm{d}\theta. \quad (7.16)$$

Hence only M_ω solves are required for the Tmatrom algorithm, where M_ω depends only on the geometry of Ω_-. In §6.1.2 it was shown that the representation (6.4) breaks down when implemented numerically, hence in practice the matrix entries should be computed using

$$T_{j\ell} = \frac{1}{4}\frac{k}{\pi}\mathrm{i}^{|j|}(1+\mathrm{i})\int_0^{2\pi}\int_0^{2\pi} g_\ell(\alpha)\mathcal{E}^{\circledast}_{\mathcal{P}_F} D(\theta,\alpha;N_T)\Lambda(\theta,\alpha)\mathrm{e}^{-\mathrm{i}j\theta}\,\mathrm{d}\alpha\,\mathrm{d}\theta, \quad (7.17)$$

where $\mathcal{E}^{\circledast}_{\mathcal{P}_F} D(\theta,\alpha;N_T)$ is the Combined Expansion Approximation of Definition 6.6, with N_T the parameter corresponding to the degree of the Taylor expansion taken. The integral (7.17) must be computed using a quadrature rule, as discussed in Appendix B. Where possible, these points should be chosen in the same spirit as (6.34), with α nodes as far as possible from the points in $[0, 2\pi)$ at which only a first order Taylor approximation is used.

Tmatrom is in some ways superior to traditional T-matrix methods (such as the Null Field approaches (7.5) and (7.6)), in that it is provably stable for any configuration. This comes at the cost of the requirement to solve $O(k)$ scattering problems before the T-matrix can be computed, which is not a requirement of the other (less stable) T-matrix methods. By coupling Tmatrom with the Embedding Formulae of Chapter 6, this $O(k)$ dependence becomes $O(1)$, and the cost of computing the more stable Tmatrom T-matrix has the same k-dependence as a traditional T-matrix method, such as (7.5) or (7.6). Therefore this combined approach offers stability, at

no extra k-dependent cost. Justifying this claim with numerical results is a key area for future work. Figure 7.1 shows the output of the combination of Tmatrom with our embedding solver and the MPSpack solver. This required 8, 12 and 30 solves on the triangle, square and pentagon respectively, a total of 50 solves, a number independent of k. For wavenumber $k = 5$, using MPSpack without solving via the Embedding Formulae results in a total of 27 solves on each scatterer, hence a total of 81 solves. So even at a relatively low wavenumber using a non-HNA solver, the Embedding Formulae can reduce the number of solves required.

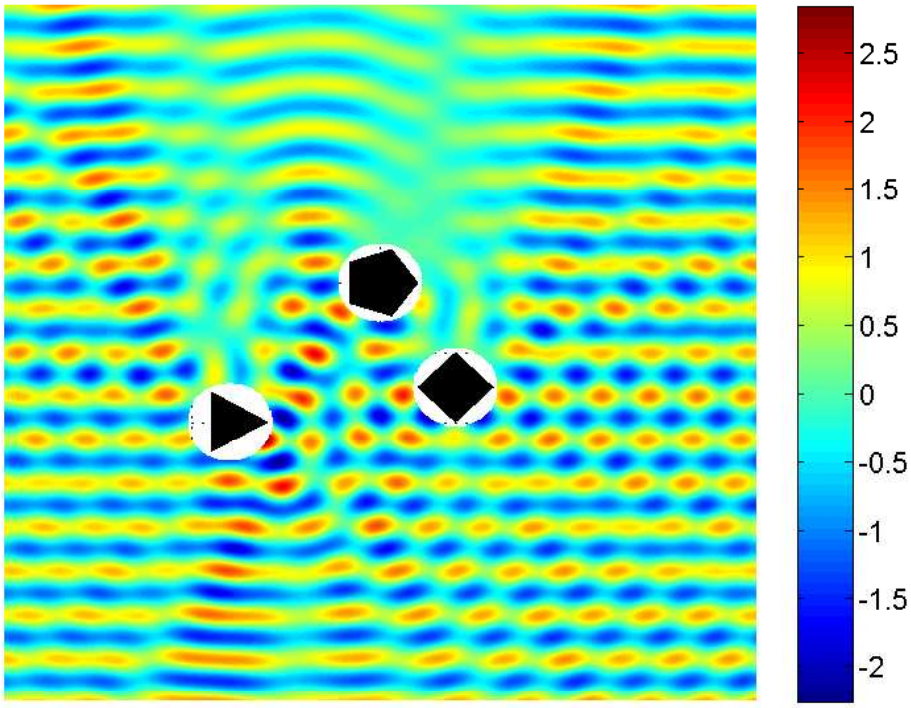

Figure 7.1: Real part of total field u for a configuration of multiple polygons, with incident field $u^{\text{inc}}_{PW}(\cdot;\pi/2)$ solved using MPSpack as the solver used for the embedding implementation, which in turn is used as the solver for Tmatrom. The expansion is only valid outside of the balls B_i containing the obstacle Ω_i, for $i = 1, 2, 3$.

We conclude this chapter with a summary of the k-dependency of different T-matrix methods. We first note that the matrix T is in principle the same regardless of if a null-field method (7.5), (7.6) or Tmatrom method (7.7) is used, hence it is recommended that the size of the truncated T-matrix grows like $O(k)$ (specifically (7.8)) for any approach. For cases where they are robust, traditional T-matrix methods

may be performed relatively quickly at low k, requiring two integrals for each entry of the T-matrix ((7.5) and (7.6)). This suggests an advantage over Tmatrom, which (i) requires a new scattering problem to be solved for each of the $O(k)$ columns of T, whilst (ii) each column in turn may require $O(k)$ such integrals if (for example) a standard Galerkin BEM solver is used. However, for polygons an HNA solver may be used to reduce the dependency of the Galerkin system to $O(1)$ (as discussed in §2.3) which overcomes (ii), and we have shown that Embedding formulae may be used to reduce the number of scattering problems to $O(1)$, which overcomes (i). Moreover, for large k and hence large T-matrices, numerical cost of the inverted matrix of (7.4) will increase for standard T-matrix methods, whilst Tmatrom does not require the inversion of any large matrices, so at large k a method combining HNA BEM and Embedding formulae with Tmatrom is advantageous over a standard T-matrix method. Investigating this combination is a key area for future work; the only k-dependence with such a method would take the form of $O(k^2)$ integrals used to compute T, which contain smooth integrands, and may be computed using sophisticated quadrature routines of [38]. The purpose of this chapter was to lay the ground work for such an implementation.

Chapter 8

Conclusions and future work

In this thesis we have presented a number of new developments. Some may be applied to general multiple scattering methods, whilst others represent advances to HNA single scattering methods (with subsequent potential contribution to multiple scattering problems). We now recap the most significant (in the opinion of the author) new results.

- Chapter 2 analysed the best approximation error of single-mesh HNA BEM (Theorem 2.9), providing estimates comparable to [35, Theorem 5.5].
- Chapter 3 generalised HNA methods to a Herglotz and source-type incident fields. Error estimates for source-type incidence required an alternative approach (Theorem 3.10) to [35], to handle the singular behaviour of the incident field. These estimates were backed up by numerical experiments in §3.2.3.
- Chapter 4 presented the first extension of HNA methods to multiple obstacles, generalising the ansatz (4.9). As a necessary component of the error estimates, we required a new bound on the solution in the domain for non-trapping polygons (Corollary 4.7). This bound may also be applied to non-convex obstacles of [15], for which the solution in the domain was *assumed* to be bounded, but not proved. Numerical results demonstrated exponential convergence of the approximation in 4.5.
- Chapter 5 presented the first k-explicit stability estimates for any multiple scattering BEM. The first of these, Theorem 5.5, requires that the obstacles are sufficiently smooth and strictly convex. The second, Theorem 5.7, guarantees stability via a geometric condition which is sufficient for the multiple scattering problem to be coercive. This holds for more general (than the other key stability

result of the chapter) star-shaped obstacles, but requires that these obstacles are sufficiently far apart. New best approximation estimates for scattering by multiple convex polygons were presented in Theorem 5.10, whilst estimates for the inverse of the Constellation Combined operator were presented in Theorem 5.6.

- Chapter 6 identified previously undocumented stability issues that arise when implementing Embedding Formulae for polygons, quantified by Theorem 6.3 and demonstrated by numerical examples in §6.1. A numerically stable alternative was proposed in Definition §6.2.3, which was subsequently analysed in §6.3. This analysis made use of Lemma 6.9, which provides a bound on arbitrary derivatives of the far-field coefficient in terms of incident angle and observation angle. In §6.4 Embedding Formulae were extended from incident plane waves to Herglotz-type functions, supplemented by numerical examples.

- Chapter 7 showed how the Embedding Formulae can be used to reduce the number of solves required for Tmatrom from $O(k)$ to $O(1)$, demonstrating with a single numerical example that even at low wavenumber, this approach can offer a saving in computational cost.

We also remark that whilst the work of Chapter 3 is based on single scattering problems, such general incident fields may be equally adapted to HNA methods for multiple scattering problems; the method of Chapter 4 can easily be generalised to cases where the incident field is not a plane wave.

8.1 Single vs. overlapping mesh

We have seen in §2.2 that the HNA method can be applied to single or overlapping meshes, and Theorem 2.9 showed that the best approximation behaves similarly for either choice. In terms of practical implementation, the numerical experiments in Chapters 3 and 4 shed additional light on the effectiveness of the single mesh space. Whilst no overlapping mesh approximations were used for the numerical experiments of this thesis, comparison against the numerical results of [35] suggests that the overlapping mesh space is more accurate, for the same number of degrees of freedom. Moreover, as was observed in Figure 4.4, the accuracy of the approximation is very dependent on the choice of the parameter α_{ij} of (2.7). The advantage is that the single-mesh space space is readily adaptable from a standard *hp* space, only the basis functions must be changed. Although the collocation HNA BEM was not investigated

in this thesis, the discussion of Remark 2.12 suggests it would be better suited to the single-mesh space.

8.2 HNA methods for multiple obstacles

The primary aim of this thesis was to generalise HNA BEM to multiple obstacles, and all of the work of Chapters 3–7 may be partitioned into (roughly) two distinct ways to do this:

(i) *Hybrid-Standard BEM basis coupling* (we will call this *H-S* for short), in which an HNA basis is used on a polygonal obstacle, and a standard basis is used on the other obstacle(s).

(ii) *Tmatrom with Embedded HNA-BEM* (we call this *T-E-H* for short), in which a HNA basis is used to solve a small number of plane wave single scattering problems, which can then be converted to a multiple scattering solution using the Embedding Formulae and Tmatrom software.

A third approach would be to use the beam source method of §3.2 to construct an iterative multiple scattering formulation, similar to that discussed in (for example) [1]. We do not consider this here, although it is a key area for future research. We now summarise both methods (*H-S* and *T-E-H*) in detail, from a practical and theoretical point of view, in terms of what has been done in this thesis, and possible future work.

Hybrid-Standard BEM basis coupling (H-S)

In Chapter 4, the ansatz of the HNA method of Chapter 2 was extended to multiple obstacles (4.9), by combining the HNA space with a standard *hp*-BEM approximation space on the additional obstacle(s). As a consequence of this new ansatz, we require that a standard BEM approximation space must be used on the *other* obstacle(s). This is advantageous in that we do not require these to be polygonal, and there is minimal restriction (4.16) on the separation of the obstacles, but disadvantageous in that the size of the standard *hp* BEM basis here must grow like $O(k)$ to maintain accuracy. We observe exponential convergence of the method in the numerical experiments tested, which is predicted under Assumption 4.8 that the standard *hp* BEM basis converges exponentially.

From a practical point of view, we expect this method to be best suited to problems for which the scatterer(s) with the standard basis has a size parameter close to one wavelength, or generally speaking when there is a polygonal obstacle which is

much larger than all of the others. Given that the current a priori bounds depend on Assumption 4.8 and the unknown conditions for Lemma 4.9, the Galerkin HNA method offers no (theoretical) advantage over the (easier to implement) collocation approach (see Remark 2.12). In practical applications, oscillatory quadrature should be implemented to reduce the k-dependence of the computational cost of the inner products, another key area for future work.

From a theoretical point of view, a useful development would be to bound the stability constants for more general multiple obstacle configurations, including polygons. The work of Chapter 5 makes significant progress towards this, for cases where the obstacles are sufficiently smooth, or sufficiently far apart. Whilst there are cases (see Remark 4.11) for which we can provide fully explicit error bounds for the solution of the Galerkin method (4.22), this is not yet possible for the general problem considered in Chapter 4, and does not predict exponential convergence. Further work to prove that the standard hp-BEM basis converges exponentially would also be beneficial, we expect that this would involve the ideas developed in [41].

Tmatrom solved using Embedding formulae with HNA-BEM (T-E-H)

This method does not require an extension of the HNA ansatz, but is based on a reformulation of the BVP (1.4)–(1.6) which combines many single scattering problems. The T-matrix formulation of Chapter 7 may be combined with the Embedding Formulae of Chapter 6, using the plane wave HNA solver of [35] (this solver fits inside of the general framework of Chapter 2). As was shown in §7.3, this extension of the Tmatrom algorithm maintains numerical stability, whilst requiring an $O(1)$ number of solves. As with the previous method, a standard approximation space may be used on obstacles for which an HNA basis is not appropriate, but here we do not need to relate these obstacles via an operator such as $\mathcal{G}_{\gamma\to\Gamma_j}$. The main physical constraint is that the obstacles must be sufficiently far apart such that pairwise disjoint balls can be constructed around each of them.

The current version of the embedding code we have developed only works for quasi-regular polygons, the next extension should be to generalise this to rational polygons. Moreover, the cost of this algorithm may be reduced, as discussed at the end of §6.5. A software package incorporating the ideas of Chapter 6 would be a useful extension to the Tmatrom package. From a practical point of view, implementing this method requires the construction of a plane wave HNA solver, then combining this with the Embedding Formulae ideas of Chapter 6. As discussed earlier in this chapter, we propose that the easiest HNA solver to implement would use a single mesh

with collocation BEM. Our embedding software package requires identical inputs to the Tmatrom software, an object-oriented *solver* class, so may be used as an optional extra to Tmatrom.

From a theoretical point of view, if an HNA basis can be used on every scattering obstacle, and each obstacle is star-shaped, we can guarantee that the method will have a unique solution, given that Assumption 6.2 holds. This can be achieved by choosing the star-combined formulation and solving via the Galerkin method, such that the approximations to the canonical solutions for the Embedding Formulae exist and are unique. The bounds of [24] provide a range of theory which may be readily applied to obtain best approximation estimates, which may be combined with the solver error which follows Theorem 6.8. The key areas in which the theory may be improved depend on the embedding component of the method. This is unsurprising as almost no work has been published discussing its numerical implementation. For fully explicit error bounds in this method, we require bounds on the constant ϵ_b of Theorem 6.8, as these are still implicit and are closely related to the (currently open) question of Assumption 6.2(i).

Appendix A

Fundamental definitions and results

Here we define function spaces, trace spaces and key operators that may map between them. As in Chapter 1, Ω denotes a general open subset of $\mathbb{R}^2$ with boundary $\partial\Omega$, whilst Ω_+ denotes the exterior domain, and Ω_- denotes the bounded interior domain. All definitions are in two-dimensions, with trace spaces of Hausdorff dimension one.

A.1 Function spaces

DEFINITION A.1 (Spaces of continuous functions)**.** *First we define the two dimensional multi-index derivative*

$$\partial^\alpha := \frac{\partial}{\partial x_1^{\alpha_1}} \frac{\partial}{\partial x_2^{\alpha_2}},$$

for $\alpha \in \mathbb{N}_0^2$*. For open* $\Omega \subset \mathbb{R}^2$*, we define the following space of p-differentiable continuous function*

$$C^p(\Omega) := \{\varphi : \Omega \to \mathbb{C} : \quad \partial^\alpha \varphi \quad \text{is continuous, for } \alpha_1 + \alpha_2 \leq p\}.$$

Now we define the space of continuous functions.

DEFINITION A.2 (L^p spaces)**.** *The* L^p *norm is defined as*

$$\|\varphi\|_{L^p(\Omega)} := \begin{cases} \left(\int_\Omega |\varphi|^p\right)^{1/p}, & p \in (1, \infty), \\ \operatorname*{ess\,sup}_{\mathbf{x}\in\Omega} |\varphi(\mathbf{x})|, & p = \infty. \end{cases}$$

We define the space of p-integrable functions defined on Ω *to be*

$$L^p(\Omega) := \left\{\varphi : \|\varphi\|_{L^p(\Omega)} < \infty\right\},$$

and the space of locally integrable functions on Ω is

$$L^p_{\mathrm{loc}}(\Omega) := \{\varphi : \chi\varphi \in L^p(\Omega) \text{ for every compactly supported } \chi \in C^\infty(\Omega)\}, \tag{A.1}$$

(this definition only makes sense for unbounded Ω).

The space $L^2(\Omega)$ is an inner product space, with inner product

$$(\varphi, \psi)_{L^2(\Omega)} := \int_\Omega \varphi\overline{\psi},$$

which induces the norm $\|\varphi\|_{L^2(\Omega)} = (\varphi, \varphi)^{1/2}_{L^2(\Omega)}$. Sobolev spaces introduce a notion of differentiability to L^2 spaces. Our first definition of a Sobolev space requires the Fourier transform of any given function φ, which we define as

$$\hat{\varphi}(\xi) := \frac{1}{2\pi}\int_{\mathbb{R}^2} \mathrm{e}^{-\mathrm{i}\mathbf{x}\cdot\xi}\varphi(\mathbf{x})\,\mathrm{d}\mathbf{x}, \quad \xi \in \mathbb{R}^2. \tag{A.2}$$

The Bessel potential space $H^s(\mathbb{R}^2)$ has the inner product

$$(\varphi, \psi)_{H^s(\mathbb{R}^2)} := \int_{\mathbb{R}^2} \left(1 + |\xi|^2\right)^s \hat{\varphi}(\xi)\overline{\hat{\psi}}(\xi)\,\mathrm{d}V(\xi), \tag{A.3}$$

which induces the norm $\|\varphi\|_{H^s(\mathbb{R}^2)} := (\varphi, \varphi)^{1/2}_{H^s(\mathbb{R}^2)}$. Here $\mathrm{d}V$ denotes the standard volume measure; $\mathrm{d}V(\mathbf{x}) = \mathrm{d}x_1\,\mathrm{d}x_2$. It is straightforward to show that $\|\varphi\|_{L^2(\mathbb{R}^2)} = \|\hat{\varphi}\|_{L^2(\mathbb{R}^2)}$, hence by the definition (A.3) we have that $H^0(\mathbb{R}^2) = L^2(\mathbb{R}^2)$, for the special case $s = 0$. Moreover, for the case $s = 1$ it follows that

$$\|\varphi\|_{H^1(\mathbb{R}^2)} = \left(\int_{\mathbb{R}^2} |\varphi|^2 + |\nabla\varphi|^2\,\mathrm{d}V\right)^{1/2},$$

by transferring derivatives to ξ using the Fourier transform (A.2). We will mostly be interested in Sobolev spaces on the boundary $\partial\Omega$, which requires the concept of a *Lipschitz hypograph*. For Lipschitz open Ω, by the definition of a Lipschitz open set (see for example [13, Definition A.2]) there exists $g : \mathbb{R} \to \mathbb{R}$ in $C^{0,1}(\mathbb{R})$ (the set of Lipschitz continuous functions) such that $\Omega = \{\mathbf{x} := (x_1, x_2) \in \mathbb{R}^2 : x_1 \in \mathbb{R}, x_2 > g(x_1)\}$. The boundary of Ω can thus be defined as $\partial\Omega := \{(x_1, g(x_1)) : x_1 \in \mathbb{R}\}$. This concept enables us to extend our definitions of L^p integrable spaces and Sobolev spaces to the boundary $\partial\Omega$, via the surface measure $\mathrm{d}s$, which we define as

$$\int_{\partial\Omega} \varphi\,\mathrm{d}s := \int_{\mathbb{R}} \varphi\big((x_1, g(x_1))\big)\sqrt{1 + |\nabla g(x_1)|^2}\,\mathrm{d}x_1.$$

We now define the L^p norm on the boundary $\partial\Omega$ as

$$\|\varphi\|_{L^p(\partial\Omega)} := \begin{cases} \left(\int_{\partial\Omega} |\varphi|^p\right)^{1/p} \mathrm{d}s, & p \in (0,\infty), \\ \operatorname*{ess\,sup}_{\mathbf{x}\in\partial\Omega} |\varphi(\mathbf{x})|, & p = \infty, \end{cases}$$

from which the space $L^p(\partial\Omega)$ follows in the same way as (A.1). Likewise, we may also define the boundary Sobolev norm by

$$\|\varphi\|_{H^s(\partial\Omega)} := \left\| \varphi\Big(\big(\cdot, g(\cdot)\big)\Big) \right\|_{H^s(\mathbb{R})}, \quad s \in \mathbb{R}$$

from which the boundary Sobolev space $H^s(\partial\Omega)$ follows in the natural way.

Some of the results in this thesis make use of the k-weighted space $H^1_k(\mathbb{R}^2)$, with norm

$$\|\varphi\|_{H^1_k(\partial\Omega)} := \left(\int_{\partial\Omega} k^2|\varphi|^2 + |\nabla_\gamma \varphi|^2 \,\mathrm{d}V \right)^{1/2}, \tag{A.4}$$

for $k > 0$. The k-weighted norm on $\partial\Omega$ analogous to A.4 follows in the same way, with Ω replaced by $\partial\Omega$, using the surface measure $\mathrm{d}s$. A more general definition can be found in [6, §2], whilst physical justification for the $H^1_k(\Omega)$ norm can be found in [43, Remark 3.8].

A.2 Trace operators

A further modification to the our standard Sobolev space, required for definition the Neumann trace (A.6), is the following:

$$\begin{aligned} H^s(\Omega;\Delta) := \big\{ \varphi \in H^s(\Omega) :\ & \text{there exists a } w \in L^2(\Omega) \\ & \text{such that } \int_\Omega wv \,\mathrm{d}V = \int_\Omega \varphi \Delta v \text{ for all } v \in C^\infty(\Omega) \big\}, \quad \text{for } s < 2. \end{aligned}$$

A non-tangential approach set $\Theta_\pm$ is required to define trace operators, a precise definition can be found in [13, A.4]. For almost every $\mathbf{x} \in \partial D$, the Dirichlet traces $\tau_\pm : H^s(\Omega_\pm) \to H^{s-1/2}(\partial\Omega)$ for $s \in (1/2, 3/2)$ are defined by

$$\tau_\pm \varphi(\mathbf{x}) := \lim_{\mathbf{y}\to\mathbf{x}, \mathbf{y}\in\Theta_\pm(\mathbf{x})} u(\mathbf{y}), \tag{A.5}$$

whilst the Neumann traces $\partial^\pm_{\mathbf{n}} : H^1(\Omega_\pm;\Delta) \to H^{-1/2}(\partial\Omega)$ are defined by

$$\partial^\pm_{\mathbf{n}} \varphi(\mathbf{x}) = \pm \frac{\partial u}{\partial \mathbf{n}}(\mathbf{x}) := \lim_{\mathbf{y}\to\mathbf{x}, \mathbf{y}\in\Theta_\pm(\mathbf{x})} \mathbf{n}(\mathbf{x}) \cdot \nabla\varphi(\mathbf{y}). \tag{A.6}$$

For a more detailed discussion of these operators, we refer to [13, p112 and §A.3-§A.5]

A.3 Bounds on the Hankel functions

Here we collect bounds on the Hankel functions which are used throughout this thesis. The first, from [12, 1.22] is

$$|H_0^{(1)}(z)| \leq \sqrt{\frac{2}{\pi z}}, \quad \text{for } z > 0, \tag{A.7}$$

whilst the second from [12, 1.23] is

$$|H_1^{(1)}(z)| \leq \sqrt{\frac{2}{\pi z}} + \frac{2}{\pi z}, \quad \text{for } z > 0. \tag{A.8}$$

The third bound, on $|H_1^{(1)'}(z)|$, requires a little work. Starting with the representation [12, 1.21],

$$H_1^{(1)}(z) = \frac{2\mathrm{i}}{\pi}\mathrm{e}^{\mathrm{i}z}\int_0^\infty \frac{(\mathrm{i}-r)\mathrm{e}^{-rz}}{r^{1/2}(r-2\mathrm{i})^{1/2}}\,\mathrm{d}r, \quad \text{for } z > 0,$$

differentiating with respect to z,

$$\begin{aligned} H_1^{(1)'}(z) &= -\frac{2}{\pi}\mathrm{e}^{\mathrm{i}z}\int_0^\infty \frac{(\mathrm{i}-r)\mathrm{e}^{-rz}}{r^{1/2}(r-2\mathrm{i})^{1/2}}\,\mathrm{d}r - \frac{2\mathrm{i}}{\pi}\mathrm{e}^{\mathrm{i}z}\int_0^\infty \frac{r^{1/2}(\mathrm{i}-r)\mathrm{e}^{-rz}}{(r-2\mathrm{i})^{1/2}}\,\mathrm{d}r, \quad \text{for } z > 0, \\ &= \mathrm{i}H_1^{(1)}(z) - \frac{2\mathrm{i}}{\pi}\mathrm{e}^{\mathrm{i}z}\int_0^\infty \frac{r^{1/2}(\mathrm{i}-r)\mathrm{e}^{-rz}}{(r-2\mathrm{i})^{1/2}}\,\mathrm{d}r, \quad \text{for } z > 0, \end{aligned}$$

bounding using (A.8) for the first term, whilst noting that $|(\mathrm{i}-r)/(r-2\mathrm{i})^{1/2}| \leq (1+r)/r^{1/2}$ for $r > 0$,

$$\begin{aligned} |H_1^{(1)'}(z)| &\leq \sqrt{\frac{2}{\pi z}} + \frac{2}{\pi z} + \frac{2}{\pi}\int_0^\infty (1+r)\mathrm{e}^{-rz}\,\mathrm{d}r, \\ &\leq \sqrt{\frac{2}{\pi z}} + \frac{4}{\pi z} + \frac{2}{\pi z^2}, \quad \text{for } z > 0. \end{aligned} \tag{A.9}$$

Finally, we will make use of the following bound for small argument, which was first derived in [35, Proof of Lemma 4.1] using [18, (10.2.2), (10.8.2) and (10.17.5)]:

$$|H_0^{(1)}(z)| \leq \hat{c}(1 + |\log z|) \quad , \text{ for } 0 < z \leq 1, \tag{A.10}$$

where $\hat{c} = (1 + 2/\pi(1 + \gamma_E + \mathrm{e}^{1/4}))$.

A.4 Regularity of fundamental solution

Here we justify the statement made in (3.12), that is

$$\Phi(\cdot, \mathbf{s}) \in H^{1-\epsilon}_{\mathrm{loc}}(\mathbb{R}^2), \quad \text{for all } \epsilon > 0, \quad \mathbf{s} \in \mathbb{R}^2,$$

as we have been unable to find a derivation of this in the literature.

A quick explanation can be obtained from [13, Theorem 2.15]; from which it follows that

$$S_k : H^{s-1/2}_{\mathrm{loc}}(\partial\Omega) \to H^{s+1}(\mathbb{R}^2), \quad \text{for } s \in [-1/2, 1/2],$$

where $\partial\Omega$ is some Lipschitz boundary containing a point $\mathbf{s}$. Considering $\delta_{\mathbf{s}} \in H^{-1/2-\epsilon}_{\mathrm{loc}}(\partial\Omega)$ for all $\epsilon > 0$, it then follows from Definition 1.10 of S_k that for $\mathbf{s} \in \partial\Omega$,

$$S_k\delta_{\mathbf{s}} = \Phi(\cdot, \mathbf{s}) \in H^{1-\epsilon}(\mathbb{R}^2), \quad \text{for } \epsilon > 0,$$

and the choice of $\partial\Omega$ is arbitrary, so can be chosen to contain any $\mathbf{s}$. As an alternative justification, we may derive the same result from first principles, making use of the following Lemma.

LEMMA A.3. *If*

$$(\Delta - 1)v = f \quad \textit{in } \mathbb{R}^2, \quad \textit{for } f \in H^s(\mathbb{R}^2), \quad s \in \mathbb{R}, \tag{A.11}$$

then

$$\|v\|_{H^{s+2}(\mathbb{R}^2)} = \|f\|_{H^s(\mathbb{R}^2)}.$$

Proof. Taking Fourier Transforms (A.2) of both sides we obtain

$$\hat{v}(\xi) = \frac{\hat{f}(\xi)}{1 + |\xi|^2}, \quad \text{for } \xi \in \mathbb{R}^2,$$

and by the definition of the fractional Sobolev norm in §A.1 it follows that

$$\|v\|_{H^{s+2}(\mathbb{R}^2)} = \int_{\mathbb{R}^2} (1 + |\xi|^2)^{s+2} \frac{|\hat{f}(s)|^2}{(1 + |\xi|^2)^2} \, \mathrm{d}V(\xi) = \|f\|_{H^s(\mathbb{R}^2)}.$$

□

We may bound $\Phi(\cdot, \mathbf{s})$ for small argument using (A.10), hence it follows that $\Phi(\cdot, \mathbf{s}) \in L^2_{\mathrm{loc}}(\mathbb{R}^2)$, and

$$\nabla\Phi(\cdot, \mathbf{s}) \in H^{-1}_{\mathrm{loc}}(\mathbb{R}^2), \quad \mathbf{s} \in \mathbb{R}^2. \tag{A.12}$$

We denote by χ some compactly supported function in $C^\infty(\mathbb{R}^2)$. Expanding the left-hand side of (A.11) by the product rule yields

$$(\Delta - 1)[\chi v] = v\Delta\chi + 2\nabla\chi \cdot \nabla v + \chi(\Delta - 1)v \tag{A.13}$$

$$= v\Delta\chi + 2\nabla\chi \cdot \nabla v + \chi(\Delta + k^2 - 1 - k^2)v. \tag{A.14}$$

Now choosing $v = \Phi(\cdot, \mathbf{s})$ we may write

$$(\Delta - 1)\left[\chi\Phi(\,\cdot, \mathbf{s})\right] = \Phi(\cdot, \mathbf{s})\Delta\chi + 2\nabla\chi \cdot \nabla\Phi(\cdot, \mathbf{s}) + \chi\delta_{\mathbf{s}} - (1 + k^2)\Phi(\cdot, \mathbf{s}).$$

We may now consider the regularity of each term on the right-hand side. It is known that $\delta_{\mathbf{s}} \in H^{-1-\epsilon}(\mathbb{R}^2)$ for all $\epsilon > 0$, and given (A.12) we can deduce that the right-hand side is in $H^{-1-\epsilon}(\mathbb{R}^2)$, for all $\epsilon > 0$. Hence, by Lemma A.3 it follows that $\chi\Phi(\cdot, \mathbf{s}) \in H^{-1-\epsilon+2}(\mathbb{R}^2)$, and $\Phi(\cdot, \mathbf{s}) \in H^{1-\epsilon}_{\text{loc}}(\mathbb{R}^2)$ for all $\epsilon > 0$, as claimed.

Appendix B

Some notes on quadrature

The subject of quadrature is not discussed in detail in the main body of the thesis. It is an integral component of the boundary element method, so we devote some time to it here, although this is not a complete account. Whilst many of the results in this appendix can be found elsewhere (possibly with the exception of the phenomenon discussed in Remark B.6 and B.7, which we have not seen in other literature), it may be useful to have all such results written in one place.

Many of the inner products that occur when implementing the boundary element method are singular and/or oscillatory, and efficient computation of such integrals is a significant area of research in its own right. When dealing with trace spaces on polygonal shapes, these singularities may be decoupled into products of one dimensional integrals, which enables us to use *Generalised Gaussian Quadrature*, requiring no grading, with far less quadrature points than with a standard routine.

B.1 One dimensional quadrature routines

Firstly, we list the the quadrature routines that we use for integrating a one-dimensional integral,

$$\int_a^b \varphi \approx \sum_{i=1}^{N_Q} \varphi(s_i) w_i, \tag{B.1}$$

with weights $(w_i)_{i=1}^{N_Q}$ and nodes $(s_i)_{i=1}^{N_Q}$ in $[a, b]$.

DEFINITION B.1 (Classical Gaussian Quadrature)**.** *Let P_i denote the ith Legendre Polynomial (see [18, 14.5(ii), 14.10]). To approximate the integral* (B.1) *over $[-1, 1]$ with $N_Q \geq 1$ quadrature points, we choose nodes $Q_C(-1, 1; N_Q) = (s_i)_{i=1}^{N_Q}$ defined by*

$$s_i \in [0, 1] : P_{N_Q}(s_i) = 0,$$

sorted in ascending order of value and indexed by i, with weights $W_C(-1,1;N_Q) = (w_i)_{i=1}^{N_Q}$

$$w_i := \frac{2}{(1-s_i^2)(L'_{N_Q}(s_i))^2}, \quad \textit{for } i = 1,\dots,N_Q.$$

This may be mapped to any $[a,b] \subset \mathbb{R}$*, defining* $Q_C(a,b;N_Q)$ *as the nodes*

$$s'_i := a + (s_i+1)(b-a)/2, \quad \textit{for } i = 1,\dots,N_Q$$

and weights $W_C(a,b;N_Q)$ *given by*

$$w'_i = (w_i+1)(b-a)/2,$$

where s_i *and* w_i *are the nodes and weights of* $Q_C(-1,1)$ *and* $W_C(-1,1;N_Q)$ *respectively.*

The fundamental theorem of Gaussian quadrature states that if the integrand φ of (B.1) is a polynomial of degree $2N_Q-1$ or less, and Gaussian weights $W_C(a,b;N_Q)$ and nodes $Q_C(a,b;N_Q)$ are used, then the approximation (B.1) is exact (see for example [48, §4.2]). It follows that Gaussian quadrature is ideal for approximating the integrals of smooth functions, which can be well approximated by a low degree polynomial.

For singular functions, we use the following alternative approach, which splits the interval into geometrically graded subintervals of increasingly small width close to the singularity.

DEFINITION B.2 (Layered Gaussian Quadrature)**.** *We split the interval* $[a,b]$ *into* $n \in \mathbb{N}$ *layered subintervals, using the grading parameter* $\sigma \in (0,1)$*, such that the endpoints of the subintervals are given by*

$$t_0 = a, \quad t_j = a + (b-a)\sigma^{n-j}, \quad \textit{for } j = 1,\dots,n,$$

noting that by this definition we have that $t_{n+1} = b$*. The layered quadrature nodes* $Q_G(t_j,t_{j+1};N_Q,\sigma,n)$ *are then defined as*

$$(s_i)_{i=N_Q j+1}^{(N_Q+1)j}, \quad \textit{given by } Q_L(t_j,t_{j+1};N_Q), \quad \textit{for } j = 0,\dots,n-1,$$

likewise, the weights are $W_G(t_j,t_{j+1};N_Q,\sigma,n)$

$$(w_i)_{i=N_Q j+1}^{(N_Q+1)j}, \quad \textit{for } i = 1,\dots,N_Q \quad \textit{as in } W_L(t_j,t_{j+1};N_Q), \quad \textit{for } j = 0,\dots,n-1.$$

Layered quadrature is a useful multi-purpose tool for singular integrals. When information about the singularity is known, alternative quadrature routines may be used which significantly reduce the number of weights and nodes required. As we shall see shortly (in B.2), we will need to integrate functions with a logarithmic singularity.

DEFINITION B.3 (Generalised Gaussian Quadrature for logarithmic singularities)**.** *For our generalised Gaussian quadrature rule (see e.g. [37]), the N_Q weights $W_G(0,1)$ and nodes $Q_G(0,1)$, are chosen to satisfy the non-linear system of $2N_Q$ equations generated by*

$$\sum_{i=1}^{N_Q} \varphi(s_i) w_i = \int_0^1 \varphi, \quad \forall \varphi \in T_m, \tag{B.2}$$

$$T_m := \begin{cases} \{x^\rho, x^\rho \log(x), \text{ for } \rho = 0, \ldots, N_Q - 1, x^{N_Q}\}, & m = 2N_Q \text{ is even} \\ \{x^\rho, x^\rho \log(x), \text{ for } \rho = 0, \ldots, N_Q\}, & m = 2N_Q + 1 \text{ is odd} \end{cases}$$

This definition is easily extended to $Q_G(0, b; N_Q)$ and $W_G(0, 1; N_Q)$, by multiplying the weights and nodes of (B.2) *by b.*

REMARK B.4. *Such weights and nodes are typically generated iteratively (see e.g. [37]), for example using a $2N_Q$-dimensional Newton iteration, seeking to minimise the error in* (B.2)*, choosing the composition of classical nodes $Q_C(0, 1; N_Q)$ and weights $W_C(0, 1; N_Q)$ as a starting point in $[0, 1]^{2N_Q}$. This need not reduce the efficiency of our numerical method; once the weights and nodes have been generated for a given N_Q, they may be stored and reused.*

Definition B.3 ensures that a linear combination of polynomials and products of logarithms with polynomials up to order N_Q can be integrated exactly, given $2N_Q$ quadrature points. The non-linear system (B.2) is shown to be uniquely solvable in [37]. When comparing the basis T_m with the Fundamental Theorem of Gaussian quadrature, it is worth noting that the polynomials which can be integrated exactly by Generalised Gauss are around half the order which can be integrated exactly using Classical Gauss. Hence, for consistency we typically choose the number of quadrature points N_Q to be twice as large for Generalised Gauss than Classical Gauss. We note that this is still a significant improvement on the accuracy of Layered Gaussian Quadrature if the same the number of points were used.

A nearly logarithmic singular integral is an integral of the following form:

$$\int_0^1 \varphi(x) \log(x + \delta) \, \mathrm{d}x, \tag{B.3}$$

where $\delta > 0$ is *small* (clarity will follow shortly, via (B.5) and Figure B.1). Classical Gaussian Quadrature works well for sufficiently smooth functions, so a sensible starting point is to test exactly how *near* the singularity must be (i.e. how small δ must

be) before the classical approach breaks down, by considering

$$\mathcal{E}(\delta, N_Q) := \left| \int_0^1 \varphi(x) \log(x+\delta)\, \mathrm{d}x - \sum_{i=1}^{N_Q} \varphi(s_i) w_i \right|, \tag{B.4}$$

where the weights $(w_i)_{i=1}^{N_Q}$ and nodes $(s_i)_{i=1}^{N_Q}$ are generated using $W_{\mathrm{C}}(0,1;N_Q)$ and $Q_{\mathrm{C}}(0,1;N_Q)$ respectively. The results of this test are visualised in figure B.1. Using this as a guide, given N_Q, one should aim to choose a threshold

$$\delta_*(N_Q) = \inf\{\delta > 0 : \mathcal{E}(\delta, N_Q) \leq \text{ desired precision}\}, \tag{B.5}$$

such that for $\delta < \delta_*$ Layered Gaussian Quadrature is used, and for $\delta \geq \delta_*$ Classical Gaussian Quadrature is used.

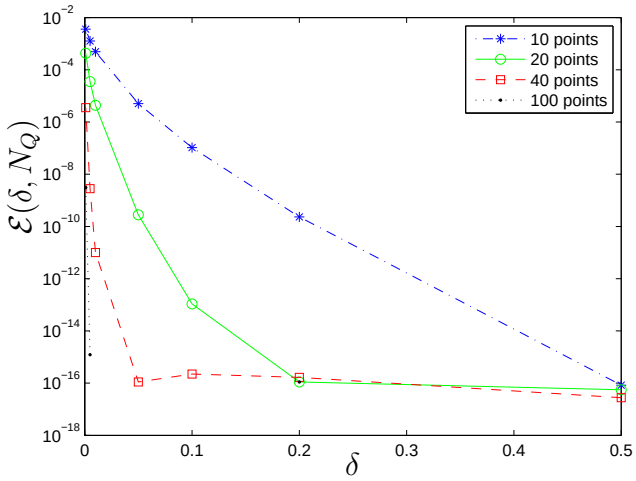

Figure B.1: Testing the error (measured as the absolute difference between the integral and its approximation) when using classical Gaussian quadrature to compute (B.3) with $\varphi \equiv 1$ for a range of δ for varying numbers of quadrature points (N_Q).

REMARK B.5. *Whilst it is possible to generate a set of Generalised Gaussian weights and nodes to compute integrals of the form of* (B.3) *exactly (using a technique similar to that discussed in Remark B.4), a new set of weights and nodes must be computed for each value of δ, so this is very impractical to do during on-the-fly computation. For a given N_Q, a third approach*[1]*, which we have not implemented, might be to generate weights and nodes for $\delta_j \in (0, \delta^*)$, for $j = 1, \ldots, N_Q{}'$. The ith weight and node may be interpolated using Chebyshev polynomials, taking δ as a variable. The Chebyshev coefficients may then be stored, and (for this choice of N_Q)*

[1] As suggested by Daan Huybrechs of KC Leuven.

weights and nodes can be produced for any given δ. Naturally, the larger the choice of N_Q, the larger the number of interpolation points will be, and the more accurate the resulting quadrature routines will be.

B.2 Computing inner products

Here we outline the procedure to compute a typical entry of the stiffness matrix of a standard Galerkin BEM for two basis functions ϕ_n and ϕ_m, supported on $\operatorname{supp}\phi_n$ and $\operatorname{supp}\phi_m$ respectively. Other inner products that occur in standard and HNA methods are discussed in §B.2.4. Here we assume that both basis functions are polynomial over their support, and that their support is less than one wavelength long. With a (non-standard) HNA basis such as those discussed in 2.2, there will typically be elements which are many wavelengths long, methods for such a case are discussed in §B.3. Everything we write here assumes the choice $\mathcal{A} = \mathcal{A}_{k,\eta}$, although a similar approach would be required for the constellation combined operator.

A typical BEM inner product will take the form

$$(\mathcal{K}\phi_n, \phi_m)_{L^2(\partial\Omega)} = \int_{\operatorname{supp}\phi_n} \int_{\operatorname{supp}\phi_m} K(\mathbf{x},\mathbf{y})\phi_n(\mathbf{x})\phi_m(\mathbf{y})\,\mathrm{d}s(\mathbf{x})\,\mathrm{d}s(\mathbf{y}), \tag{B.6}$$

where ϕ_n and ϕ_m are basis functions of the approximation space, $\mathcal{K} := \mathcal{A}_{k,\eta} - \mathcal{I}$,

$$K(\mathbf{x},\mathbf{y}) := 2\left(\frac{\partial\Phi(\mathbf{x},\mathbf{y})}{\partial\mathbf{n}(\mathbf{x})} - \mathrm{i}\eta\Phi(\mathbf{x},\mathbf{y})\right), \quad (\mathbf{x},\mathbf{y}) \in [c,d]\times[a,b],$$

which by the definition (1.7) of the fundamental solution, we can write the kernel in full

$$K(\mathbf{x},\mathbf{y}) = -\frac{\mathrm{i}k\mathbf{n}(\mathbf{x})\cdot(\mathbf{x}-\mathbf{y})}{2|\mathbf{x}-\mathbf{y}|}H_1^{(1)}(k|\mathbf{x}-\mathbf{y}|) + \frac{\eta}{2}H_0^{(1)}(k|\mathbf{x}-\mathbf{y}|). \tag{B.7}$$

The integrals that require the most care will be those for which K is singular. We note that the second term on the right-hand side of (B.7) only exists when $\mathbf{x}$ and $\mathbf{y}$ are on different sides of Γ, and is smooth as $|\mathbf{x}-\mathbf{y}| \to 0$, despite $|H_1^{(1)}(z)| \sim 2/|\pi z|$ (from [18, 10.7.3]). To see why, we assume that $\mathbf{x}$ and $\mathbf{y}$ are on neighbouring sides (otherwise the argument of $H_1^{(1)}$ cannot approach zero), and let $\mathbf{P}_j$ denote the vertex between these two sides. It follows that $\mathbf{n}(\mathbf{x})\cdot(\mathbf{x}-\mathbf{y})/|\mathbf{x}-\mathbf{y}| \sim |\mathbf{P}_j - \mathbf{y}|$ as $\mathbf{P}_j \to \mathbf{y}$, balancing the singular behaviour of the Hankel function. Hence, it follows by [18, 10.7.3] that

$$K(\mathbf{x},\mathbf{y}) \sim \frac{2\eta}{\pi}\log(k|\mathbf{x}-\mathbf{y}|), \quad |\mathbf{x}-\mathbf{y}| \to 0. \tag{B.8}$$

We parametrise $\mathbf{x}(s)$ and $\mathbf{y}(t)$ as in (2.1), with s and t in $[0, L_\Gamma]$, hence we can rewrite (B.6) as

$$(\mathcal{K}\phi_n, \phi_m)_{L^2(\partial\Omega)} = \int_a^b \int_c^d \tilde{K}(s,t)\tilde{\phi}_n(s)\tilde{\phi}_m(t)\,\mathrm{d}s\,\mathrm{d}t. \tag{B.9}$$

where

$$\mathbf{x}([c,d]) = \operatorname{supp}\phi_n, \quad \mathbf{y}([a,b]) = \operatorname{supp}\phi_m, \quad \tilde{K}(s,t) := K(\mathbf{x}(s), \mathbf{y}(t)),$$
$$\tilde{\phi}_n(s) := \phi_n(\mathbf{x}(s)), \quad \tilde{\phi}_n(t) := \phi_m(\mathbf{x}(t)).$$

We want to separate explicitly the singular components of (B.9), hence we can write

$$(\mathcal{K}\phi_n, \phi_m)_{L^2(\partial\Omega)} = \int_a^b \int_c^d \log(kr(s,t))v(s,t)\,\mathrm{d}s\,\mathrm{d}t, \tag{B.10}$$

where r is chosen such that $r(s,t) = |\mathbf{x}(s) - \mathbf{y}(t)|$, and $v(s,t) := \tilde{\phi}_n(s)\tilde{\phi}_m(t)\tilde{K}(s,t)/\log(kr(s,t))$ is smooth, given (B.8). The type of singularities that occur can be split into four distinct types:

(i) $[a,b] = [c,d]$, diagonal singularity

(ii) $b = c$, (or) $a = d$, point singularity

(iii) $b \lessapprox c$, (or) $a \gtrapprox d$, near singularity

(iv) No singularity

Case (i)-(iii) can be made simpler by splitting the square into two triangles along the hypotenuse, and using the *Duffy Transformation* (e.g. [44]) to transform these domains into two squares, which yields the following identity:

$$\int_a^b \int_c^d g(x,y)\,\mathrm{d}x\,\mathrm{d}y = (b-a)(d-c)\int_0^1 \int_0^1 G(\xi, \xi\tau)x\,\mathrm{d}\xi\,\mathrm{d}\tau, \tag{B.11}$$

where

$$G(x,y) := g(c + (d-c)x, a + (b-a)y) + g(c + (d-c)y, a + (b-a)x). \tag{B.12}$$

If the integration domain $[a,b]\times[c,d]$ is considered as a rectangle, this moves singular behaviour from the diagonal (case (i)) or corner (case (ii) and (iii)) to the edge(s) of a square, enabling us to treat the singularity more effectively (see Figure B.2). We now explain the approach to do this in the cases (i)-(iii).

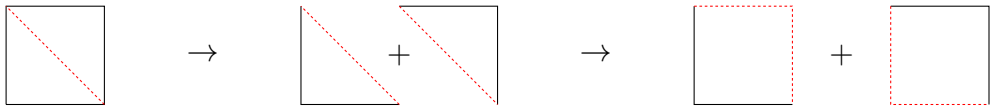

Figure B.2: Representation of the Duffy transform, mapping a function defined on a square domain with a diagonal singularity (represented by a dashed line) to two squares, each with a singularity at two edges. Such a transform makes grading towards the singularity more straightforward when implementing quadrature. A similar approach works for corner/point singularities, although this results in two squares each with one singular edge.

B.2.1 Diagonal singularity

We are in the setting $[c, d] = [a, b]$, hence we consider

$$(\mathcal{K}\phi_n, \phi_m)_{L^2(\partial\Omega)} = \int_a^b \int_a^b \log(kr(s,t))v(s,t)\,\mathrm{d}s\,\mathrm{d}t, \tag{B.13}$$

with $r(s,t) = |s-t|$ (this follows by the parametrisation of $\mathbf{x}$ and $\mathbf{y}$). Choosing g of (B.11) to be $\log(kr(s,t))v(s,t)$, we obtain

$$\begin{aligned} G(\xi,\xi\tau) &= \log(k(b-a)|\xi(1-\tau)|)V(\xi,\xi\tau) - \log(k((b-a)|\xi(\tau-1)|))V(\xi\tau,\xi) \\ &= \log(k(b-a)|\xi(1-\tau)|)\left(V(\xi,\xi\tau) - V(\xi\tau,\xi)\right) \\ &= \left(\log(k(b-a)) + \log(\xi) + \log(1-\tau)\right)\left(V(\xi,\xi\tau) - V(\xi\tau,\xi)\right), \end{aligned} \tag{B.14}$$

where $V(s,t) = v(c+(d-c)s, a+(b-a)t)$ is a combination of sums, compositions and products of smooth functions, and is therefore smooth. Hence we can decouple the singularities of the inner product to obtain the representation

$$\begin{aligned} (\mathcal{K}\phi_n, \phi_m)_{L^2(\partial\Omega)} = &\log(k(b-a)) \int_a^b \int_a^b \left(V(\xi,\xi\tau) - V(\xi\tau,\xi)\right)\xi\,\mathrm{d}\xi\,\mathrm{d}\tau \\ &+ \int_0^1 \log(1-\tau) \int_a^b \left(V(\xi,\xi\tau) - V(\xi\tau,\xi)\right)\xi\,\mathrm{d}\xi\,\mathrm{d}\tau \\ &+ \int_0^1 \log(\xi)\xi \int_a^b \left(V(\xi,\xi\tau) - V(\xi\tau,\xi)\right)\mathrm{d}\tau\,\mathrm{d}\xi \end{aligned}$$

The approach taken in our routine is to approximate the integral using Generalised Gaussian Quadrature of Definition B.3, grading towards zero in the ξ direction and towards one in the τ direction (by subtracting the nodes in the definition from 1). It follows that the logarithmic singularities are handled by this routine, and no grading is necessary.

B.2.2 Point singularity

We now consider (assuming WLOG $a < c$)

$$(\mathcal{K}\phi_n, \phi_m)_{L^2(\partial\Omega)} = \int_a^b \int_b^c \log(kr(s,t))v(s,t)\,\mathrm{d}s\,\mathrm{d}t \tag{B.15}$$

and a slightly different approach is required here. We adjust our integration variables so they are in terms of the distance from b, and choose g of (B.11) to be $g(s,t) = \log(kr(s,t))v(s,t)$, yielding

$$\begin{aligned}&(\mathcal{K}\phi_n, \phi_m)_{L^2(\partial\Omega)}\\ =&(b-a)(c-b)\int_0^1\int_0^1 \left[\log(kR(\xi,\xi\tau))V(\xi,\xi\tau) + \log(kR(\xi\tau,\xi))V(\xi\tau,\xi)\right]\xi\,\mathrm{d}\xi\,\mathrm{d}\tau.\end{aligned} \tag{B.16}$$

where $V(s,t) = v(b+s(c-b), b-t(b-a))$, and we use two alternate definitions for R (which is related to the function r), the second of which is only applicable when the two basis functions are supported on neighbouring sides, touching at a corner of Ω_-,

$$R(s,t) := \begin{cases} s(c-b) + t(b-a), & \text{same side,} \\ \left(s^2(c-b)^2 + t^2(b-a)^2 - 2st(c-b)(b-a)\cos(\theta)\right)^{1/2}, & \text{neighbouring sides,}\end{cases}$$

where θ denotes the internal angle at the corner between the neighbouring sides. Henceforth assume that we are in the *same side* case, the case of *neighbouring sides* follows similarly. Focusing on the first singular term of (B.16), we observe

$$\begin{aligned}\log(kR(\xi,\xi\tau)) &= \log(k(\xi(c-b) + \tau\xi(b-a)))\\ &= \log k + \log\xi + \log((c-b) + \tau(b-a)).\end{aligned} \tag{B.17}$$

Using the representation (B.17),

$$\begin{aligned}(\mathcal{K}\phi_n, \phi_m)_{L^2(\partial\Omega)} =& \log k \int_0^1\int_0^1 V(\xi,\xi\tau)\xi\,\mathrm{d}\xi\,\mathrm{d}\tau + \int_0^1 \xi\log\xi\int_0^1 V(\xi,\xi\tau)\,\mathrm{d}\tau\,\mathrm{d}\xi\\ &+ \int_0^1 \log((c-b)+\tau(b-a))\int_0^1 V(\xi,\xi\tau)\xi\,\mathrm{d}\xi\,\mathrm{d}\tau.\end{aligned}$$

This breakdown of the integral shows that the integrand is only singular as $\xi \to 0$, but the singularity does not depend on τ (assuming that $(b-a)$ and $(c-b)$ are similar in length, the case when they are not is discussed below in Remark B.6). Similar arguments apply to the second singular term of (B.13). Hence, we approximate the integral using Generalised Gaussian quadrature for $\xi \in (0,1)$ and Classical Gaussian quadrature for $\tau \in (0,1)$. The Generalised Gauss will handle the logarithmic singularity, and as $V(\xi,\xi\tau)\xi$ and $V(\xi\tau,\xi)\xi$ consist of sums, products and compositions of smooth functions, both are therefore smooth.

REMARK B.6. *For a sufficiently elongated (long and thin) domain, the approach we present here breaks down. Such integrals occur frequently in Galerkin BEMs with an approximation space on a graded mesh, when basis functions supported on large elements are integrated against basis functions on small elements. To see why, we must consider the final term in the integral of* (B.17)*, which may be rewritten as*

$$\log((c-b)+\tau(b-a)) = \log(b-a) + \log\left(\frac{c-b}{b-a}+\tau\right),$$

hence if $(b-a) \gg c-b$*, the integrand has a near singularity (in the sense of Definition B.3) with* $\delta = (c-b)/(b-a)$*. Similar arguments to* (B.17) *follow for the second singular term of* (B.13)*, yielding near singularities with* $\delta = (b-a)/(c-b)$*. We choose the same parameter* δ_* *as in* (B.5)*, and treat these near singularities in the same way, with layered Gaussian quadrature.*

B.2.3 Near point singularity

These integrals may be considered to be of the form

$$(\mathcal{K}\phi_n, \phi_m)_{L^2(\partial\Omega)} = \int_a^{b_-}\int_{b_+}^{c} K(\mathbf{x},\mathbf{y})\phi_n(\mathbf{x})\phi_m(\mathbf{y})\,\mathrm{d}s(\mathbf{x})\,\mathrm{d}s(\mathbf{y}), \tag{B.18}$$

for $a < b_- < b_+ < c$, with b_- near to b_+. If ϕ_n and ϕ_m are supported on different sides of Γ, we define $b \in (b_-, b_+)$ such that $\mathbf{x}_\Gamma(b) = \mathbf{P}_j$ (using the parametrisation (2.1)) is the corner between the two sides. Reformulating the integral as in §B.2.2, we may write

$$(\mathcal{K}\phi_n, \phi_m)_{L^2(\partial\Omega)} = (b-a)(c-b)\int_0^1\int_0^1 [\log(kR(\xi,\xi\tau))V(\xi,\xi\tau) + \log(kR(\xi\tau,\xi))V(\xi\tau,\xi)]\,\xi\,\mathrm{d}\xi\,\mathrm{d}\tau. \tag{B.19}$$

where $V(s,t) = v(b_+ - s(c-b_+), b_- + t(b_- - a))$, whilst *either*

$$R(s,t) = s(c-b_+) + t(b_- - a) + (b_+ - b_-),$$

if ϕ_n and ϕ_m are supported on the same side of Γ, *or*

$$\begin{aligned} R(s,t) := & \\ & \big((s(c-b_+)+b_+-b)^2 + (t(b_- - a)+b-b_-)^2 \\ & - 2(s(c-b_+)+b_+-b)(t(b_- - a)+b-b_-)\cos(\theta)\big)^{1/2}, \end{aligned}$$

if ϕ_n and ϕ_m are supported on neighbouring sides of Γ, where θ is the internal angle at $\mathbf{P}_j$.

Due to two-dimensional analogue of reasons discussed in Remark B.5, we used Layered Gaussian Quadrature (of Definition B.2) in ξ and τ.

REMARK B.7. *In the case of near singularities, an (unstable) approach is to integrate fully up the singularity, and subtract off the difference, i.e.*

$$\begin{aligned}\int_0^1 \log(x+\delta)\varphi(x)\,\mathrm{d}x &= \int_\delta^{1+\delta} \log(x)\varphi(x-\delta)\,\mathrm{d}x \\ &= \int_0^{1+\delta} \log(x)\varphi(x-\delta)\,\mathrm{d}x - \int_0^{\delta} \log(x)\varphi(x-\delta)\,\mathrm{d}x,\end{aligned}$$

provided that φ is smooth and is defined on $[-\delta, 1] \supset [0,1]$. Theoretically, this works for one-dimensional near singularities such as (B.3)*. However, in two dimensions this approach corresponds to the subtraction of thin strips along the edge of the rectangle $[a,b]\times[b,c]$ for some $b \in [b_-, b_+]$. These thin strips are inherently long and thin with singularities at the corner, and as discussed in Remark B.6, Generalised Gaussian quadrature breaks down in such a case.*

B.2.4 Other inner products

We note that the representation (B.6) does not cover all inner products, one dimensional integrals, following from the identity component of $\mathcal{A}$ and the right-hand side $(f, \phi_m)_{L^2(\partial\Omega)}$ are more straightforward to compute efficiently, and may be handled using techniques described in the previous section §B.1. Other integrals that do not follow this structure are $(\mathcal{A}\Psi, \phi_m)_{L^2(\partial\Omega)}$ when u^i is the beam source of Definition 3.6, as Ψ takes the form of a triple integral, similarly $(\mathcal{A}\mathcal{G}_{\gamma\to\Gamma_j}\phi_n, \phi_m)_{L^2(\partial\Omega)}$ of §4.4. The latter of these may be handled by considering $\mathcal{G}_{\gamma\to\Gamma_j}\phi_n$ as a separate function, which will require one-dimensional quadrature to compute (in particular, layered quadrature will be required when $\operatorname{supp}\phi_n \subset \gamma$), but is itself smooth on Γ; and techniques of this section may be applied, with ϕ_n replaced by $\mathcal{G}_{\gamma\to\Gamma_j}\phi_n$.

B.2.5 Parameter values used

All numerical examples in this thesis were performed in MATLAB, for which standard machine precision accuracy is 10^{-16}. These parameters were chosen to such that all integrals were accurate to machine precision.

$$N_Q = 20, \quad n = 16, \quad \sigma = 0.15, \quad \delta_* = 0.2.$$

B.3 Oscillatory quadrature

The oscillatory integrals computed in the methods of this thesis are handled using a basic composite quadrature approach. The domain is split up into rectangles no

wider or taller than half a wavelength each, and these are integrated separately. As k gets large, the number of composite integrals will increase asymptotically like k^2 (in fact k^3 for certain triple integrals). There are oscillatory routines available, such as Filon, Secant and the Method of Steepest Descent (for a review of these, see [39] or [13, §4]), which can be used to integrate independently of frequency. These are difficult to implement as they require an invertible change of integration variables, which often requires $[a, b] \times [c, d]$ to be split into sub-domains to ensure injectivity of the inverse map. The inclusion of these routines is appealing, for the sake of removing the frequency dependent quadrature routines from an otherwise (almost) frequency independent method.

Appendix C

Implementation of Embedding Formulae

This appendix contains efficient techniques and extensions related to the Combined Embedding Expansion Approximation of Definition 6.21.

C.1 Fast algorithm for computing far-field derivatives

We can represent derivatives of the far-field coefficient as

$$\frac{\partial^n D}{\partial \theta^n}(\theta, \alpha) = -\int_\Gamma \frac{\partial^n K}{\partial \theta^n}(\theta, \mathbf{y}) \frac{\partial u_\alpha}{\partial \mathbf{n}}(\mathbf{y})\, \mathrm{d}s(\mathbf{y}),$$

where $K(\theta, \mathbf{x}) := \mathrm{e}^{-\mathrm{i}k[x_1 \cos\theta + x_2 \sin\theta]}$. We require an efficient method to compute derivatives of the kernel K. We can write these derivatives as $\partial^n K/\partial\theta^n = g_n \cdot K$ where g_n can be defined iteratively as in (6.28),

$$g_1(\theta, \mathbf{y}) := -\mathrm{i}k[-y_1 \sin(\theta) + y_2 \cos(\theta)] \tag{C.1}$$

and

$$g_n(\theta, \mathbf{y}) = g_{n-1}(\theta, \mathbf{y}) g_1(\theta, \mathbf{y}) + \frac{\partial g_{n-1}}{\partial \theta}(\theta, \mathbf{y}), \quad \text{for } n \geq 2,$$

by repeated application of the product and chain rules. We can then write a general formula for g_n,

$$g_n(\theta, \mathbf{y}) = \left(g_1(\theta, \mathbf{y}) + \frac{\partial}{\partial \theta}\right)^n g_1(\theta, \mathbf{y}), \quad \text{for } n \geq 2.$$

In practice, the operation which maps g_{n-1} to g_n can be computed linearly in finite dimensions on functions expressed in a Fourier basis $\{\mathrm{e}^{\mathrm{i}\ell\theta}\}_{\ell \in \mathbb{Z}}$, with finitely many non-zero coefficients. For example, we can rewrite (C.1)

$$g_1(\theta, \mathbf{y}) := c_{-1}(\mathbf{y}) \mathrm{e}^{-\mathrm{i}\theta} + c_1(\mathbf{y}) \mathrm{e}^{\mathrm{i}\theta},$$

$$\text{where} \quad c_{-1}(\mathbf{y}) = -\mathrm{i}k\frac{y_2 - \mathrm{i}y_1}{2} \quad \text{and} \quad c_1(\mathbf{y}) = -\mathrm{i}k\frac{y_2 + \mathrm{i}y_1}{2}.$$

For simplicity, we will drop the argument $(\mathbf{y})$ from c_{-1} and c_1 for now. More generally, if a function can be represented exactly using $2n+1$ coefficients $b_{-n}, \ldots, b_n$, then (in terms of coefficients) the operation of multiplying by g_1 (of (C.1)) is represented by

$$\cdot \times g_1 \simeq \begin{bmatrix} c_{-1} & 0 & \cdots & & \\ 0 & c_{-1} & \ddots & & \\ c_1 & 0 & \ddots & & \vdots \\ 0 & \ddots & \ddots & \ddots & 0 \\ \vdots & \ddots & & \ddots & c_{-1} \\ & & \ddots & \ddots & 0 \\ & & & 0 & c_1 \end{bmatrix} \quad \text{and}$$

whilst differentiation with respect to θ is represented by

$$\frac{\partial}{\partial\theta} \simeq \begin{bmatrix} -n & 0 & \ldots & & \\ 0 & \ddots & \ddots & & \\ \vdots & \ddots & & \ddots & \vdots \\ & & \ddots & \ddots & 0 \\ & & \ldots & 0 & n \end{bmatrix}.$$

Therefore, the operator $g_1(\theta, \mathbf{y}) + \partial/\partial\theta$ acting on a function of the form $\varphi(\theta; \mathbf{y}) = \sum_{\ell=-n}^{n} b_\ell(\mathbf{y})\mathrm{e}^{\mathrm{i}\ell\theta}$ is represented by

$$G_n := \begin{bmatrix} c_{-1} & 0 & \cdots & & \\ -n & c_{-1} & \ddots & & \\ c_1 & -n+1 & \ddots & & \vdots \\ 0 & \ddots & \ddots & \ddots & 0 \\ \vdots & \ddots & & n-1 & c_{-1} \\ & & \ddots & \ddots & n \\ & & & 0 & c_1 \end{bmatrix},$$

and the fast computation of the far-field kernel follows by repeated multiplication of these matrices

$$g_n(\theta; \mathbf{y}) = \left(g_1(\theta, \mathbf{y}) + \frac{\partial}{\partial\theta}\right)^n g_1(\theta; \mathbf{y}) = \left[G_n \times \ldots \times G_1[c_{-1}, c_1]^T\right]^T \left[\mathrm{e}^{\mathrm{i}\ell\theta}\right]_{\ell=-n}^{n}.$$

Given c_{-1}, c_1 and n, arrays of G_n may be computed very easily, allowing for fast (non-symbolic) computation of far-field derivatives.

C.2 Avoiding numerical instabilities in computation of Taylor expansion

Practical implementation of (6.17) also requires care when $0 < |\theta - \theta_0| \ll 1$ is small, although this is easier to remedy than for the naive implementation (6.10). This is because numerical errors in the denominator of

$$\frac{\theta - \theta_0}{\Lambda(\theta, \alpha)} = \frac{\theta - \theta_0}{\cos(p\theta) - (-1)^p \cos(p\alpha)}$$

can cause the value of the total fraction to become significantly inaccurate. Using the identity (6.13) and Taylor expanding about θ_0 yields the stable (in a region around θ_0) representation, for $\alpha \notin \Theta_*$,

$$\frac{\theta - \theta_0}{\Lambda(\theta, \alpha)} = \left(\sum_{n=1}^{\infty} \frac{(\theta - \theta_0)^{n-1}}{n!} p^n \cos(p\theta_0 + n\pi/2) \right)^{-1},$$

in practice the sum should be truncated after an appropriate number of terms.

C.3 Computing multi-variate expansion to nth order

The Taylor expansion we present in §6.2.2 is first order. Here we outline a procedure to extend to higher order multi-variate Taylor expansion. This requires computation of arbitrary mixed derivatives of the far-field coefficient $D(\theta, \alpha)$.

Computation of derivatives in θ only is far more straightforward from the integral representation (6.3), the derivatives in α only follow by reciprocity (Theorem 6.4). Practically, only half of the non-symmetric mixed derivatives need to be computed, again thanks to reciprocity, as we have

$$\frac{\partial^{n_\theta + n_\alpha}}{\partial \theta^{n_\theta} \partial \alpha^{n_\alpha}} D(\theta_*, \alpha_*) = \frac{\partial^{n_\theta + n_\alpha}}{\partial \theta^{n_\alpha} \partial \alpha^{n_\theta}} D(\alpha_*, \theta_*).$$

But this offers little consolation considering the effort required to compute the mixed derivatives, which cannot be obtained using the representation (6.3). We can obtain an exact representation for these using the representation (6.4), for example

$$\begin{aligned} &\frac{\partial D}{\partial \alpha}(\theta, \alpha) \\ &= \frac{\partial}{\partial \alpha} \left[\frac{1}{\Lambda(\theta, \alpha)} \sum_m B_m(\alpha) \hat{D}(\theta, \alpha_m) \right] && \text{(C.2)} \\ &= \frac{\sum_m [B_m(\alpha) \frac{\partial \Lambda}{\partial \alpha}(\theta, \alpha) - B'_m(\alpha) \Lambda(\theta, \alpha)] \hat{D}(\theta, \alpha_m)}{[\Lambda(\theta, \alpha_m)]^2}, && \text{(C.3)} \end{aligned}$$

where the coefficients B'_m (derivatives of B_m of (6.6)) can be determined by solving the system of equations

$$\sum_{m=1}^{N_T} B'_m \hat{D}(\alpha_n, \alpha_m) = (-1)^{p+1} \frac{\partial \hat{D}}{\partial \theta}(\alpha, \alpha_n), \quad \text{for } n = 1, \ldots, N_T. \tag{C.4}$$

Noting that

$$\frac{\partial^2 \Lambda(\theta, \alpha)}{\partial \theta \partial \alpha = 0},$$

for all θ, α, it follows from (C.2) that

$$\frac{\partial^2 D}{\partial \alpha \partial \theta}(\theta, \alpha) = \frac{-\sum_m B'_m(\alpha) \left[\frac{\partial [\Lambda(\theta, \alpha_m)^2]}{\partial \theta} \hat{D}(\theta, \alpha_m) + \Lambda(\theta, \alpha) \frac{\partial \hat{D}(\theta, \alpha_m)}{\partial \theta} + 2\hat{D}(\theta, \alpha_m) \frac{\partial \Lambda(\theta, \alpha_m)}{\partial \theta} \right]}{[\Lambda(\theta, \alpha)]^2}. \tag{C.5}$$

In the above case, which is the lowest order mixed derivative, to compute the limit as $(\theta, \alpha) \to (\theta_*, \alpha_*)$, more applications of L'Hopital's rule are required, making this approach less practical.Clearly, whilst any desired accuracy close to problematic points (θ_*, α_*) is achievable, a significant amount of symbolic work is required beforehand. Formulae for higher order cross terms will become increasingly arduous to compute, hence to compute to arbitrary precision may require the use of symbolic solver. We denote such an approximation by

$$\begin{aligned} & D(\theta, \alpha) \\ & \overbrace{\approx \sum_{n=0}^{N_T{}^*} \left[\frac{(\theta - \theta_*)^n}{n!} \frac{\partial^n \theta \mathcal{P}_F D}{\partial \theta^n}(\theta_*, \alpha_{m_1}) + \frac{(\alpha - \alpha_*)^n}{n!} \frac{\partial^n \theta \mathcal{P}_F D}{\partial \theta^n}(\alpha_*, \alpha_{m_2}) \right]}^{\text{Non-mixed partial derivatives using reciprocity}} \\ & \underbrace{+ \sum_{\substack{n_\theta + n_\alpha \leq N_T{}^* \\ n_\theta, n_\alpha \in \mathbb{N}}} \frac{(\theta - \theta_*)^{n_\theta} (\alpha - \alpha_*)^{n_\alpha}}{n_\theta! n_\alpha!} \lim_{(\theta, \alpha) \to (\theta_*, \alpha_*)} \frac{\partial^{N_T{}^*}}{\partial \theta^{n_\theta} \partial \alpha^{n_\alpha}} \left[\frac{\sum_{m=1}^{N_T} b_m(\alpha) \mathcal{P}_F \hat{D}(\theta, \alpha_m)}{\Lambda(\theta, \alpha)} \right]}_{\text{Mixed partial derivatives}}, \end{aligned}$$

for $0 < |\theta - \theta_0| \ll 1$ and $0 < |\theta - \theta_*| \ll 1$, with $\theta_0 \in \Theta_\alpha$ and $\theta_* \in \Theta_*$, where A_{M_ω} has been chosen such that $\theta_* = \alpha_{m_1} \in \Theta_*$ and $\theta_* = \alpha_{m_2} \in \Theta_*$.

Bibliography

[1] A. Anand, Y. Boubendir, F. Ecevit, and F. Reitich. Analysis of multiple scattering iterations for high-frequency scattering problems. II.The three-dimensional scalar case. *Numer. Math.*, 114(3):373–427, 2010.

[2] D. N. Arnold and W. L. Wendland. On the asymptotic convergence of collocation methods. *Math. Comp.*, 41(164):349–381, 1983.

[3] K. E. Atkinson. *The Numerical Solution of Integral Equations of the Second Kind*. Cambridge University Press, 1997. Cambridge Books Online.

[4] A. H. Barnett and T. Betcke. Stability and convergence of the method of fundamental solutions for Helmholtz problems on analytic domains. *J. Comput. Phys.*, 227(14):7003–7026, 2008.

[5] A. H. Barnett and T. Betcke. An exponentially convergent nonpolynomial finite element method for time-harmonic scattering from polygons. *SIAM J. Sci. Comput.*, 32(3):1417–1441, 2010. MPSpack software available to download from https://github.com/ahbarnett/mpspack.

[6] D. Baskin, E. A. Spence, and J. Wunsch. Sharp high-frequency estimates for the Helmholtz equation and applications to boundary integral equations. *SIAM J. Appl. Math.*, 48(1):229–267, 2016.

[7] T. Betcke, S. N. Chandler-Wilde, I. G. Graham, S. Langdon, and M. Lindner. Condition number estimates for combined potential boundary integral operators in acoustics and their boundary element discretisation. *Numer. Methods PDEs*, 27:31–69, 2011.

[8] T. Betcke and E. A. Spence. Numerical estimation of coercivity constants for boundary integral operators in acoustic scattering. *SIAM J. Numer. Anal*, 49(4):1572–1601, 2011.

[9] N. R. T. Biggs. A new family of embedding formulae for diffraction by wedges and polygons. *Wave Motion*, 43(7):517–528, 2006.

[10] S. N. Chandler-Wilde. The impedance boundary value problem for the Helmholtz equation in a half-plane. *Math. Methods Appl. Sci.*, 20(10):813–840, 1997.

[11] S. N. Chandler-Wilde, A. Gibbs, A. Moiola, and S. Langdon. Hybrid numerical asymptotic approximation for multiple scattering problems. In *Proceedings of the 12th International Conference on Mathematical and Numerical Aspects of Wave Propagation*, pages 130–131, Karlsruhe, Germany, July 2015. Book of abstracts available at: http://waves2015.math.kit.edu/boa/book-of-abstracts.pdf.

[12] S. N. Chandler-Wilde, I. G. Graham, S. Langdon, and M. Lindner. Condition number estimates for combined potential boundary integral operators in acoustic scattering. *J. Integral Equations Appl.*, 21(2):229–279, 2009.

[13] S. N. Chandler-Wilde, I. G. Graham, S. Langdon, and E. A. Spence. Numerical-asymptotic boundary integral methods in high-frequency acoustic scattering. *Acta Numer.*, 21:89–305, 2012.

[14] S. N. Chandler-Wilde and D. P. Hewett. Acoustic scattering by fractal screens: mathematical formulations and wavenumber-explicit continuity and coercivity estimates. *arXiv preprint arXiv:1401.2805*, 2014.

[15] S. N. Chandler-Wilde, D. P. Hewett, S. Langdon, and A. Twigger. A high frequency boundary element method for scattering by a class of nonconvex obstacles. *Numer. Math.*, 129(4):647–689, 2015.

[16] S. N. Chandler-Wilde and S. Langdon. A Galerkin boundary element method for high frequency scattering by convex polygons. *SIAM J. Numer. Anal.*, 45(2):610–640, 2007.

[17] D. Colton and R. Kress. *Inverse acoustic and electromagnetic scattering theory*, volume 93 of *Applied Mathematical Sciences*. Springer, New York, third edition, 2013.

[18] NIST Digital Library of Mathematical Functions. http://dlmf.nist.gov/, Release 1.0.10 of 2015-08-07.

[19] T. J. Dufva, J. Sarvas, and J. C-E. Sten. Unified derivation of the translational addition theorems for the spherical scalar and vector wave functions. *Prog. Electromagn. Res. B.*, 4:79–99, 2008.

[20] J. Galkowski, E. H. Müller, and E. A. Spence. Wavenumber-explicit analysis for the Helmholtz h-BEM: error estimates and iteration counts for the Dirichlet problem. *arXiv preprint arXiv:1608.01035*, 2016.

[21] M. Ganesh and S. C. Hawkins. A high-order algorithm for multiple electromagnetic scattering in three dimensions. *Numer. Algorithms*, 50(4):469–510, 2009.

[22] M. Ganesh and S. C. Hawkins. A stochastic pseudospectral and T-matrix algorithm for acoustic scattering by a class of multiple particle configurations. *J. Quant. Spectrosc. Radiat. Transfer*, 123:41–52, 2013.

[23] M. Ganesh and S. C. Hawkins. Algorithm XXX: TMATROM-a T-matrix reduced order model software. *ACM Trans. Math. Software*, 2017. To appear. Preprint available at: http://inside.mines.edu/.

[24] M. Ganesh, S. C. Hawkins, and R. Hiptmair. Convergence analysis with parameter estimates for a reduced basis acoustic scattering T-matrix method. *IMA J. Numer. Anal.*, 32(4):1348–1374, 2012.

[25] C. Geuzaine, O. Bruno, and F. Reitich. On the $O(1)$ solution of multiple-scattering problems. *IEEE Trans. Magn.*, 41(5):1488–1491, 2005.

[26] A Gibbs, S Langdon, and A Moiola. Hybrid numerical asymptotic approximation for source-type incidence. *(In preparation)*, 2017.

[27] A. Gibbs, S. Langdon, and A. Moiola. Stable implementation of embedding formulae for computation of far field patterns. In *Proceedings of the 13th International Conference on Mathematical and Numerical Aspects of Wave Propagation*, pages 157–158, Minneapolis, USA, May 2017. Book of abstracts available at: www.cce.umn.edu/documents/CPE-Conferences/WAVES2017BookofAbstracts.pdf.

[28] A Gibbs, S Langdon, and A Moiola. Stable implementation of embedding formulae for computation of far-field patterns. *(In preparation)*, 2017.

[29] A Gibbs, S Langdon, A Moiola, and E. A. Spence. h-BEM analysis of multiple scattering problems. *(In preparation)*, 2017.

[30] I. G. Graham, M. Löhndorf, J. M. Melenk, and E. A. Spence. When is the error in the h-BEM for solving the Helmholtz equation bounded independently of k? *BIT Numer. Math.*, 55(1):171–214, 2014.

[31] S. P. Groth, D. P. Hewett, and S. Langdon. Hybrid numerical-asymptotic approximation for high-frequency scattering by penetrable convex polygons. *IMA J. Appl. Math.*, 80(2):324–353, 2015.

[32] W. Gui and I. Babuˇska. The h, p and h-p versions of the finite element method in 1 dimension. parts I–III. *Numer. Math.*, 49(6):577–683, 1986.

[33] J. Hargreaves, D. P. Hewett, Y. Lam, and S. Langdon. A high frequency boundary element method for scattering by three-dimensional screens. In *Proceedings of the 12th International Conference on Mathematical and Numerical Aspects of Wave Propagation*, pages 202–203, Karlsruhe, Germany, July 2015. Book of abstracts available at: http://waves2015.math.kit.edu/boa/book-of-abstracts.pdf.

[34] D. P. Hewett, S. Langdon, and S. N. Chandler-Wilde. A frequency-independent boundary element method for scattering by two-dimensional screens and apertures. *IMA J. Numer. Anal.*, 35(4):1698–1728, 2015.

[35] D. P. Hewett, S. Langdon, and J. M Melenk. A high frequency hp boundary element method for scattering by convex polygons. *SIAM J. Numer. Anal.*, 51(1):629–653, 2013. Appendix present in the preprint MPS-2011-18 at http://www.reading.ac.uk/maths-and-stats/research/maths-preprints.aspx, Department of Mathematics and Statistics, University of Reading, UK.

[36] R. Hiptmair, A. Moiola, and I. Perugia. Plane wave discontinuous galerkin methods: Exponential convergence of the hp-version. *FoCM*, 16(3):637–675, 2016.

[37] D. Huybrechs and R. Cools. On generalized Gaussian Quadrautre rules for singular and nearly singular integrals. *SIAM J. Numer. Anal.*, 47:719–739, 2009.

[38] D. Huybrechs and S. Olver. Superinterpolation in highly oscillatory quadrature. *Found. Comput. Math.*, 12(2):203–228, 2012.

[39] D. Huybrechs and S. Vandewalle. The construction of cubature rules for multivariate highly oscillatory integrals. *Math. Comp.*, 76(260):1955–1980, 2007.

[40] Mitsuru Ikawa. Decay of solutions of the wave equation in the exterior of several convex bodies. In *Ann. Inst. Fourier (Grenoble)*, volume 38, pages 113–146, 1988.

[41] M. Löhndorf and J. M. Melenk. Wavenumber-explicit *hp*-BEM for high frequency scattering. *SIAM J. Numer. Anal.*, 49(6):2340–2363, 2011.

[42] W. McLean. *Strongly elliptic systems and boundary integral equations*. Cambridge University Press, Cambridge, 2000.

[43] A. Moiola and E. A. Spence. Is the Helmholtz equation really sign-indefinite? *SIAM Rev.*, 56(2):274–312, 2014.

[44] S. E. Mousavi and N. Sukumar. Generalized Duffy transformation for integrating vertex singularities. *Comput. Mech.*, 45(2-3):127–140, 2010.

[45] Jean-Claude Nédélec. *Acoustic and electromagnetic equations*, volume 144 of *Applied Mathematical Sciences*. Springer-Verlag, New York, 2001. Integral representations for harmonic problems.

[46] S. Nonnenmacher and M. Zworski. Quantum decay rates in chaotic scattering. *Acta. Math.*, 203(2):149–233, 2009.

[47] E. Parolin. A hybrid numerical-asymptotic boundary element method for high-frequency wave scattering. Master's thesis, University of Oxford, 2015.

[48] A. Quarteroni and A. Valli. *Numerical approximation of partial differential equations*, volume 23. Springer Science & Business Media, 2008.

[49] S. A. Sauter and C. Schwab. *Boundary element methods*. Springer, 2010.

[50] E. A. Spence. Wavenumber-explicit bounds in time-harmonic acoustic scattering. *SIAM J. Math. Anal.*, 46(4):2987–3024, 2014.

[51] E. A. Spence. *"When all else fails, integrate by parts" - an overview of new and old variational formulations for linear elliptic PDEs*, chapter 6. SIAM, 2015. Author's personal copy available at: http://people.bath.ac.uk/eas25/ibps.pdf, any numbered theorems, equations etc. inside of this thesis are referring to this version.

[52] E. A. Spence, S. N. Chandler-Wilde, I. G. Graham, and V. P. Smyshlyaev. A new frequency-uniform coercive boundary integral equation for acoustic scattering. *Comm. Pure Appl. Math.*, 64(10):1384–1415, 2011.

[53] E. A. Spence, I. V. Kamotski, and V. P. Smyshlyaev. Coercivity of combined boundary integral equations in high-frequency scattering. *Communications on Pure and Applied Mathematics*, 68(9):1587–1639, 2015.

[54] O. Steinbach. *Numerical approximation methods for elliptic boundary value problems: finite and boundary elements*. Springer Science & Business Media, 2007.

[55] P. C. Waterman. New formulation of acoustic scattering. *J. Acoust. Soc. Am.*, 45(6):1417–1429, 1969.

[56] W. J. Wiscombe. Improved Mie scattering algorithms. *Appl. Optics*, 19(9):1505–1509, 1980.

[57] Jared Wunsch. Resolvent estimates with mild trapping. *J. É. D. P.*, pages 1–15, 2012.